Dissertation zur Erlangung des Doktorgrades
der Fakultät für Chemie und Pharmazie
der Ludwig-Maximilians-Universität München

CARTRIDGE FILLING WITH BIOPHARMACEUTICALS WITH FOCUS ON THE OPTIMIZATION OF THE SILICONIZATION PROCESS

Stefanie Funke
aus
Zwickau, Deutschland

2016

ERKLÄRUNG

Diese Dissertation wurde im Sinne von § 7 der Promotionsordnung vom 28. November 2011 von Herrn Prof. Dr. Wolfgang Frieß betreut.

EIDESSTATTLICHE VERSICHERUNG

Diese Dissertation wurde eigenständig und ohne unerlaubte Hilfe erarbeitet.

Basel, 02. Juni 2016

.....

Stefanie Funke

Dissertation eingereicht am:	03. Juni 2016
1. Gutachter:	Prof. Dr. Wolfgang Frieß
2. Gutachter:	Prof. Dr. Gerhard Winter
Mündliche Prüfung am:	07. Juli 2016

Für meine Eltern

ACKNOWLEDGEMENT

This thesis was prepared at the Department of Pharmacy, Pharmaceutical Technology and Biopharmaceutics at the Ludwig-Maximilians-Universität München (LMU) in cooperation with F. Hoffmann-La Roche Ltd, Pharmaceutical Development & Supplies, PTD Biologics Europe (PTDE-P).

Foremost, I would like to express my gratitude to my supervisor Prof. Dr. Wolfgang Frieß. I am deeply thankful for his enthusiastic guidance and scientific input. His creativity, encouragement and patience were invaluable to develop my own scientific ideas and confidence in my work. On both personal and professional level I very much appreciated his advice. Thank you for giving me the opportunity to join your group - I really enjoyed the fantastic atmosphere during everyday life and exciting group activities.

I also would like to thank Prof. Dr. Gerhard Winter for being co-referee of this thesis. Also highly appreciated is his dedication to create excellent work conditions as chair of Pharmaceutical Technology and Biopharmaceutics, and to encourage scientific discussion during Thursday´s seminars.

I highly appreciated the collaboration with the team from F. Hoffmann-La Roche Ltd. I want to thank Julia Matilainen for her enthusiastic supervision and input during this work as well as for her personal guidance during my numerous stays in Basel. Thank you so much for your continuous effort! Many thanks are also expressed to Heiko Nalenz for co-supervising this project and for his valuable support during our telecons, meetings and experiments performed in Basel. I am also deeply thankful to Karoline Bechtold-Peters, who initiated the project and made way for the collaboration. I really enjoyed working on this project. Thank you for your input and ideas. Very special thanks also go to Hanns-Christian Mahler for his valuable scientific advice. To the entire team in Basel I want to express my gratitude for supporting this project: Pierre Windenberger, Alexander Hein and Michel Schaffner for setting up the pilot-scale siliconization unit and associated equipment, Holger Röhl and Jean-Pierre Büttiker for providing access to the 3D-laser scanning microscope and helpful information on the “vartridge” design, Anacelia Rios Quirez and Emilien Folzer for the introduction into NTA and RMM particle analysis, Constanze Hediger for her help with HIC, Sascha Dreher, Thorben Hammerich, Lothar Vorgrimler and Jean Grausse for the opportunity to use different methods in the lab during initial method evaluation for this thesis.

Thanks to Prof. Dr. Franz Bracher, Christoph Müller and Florian Vetter from the Department of Pharmacy, Center for Drug Research at the LMU, for performing the GC-MS measurements and for proofreading parts of this work for peer-reviewed publication. Furthermore, I want to thank Norma Minar and Constantin Schirnding from the Department of Chemistry and Center for NanoScience at the LMU for their kind support on AFM measurements. Prof. Dr. Angelika Vollmar and her group from the Department of Pharmacy, Center for Drug Research at the LMU, are also kindly acknowledged for enabling access to the FACS instrument.

Daniela Held from PSS Polymer Standards Service GmbH is kindly acknowledged for her help to analyze the GPC results. Additional thanks go to Stefan Ebert from Bausch + Ströbel Maschinenfabrik GmbH + Co. KG for his technical support on the pilot-scale siliconization unit during numerous phone calls and email conversations. Coriolis Pharma is kindly acknowledged for the possibility to use the MFI instrument. Special thanks go to Daniel Weinbuch, who shared his MFI experience with me.

My thanks are also extended to Prof. Dr. Christian Wahl-Schott, Prof. Dr. Stefan Zahler, Prof. Dr. Franz Bracher and Prof. Dr. Ernst Wagner for kindly being members of my thesis advisory board.

Thank you to all the students who were involved in this project: Daniela Maier, Samuel Scholl, Stephanie Raschke and Linh Hoang Thuy. Thank you for your excellent work!

Many thanks and the kindest regards go to all my former colleagues at the institute. I am deeply grateful for the legendary atmosphere and the good times we spent together in the lab and on weekends having barbecues, skiing, hiking, canoeing, or eating kilos of chocolate. Thank you Verena for the warm atmosphere we shared during our collaboration on the Roche projects. It felt most comfortable working with you in such a friendly and scientifically driven manner. I also wish to address a special thanks to my lab mate Imke, who offered help at any time and shared precious LMU campus knowledge with me.

Finally, I deeply thank my family and Roman for their support, never ending confidence and encouragement during those intensive years.

TABLE OF CONTENT

I GENERAL INTRODUCTION

1 READY-TO-USE DRUG/DEVICE COMBINATION PRODUCTS (DDCP)

Over the last decades, ready-to-use DDCPs have changed the perspectives of patients and health care professionals towards injectables. In-line with the success of therapeutic proteins to treat a wide range of severe oncology and immune disorders [1], the use of DDCPs for therapeutic proteins has considerably grown by 22 % from 2010 to 2015 compared to 11 % for other injectables [2]. It is forecasted that the market will grow from 2 billion sold pre-filled syringes (PFS) in 2009 to 6.83 billion units in 2025 [3]. While the glass PFS market was worth $3.59 billion in 2015, revenues are predicted to reach $5.51 billion in 2022 with Becton Dickinson, Schott, Nipro Glass, Nuova Ompi and Gerresheimer being the dominating syringe suppliers [4]. Likewise, advanced DDCPs such as auto-injectors pre-loaded with cartridges or syringes have evolved to further improve the ease of self-administration by automatic needle insertion and drug delivery (e.g., spring-controlled). Self-administration of DDCPs allows patients to take their medication with a high level of convenience at home or during travelling [5]. For health care professionals, DDCPs are the primary choice for immediate and safe medication (85% of health care professionals prefer DDCPs over other parenteral delivery systems) [6]. The expected market growth is primarily attributed to an increasing demand for injectable therapeutic proteins [4]. In addition, DDCPs are also used for the parenteral administration of small molecular drugs (Tab. I-1).

Recently, large volume (up to 10 mL), wearable DDCPs, i.e., patch pumps such as SmartDose®, SteadyMed®, which are well-known in insulin therapy, have gained more attention within the highly competitive biopharmaceutical market [7,8]. These systems eliminate the need for multiple injections or infusions.

Tab. I-1. Selected medications available as DDCP modified from [2,6,7] (by May 6, 2016).

Brand name	INN [a]	LM [b]/SM [c]	Indication/Disease (selection)	DDCP
Aranesp	Darbepoetin alpha	LM	Anemia	PFS
APO-go	Apomorphine HCl	SM	Parkinson´s disease	PFS, injector
Avonex	Interferon β-1a	LM	Multiple sclerosis	PFS, injector
Clexane	Enoxaparin sodium	SM	Deep vein thrombosis	PFS
Emerade	Epinephrine tartrate	SM	Anaphylaxis	Injector
Enbrel	Etanercept	LM	TNF blocker	PFS, injector
Engerix	Hepatitis B (rDNA) vaccine	LM	Hepatitis B	PFS
Heparin-Calcium-5000 ratiopharm	Heparin calcium	SM	Anticoagulant	PFS
Humira	Adalimumab	LM	Rheumatoid arthritis	PFS, injector
IntronA	Interferon α-2b	LM	Chronic hepatitis B	Injector
Lantus SoloSTAR	Insulin glargine	LM	Diabetes	Pen
Metex	Methotrexat	SM	Rheumatoid arthritis	PFS, injector
Neupogen	Filgrastim	LM	Neutropenia	PFS
Pegasys	Peginterferon alpha-2a	LM	Chronic hepatitis B & C	PFS
RoActemra	Tocilizumab	LM	Rheumatoid arthritis	PFS
Roferon	Interferon α-2a	LM	Leukaemia	PFS

[a] *International non-proprietary name*
[b] *Large molecule*
[c] *Small molecule*

The interest dedicated to DDCPs can be tracked back to several advantages for both industry and the intended user population. The main reasons include the following (modified from [4]):

- increased sterility assurance
- reduced handling requirements improve ease and speed of administration (no separate reconstitution or filling step from another container (vial, ampoule) to the syringe)
- potential for self-administration by the patient
- improved dosing accuracy
- benefits for the safety of patients and health care professionals with regard to post-administration needle-stick injuries, e.g., by integrated needle safety devices
- brand differentiation in the course of life-cycle management
- less overfill of costly therapeutics (2-3 % compared to 20-25 % for ampoules/vials [3]) and consequently reduced waste and costs

- ease of manufacture by purchasing ready-to-fill (pre-washed, pre-sterilized, depyrogenated, siliconized) syringes

However, significant variations in design, format, construction material, surface treatment (e.g., coating) and secondary components (plunger rod, tip, cap, rigid needle shield etc.) for most DDCPs also pose numerous technical challenges. These include selection of appropriate on-site filling and assembly technologies, functional performance, compatibility with the therapeutic protein during shelf life and matching user requirements [9,10].

2 SILICONIZATION PROCESSES FOR PRIMARY PACKAGING GLASS BARRELS

Numerous parenteral packaging components are to some extent lubricated with silicone oil to improve functional performance and machinability. Rubber components such as vial stoppers and syringe pistons are less sticky after siliconization, which ensures discharging from stopper washing bowls, seamless feed from hoppers to machine paths as well as transfer through machine guides. Siliconization further reduces the force to insert vial stoppers [11]. In addition, siliconized vials show better drainage and less fogging after siliconization [12]. From a patient´s perspective, needle lubrication results in less injection pain due to lower frictional forces during skin penetration. Adequate siliconization of the inner syringe/cartridge glass barrel is essential for a smooth, easy and consistent injection of DDCPs [11]. Thus, among the different functional performance tests for DDCP, e.g., seal integrity testing, tip cap removal force, the forces to initiate (referred to as break-loose force) and to maintain the movement of the piston within the glass barrel (gliding force) are still the most important measurable outputs and are often somehow related to the degree of siliconization [3].

In addition, silicone oil free systems are being promoted. These techniques include lubricious, biocompatible coatings for plunger stoppers, which enable adequate extrusion performance in silicone oil free syringes, e.g., fluoropolymer coatings (FluroTec®) or proprietary i-coating™, often in combination with polymer based syringes (Plajex™, CrystalZenith®) [13–15]. Studies suggest a great potential of these systems for highly sensitive protein therapeutics with low protein aggregate and subvisible particle levels, but suitability has still to be confirmed with more systematic investigations [16].

Usually, siliconization of the inner glass barrel is performed by spraying-on either silicone oil (referred to as spray-on siliconization) without further treatment [17] or diluted silicone emulsion

that is baked-on the glass surface at approximately 300 °C for 10-30 min (referred to as bake-on siliconization) [18,19]. Automated siliconization units precisely regulate the spray amount, nozzle position, nozzle speed as well as the air atomization pressure and spray time [17,20]. Both processes are applicable for luer cone PFS and cartridges. In contrast, staked-in needle PFS need to be spray-on siliconized due to the low heat resistance of the glue used for embedding the needle into the fluid path of the syringe cone. Generally, siliconization can also be performed by wiping, dipping or washing the component in a solvent-based silicone solution or silicone emulsion followed by drying at room temperature or elevated temperature [21–24].

The most widely applied silicone oil for spray-on siliconization is trimethylsiloxy-endcapped polydimethylsiloxane, e.g., silicone oil as lubricant [25] or dimethicone [26], with viscosities ranging from 1,000 cSt to 12,500 cSt [17,21]. The physical and chemical requirements for non-parenteral use (i.e., as lubricant) are defined in the relevant monographs in the Ph. Eur., depending on the fluid viscosity [25,26].

Silicone emulsion for bake-on siliconization, e.g., dimethicone emulsion, contains additional stabilizers such as preservatives (methyl paraben and propyl paraben), non-ionic surfactants (Tween 20 and Triton X-100) and co-solvents (propylene glycol) up to 5 % each and about 35 % dimethicone, 350 cSt, in water [27,28]. Even though diluted emulsions are applied and hence these stabilizers level-off, there might be concerns with respect to a potential interaction with the drug.

Silicone oil has been safely used as lubricant over decades [25], for the treatment of retinal detachment and soft tissue augmentation due to its biological inertness [29]. However, certain low molecular weight siloxanes, which may be present in silicone oil as residues from polymer synthesis [30,31] have been associated with toxicological concerns [32,33]. These low molecular weight siloxanes may also appear as thermal decomposition products [34–36] during bake-on siliconization. Nevertheless, adequate heat-treatment is essential to remove the emulsion water and for concomitant sterilization and depyrogenation [9,17,19,28].

Although bake-on siliconization is widely implemented in industry, there is currently a substantial gap in understanding the thermal impact on the applied silicone emulsion. A systematical evaluation of the change in the silicone level, extrusion performance and chemical composition upon bake-on may help to define an adequate processing window with regard to burn-in time and temperature.

For both siliconization processes, it is critical to target an adequate silicone level in order to meet the intended piston extrusion performance, also in context of long-term product storage, but at the same time keeping the overall silicone quantity as low as possible. Spray-on siliconization processes most commonly apply relatively high silicone levels of 0.2-1 mg/barrel due to limitations of the siliconization equipment to precisely spray lower amounts of viscous silicone oil [10,16,17,37–42]. In bake-on processes, silicone levels below 0.1 mg/barrel are achieved by adjusting the spray amount and/or concentration of the silicone emulsion [37,43,44].

Likewise, a homogeneous distribution of the silicone within the glass barrel is challenging. An uneven silicone distribution may lead to a poor injection performance, stalling of the piston during injection or "chattering" with repetitive halting of the piston [10,45]. In this context, great effort is made by suppliers to optimize the silicone distribution using different static or dynamic spray nozzle positions [17,20], but technical aspects are rarely published and considered as proprietary know-how. Overall, siliconization processes are not well standardized and as such, there is a high variability in the silicone level, distribution and leaching from individual siliconized containers [43,46].

3 CHARACTERIZATION METHODS FOR SILICONIZED PRIMARY PACKAGING GLASS BARRELS

Reliable analytical techniques are the prerequisites for the optimization of siliconization processes. Silicone levels of approximately 0.2-7.3 mg/barrel have been quantified using Fourier transform infrared (FTIR) spectroscopy or atomic absorption spectroscopy after solvent extraction [37,42,47]. For silicone levels between 0.2 mg and 1.0 mg/barrel, quantification has been performed simply gravimetrically by weighing the syringe before and after siliconization [17]. The functional performance of DDCPs is assessed by extrusion force measurements, which may serve as an indirect measure for siliconization quantity and distribution within the glass barrel.

A rather subjective qualitative evaluation of the silicone distribution within the glass barrel can be performed by spreading glass or talcum dust or suspension, which adhere to the siliconized areas on the glass surface [17,48]. The relatively thick spray-on silicone layers usually exhibit individual plaque-like structures, which can be assessed by optical microscopy [41,42,45]. In addition, upon contact with aqueous media the silicone layer forms micro-droplet structures that can be tracked along the syringe barrel by schlieren visualization (e.g., Flex-Bench-Top

Lubricant Characterization System from Zebrasci, Inc.). Other spectroscopic techniques such as interferometry with white light (e.g., Layer Explorer from rap.ID Particle Systems GmbH) have been applied to determine silicone layer thicknesses up to approximately 1 µm with a lower limit of quantification of approximately 80 nm [39,41,42,45,48,49]. In addition, interferometric profilers that apply a red laser beam have been proposed to determine silicone layers as thin as 20 nm [50], but no data have been published yet.

A combination of these methods should enable the full characterization of siliconized syringes and cartridges in terms of silicone quantity, silicone layer thickness and distribution. Quantification limits as low as 0.2 µg/mL have been reported for FTIR. Together with easy sample preparation (e.g., solvent extraction) and fast measurement, this makes FTIR a promising technique to quantify baked-on silicone levels even below 0.1 mg/barrel. The relatively new spectroscopic methods based on schlieren visualization or interferometry have not been systematically investigated yet, which limits the applicability even for spray-on silicone layers. In particular for thin, baked-on silicone layers of less than 100 nm these methods lack sufficient sensitivity. Hence there is currently a gap in analytical methods to characterize very thin baked-on silicone layers.

4 DRUG PRODUCT COMPATIBILITY WITH SILICONIZED PRIMARY PACKAGING SYSTEMS

Protein drugs are generally prone to both chemical instabilities, e.g., deamidation or oxidation, and physical instabilities such as particle formation and adsorption. These protein instabilities are induced by various factors including higher temperature, freezing and thawing and mechanical agitation by shaking or stirring [51–53]. Protein aggregates and particles have been associated with immunological concerns [54–57] and adverse clinical effects [58,59]. The topic is highly debated, since on the other hand, marketed products with some levels of particles have been safely used for years [46].

The protein-inherent degradation pathways might also be triggered by various surfaces proteins encounter during formulation (filters), manufacturing (tanks, columns, tubing), shipping (bags), storage (DDCPs, bags) and delivery (infusion bags, DDCPs) [60,61]. DDCPs should offer protection of the drug product during storage and facilitate drug delivery during administration. However, the different component surfaces can interact with the drug product and may thus be critical for product quality. This includes siliconized surfaces or droplets that have leached into

the drug product formulation. Other product-related impurities for PFS formats have been traced back to tungsten/tungsten oxide as residues from tungsten pins used to form the syringe fluid path and to the adhesive process used to attach the needle in the syringe fluid path [4,62–64]. Leaching impurities from uncoated rubber materials may also play a critical role, e.g., the increased incidence of pure red cell aplasia in chronic kidney disease patients treated with Eprex (epoetin alfa) in a PFS format was postulated to be related to such impurities [65,66]. Also, the glass barrel adds to the impurity profile [9]. The following section focuses on silicone-protein interactions. Effects of other surfaces and leachable have been thoroughly reviewed in the referenced literature.

Silicone can detach from the inner glass wall and appear as silicone droplets in the drug product formulation, which renders two potential problems. Firstly, silicone droplets increase the number of particles, for which limits are set by the pharmacopoeias [67–71]. Secondly, protein stability may be perturbed leading to homogeneous protein aggregates and particles or heterogeneous protein-silicone particles. Early studies observed particles and a loss of insulin activity associated with the release of silicone droplets [72]. In siliconized syringes and silicone-spiked formulations without surfactant, aggregation and particle formation was reported for several proteins upon agitation [16,22,40,73–76], at increased temperatures [38,77] or periodical rupture of the silicone oil-water interface [78]. However, in most of the performed spiking studies, the silicone concentrations were considerably higher than typically present in DDCPs. Furthermore, the addition of surfactant efficiently mitigated the observed protein instabilities [74,75,78–81]. Interestingly, minimal silicone migration was reported for baked-on siliconized containers as compared to spray-on siliconized containers with higher silicone levels [22,38,39,41]. Overall, it appears that in most cases, particle levels and turbidity increased due to silicone migration rather than compromised protein stability [19,40,82–85].

Due to their surface activity proteins readily adsorb to container materials. Since the adsorbed amounts of most proteins are considerably low, loss in protein content may be only of concern for diluted or low concentration protein therapeutics [86,87]. In contrast, structural alteration upon adsorption followed by exchange or desorption back into solution often receives more attention since these altered structures are considered as precursors for protein aggregation [88–90]. In the absence of polysorbate 80, a loss in protein content and structural alteration was reported for albinterferon α_{2b} likely through protein adsorption to silicone droplets [74]. Silicone oil induced

protein loss was also observed for several other proteins, e.g., anti-SA IgG1, abatacept, lysozyme and trastuzumab, but the effect on protein stability was minimal [75,81].

Given the cited reports in addition to optimized formulation approaches, optimized siliconization processes to reduce the silicone levels and the usage as lubricant for years, silicone oil does not seem to pose a serious risk for protein stability. However, the increased use of DDCPs as storage and delivery systems for therapeutic proteins makes a more thorough investigation of the extent of silicone leaching, the driving factors and concomitant protein adsorption and particle formation necessary.

5 ABBREVIATIONS

DDCP	Drug/device combination product
FACS	Fluorescence activated cell sorting
FTIR	Fourier transform infrared (spectroscopy)
LM	Large molecule
PFS	Pre-filled syringe
SM	Small molecule

6 REFERENCES

[1] J.G. Elvin, R.G. Couston, C.F. van der Walle, Therapeutic antibodies: market considerations, disease targets and bioprocessing., Int. J. Pharm. 440 (2013) 83–98.

[2] J. Wright, Developing containers and devices to meet emerging and evolving parenteral needs, (2011). http://ondrugdelivery.com/publications/Prefilled Syringes Sep 2011/Prefilled Syringes September 2011 Low Res.pdf (accessed May 5, 2016).

[3] R.G. Ingle, A.S. Agarwal, Pre-filled syringe - a ready-to-use drug delivery system: a review, Expert Opin. Drug Deliv. 11 (2014) 1391–1399.

[4] J. Jezek, N.J. Darton, B.K. Derham, N. Royle, I. Simpson, Biopharmaceutical formulations for pre-filled delivery devices, Expert Opin. Drug Deliv. 10 (2013) 811–828.

[5] A. Blauvelt, J.C. Prinz, A.B. Gottlieb, K. Kingo, H. Sofen, M. Ruer-Mulard, et al., Secukinumab administration by pre-filled syringe: efficacy, safety and usability results from a randomized controlled trial in psoriasis (FEATURE)., Br. J. Dermatol. 172 (2015) 484–493.

[6] A. Agarwal, The lucrative challenges for pre filled syringe technology, (2013). http://blog.pharmatechnologyindex.com/2013/01/the-lucrative-challenges-of-pre-filled-syringe-technology/ (accessed April 30, 2016).

[7] West Pharmaceutical Services Inc., SmartDose®, Electronic wearable injector, (2015). http://www.westpharma.com/SiteCollectionDocuments/SmartDose sell sheet 7247.pdf (accessed March 17, 2016).

[8] S.T. Inc., SteadyMed® patch pump, (2015). http://www.steadymed.com/technology/ (accessed March 17, 2016).

[9] G. Sacha, J.A. Rogers, R.L. Miller, Pre-filled syringes: a review of the history, manufacturing and challenges, Pharm. Dev. Technol. 20 (2015) 1–11.

[10] G.A. Sacha, W. Saffell-Clemmer, K. Abram, M.J. Akers, Practical fundamentals of glass, rubber, and plastic sterile packaging systems, Pharm. Dev. Technol. 15 (2010) 6–34.

[11] PDA, Technical report No. 12. Siliconization of parenteral drug packaging components, J. Parenter. Sci. Technol. 42 (1988) S2–S13.

[12] A.M. Abdul-Fattah, R. Oeschger, H. Roehl, I. Bauer Dauphin, M. Worgull, G. Kallmeyer, et al., Investigating factors leading to fogging of glass vials in lyophilized drug products., Eur. J. Pharm. Biopharm. 85 (2013) 314–326.

[13] K. Yoshino, K. Nakamura, A. Yamashita, Y. Abe, K. Iwasaki, Y. Kanazawa, et al., Functional evaluation and characterization of a newly developed silicone oil-free prefillable syringe system., J. Pharm. Sci. 103 (2014) 1520–1528.

[14] West Pharmaceutical Service Inc., CZ: The first silicone oil- and tungsten-free insert needle syringe, (2014). http://www.westpharma.com/SiteCollectionDocuments/CZ Combined Brochure.pdf (accessed March 17, 2016).

[15] E.G.; Ashmead, E.C.. Gunzel, M.P.. Moritz, Syringe stopper, U.S. Patent US8722178 B2, 2014.

[16] E. Krayukhina, K. Tsumoto, S. Uchiyama, K. Fukui, Effects of syringe material and silicone oil lubrication

on the stability of pharmaceutical proteins, J. Pharm. Sci. 104 (2015) 527–535.

[17] E. Chan, A. Hubbard, S. Sane, Y.-F. Maa, Syringe siliconization process investigation and optimization, PDA J. Pharm. Sci. Technol. 66 (2012) 136–150.

[18] T. Mundry, Einbrennsilikonisierung bei pharmazeutischen Glaspackmitteln - Analytische Studien eines Produktionsprozesses, Dissertation, Humboldt-Universität Berlin, 1999.

[19] K.B. Auge, A.W. Blake-Haskins, S. Devine, S. Rizvi, Y.-M. Li, M. Hesselberg, et al., Demonstrating the stability of albinterferon alfa-2b in the presence of silicone oil, J. Pharm. Sci. 100 (2011) 5100–5114.

[20] A. Sardella, Fine tuning of process parameters for improving biocompatibility of prefilled syringes, Drug Deliv. (2010) 18–22.

[21] T. Buch-Rasmussen, P. Jannasch, E. Bonne Jorgsen, I. Johannesen, S. Ndoni, N. Berg Madsen, Coating systems providing low friction, U.S. Patent 6,482,509 B2, 1999.

[22] A. Gerhardt, B.H. Nguyen, R. Lewus, J.F. Carpenter, T.W. Randolph, Effect of the siliconization method on particle generation in a monoclonal antibody formulation in pre-filled syringes, J. Pharm. Sci. 104 (2015) 1601–1609.

[23] A. Colas, Silicones in pharmaceutical applications. Part 5: Siliconization of parenteral packaging components, (2006). http://www.dowcorning.com/content/publishedlit/52-1094-01.pdf (accessed July 16, 2015).

[24] A.J.M. D`Szouza, D.B. Montgomery, Medical components having coated surfaces exhibiting low frictiong and low reactivity, U.S. Patent US 2011/0313363 A1, 2011.

[25] European Directorate for the Quality of Medicines & HealthCare (EDQM), Ph. Eur. 3.1.8 Siliconöl zur Verwendung als Gleitmittel, (2014).

[26] European Directorate for the Quality of Medicines & HealthCare (EDQM), Ph. Eur. 7.2/0138 Dimeticon, (2014).

[27] Dow Corning Corporation, Material safety data sheet. Dow Corning 365, 35 % Dimethicone NF Emulsion, 2013.

[28] Dow Corning Corporation, Frequently asked questions. Dow Corning 365, 35 % Dimethicone NF Emulsion, 2002.

[29] R.S. Narins, K. Beer, Liquid injectable silicone: A Review of its history, immunology, technical considerations, complications, and potential, Plast Reconstr Surg. 118 (2006) 77S–84S.

[30] J. Ackermann, V. Damrath, Chemie und Technologie der Silicone II. Herstellung und Verwendung von Siliconpolymeren, Chemie Unserer ZEit. 3 (1989) 86–99.

[31] A. Ballistreri, D. Garozzo, G. Montaudo, Mass spectral characterization and thermal decomposition mechanism of poly(dimethylsiloxane), Macromolecules. 17 (1984) 1312–1315.

[32] C. Rücker, K. Kümmerer, Environmental chemistry of organosiloxanes, Chem. Rev. 115 (2015) 466–524.

[33] C. Lassen, C.L. Hansen, S. Hagen Mikkelsen, J. Maag, Siloxanes - Consumption, Toxicity and Alternatives, Environmental project No. 1031 of the Danish Ministry of the Environment, (2005). http://www2.mst.dk/Udgiv/publications/2005/87-7614-756-8/pdf/87-7614-757-6.pdf (accessed July 13, 2015).

[34] G. Camino, S.. Lomakin, M. Lageard, Thermal polydimethylsiloxane degradation. Part 2. The degradation mechanisms, Polymer (Guildf). 43 (2002) 2011–2015.

[35] G. Camino, S.. Lomakin, M. Lazzari, Polydimethylsiloxane thermal degradation Part 1. Kinetic aspects, Polymer (Guildf). 42 (2001) 2395–2402.

[36] T.H. Thomas, T.C. Kendrick, Thermal analysis of polydimethylsiloxanes. I. Thermal degradation in controlled atmospheres, J. Polym. Sci. Part A-2 Polym. Phys. 7 (1969) 537–549.

[37] J.S. Bee, V.V. Frey, U. Javed, J. Chung, M.L. Corcoran, P.S. Roussel, et al., Characterization of the Initial Level and Migration of Silicone Oil Lubricant in Empty Prefilled Syringes for Biologics Using Infrared Spectroscopy, PDA J. Pharm. Sci. Technol. 68 (2014) 494–503.

[38] A. Badkar, A. Wolf, L. Bohack, P. Kolhe, Development of Biotechnology Products in Pre-filled Syringes: Technical Considerations and Approaches, AAPS PharmSciTech. 12 (2011) 564–572.

[39] F. Felsovalyi, S. Janvier, S. Jouffray, H. Soukiassian, P. Mangiagalli, Silicone-oil-based subvisible particles: their detection, interactions, and regulation in prefilled container closure systems for biopharmaceuticals, J. Pharm. Sci. 101 (2012) 4569–4583.

[40] S. Majumdar, B.M. Ford, K.D. Mar, V.J. Sullivan, R.G. Ulrich, A.J.M. D'Souza, Evaluation of the effect of syringe surfaces on protein formulations, J. Pharm. Sci. 100 (2011) 2563–2573.

[41] R.A. Depaz, T. Chevolleau, S. Jouffray, R. Narwal, M.N. Dimitrova, Cross-linked silicone coating: a novel prefilled syringe technology that reduces subvisible particles and maintains compatibility with biologics, J. Pharm. Sci. 103 (2014) 1384–1393.

[42] M. Lankers, Analyse von Silikonschichtdicken bei der Herstellung von Fertigspritzen mit Hilfe von Refektometriemessungen, Pharm. Ind. 72 (2010) 2148–2153.

[43] L. Khandke, R. Malone, X. Yang, H. Han, J.L. Look, Z. Jin, et al., Novel formulations which stabilize and inhibit precipitation of immunogenic compositions, U.S. Patent 2011/0172393 A1, 2011.

[44] B. Reuter, Silicone oil and its applications for parenteral products, PDA Europe Workshop, Cologne, (2010).

[45] Z.-Q. Wen, A. Vance, F. Vega, X. Cao, B. Eu, R. Schulthesis, Distribution of Silicone Oil in Prefilled Glass Syringes Probed with Optical and Spectroscopic Methods, PDA J. Pharm. Sci. Technol. 63 (2009) 149–158.

[46] S.K. Singh, N. Afonina, M. Awwad, K. Bechtold-Peters, J.T. Blue, D. Chou, et al., An industry perspective on the monitoring of subvisible particles as a quality attribute for protein therapeutics, J. Pharm. Sci. 99 (2010) 3302–3321.

[47] J.R. Miller, J.J. Helprin, J.S. Finlayson, Silicone lubricant flushed from disposable syringes: Determination by atomic absorption spectrophotometry, J. Pharm. Sci. 58 (1969) 455–456.

[48] C. Petersen, Syringe Siliconisation. Trends, Methods, Analysis Procedures, Int. Pharm. Ind. 4 (2012) 92–99.

[49] rap.ID Particle Systems GmbH, Silicone layer information, Layer Explorer (LE) devices for different applications, (n.d.). http://www.siliconization.com/layerexplorer/le.html (accessed March 27, 2014).

[50] rap.ID Particle Systems GmbH, Layer Explores UT, Control baked-on siliconization, Information brochure

[51] H.-C. Mahler, W. Friess, U. Grauschopf, S. Kiese, Protein aggregation: pathways, induction factors and analysis., J. Pharm. Sci. 98 (2009) 2909–2934.

[52] M.C. Manning, D.K. Chou, B.M. Murphy, R.W. Payne, D.S. Katayama, Stability of protein pharmaceuticals:

an update., Pharm. Res. 27 (2010) 544–575.

[53] W. Wang, S. Nema, D. Teagarden, Protein aggregation--pathways and influencing factors., Int. J. Pharm. 390 (2010) 89–99.

[54] A.S. Rosenberg, Effects of protein aggregates: an immunologic perspective, AAPS J. 8 (2006) E501–E507.

[55] H. Schellekens, Bioequivalence and the immunogenicity of biopharmaceuticals., Nat. Rev. Drug Discov. 1 (2002) 457–462.

[56] V. Rombach-Riegraf, A.C. Karle, B. Wolf, L. Sordé, S. Koepke, S. Gottlieb, et al., Aggregation of human recombinant monoclonal antibodies influences the capacity of dendritic cells to stimulate adaptive T-cell responses in vitro., PLoS One. 9 (2014) 2128–2135.

[57] M. Shomali, S. Tanriverdi, A.J. Freitag, J. Engert, G. Winter, M. Siedler, et al., Dose levels in particulate-containing formulations impact anti-drug antibody responses to murine monoclonal antibody in mice., J. Pharm. Sci. 104 (2015) 1610–1621.

[58] L. Doessegger, H. Mahler, P. Szczesny, H. Rockstroh, G. Kallmeyer, A. Langenkamp, et al., The potential clinical relevance of visible particles in parenteral drugs, J. Pharm. Sci. 101 (2012) 2635–2644.

[59] S. Bukofzer, J. Ayres, A. Chavez, M. Devera, J. Miller, D. Ross, et al., Industry perspective on the medical risk of visible particles in injectable drug products., PDA J. Pharm. Sci. Technol. 69 (2015) 123–139.

[60] J.S. Bee, T.W. Randolph, J.F. Carpenter, S.M. Bishop, M.N. Dimitrova, Effects of surfaces and leachables on the stability of biopharmaceuticals, J. Pharm. Sci. 100 (2011) 4158–4170.

[61] B. Sharma, Immunogenicity of therapeutic proteins. Part 2: impact of container closures., Biotechnol. Adv. 25 (2007) 318–324.

[62] M. Adler, Challenges in the development of pre-filled syringes for biologics from a formulation scientist´s point od view, Am. Pharm. Rev. 15 (2012).

[63] Y. Nashed-Samuel, D. Liu, K. Fujimori, L. Perez, H. Lee, Extractables and leachables implications on biological products in prefilled syringes, Am. Pharm. Rev. 14 (2011).

[64] D. Jenke, Suitability-for-use considerations for prefilled syringes, (2008). http://www.pharmtech.com/suitability-use-considerations-prefilled-syringes (accessed March 17, 2014).

[65] K. Boven, S. Stryker, J. Knight, A. Thomas, M. van Regenmortel, D.M. Kemeny, et al., The increased incidence of pure red cell aplasia with an Eprex formulation in uncoated rubber stopper syringes, Kidney Int. 67 (2005) 2346–2353.

[66] F. Locatelli, Erythropoiesis-stimulating agents and antibody-mediated pure red-cell aplasia: here are we now and where do we go from here?, Nephrol. Dial. Transplant. 19 (2004) 288–293.

[67] United States Pharmacopeial Convention, United States Pharmacopeia. General chapter -788-. Particulate matter in injections, (2012).

[68] European Directorate for the Quality of Medicines & HealthCare (EDQM), Ph. Eur. 2.9.19 Partikelkontamination - Nicht sichtbare -Partikeln, (2014).

[69] European Directorate for the Quality of Medicines & HealthCare (EDQM), Ph.Eur. 2.9.20 Partikelkontamination - Sichtbare Partikel, (2014).

[70] United States Pharmacopeial Convention, United States Pharmacopeia. General chapter -789-. Particulate

matter in opthalmic solutions, (2012).

[71] United States Pharmacopeial Convention, United States Pharmacopeia. General chapter -787-.Subvisible particulate matter in therapeutic protein injections, (2014).

[72] E. Chantelau, M. Berger, Pollution of insulin with silicone oil, a hazard of disposable plastic syringes, Lancet. (1985) 1459.

[73] A. Gerhardt, N.R. Mcgraw, D.K. Schwartz, J.S. Bee, J.F. Carpenter, T.W. Randolph, Protein aggregation and particle formation in prefilled glass syringes, J. Pharm. Sci. 103 (2014) 1601–1612.

[74] P. Basu, A.W. Blake-Haskins, K.B. O'Berry, T.W. Randolph, J.F. Carpenter, Albinterferon α2b adsorption to silicone oil-water interfaces: effects on protein conformation, aggregation, and subvisible particle formation, J. Pharm. Sci. 103 (2014) 427–436.

[75] R. Thirumangalathu, S. Krishnan, M.S. Ricci, D.N. Brems, T.W. Randolph, J.F. Carpenter, Silicone oil- and agitation-induced aggregation of a monoclonal antibody in aqueous solution, J. Pharm. Sci. 98 (2009) 3167–3181.

[76] M.K. Joubert, Q. Luo, Y. Nashed-Samuel, J. Wypych, L.O. Narhi, Classification and characterization of therapeutic antibody aggregates., J. Biol. Chem. 286 (2011) 25118–25133.

[77] L.S. Jones, A. Kaufmann, C.R. Middaugh, Silicone oil induced aggregation of proteins, J. Pharm. Sci. 94 (2005) 918–927.

[78] S.B. Mehta, R. Lewus, J.S. Bee, T.W. Randolph, J.F. Carpenter, Gelation of a monoclonal antibody at the silicone oil-water interface and subsequent rupture of the interfacial gel results in aggregation and particle formation., J. Pharm. Sci. 104 (2015) 1282–1290.

[79] K.A. Britt, D.K. Schwartz, C. Wurth, H.-C. Mahler, J.F. Carpenter, T.W. Randolph, Excipient effects on humanized monoclonal antibody interactions with silicone oil emulsions, J. Pharm. Sci. 101 (2012) 4419–4432.

[80] A. Gerhardt, K. Bonam, J.S. Bee, J.F. Carpenter, T.W. Randolph, Ionic strength affects tertiary structure and aggregation propensity of a monoclonal antibody adsorbed to silicone oil-water interfaces, J. Pharm. Sci. 102 (2013) 429–440.

[81] D.B. Ludwig, J.F. Carpenter, J.-B. Hamel, T.W. Randolph, Protein adsorption and excipient effects on kinetic stability of silicone oil emulsions, J. Pharm. Sci. 99 (2010) 1721–1733.

[82] B. Demeule, S. Messick, S.J. Shire, J. Liu, Characterization of particles in protein solutions: reaching the limits of current technologies., AAPS J. 12 (2010) 708–715.

[83] A. Lubiniecki, D.B. Volkin, M. Federici, M.D. Bond, M.L. Nedved, L. Hendricks, et al., Comparability assessments of process and product changes made during development of two different monoclonal antibodies., Biologicals. 39 (2011) 9–22.

[84] L. Liu, D.A. Ammar, L.A. Ross, N. Mandava, M.Y. Kahook, J.F. Carpenter, Silicone oil microdroplets and protein aggregates in repackaged bevacizumab and ranibizumab: effects of long-term storage and product mishandling, Invest. Ophthalmol. Vis. Sci. 52 (2011) 1023–1034.

[85] J.G. Barnard, K. Babcock, J.F. Carpenter, Characterization and quantitation of aggregates and particles in interferon-β products: potential links between product quality attributes and immunogenicity., J. Pharm. Sci.

102 (2013) 915–928.

[86] K. Nakanishi, T. Sakiyama, K. Imamura, On the adsorption of proteins on solid surfaces, a common but very complicated phenomenon, J. Biosci. Bioeng. 91 (2001) 233–244.

[87] C.J. Burke, B.L. Steadman, D.B. Volkin, P.-K. Tsai, M.W. Bruner, C.R. Middaugh, The adsorption of proteins to pharmaceutical container surfaces, Int. J. Pharm. 86 (1992) 89–93.

[88] V. Sluzky, J.A. Tamada, A.M. Klibanov, R. Langer, Kinetics of insulin aggregation in aqueous solutions upon agitation in the presence of hydrophobic surfaces, Proc. Natl. Acad. Sci. 88 (1991) 9377–9381.

[89] W. Norde, C.E. Giacomelli, BSA structural changes during homomolecular exchange between the adsorbed and the dissolved states, J. Biotechnol. 79 (2000) 259–268.

[90] T. Vermonden, C.E. Giacomelli, W. Norde, Reversibility of Structural Rearrangements in Bovine Serum Albumin during Homomolecular Exchange from AgI Particles, Langmuir. 17 (2001) 3734–3740.

II OBJECTIVES AND OUTLINE OF THE THESIS

This thesis aimed at the optimization of the bake-on siliconization process for 5 mL cartridges and the investigation of silicone-associated interactions after cartridge-filling with drug product with regard to particle formation and protein adsorption.

The first main objective was to establish novel analytical techniques for the characterization of thin baked-on silicone layers, which have not been accessible with standard techniques so far. Fourier transform infrared spectroscopy and 3D-laser scanning microscopy were introduced to quantify low, baked-on silicone levels after solvent extraction and to determine the thickness of these thin layers **(chapter III)**.

Although siliconization processes are widely implemented in industry, information is rarely published or still considered proprietary know-how. The application of the established, sensitive methods allowed a straightforward optimization of the bake-on siliconization process to fill this gap in process understanding. In **chapter IV**, the spray-on process of silicone emulsion was thoroughly evaluated. Important process parameters such as the spray quantity, spray nozzle position, spray pressure, time for pump dosing and the nozzle design were studied with focus on the impact on the baked-on silicone level, layer thickness and distribution within the cartridge barrel. The concentration of the silicone emulsion was adapted to challenge adequate, but limited silicone levels to ensure extrusion performance of the piston after long-term storage. Comparable to a commercial bake-on siliconization process, the sprayed-on silicone emulsion was baked-on in a heat-tunnel. In **chapter V**, the impact of different burn-in times and temperatures on the silicone layer characteristics was investigated. In addition, the focus was set on the thermal decomposition of silicone and pharmaceutically relevant stabilizers of the emulsion in terms of weight loss, formation of cyclic low molecular weight siloxanes and change in molecular weight distribution of the silicone polymer. The formation of covalent bonds between silicone and the glass surface upon bake-on, which is postulated in literature, was functionally addressed by contact angle measurements. In addition, a heat-oven was assessed as an experimental model to mimic the heat-tunnel.

Subsequently, the effect of different baked-on silicone levels on the particle formation in cartridges filled with placebo and monoclonal antibody solution was investigated **(chapter VI)**. For placebo, different stresses such as cartridge expelling, shaking or a combination of both

factors were applied to determine the most detrimental effect on silicone leaching from the siliconized container surface. A toolbox of methods was employed to cover a broad aggregate and particle size range. Overall, the results aimed to clarify a potential impact of silicone oil droplets from baked-on silicone layers on protein particle formation.

In **chapter VII**, the focus was set on two novel methods to characterize protein adsorption to silicone surfaces. The adsorption behavior of a monoclonal antibody on silicone and heat-treated silicone was investigated using a quartz crystal microbalance to mimic spray-on and bake-on siliconized drug product containers. Furthermore, fluorescence activated cell sorting using fluorescently labeled monoclonal antibody was introduced as promising technique to monitor concentration and time-dependent adsorption processes. The fluorescence activated cell sorting method was further challenged with focus on limitations associated with the application of fluorescently labeled protein species. Electrostatic and hydrophobic interactions were evaluated as driving forces for protein adsorption using both techniques.

Finally, the main results were summarized in **chapter VIII.**

Overall, this thesis shall highlight the complex set of parameters during the development of siliconized drug/device combinations products from early siliconization process set-up to final challenges related to drug product quality.

III ANALYSIS OF THIN BAKED-ON SILICONE LAYERS BY FOURIER TRANSFORM INFRARED SPECTROSCOPY AND 3D-LASER SCANNING MICROSCOPY

The following chapter is published as research article in the European Journal of Pharmaceutics and Biopharmaceutics:

S. Funke, J. Matilainen, H. Nalenz, K. Bechtold-Peters, H.-C. Mahler, W. Friess. Analysis of thin baked-on silicone layers by FTIR and 3D-Laser Scanning Microscopy. Eur. J. Pharm. Biopharm. 96 (2015) 304–313.

KEYWORDS

Cartridge, FTIR, 3D-laser scanning microscopy, silicone distribution, silicone layer thickness, siliconization

GRAPHICAL ABSTRACT

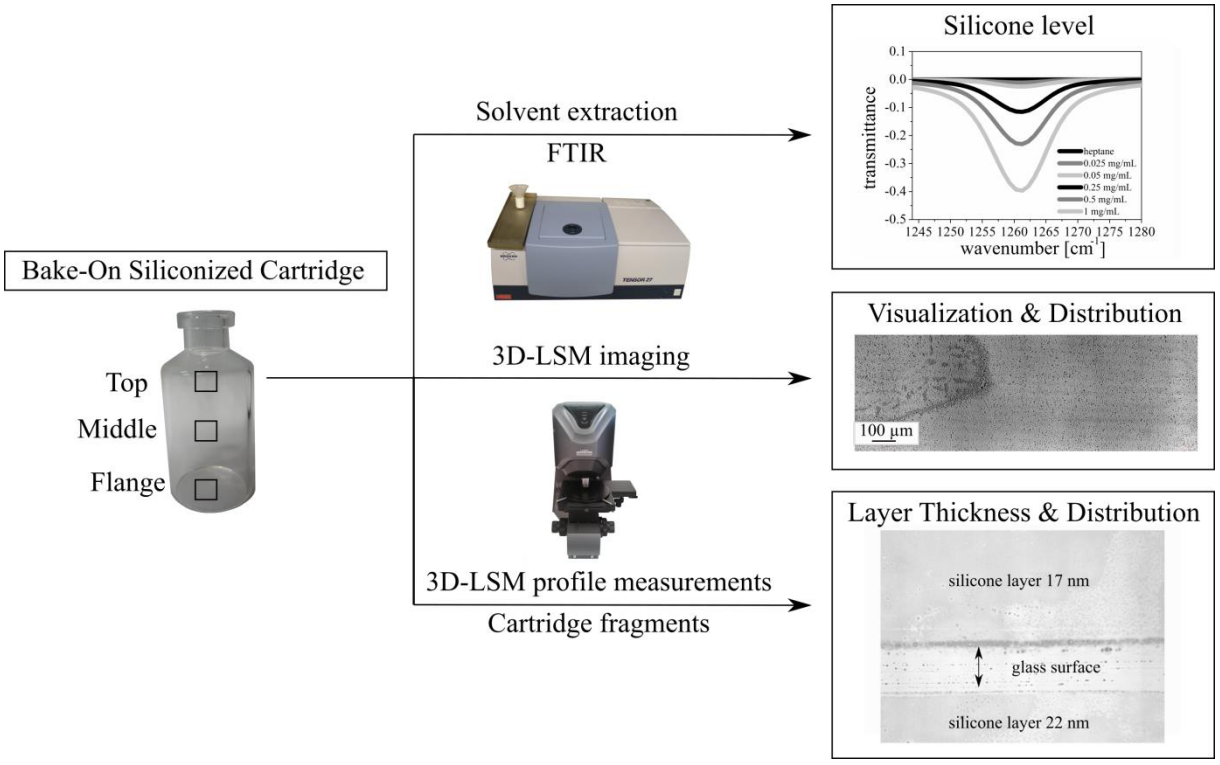

ABSTRACT

Pre-filled syringes (PFS) and auto-injection devices with cartridges are increasingly used for parenteral administration. To assure functionality, silicone oil is applied to the inner surface of the glass barrel. Silicone oil migration into the product can be minimized by applying a thin, but sufficient layer of silicone oil emulsion followed by thermal bake-on versus spraying-on silicone oil. Silicone layers thicker than 100 nm resulting from regular spray-on siliconization can be characterized using interferometric profilometers. However, the analysis of thin silicone layers generated by bake-on siliconization is more challenging. In this paper, we have evaluated Fourier transform infrared (FTIR) spectroscopy after solvent extraction and a new 3D-laser scanning microscopy (3D-LSM) to overcome this challenge. A multi-step solvent extraction and subsequent FTIR spectroscopy enabled to quantify baked-on silicone levels as low as 21-325 µg per 5 mL cartridge. 3D-LSM was successfully established to visualize and measure baked-on silicone layers as thin as 10 nm. 3D-LSM was additionally used to analyze the silicone oil distribution within cartridges at such low levels. Both methods provided new, highly valuable insights to characterize the siliconization after processing, in order to achieve functionality.

1 INTRODUCTION

Pre-filled syringes (PFS) and cartridges, which are usually assembled with pens and other devices to drug/device combination products, are increasingly used for parenteral administration, mainly because they are both convenient and easy-to-handle for the intended user population, such as health care professionals and patients. PFS and cartridges additionally assure accurate dose delivery and often require less overfill [1,2]. The manufacturing process comprises several unit operations from washing, siliconization, thermal depyrogenation to piston placing, filling, further assembly, labelling and packaging.

For different aspects of such products, siliconization of the primary packaging barrel is an essential step. The interior of the glass barrels is lubricated to reduce the forces required to initiate (break-loose) and perform injection (glide), i.e., siliconization enables moving the piston during drug administration [3,4].

However, apart from the functionality of the device over the shelf life of a product, possible interactions of the silicone with the active ingredient (e.g., protein) and formulation (solution) need to be considered [5]. Silicone oil has been reported to increase turbidity and subvisible particle levels due to migration into protein solution [6–9]. Increased levels of spiked silicone oil have been shown to perturb liquid formulations of some proteins upon agitation [10,11], at increased temperatures [12,13] as well as upon agitation at increased temperatures [10]. However, there are also numerous proteins, where silicone did not impact stability. Adequate formulation development, e.g., the addition of surfactants, has also been reported to protect proteins sensitive to silicone oil from related degradation. The presence of silicone oil during quiescent storage at room temperature has also not resulted in protein aggregation or precipitation [14]. Consequently, it is required to carefully develop siliconization processes to assure functionality of the injection device at sufficient silicone levels, and to study product stability within the intended process range and design space.

Typically, two different siliconization procedures are used for syringes. Siliconization of luer tip syringes is usually performed using silicone emulsion (e.g., Dow Corning 365 35 % Dimethicone NF Emulsion) followed by a high temperature baking process for depyrogenation. Before administration, a needle of choice can be attached to the luer tip. Cartridges as part of delivery systems are combined with separate pen needles, and can therefore be bake-on siliconized. In case of staked-in needles (SIN), where an adhesive (glue) is used to affix a needle into the fluid path, bake-on siliconization is not applicable due to the low heat resistance of the adhesive.

Therefore, SIN PFS are processed via spray-on siliconization using silicone oil (e.g., Dow Corning 360 Medical Fluid) [13,15,16]. The process step of siliconization can be performed either at the syringe manufacturer (suppliers) or the pharmaceutical company. Often, a bake-on siliconization process is performed prior to fill/finish operations during product manufacturing, whereas spray-on siliconization of trayed syringes is performed at the supplier.

Relatively high silicone levels of approximately 0.2-1.0 mg/container [4,13,15,17] obtained by spraying-on silicone oil can be rather easily characterized. In contrast, the analysis of silicone levels below 0.1 mg/container [18] as often generated by bake-on siliconization, is still challenging with the available methods.

A simple, though not very precise technique for silicone quantification after spray-on is a gravimetric approach by weighing the empty syringe before and after the siliconization process [15].

Siliconization levels of glass barrel interiors and rubber closures in the range of 0.4-1.3 mg/closure and 0.2-7.3 mg/barrel were determined using atomic absorption spectrometry (AAS) and inductively coupled plasma-optical emission spectrometry (ICP-OES) after solvent extraction [19–21]. In particular, Lankers *et al.* could exemplarily quantify 0.2-0.3 mg silicone oil/container using AAS after toluene extraction [20]. ICP-OES and AAS are considered as highly sensitive techniques to quantify silicone concentrations ≤ 1 µg/mL [17,19]. Reverse-phase high-performance liquid chromatography in combination with evaporative light scattering detection has been employed to quantify silicone oil in water after liquid-liquid extraction reaching a quantification limit of 88 µg/mL silicone oil [6].

Because of their sensitivity, the above-mentioned methods are suited for the quantification of low baked-on silicone levels. However, these methods require high technical effort. Therefore, these techniques are often not selected as routine methods for the quantification of low baked-on silicone levels.

Colorimetric silicone determination, as used in food analysis, is based on acidic heat-induced sample decomposition and formation of silica, which forms a complex with ammonium molybdate. Silica can be quantified down to 3 µg/mL and is calculated back to silicone of a known molecular structure [22]. But this correlation between silica and silicone oil is prone to error with the complex structure of polydimethylsiloxane (PDMS) and even less suitable for the analysis of silicone levels after bake-on due to heat induced chemical changes of the PDMS.

Fourier transform infrared (FTIR) spectroscopy after solvent extraction is another suitable

method to determine silicone levels on glass barrels and stoppers [6,17,23,24] and silicone oil in water emulsions after liquid-liquid extraction [14,25,26]. The extracted silicone oil is quantified via the intensity of the characteristic Si–CH_3 band at 1260 cm^{-1} [27,28]. FTIR achieves quantification limits of 0.2 µg/mL [29], simple potassium bromide or calcium fluoride cells are used and above all, it is a fast technique. Although described only for spray-on siliconized containers in the literature up to now, it offers great potential also for the quantification of baked-on silicone layers. In addition, Mundry suggested a correlation between the intensity of individual absorption bands in FTIR versus molecular weight and viscosity, respectively [30].

The qualitative silicone distribution can be visualized by glass and talcum dust tests, optical microscopy and schlieren visualization (e.g., commercially available from ZebraScience, Inc., Temecula, USA). Glass and talcum powders or suspensions stick to glass surfaces, which have been coated with sprayed-on or baked-on silicone. Non-siliconized glass areas can be identified; however, the results are rather subjective. Furthermore, silicone amount and silicone layer homogeneity cannot be determined [15,20,31].

Thick silicone layers usually show plaque-like structures, which can be visualized by optical microscopy [20,32]. In contrast, thin baked-on silicone layers cannot be visualized by simple optical microscopy.

Schlieren visualization observes the optical inhomogeneity along the silicone coated container based on the differences in the refractive indices (RI) of silicone oil (RI app. 1.40 [33]) and the borosilicate glass matrix (RI app. 1.49 [34]). When passing inhomogeneous media, light refracts and deflects, resulting in schlieren, which are not visible to the eye. The glass container is placed between a digital microscope equipped with a microscopic lens and a zebra strip pattern in front of a back light. Side light is used to illuminate small areas of the syringe. A two-axis motion system moves the syringe in order to visualize the entire glass barrel. In filled containers, high levels of spray-on silicone lead to micron-sized droplets upon contact with aqueous media. Schlieren visualization tracks these droplets, and thus provides fast qualitative information about the silicone distribution [31,32]. Thin baked-on silicone layers, however, do not form large silicone droplets upon contact with aqueous media, therefore, they are hardly accessible by schlieren visualization.

Eu *et al.* showed the direct visualization of protein adsorption on non-siliconized container surfaces by gold nanoparticles [35]. Therefore, gold nanoparticles are only suitable to indirectly visualize the silicone distribution.

Semi-quantitative information about the layer thickness can be obtained by interferometric profilometers using vertical scanning interferometry (VSI) with white light (commercially available as Layer Explorer, rap.ID Particle Systems GmbH, Berlin, Germany). Interference reflection spectroscopy is also based on the difference in RI of silicone oil and the glass matrix. Since this delta is small, VSI achieves a theoretical detection limit of 80 nm [36], but silicone layers below 100 nm have only been exemplarily determined with this method in the literature [17,20,37]. For sprayed-on silicone layers above 100 nm, VSI is a reliable, fast and non-destructive method, which scans the container barrel line-by-line [17,20,31,32,37]. The use of phase shift interferometry of a red laser beam to determine thin silicone layers down to 20 nm has been claimed [38], but no data have been published yet.

As an alternative, thin films can be studied by ellipsometry. Based on the change in the state of polarization of light upon reflection from a surface, ellipsometry is an accurate technique for thin films of known RI deposited on substrates with high reflectance such as metals. Barium fluoride layers on chromium ferrotype surfaces in the range of approximately 630-680 Å and fibrinogen layers adsorbed on hydrophobic and hydrophilic chromium surfaces as thin as 15 Å have been characterized by ellipsometry. Silicone coatings deposited onto polycarbonate have been determined in the range of 250-1500 nm. The sensitivity of this technique to surface coatings decreases with decreasing difference in RI between the coating and the substrate [39], and therefore, thin silicone layers on glass substrates are hardly accessible.

Scanning electron microscopy has been utilized to characterize film thicknesses in the lower µm-range, but requires a tedious preparation of perpendicular cross sections, which are mounted face-up for analysis. Metal or carbon sputtering of the probes, which has to be applied for sample preparation, and artifacts caused by vacuum, can additionally alter the measured layer thickness [40,41].

Furthermore, time-of-flight secondary ion mass spectrometry (ToF SIMS) has been performed to determine the lubricant thickness of cross-linked XSi^{TM} siliconized and spray-on siliconized syringes in the range of 10-250 nm [37].

In summary, high levels of effort in sample preparation and analysis, insufficient detection limits as well as the optical properties of siliconized glass surfaces exclude the discussed methods to routinely characterize and measure the thickness of thin baked-on silicone layers.

The objective of this study was to develop a silicone extraction and FTIR quantification method to characterize baked-on silicone layers with low quantification limits. In addition, 3D laser

scanning microscopy (3D-LSM) was evaluated as a novel analytical technique for both qualitative visual evaluation of silicone layers with high resolution and the determination of the thickness of thin baked-on silicone layers. 3D-LSM was compared with Atomic Force Microscopy (AFM) and step height standards to further assess its potential to visualize and quantify very thin silicone layers on glass. Advancing further techniques for the characterization of silicone layers improve process understanding, and thus increase reliability in process design and functionality of drug/device combination products.

2 MATERIALS AND METHODS

2.1 MATERIALS

365 35 % Dimethicone NF Emulsion was purchased from Dow Corning GmbH (Wiesbaden, Germany). Dilutions were prepared with highly purified water. Cartridges with 5 mL barrels (barrel length 32 mm, inner diameter 19 mm, outer diameter 22 mm) were obtained from F. Hoffmann-La Roche Ltd (Basel, Switzerland).

2.2 BAKE-ON SILICONIZATION PROCESS

An external mixing, two-fluid nozzle was employed to nebulize 365 Dimethicone NF Emulsion on a SVS9061 pilot-scale unit from Bausch + Ströbel Maschinenfabrik Ilshofen GmbH+Co. KG (Ilshofen, Germany) into 5 mL cartridges. A spray quantity of 16 mg was maintained using a high precision rotary piston pump with a gliding disk from Saphirwerk AG (Brügg, Switzerland). Emulsion concentrations ranging from 0.35 % (w/w) to 3.5 % (w/w) were prepared by weighing on an analytical balance AT261 and precision balance PM-4000 both from Mettler-Toledo GmbH (Gießen, Germany). The cartridges were subsequently treated in a Bosch TSQ U03 heat-tunnel (Robert Bosch GmbH, Stuttgart, Germany) at 316 °C for 12 min.

2.3 EXTRACTION AND FOURIER TRANSFORM INFRARED (FTIR) QUANTIFICATION

The silicone content in baked-on siliconized cartridges was determined by a combination of solvent extraction and quantitative FTIR spectroscopy (Fig. III-1).

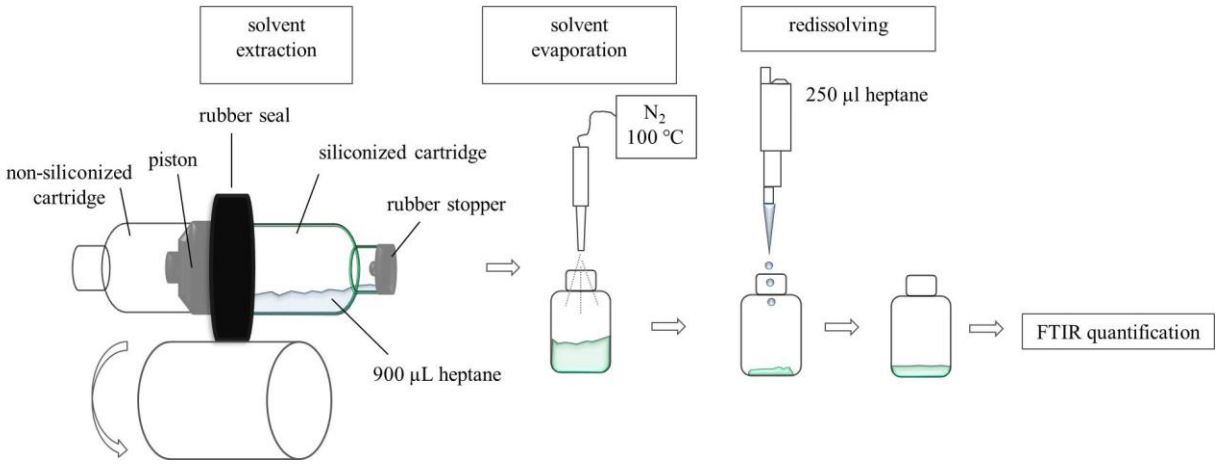

Fig. III-1. Multi-step scheme for the extraction and FTIR quantification of baked-on silicone oil.

The siliconized cartridges were closed using a rubber stopper at the needle-side and a second, non-siliconized cartridge containing a placed piston. A rubber seal was used to closely fasten both cartridges at the flange-side. The non-siliconized cartridge, the piston, and the rubber seal had been previously washed. Silicone oil was extracted from the siliconized cartridge interior barrel into 900 µL heptane under horizontal rotation at 50 rpm for 10 min. Two rinsing steps were performed using 900 µL heptane. The solvent extracts were combined in a 2R vial and heptane was evaporated to dryness using a flowtherm evaporator at 100 °C and constant nitrogen flow of 210 mL/min from Barkey GmbH & Co. KG (Leopoldshöhe, Germany). The dried extract was redissolved in 250 µL heptane. This solution was injected into a 250 µm path length FTIR calcium fluoride liquid cell from Bruker Optik GmbH (Ettlingen, Germany).

PDMS was quantified as area under the curve (AUC) of the transmittance spectrum between 1280 cm^{-1} and 1244 cm^{-1} (PDMS has a characteristic transmittance at 1260 cm^{-1} due to the symmetric deformation vibration of the Si-CH_3 moieties [27]) using a Tensor 27 FTIR equipped with a high sensitivity broad-band mercury cadmium telluride detector from Bruker Optik GmbH (Ettlingen, Germany) (Fig. III-2a). High resolution of 4 cm^{-1} and 64 scans were used. Prior to each sample, the same number of background scans was performed using heptane. Silicone oil solutions in heptane ranging from 0.025 mg/mL to 1.0 mg/mL were used for calibration (Fig. III-2b).

a. b.

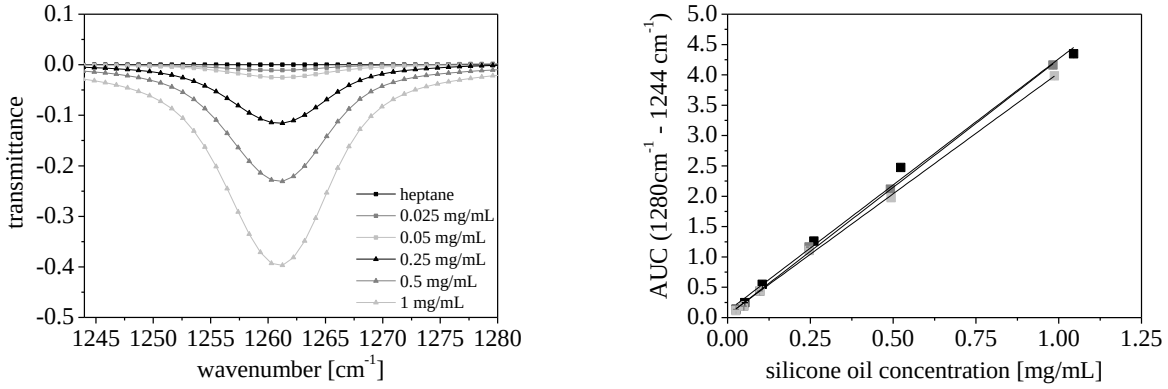

Fig. III-2. Analysis of silicone oil solutions in heptane by FTIR. (a) Infrared transmittance spectra of silicone oil in heptane solutions (0.025-1.0 mg/mL, individual heptane blanks subtracted). (b) Silicone oil concentration standard curves (R^2 = 0.994-0.999).

According to considerations provided in ICH Q2 R1 Validation Analytical Procedure, the limit of detection (LOD) of the developed FTIR method was found to be below 1 µg/mL (number of calibration curves n = 22). The limit of quantification (LOQ) was 18 µg/mL (n = 22), equivalent

to 4 µg per cartridge based on 250 µL dissolution volume.

A second solvent extraction of a baked-on siliconized cartridge (202 µg ± 12 µg) was performed as described above (900 µL heptane, two rinsing steps à 900 µL). Analysis of this second solvent extract revealed silicone concentrations below LOQ. Thus, one solvent extraction employing three solvent steps with heptane was sufficient for quantitative silicone recovery from the baked-on silicone layer.

For a second recovery experiment, 2 mL of a 0.025 mg/mL and 0.05 mg/mL silicone solution in heptane, respectively, were filled into non-siliconized cartridges. Horizontal rotation, rinsing steps, solvent evaporation, and FTIR quantification were performed as previously described. The spiked in heptane solutions containing 50 µg and 100 µg silicone oil were recovered with 95 ± 3 % and 105 ± 3 %, respectively.

2.4 3D-LASER SCANNING MICROSCOPY (3D-LSM)

The silicone layer thickness was determined using a VK-X210 microscope from Keyence Deutschland GmbH (Neu-Isenburg, Germany). 3D-LSM allowed height measurements based on confocal profiling. The sample was scanned in vertical steps of 0.5 nm so that each point of the sample passed the focus of the laser (λ 408 nm). The height of the surface at each point was determined by detecting the position of the peak maximum of the axial reflectance response in a 16-Bit photomultiplier. In addition to conventional lenses, the microscope was equipped with an ultra-long range objective (working distance 4.7 mm, magnification 100 x) to facilitate height measurements of curved samples.

Cartridges were covered with adhesive tape, broken up and individual fragments were removed from the adhesive tape to enable direct measurements of the thin baked-on silicone layer. Breakage as performed by our procedure did not substantially change the silicone layer. Cartridge fragments from the flange, middle and top of the cartridge were analyzed to determine the silicone distribution within the barrel.

An artificial glass baseline was created by scratching a 20 G cannula from B. Braun Melsungen AG (Melsungen, Germany) over the glass surface to remove the silicone layer. Thicker, partially fluid silicone layers may blur out the baseline over time. With regard to thin, baked-on silicone layers, scratching was the best method possible to create a straight, defined baseline with a steep slope compared to the silicone layer. Although we never observed any change or disappearance of the scratch over time, the time between scratching and measurement was kept as short as

possible, i.e., not more than 1 min.

Height profile measurements of 100 µm x 143 µm cartridge areas were performed using VK Viewer Software from Keyence (Deutschland GmbH, Neu-Isenburg, Germany) in EasyMode. VK Analyzer Software from Keyence Deutschland GmbH (Neu-Isenburg, Germany) was utilized to determine the average layer thickness (ALT) as the difference in the average height between the glass surface and the silicone layer in multi-line average profile (400 lines) after area and line tilt correction (2^{nd} curved line and area auto, respectively).

The 3D-LSM measurements were compared with step height standards from John P. Kummer GmbH (Augsburg, Germany) of 17.3 ± 1.6 nm and 89.4 ± 1.2 nm chrome coating on a quartz substrate. The height of the step was measured in Easy Mode by VK Viewer software and calculated as the difference between the average height along the base of the step and the top of the step in multi-line average profile (200 lines) using VK Analyzer software. At 10 x magnification the tilt of the quartz substrate was leveled using automatic area and line plane correction.

To confirm the 3D-LSM measurements, a theoretical average layer thickness was calculated from the silicone level quantified via FTIR applying a silicone density of 0.972 g/cm^3 [33] and a cartridge interior surface of 2422 mm^2.

Both the integrated optical microscope and 3D-LSM images were additionally employed to visualize the distribution of the silicone within an intact cartridge. Lower magnification (10 x) was used to visualize larger cartridge areas of 1.2 mm x 0.5 mm.

2.5 ATOMIC FORCE MICROSCOPY (AFM)

AFM was performed on a NSCRIPTOR™ DPN® System from NanoInk Inc. (Candor, NY, USA). Samples were measured in tapping mode using rectangular, silicon cantilevers with highly doped single crystal silicon probes from Applied NanoStuctures Inc. (Mountain View, CA, USA), having a nominal resonant frequency of 300 kHz, a nominal spring constant of 37 N/m and a guaranteed tip radius below 10 nm. Cartridge fragments were prepared as previously described. Forward and reverse scans of 30 µm x 30 µm cartridge areas were performed. The ALT was determined as the difference between horizontal lines, i.e., the glass surface and the silicone layer, after profile extraction of 110 px multi-lines and tilt correction by mean plane subtraction using Gwyddion Software 2.34. (free software, development is supported by the Czech Metrology Institute: http://www.cmi.cz/distance) (supporting information Fig. S III-1).

2.6 EXTRUSION FORCE MEASUREMENTS

To assess device functionality, break-loose forces, maximum and minimum gliding forces were analyzed using a material testing instrument TA.XT.plus from Winopal Forschungsbedarf GmbH (Elze, Germany). A piston was inserted manually into the empty, siliconized cartridge prior to filling with 5.16 mL purified water. After stoppering and capping, the cartridge was emptied by pushing down the piston using a steady compression rate of 5.6 mm/min over a distance of 17.5 mm. The barrel length was approximately 32 mm and the "height" of the cartridge shoulder was approximately 5 mm. Therefore, the maximum travel distance for the 20 mm piston was approximately 17 mm, which was reflected in the chosen measurement set-up. Consequently, the entire cartridge barrel was tested.

3 RESULTS AND DISCUSSION

3.1 SILICONE LEVELS IN BAKED-ON SILICONIZED CARTRIDGES

The silicone levels in baked-on siliconized cartridges were determined using FTIR. For the FTIR method, a LOQ of 18 µg/mL, equivalent to 4 µg silicone per cartridge, was found. With increasing silicone oil emulsion concentrations ranging from 0.35 % (w/w) to 3.5 % (w/w) the amount of baked-on silicone increased steadily from 21 µg to 325 µg per cartridge (Fig. III-3).

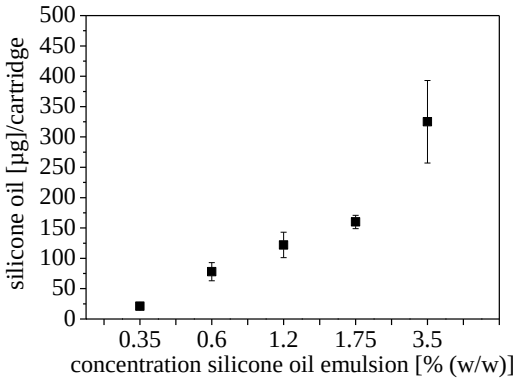

Fig. III-3. Silicone levels (n = 3) after bake-on siliconization using a spray quantity of 16 mg.

FTIR has already been employed for the trace analysis of silicone oil in food (e.g., pineapple juice, beer and yeast) with a recommended final concentration of at least 50 µg/mL silicone in the solvent solution [22]. After optimized solvent extraction and complex sample preparation including the removal of interfering components, an improved sensitivity of 0.2-2 µg/mL could be achieved using potassium bromide disks [29]. For pharmaceutical applications, FTIR has been utilized to determine silicone amounts of 219 µg on glass barrels [17], down to 4 µg/mL and in the range of 25-75 µg on stoppers [17,23], respectively. However, comparison of silicone amounts determined in this study and in the literature is aggravated since most method details, LOD and LOQ are not described [6,17,23]. For quantification of silicone oil in aqueous emulsions by FTIR after liquid-liquid extraction [14,25,26], a LOD of 80 µg/mL and a LOQ of 190 µg/mL have been reported [26].

In our work, we found good reproducibility, accuracy (spike recoveries were 95–105 %) and better sensitivity (LOD < 1 µg/mL, LOQ = 18 µg/mL) compared to the literature. The simple extraction process and fast extract analysis by FTIR spectroscopy using a liquid cell appear to be valuable tools for the determination of silicone levels below 0.1 mg/container as present in bake-on siliconization processes [18] and for sprayed-on silicone levels of approximately 0.2-

1.0 mg/container [4,13,15,17]. The quantification of the silicone levels within certain cartridge sections can also help to understand changes in extrusion, such as plunger sticking or so called "chattering" [4].

In addition to the silicone levels, the corresponding break-loose forces as well as the maximum and minimum gliding forces were analyzed. Reliable functionality over the product shelf life is one of the most important measurable outputs of a drug/device combination product. Depending on the combination product, injection forces are limited by patient´s strength or by an internal spring mechanism. The mean break-loose and gliding forces remained well below 30 N and 15 N, respectively, as reference values in this study. But still, both break-loose and gliding forces have to be carefully evaluated for each injection device. However, in other studies maximum forces were fixed at 30 N [42] and patient-friendly injection was reported with gliding forces up to 15-20 N [43]. Another study showed that rheumatoid arthritis patients could exert maximum forces up to 45 N [44]. Thus, functionality of the device was maintained for all siliconization conditions tested. The break-loose forces marginally increased from 3 N, achieved using a silicone concentration of 1.75 % (w/w) and 3.5 % (w/w), to 4.5-5 N after application of emulsions with lower silicone concentrations. A similar trend was observed in the gliding forces, which increased from 2-3 N to 3-5.5 N. The exemplarily shown force profiles for the lowest concentration of 0.35 % (w/w) and the highest concentration of 3.5 % (w/w) indicated a smooth gliding of the piston along the cartridge barrel (Fig. III-4).

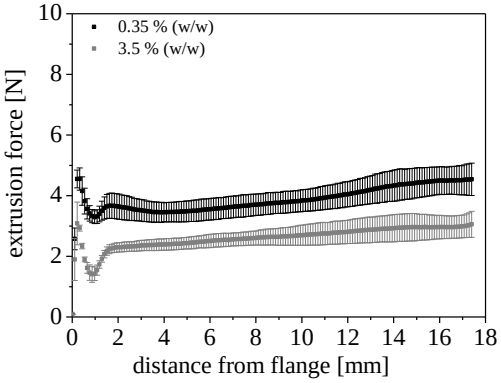

Fig. III-4. Exemplary extrusion force profiles after bake-on siliconization using a spray quantity of 16 mg and 0.35 % (w/w) and 3.5 % (w/w) emulsion.

The gliding forces slightly increased toward the top of the cartridge. A comprehensive study of the impact of spray parameters on the spray pattern of the silicone emulsion and silicone layer characteristics, e.g., extrusion performance, baked-on silicone levels and layer thickness

distribution along the cartridge barrel, are presented in chapter IV.

3.2 SILICONE LAYER SURFACE AND DISTRIBUTION

Optical microscopy can be used to visualize the surface of sprayed-on silicone layers, which were reported to show plaque-like and micro-droplet structures surrounded by a thin film layer [20,32,37]. These structures obtained by silicone fluid can be related to models that describe the wetting of polymers on solid surfaces with spherical capped droplets as a set of horizontal layers in parallel to a precursor film in front of the drop [45,46]. Micro-droplets are visible due to the high contrast and colored interference rings. Optical microscopy, however, failed to visualize thin baked-on silicone layers even at the highest emulsion concentration tested in our study of 3.5 % (w/w). These thin baked-on layers only exhibited a homogeneous purplish texture without any plaques or droplets (Fig. III-5a).

On the contrary, 3D-LSM revealed the surface characteristics of the baked-on silicone layers and the differences over the barrel after preparation from silicone emulsion concentrations from 0.6 % (w/w) to 3.5 % (w/w) (Fig. III-5b). 3D-LSM images were similar for triplicates. However, at an emulsion concentration of 0.35 % (w/w) the silicone layer was too thin to be visualized, even by 3D-LSM.

Within the analyzed cartridge areas of 1.2 mm x 0.5 mm the baked-on silicone layer was homogeneously distributed. From flange to top, 3D-LSM suggested thinner silicone layers in the middle and at the top of the cartridge. The more pronounced siliconization at the flange was attributed to the applied nozzle-to-flange distance of 20 mm, where the spray cone exactly reached the flange (see chapter IV).

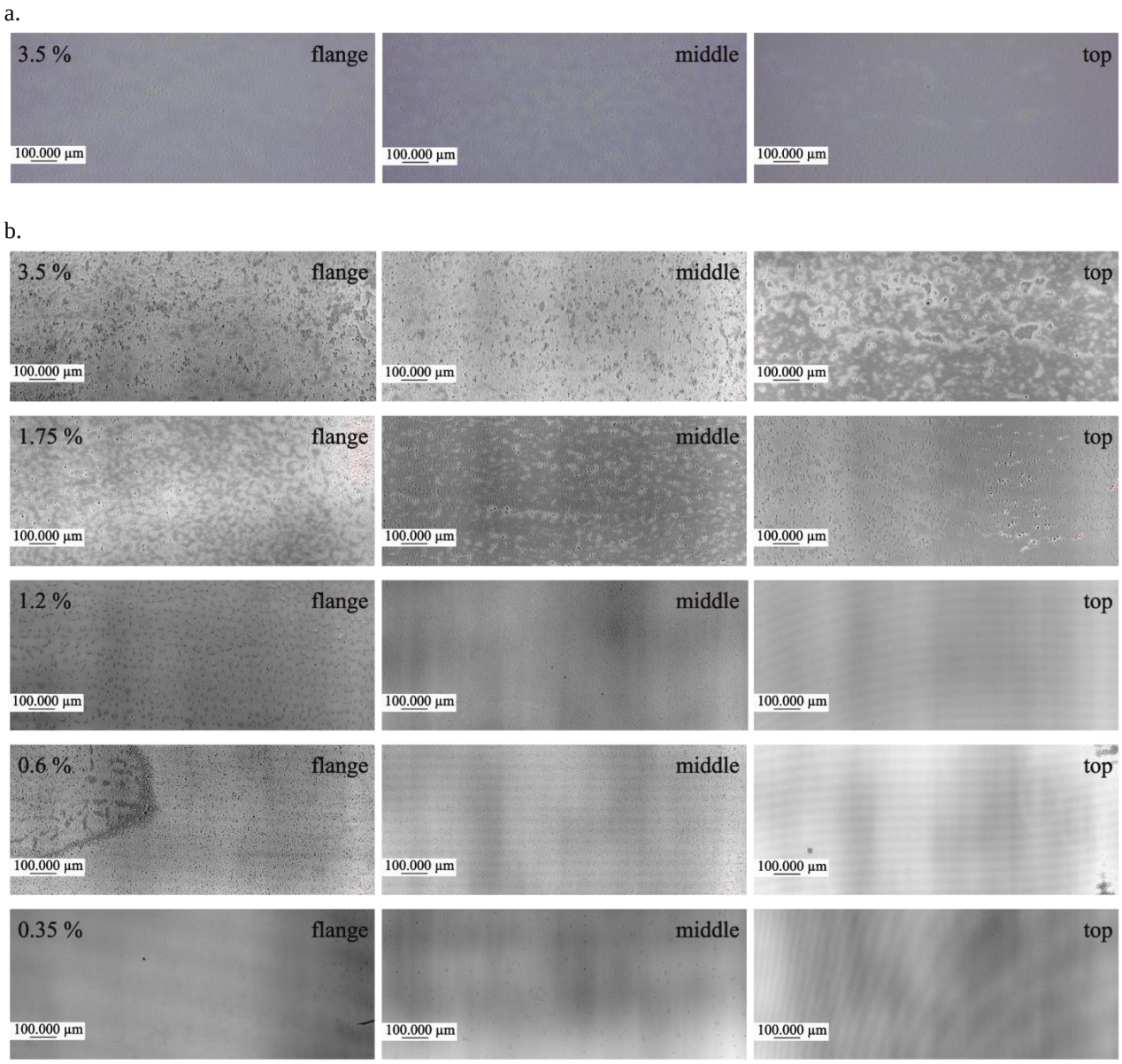

Fig. III-5. Silicone layer after bake-on siliconization (16 mg of a 0.35-3.5 % (w/w) emulsion) at various positions. (a) Optical microscopy, 10 x magnification. (b) 3D-LSM, 10 x magnification.

Thus, 3D-LSM imaging was successfully established to visualize thin baked-on silicone layers and to track even minor difference in the visual appearance of the silicone surface using intact cartridges. The images can be utilized to investigate the distribution of thin baked-on silicone layers in different sections within the cartridges. Consequently, 3D-LSM imaging is a new, non-destructive, highly sensitive and fast technique to visualize and investigate thin baked-on silicone layers, which so far were not accessible with optical microscopy.

3.3 SILICONE LAYER THICKNESS AND DISTRIBUTION

3.3.1 ESTABLISHMENT OF 3D-LSM TO DETERMINE THIN SILICONE LAYERS

In addition to the visual appearance as determined by 3D-LSM imaging, the thickness of the baked-on silicone layers was determined by 3D-LSM height measurements. To qualify measurements of the silicone layer thickness by 3D-LSM, a comparison with chrome-coated step height standards was performed. The measured ALT was comparable to the certified heights of 17.3 ± 1.6 nm and 89.4 ± 1.2 nm (the accuracy was 88-110 %) (Tab. III-1; supporting information Fig. S III-2).

100 x magnification, which has been further used for layer thickness determinations in baked-on siliconized cartridges, precisely measured the theoretical values with a standard deviation of approximately 2-3 nm.

Tab. III-1. Measured ALT (n = 6) of step height standards compared to certified values of 17.3 ± 1.6 nm and 89.4 ± 1.2 nm.

Certified height [nm]	Magnification	Average layer thickness [nm]	Accuracy [%]
17.3 ± 1.6	100 x	19.0 ± 1.8	110
	10 x	16.5 ± 4.4	95
89.4 ± 1.2	100 x	79.6 ± 2.8	89
	10 x	78.3 ± 7.7	88

Therefore, the lower detection limit for silicone layers was further challenged. Fig. III-6 exemplarily shows the surfaces and the respective multi-line average height profiles of silicone layers of approximately 10 nm, 20 nm and 50-60 nm thickness.

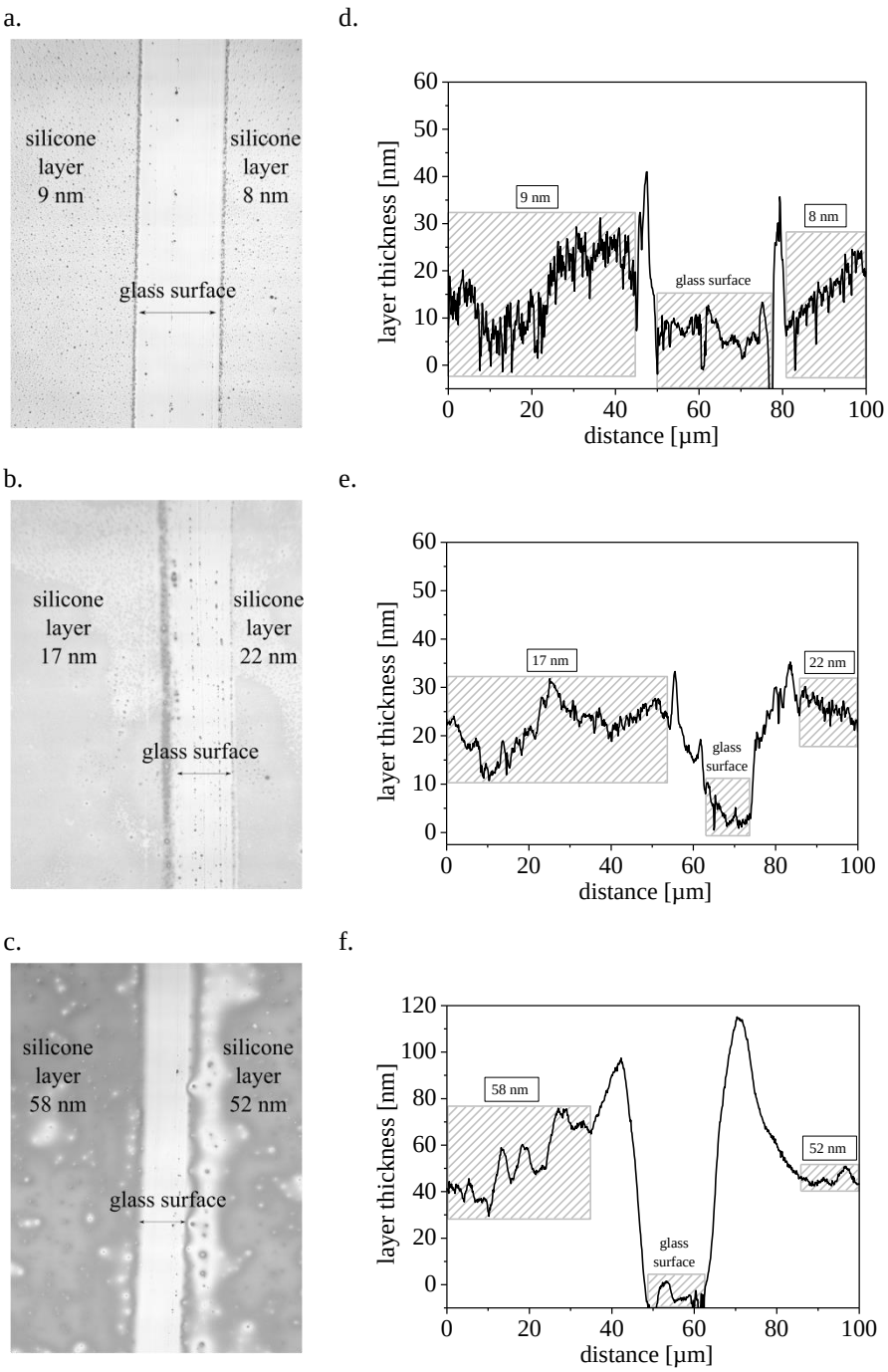

Fig. III-6. Analysis of ALT by 3D-LSM. Determination of the detection limit. 3D-LSM image of the analyzed cartridge section (100 µm x 143 µm). (a) 3D-LSM image ALT of approximately 10 nm. (b) 3D-LSM image ALT of approximately 20 nm. (c) 3D-LSM image ALT of approximately 60 nm. Respective multi-line average height profile of 400 individual profile lines after area and line tilt correction (2nd curved line and area auto, respectively) of an 100 µm x 143 µm cartridge section. The average silicone layer thickness was calculated as the difference in the average height between the glass surface and the silicone layer as indicated by the lined boxes. (d) Multi-line average height profile of approximately 10 nm. (e) Multi-line average height profile of approximately 20 nm. (f) Multi-line average height profile of approximately 60 nm.

Due to the preparation method, the height profiles showed a negative step, where the silicone layer had been artificially removed by a 20 G cannula. By this scratching the silicone layer was not only removed from the glass surface, but rather pushed aside by the cannula, which resulted in thicker silicone build-ups next to the baseline. These artificial builds-ups were not considered for the silicone layer thickness determinations. Silicone layers of approximately 50-60 nm and 20 nm showed a distinct height difference compared to the negative glass baseline. The height profile of 10 nm baked-on silicone layers could still be analyzed, but demonstrated substantial noise. The use of 3D-LSM for quantitative evaluation of silicone layers thinner than 10 nm cannot be recommended.

In contrast, an interferometric profilometer using VSI with white light, which is most commonly utilized for silicone layer thickness determinations [17,20,32,37], only achieves a theoretical detection limit of 80 nm [36]. It suffers from the poor difference in the RI of silicone (1.40) [33] and borosilicate glass (1.49) [34]. Compared to interferometry, 3D-LSM height measurements required a destructive sample preparation, but achieved a better sensitivity.

The ALT of silicone layers prepared from 1.75 % (w/w) silicone emulsion was further evaluated at four different radial directions (0°, 90°, 180°, 270°) along three sections of the cartridge barrel (flange, middle, top). Three cartridges were selected (n1, n2, n3) (Fig. III-7).

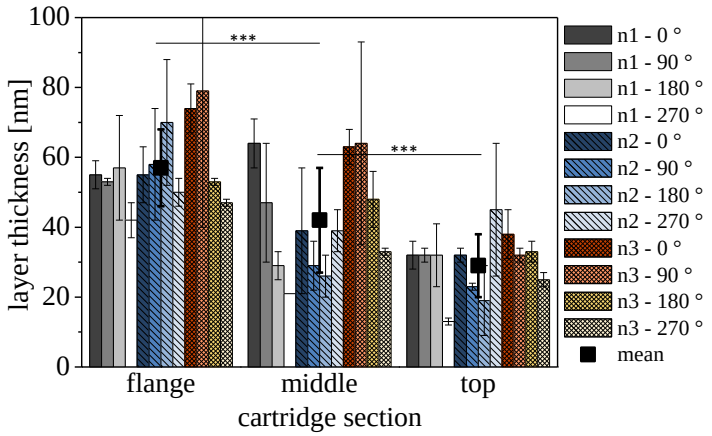

Fig. III-7. Silicone layer thickness after bake-on siliconization using 16 mg of a 1.75 % (w/w) emulsion. Layer thickness was evaluated at four radial directions in three sections within the cartridge barrel (n = 3, * $p \leq 0.05$, ** $p \leq 0.01$, *** $p \leq 0.001$).

The mean silicone layer thickness decreased significantly from 58 ± 11 nm to 29 ± 9 nm from the flange to the top of the cartridge. The more pronounced siliconization at the flange was attributed to the applied nozzle-to-flange distance of 20 mm, where the spray cone exactly reached the

flange (see chapter IV). The 3D-LSM height measurements thus confirmed the results from the visual appearance of the surface as observed in the 3D-LSM images. The ALTs varied 10-30 nm depending on the radial direction measured. Thus, to track the radial silicone distribution along the cartridge barrel, it is recommended to measure a set of at least four different radial directions.
Overall, based on our results, we consider 3D-LSM a valuable tool to investigate the effects of different spray parameters on the radial silicone layer distribution and to evaluate silicone redistributions during storage, as relevant for spray-on siliconized glass barrels [20]. However, the technique requires sophisticated software handling due to the curvature of the sample. The total measurement time including sample preparation, height measurements and data analysis takes approximately 5 min. In particular, full cartridge mapping in 3D-LSM is labor-intensive and time-consuming as the cartridge fragments need to be carefully selected after breakage. In contrast, VSI facilitates in-situ thickness measurements of usually one to six radial lines with a spot distance of 1 mm along the barrel length and requires only seconds per measurement [20,36]. Consequently, interferometric profilometers offer more convenient mapping of siliconization, but with far less sensitivity.
To further assess the suitability of 3D-LSM, layer thicknesses were exemplarily determined using AFM for comparison (Tab. III-2).

Tab. III-2. Silicone layer thickness after bake-on siliconization using 16 mg of a 1.75 % (w/w) emulsion [a].

Cartridge section	ALT (3D-LSM)	ALT (AFM)	ALT (theoretical)
Flange	57 ± 11 nm	57 ± 7 nm	
Middle	42 ± 15 nm	56 ± 8 nm	68 ± 5 nm
Top	29 ± 9 nm	47 ± 9 nm	

[a] *ALT was calculated as the mean from individual layer thicknesses at four different radial directions along three sections of the cartridge barrel (n = 3) in 3D-LSM. In AFM, ALT was calculated as the mean from the layer height of the forward and reverse scan (n = 1). The mean theoretical silicone layer thickness derived from the silicone level quantified via FTIR applying a silicone density of 0.972 g/cm^3 [33] and a cartridge interior surface of 2422 mm^2.*

The mean layer thickness values obtained by 3D-LSM were in good agreement with the layer thickness values determined by AFM in the middle and flange region of the cartridge barrel. A significant difference was observed at the top ($p \leq 0.05$). 3D-LSM mean layer thickness results were derived from cartridge mapping at four radial directions using three different cartridges, whereas AFM was based on single measurements in forward and reverse scan, which puts the results in perspective. In addition, AFM is based on mechanical profiling using an oscillating probe in tapping mode, whereas 3D-LSM is an optical profiler. However, 3D-LSM stood out

with its higher throughput and high-resolution images. Furthermore, 3D-LSM offered contact-free profiling, which is in particular suitable for soft, flexible silicone layers. We therefore believe that 3D-LSM is a suitable method to determine thin, baked-on silicone layers.

3.3.2 THICKNESS AND DISTRIBUTION OF THIN BAKED-ON SILICONE LAYERS

To investigate the silicone distribution after bake-on siliconization using different emulsion concentrations (0.35-3.5 % (w/w)), cartridge fragments were randomly collected from different radial directions, assuming that each radial directions was selected at least once and to simplify the analytical process. Silicone layers obtained from 0.35 % (w/w) emulsion reached the LOQ of 10 nm. With increasing emulsion concentrations of 0.6 % (w/w) to 1.75 % (w/w) the ALT increased from 20 nm to 70-80 nm (Fig. III-8).

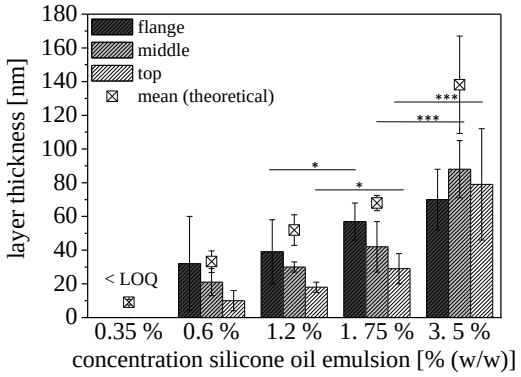

Fig. III-8.ALT after bake-on siliconization using 16 mg. Layer thickness was evaluated at one radial direction in three sections within the cartridge barrel (n = 3, * $p \leq 0.05$, ** $p \leq 0.01$, *** $p \leq 0.001$).

The middle and top sections of the cartridges exhibited a reduced ALT compared to the flange, which can be attributed to the spray position of 20 mm below the flange. These quantitative data appeared to be consistent with the results obtained from 3D-LSM imaging, which also showed a decrease in siliconization from the flange to the top (Fig. III-5).

The theoretical layer thicknesses ranged from 9 ± 2 nm to 139 ± 29 nm with increasing emulsion concentrations. These numbers were systematically higher compared to the measured ALTs at the cartridge top and middle, whereas they were in good agreement with the measured ALT at the flange. Calculations of the mean theoretical layer thickness were based on the assumption of an ideally distributed homogeneous silicone layer within the entire cartridge barrel. Inhomogeneities in the silicone oil distribution from the flange to the top as observed in the 3D-LSM imaging can

explain the slight differences between the theoretical and measured silicone layer thicknesses.
In contrast, Wen *et al.* reported a factor of two between the median layer thickness of 200 nm as obtained by VSI and the theoretical layer thickness of 430 nm. They refer this to an even more pronounced inhomogeneous silicone distribution, which is also reflected in the layer thicknesses ranging from 100 nm to 700 nm [32]. Lankers converted the silicone layer thicknesses obtained from VSI into theoretical silicone contents. The obtained values systematically deviated from silicone quantification by AAS analysis following toluene extraction. The sprayed-on silicone layers also depicted plaque-like structures [20].
The thickness of sprayed-on and cross-linked silicone layers was reported in the range of roughly 50-400 nm with some areas up to 900 nm thickness as determined by VSI [17,20,32,37]. To our knowledge, baked-on silicone layers of approximately 50-100 nm were only exemplarily determined using VSI [20]. ToF SIMS was also employed to determine the thickness of sprayed-on silicone layers in the range of 17 nm to 47 nm. It additionally facilitates to identify different silicone species in cross-linked silicone layers [37], but due to the intensive sample preparation, difficult measurement procedures and data analysis it cannot be considered a routine method. In contrast, 3D-LSM combined both, an acceptable measurement time of 5 min per sample and a highly sensitive detection limit as low as 10 nm.

4 CONCLUSION

Baked-on siliconized cartridges were examined using FTIR spectroscopy after solvent extraction to quantify the baked-on silicone levels. 3D-LSM was utilized to determine the distribution and thickness of the baked-on silicone layer quantitatively as well as visually.

The baked-on silicone level increased from 21 µg to 325 µg with increasing concentrations of the silicone oil emulsion from 0.35 % (w/w) to 3.5 % (w/w). FTIR spectroscopy showed a good linear response and excellent sensitivity below 1 µg/mL and a LOQ of 18 µg/mL silicone oil in the extract corresponding to 4 µg per cartridge. Simultaneously, the ALT increased from approximately 10 nm to 70-80 nm. 3D-LSM imaging visualized the concentration-dependent change in the silicone surface structure. A decreased layer thickness toward the top of the cartridge was visualized in 3D-LSM imaging and was similarly observed in the ALT measurements. It was attributed to the spray position of 20 mm below the flange, where the spray cone exactly reached the flange (see chapter IV). 3D-LSM is a highly sensitive technique to visualize and determine thin baked-on silicone layers below 100 nm.

Future work aims toward investigating the link between the applied siliconization parameters and the silicone distribution within the cartridge barrel. An improved characterization of the silicone distribution and a sensitive quantification of the silicone levels may allow further optimization of siliconization processes.

5 SUPPORTING INFORMATION

a. b.

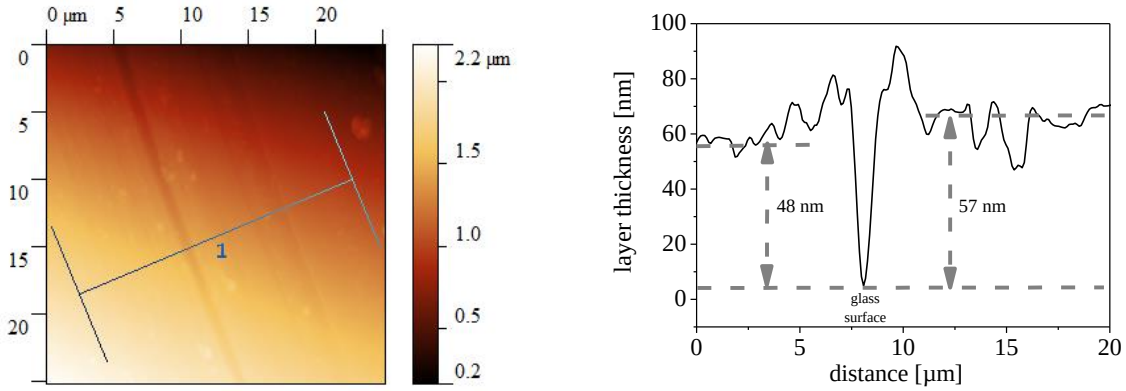

Fig. S III-1. Analysis of ALT by AFM. (a) Exemplary AFM image of an analyzed cartridge section (30 µm x 30 µm). Line depicts the 110 px multi-line average height profile. (b) 110 px multi-line average height profile. The ALT was determined as the difference between horizontal lines, i.e., the glass surface and the silicone layer, after profile extraction of 110 px multi-lines and tilt correction by mean plane subtraction.

a. b.

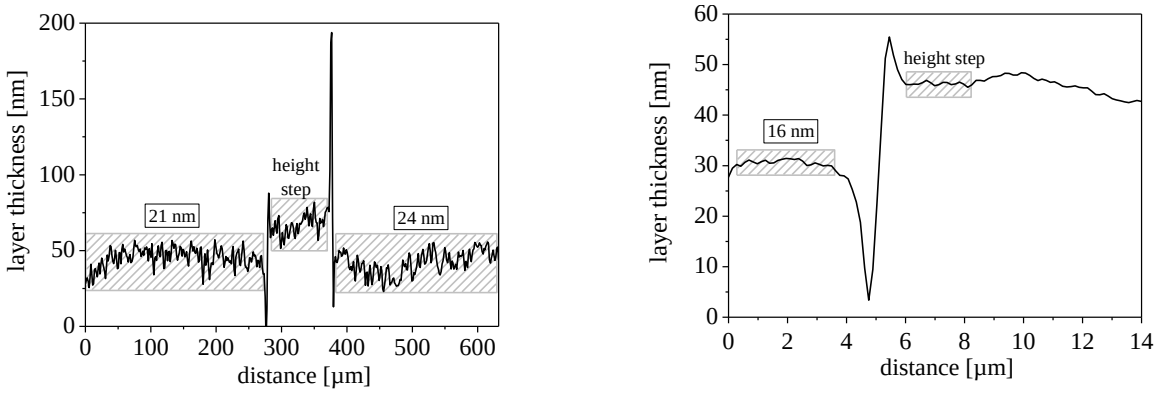

Fig. S III-2.Analysis of ALT of 17.3 ± 1.6 nm step height standards by 3D-LSM. Multi-line average height profile of 200 individual profile lines. The ALT was calculated as the difference between the average height along the base of the step and the top of the step as indicated by the lined boxes. (a) 10 x magnification. At 10 x magnification the tilt of the quartz substrate was leveled using automatic area and line plane correction. (b) 100 x magnification.

6 ABBREVIATIONS

3D-LSM	3D-laser scanning microscopy;
AAS	Atomic absorption spectrometry;
AFM	Atomic force microscopy
ALT	Average layer thickness
AUC	Area under the curve
FTIR	Fourier transform infrared (spectroscopy)
ICP-OES	Inductively coupled plasma optical emission spectrometry
LOD	Limit of detection
LOQ	Limit of quantification
PDMS	Polydimethylsiloxane
PFS	Pre-filled syringes
RI	Refractive index
SIN	Staked-in needle
ToF SIMS	Time-of-flight secondary ion mass spectrometry
VSI	Vertical scanning interferometry
XSi^{TM}	Cross-linked silicone layer, prepared by proprietary treatment of Becton-Dickinson

7 REFERENCES

[1] B. Harrison, M. Rios, Big Shot: Developments in Prefilled Syringes, Pharm. Technol. 30 (2007) 42–48.

[2] S. Makwana, B. Biswajit, Y. Makasana, A. Dharamasi, Prefilled syringes: An innovation in parenteral packaging, Int. J. Pharm. Inverstigations. 1 (2011) 200–206.

[3] N. Rathore, R.S. Rajan, Current perspectives on stability of protein drug products during formulation, fill and finish operations., Biotechnol. Prog. 24 504–514.

[4] G.A. Sacha, W. Saffell-Clemmer, K. Abram, M.J. Akers, Practical fundamentals of glass, rubber, and plastic sterile packaging systems, Pharm. Dev. Technol. 15 (2010) 6–34.

[5] M. Adler, Challenges in the development of pre-filled syringes for biologics from a formulation scientist´s point od view, Am. Pharm. Rev. 15 (2012).

[6] K.B. Auge, A.W. Blake-Haskins, S. Devine, S. Rizvi, Y.-M. Li, M. Hesselberg, et al., Demonstrating the stability of albinterferon alfa-2b in the presence of silicone oil, J. Pharm. Sci. 100 (2011) 5100–5114.

[7] S. Majumdar, B.M. Ford, K.D. Mar, V.J. Sullivan, R.G. Ulrich, A.J.M. D'Souza, Evaluation of the effect of syringe surfaces on protein formulations, J. Pharm. Sci. 100 (2011) 2563–2573.

[8] B. Demeule, S. Messick, S.J. Shire, J. Liu, Characterization of particles in protein solutions: reaching the limits of current technologies., AAPS J. 12 (2010) 708–715.

[9] A. Lubiniecki, D.B. Volkin, M. Federici, M.D. Bond, M.L. Nedved, L. Hendricks, et al., Comparability assessments of process and product changes made during development of two different monoclonal antibodies., Biologicals. 39 (2011) 9–22.

[10] R. Thirumangalathu, S. Krishnan, M.S. Ricci, D.N. Brems, T.W. Randolph, J.F. Carpenter, Silicone oil- and agitation-induced aggregation of a monoclonal antibody in aqueous solution, J. Pharm. Sci. 98 (2009) 3167–3181.

[11] A. Gerhardt, K. Bonam, J.S. Bee, J.F. Carpenter, T.W. Randolph, Ionic strength affects tertiary structure and aggregation propensity of a monoclonal antibody adsorbed to silicone oil-water interfaces, J. Pharm. Sci. 102 (2013) 429–440.

[12] L.S. Jones, A. Kaufmann, C.R. Middaugh, Silicone oil induced aggregation of proteins, J. Pharm. Sci. 94 (2005) 918–927.

[13] A. Badkar, A. Wolf, L. Bohack, P. Kolhe, Development of Biotechnology Products in Pre-filled Syringes: Technical Considerations and Approaches, AAPS PharmSciTech. 12 (2011) 564–572.

[14] K.A. Britt, D.K. Schwartz, C. Wurth, H.-C. Mahler, J.F. Carpenter, T.W. Randolph, Excipient effects on humanized monoclonal antibody interactions with silicone oil emulsions, J. Pharm. Sci. 101 (2012) 4419–4432.

[15] E. Chan, A. Hubbard, S. Sane, Y.-F. Maa, Syringe siliconization process investigation and optimization, PDA J. Pharm. Sci. Technol. 66 (2012) 136–150.

[16] Y. Nashed-Samuel, D. Liu, K. Fujimori, L. Perez, H. Lee, Extractables and leachables implications on biological products in prefilled syringes, Am. Pharm. Rev. 14 (2011).

[17] F. Felsovalyi, S. Janvier, S. Jouffray, H. Soukiassian, P. Mangiagalli, Silicone-oil-based subvisible particles: their detection, interactions, and regulation in prefilled container closure systems for biopharmaceuticals, J.

Pharm. Sci. 101 (2012) 4569–4583.

[18] L. Khandke, R. Malone, X. Yang, H. Han, J.L. Look, Z. Jin, et al., Novel formulations which stabilize and inhibit precipitation of immunogenic compositions, U.S. Patent 2011/0172393 A1, 2011.

[19] É. José dos Santos, A.B. Herrmann, R.E. Sturgeon, J.S. Azevedo Silva, A.J. Curtius, Rapid determination of silicone oil lubricant in elastomeric closures by ICP-OES, Anal. Methods. 5 (2013) 4263–4267.

[20] M. Lankers, Analyse von Silikonschichtdicken bei der Herstellung von Fertigspritzen mit Hilfe von Refektometriemessungen, Pharm. Ind. 72 (2010) 2148–2153.

[21] J.R. Miller, J.J. Helprin, J.S. Finlayson, Silicone lubricant flushed from disposable syringes: Determination by atomic absorption spectrophotometry, J. Pharm. Sci. 58 (1969) 455–456.

[22] H.J. Horner, J.E. Weiler, N.C. Angelotti, Visible and Infrared Spectroscopic Determination of Trace Amounts of Silicones in Foods and Biological Materials, Anal. Chem. 32 (1960) 858–861.

[23] F. Pavanetto, B. Conti, I. Genta, T. Modena, Particulate contamination from siliconized rubber stoppers, Int. J. Pharm. 74 (1991) 175–181.

[24] PDA, Technical report No. 12. Siliconization of parenteral drug packaging components, J. Parenter. Sci. Technol. 42 (1988) S2–S13.

[25] P. Basu, A.W. Blake-Haskins, K.B. O'Berry, T.W. Randolph, J.F. Carpenter, Albinterferon α2b adsorption to silicone oil-water interfaces: effects on protein conformation, aggregation, and subvisible particle formation, J. Pharm. Sci. 103 (2014) 427–436.

[26] D.B. Ludwig, J.F. Carpenter, J.-B. Hamel, T.W. Randolph, Protein adsorption and excipient effects on kinetic stability of silicone oil emulsions, J. Pharm. Sci. 99 (2010) 1721–1733.

[27] E. Pretsch, P. Bühlmann, C. Affolter, Determination of organic compounds. Tables of spectral data, Springer-Verlag Berlin, 2000.

[28] Wissenschaftliche Verlagsgesellschaft Stuttgart, Commentary on Ph. Eur. 3.1.8. Siliconöl zur Verwendung als Gleitmittel, (2004).

[29] A. Sinclair, T.R. Hallam, The determination of dimethylpolysiloxane in beer and yeast, Analyst. 96 (1971) 149–154.

[30] T. Mundry, Einbrennsilikonisierung bei pharmazeutischen Glaspackmitteln - Analytische Studien eines Produktionsprozesses, Dissertation, Humboldt-Universität Berlin, 1999.

[31] C. Petersen, Syringe Siliconisation. Trends, Methods, Analysis Procedures, Int. Pharm. Ind. 4 (2012) 92–99.

[32] Z.-Q. Wen, A. Vance, F. Vega, X. Cao, B. Eu, R. Schulthesis, Distribution of Silicone Oil in Prefilled Glass Syringes Probed with Optical and Spectroscopic Methods, PDA J. Pharm. Sci. Technol. 63 (2009) 149–158.

[33] Dow Corning Corporation, Product Information. Dow Corning 360 Medical Fluid. Ref. No. 51-0374N-01, (2009).

[34] Refractive index database, (2014). http://refractiveindex.info (accessed October 10, 2014).

[35] B. Eu, A. Cairns, G. Ding, X. Cao, Z.-Q. Wen, Direct visualization of protein adsorption to primary containers by gold nanoparticles., J. Pharm. Sci. 100 (2011) 1663–1670.

[36] rap.ID Particle Systems GmbH, Silicone layer information, Layer Explorer (LE) devices for different applications, (n.d.). http://www.siliconization.com/layerexplorer/le.html (accessed March 27, 2014).

[37] R.A. Depaz, T. Chevolleau, S. Jouffray, R. Narwal, M.N. Dimitrova, Cross-linked silicone coating: a novel prefilled syringe technology that reduces subvisible particles and maintains compatibility with biologics, J. Pharm. Sci. 103 (2014) 1384–1393.

[38] rap.ID Particle Systems GmbH, Layer Explores UT, Control baked-on siliconization, Information brochure

[39] B. Parbhoo, S. Izrael, J.M. Salamanca, J.L. Keddie, Use of ellipsometry and gravimetry to develop calibration standards for measuring silicone coat weight and thickness with x-ray fluorescence spectroscopy, Surf. Interface Anal. 29 (2000) 341–345.

[40] J. Bastacky, C.Y. Lee, J. Goerke, H. Koushafar, D. Yager, L. Kenaga, et al., Alveolar lining layer is thin and continuous: low-temperature scanning electron microscopy of rat lung, J Appl Physiol. 79 (1995) 1615–1628.

[41] B. Buszewski, P. Olszowy, S. Pikus, M. Kozak, Electropolymerized nanoporous polymeric SPME coatings: preparation and characterization by small angle X-ray scattering and scanning electron microscopy, Monatshefte Fur Chemie. 145 (2014) 527–531.

[42] V. Burckbuchler, G. Mekhloufi, A.P. Giteau, J.L. Grossiord, S. Huille, F. Agnely, Rheological and syringeability properties of highly concentrated human polyclonal immunoglobulin solutions, Eur. J. Pharm. Biopharm. 76 (2010) 351–356.

[43] L. Joseph, S. Martin, P. Kohle, K. Muthurania, Development of Syringeability Guide for Subcutaneous Protein Formulations, (2010). http://www.readbag.com/aapsj-abstracts-am-2010-w5265 (accessed August 14, 2015).

[44] A. Sheikhzadeh, J. Yoon, D. Formosa, The effect of a new syringe design on the ability of rheumatoid arthritis patients to inject a biological medication, Appl. Ergon. 43 (2012) 368–375.

[45] J. De Coninck, M.J. de Ruijter, M. Voué, Dynamics of wetting, Curr. Opin. Colloid Interface Sci. 6 (2001) 49–53.

[46] P. de Gennes, Wetting: statics and dynamics, Rev. Mod. Phys. 57 (1985) 827–863.

IV Optimization of the Bake-On Siliconization of Cartridges. Part I: Optimization of Spray-On Parameters

Parts of the following chapter are published as research article in the European Journal of Pharmaceutics and Biopharmaceutics:

S. Funke, J. Matilainen, H. Nalenz, K. Bechtold-Peters, H.-C. Mahler, W. Friess. Optimization of the Bake-On Siliconization Process of Cartridges. Part I: Optimization of Spray-On Parameters. Eur. J. Pharm. Biopharm 104 (2016) 200–215. © 2016 Elsevier B.V.

Keywords

Cartridge, FTIR, functionality, 3D-laser scanning microscopy, siliconization, spray process, silicone distribution, silicone layer thickness

Graphical Abstract

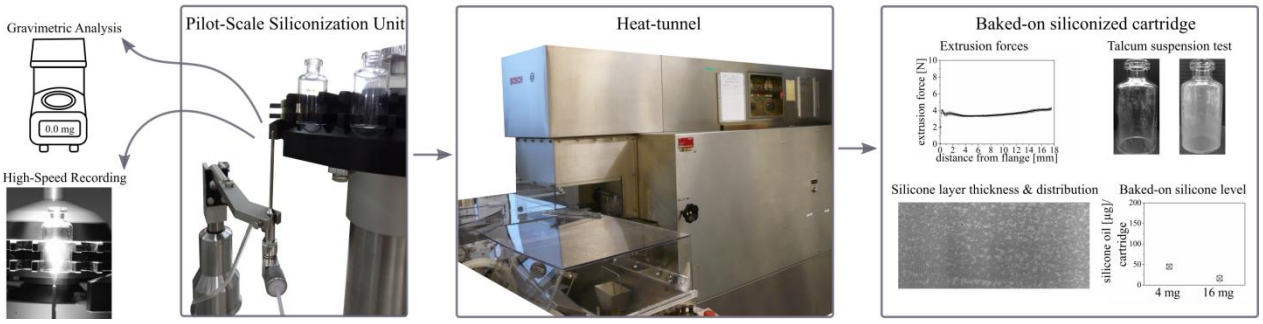

ABSTRACT

Biopharmaceutical products are increasingly commercialized as drug/device combinations to enable self-administration. Siliconization of the inner syringe/cartridge glass barrel for adequate functionality is either performed at the supplier or drug product manufacturing site. Yet, siliconization processes are often insufficiently investigated. In this study, an optimized bake-on siliconization process for cartridges using a pilot-scale siliconization unit was developed. The following process parameters were investigated: spray quantity, nozzle position, spray pressure, time for pump dosing and the silicone emulsion concentration.

A spray quantity of 4 mg emulsion showed best, immediate atomization into a fine spray. 16 and 29 mg emulsion, hence 4 to 7-times the spray volume, first generated an emulsion jet before atomization was achieved. The poor atomization of higher quantities correlated with an increased spray loss and inhomogeneous silicone distribution, e.g., due to runlets forming build-ups at the cartridge lower edge and depositing on the star wheel. A prolonged time for pump dosing of 175 ms led to a more intensive, long-lasting spray compared to 60 ms as anticipated from a higher air-to-liquid ratio. A higher spray pressure of 2.5 bar did not improve atomization but led to an increased spray loss. At a 20 mm nozzle-to-flange distance the spray cone exactly reached the cartridge flange, which was optimal for thicker silicone layers at the flange to ease piston break-loose. Initially, 10 µg silicone was sufficient for adequate extrusion in filled cartridges. However, both maximum break-loose and gliding forces in filled cartridges gradually increased from 5-8 N to 21-22 N upon 80 weeks of storage at room temperature. The increase for a 30 µg silicone level from 3-6 N to 10-12 N was moderate. Overall, the study provides a comprehensive insight into critical process parameters during the initial spray-on process and the impact of these parameters on the characteristics of the silicone layer, also in context of long-term product storage. The presented experimental toolbox may be utilized for development or evaluation of siliconization processes.

1 INTRODUCTION

Pre-filled syringes (PFS) and drug/device combination products equipped with cartridges are increasingly used to enable self-administration of parenteral medications. They are safe, less prone to contamination, user-friendly and often require less overfill [1–5].

Usually, the primary container is lubricated with silicone oil to reduce the friction between the container wall and the piston, which in turn facilitates good injectability, function and reliable dosage with sufficient precision during injection [6–8]. Of note, functionality is still one of the major concerns for drug/device combination products [9,10].

Siliconization is an established unit operation. Typically, two different siliconization procedures are used referred to as spray-on and bake-on siliconization [11,12].

Staked-in needle syringes, where an adhesive (glue) is used to embed a needle into the fluid path, are processed via spray-on siliconization using silicone oil. Bake-on siliconization, however, is not applicable to staked-in needle PFS due to the low heat resistance of the adhesive (glue) needed to fix the needle into the fluid path. Polydimethylsiloxanes, e.g., Dow Corning 360 Medical Fluid [13] with viscosities ranging from about 1000 cSt [14] to 12500 cSt [15], is most commonly applied as lubricant, but other linear or branched polydialkysiloxanes such as polydipropylsiloxane, polydihexylsiloxane are possible alternatives [15]. Due to the viscosity of silicone oil, it may be difficult to precisely deliver a small amount of the lubricant [16]. Spray-on silicone layers exhibit individual plaque-like and micro-droplet structures [9,17,18] and an uniform homogeneous coating is most likely not readily formed [19]. Therefore, in spray-on siliconization processes most commonly higher silicone levels of 0.2-1 mg/barrel are applied [8,13,16–18,20–23] compared to < 0.1 mg/barrel for bake-on siliconization processes, where heat promotes the formation of a homogeneous silicone layer [20,24,25]. To overcome these drawbacks, silicone oil could be applied as a mixture with volatile organic solvents, e.g., alkanes, alkenes or with low viscosity liquid silicones (0.1-200 cSt). After evaporation of the solvent or low viscosity silicone, the high viscosity silicone remains as lubricant on the glass surface [19,26,27].

Luer tip syringes with open syringe cones are usually applying bake-on siliconization, using a (diluted) silicone emulsion, e.g., Dow Corning 365 35 % Dimethicone NF Emulsion, followed by a high temperature process at approximately 300 °C to remove the emulsion water and to decompose emulsion stabilizers as well as concomitant pyrogens [28–31]. Before administration, a needle can be attached to the luer tip following respective instructions for use of the

pharmaceutical manufacturer [8]. Cartridges as part of delivery systems are combined with separate pen needles, and can therefore also be bake-on siliconized. The absolute spray amount of a diluted silicone emulsion can be precisely adjusted, thereby providing accurate control of the total silicone oil content. The thin, but sufficient baked-on silicone layer assures functionality during storage and minimizes silicone migration into the drug product [16,18,21,26,32]. Although different silicone levels are likely of less relevance for patient safety, it may also be beneficial for few, very silicone-sensitive protein therapeutics [12,21].

Recently, alternative coating methods utilize cross-linked silicone to further prevent silicone leaching from the barrel interior [16,18,23,26,27,33]. In addition, silicone-oil free systems are being promoted. These techniques include lubricious, biocompatible coatings for plunger stoppers, which may enable adequate extrusion performance in silicone oil free syringes, e.g., fluoropolymer coatings (FluroTec®) or proprietary i-coating™, often in combination with polymer based syringes (Plajex™, CrystalZenith®) [34–36]. Studies suggest a great potential of these systems for highly sensitive protein therapeutics with low protein aggregate and subvisible particle levels, but suitability has still to be confirmed with more systematic investigations. Additionally, extractables/leachables, oxidation and packaging sterilization may be amongst the challenges to be overcome [22].

So far, siliconization media are well-characterized, whereas the siliconization process itself varies from a dipping, spray-on, wipe-on to a washing procedure of the component to be siliconized [15,19,27]. Technical aspects of a spray-on process using automated siliconization units were described in literature [13,37], but are often considered as proprietary know-how and therefore rarely published. Consequently, there is a high variability in the silicone content, distribution and leaching from individual PFS [24,38], which increases the need for clearly defined siliconization processes. As the demand for PFS and drug/device combination product increases, the understanding and optimization of siliconization processes becomes even more relevant. Automated siliconization units precisely regulate the spray amount, static or dynamic nozzle position including nozzle speed as well as the air atomization pressure and spray time [13,37]. Thus, a carefully designed siliconization process results in clearly defined, limited silicone levels and reproducible silicone distributions without compromising functionality.

The objective of the present study was to establish an optimized bake-on siliconization process using a pilot-scale siliconization unit. In particular, we investigated different nozzle positions below the cartridge flange, and variations in spray quantities, pressures and times for pump

dosing to control and optimize the spray pattern as well as the silicone distribution and layer thickness along the cartridge barrel. The concentration of the silicone emulsion was clearly defined to yield adequate silicone levels ensuring adequate piston extrusion performance even after long-term storage.

2 MATERIALS AND METHODS

2.1 MATERIALS

DC 365 35 % Dimethicone NF Emulsion purchased from Dow Corning GmbH (Wiesbaden, Germany) was diluted to 0.06-3.5 % (w/w) using highly purified water. Non-siliconized 5 mL cartridges, pistons, serum stoppers and aluminium seals were obtained from F. Hoffmann-La Roche Ltd (Basel, Switzerland). Elastomeric components were coated with fluoropolymer (FluroTec®). Talcum (Ph. Eur. grade) was purchased from VWR International GmbH (Darmstadt, Germany).

2.2 BAKE-ON SILICONIZATION PROCESS

Experiments in this study were performed using a SVS9061 pilot-scale siliconization unit from Bausch + Ströbel (B+S) Maschinenfabrik Ilshofen GmbH+Co. KG (Ilshofen, Germany). The set-up employed a high precision rotary piston pump with a gliding disk from Saphirwerk AG (Brügg, Switzerland) to deliver silicone emulsion through an external mixing two-fluid nozzle with a swirl inset. A sensor dummy (diameter 0.6 mm) was inserted into the inner concentric tube (diameter 0.8 mm), which resulted in a hollow cone emulsion stream with an annular slit thickness of 0.1 mm (supporting Information Fig. S IV-1). The delivered amount was manually adjusted by a micrometer screw with nominal settings from one to three millimetres in 0.1 mm increments [39]. The screw setting defined the position of the gliding disk, thereby optimizing the gap between the piston and the bottom of the cylinder. Therefore, the micrometer screw allowed the absolute adjustment of dosing volume. A servo automated actuator controlled both static and dynamic nozzle positions while in turn an operator touch screen provided full control of the servo automated actuator settings. For atomization, compressed air was manually controlled by a pressure reducer (0.8-2.5 bar) and automatically monitored on the operator touch screen. Compressed air was adjusted by a gauge valve prior to emulsion dosing. The time for pump dosing was set on the operator touch screen. Up to 18 cartridges were fed manually into the star wheel with flange downwards. Finally, a two-hand circuit was used to safely initiate the spray process.

The cartridges were subsequently treated in a TSQ U03 heat-tunnel from Robert Bosch GmbH (Stuttgart, Germany) at 316 °C for 12 min.

In addition, the pilot-scale siliconization unit was equipped with a KA2 automatic spray valve

and a simple, external mixing two-fluid nozzle from Optima packaging group GmbH (Schwäbisch Hall, Germany).

2.3 GRAVIMETRIC ANALYSIS

After every adjustment of the pump screw or spray parameters, the emulsion spray was initially collected in a 2R vial, which was previously loaded with a tissue to soak up the absolute spray amount without evaporation loss. The vial was weighted before and after the siliconization process using an AT261 DeltaRange System high precision balance from Mettler-Toledo GmbH (Gießen, Germany). The absolute spray amounts were converted into theoretically sprayed silicone amounts using the corresponding concentration of the silicone emulsion.

2.4 HIGH-SPEED RECORDING

An Exilim Digital Camera EX-F1 form Casio Europe GmbH (Norderstedt, Germany) in high-speed recording (600 fps) and continuous shooting mode (60 fps) was employed to characterize the spray pattern.

2.5 TALCUM SUSPENSION TEST

The cartridge flange was covered with parafilm and filled with 2 ml of 4 % (w/w) talcum suspension in purified water. The cartridge was rotated ten times in horizontal position before discarding the suspension. Talcum coated cartridges were visually inspected using a DMC-LS75 digital camera from Panasonic Marketing Europe GmbH (Hamburg, Germany). Talcum adheres to silicone coated surfaces and therefore provides a first visual assessment related to silicone level and distribution over the cartridge barrel.

2.6 EXTRACTION AND FOURIER TRANSFORM INFRARED (FTIR) QUANTIFICATION

The baked-on silicone amount was determined by a combination of heptane extraction and quantitative FTIR spectroscopy. The baked-on silicone distribution was characterized by extracting specific zones at the flange, middle and top of the cartridge barrel (length 32 mm). The flange and top zone were equivalent to a filling height of the inner barrel of approximately 10 mm. The flange-side was closed using a second non-siliconized cartridge with a placed piston. Both cartridges were connected using a tight rubber seal. The siliconized cartridge with the flange downwards was filled with 2.5 mL heptane, thereby extracting the flange zone. Note that during

flange extraction, silicone was also extracted from the cartridge edge. The silicone in the top zone was extracted by filling 2.8 mL of heptane into the cartridge with the flange upwards after closing the needle-side with a stopper. Two rinsing steps were performed using the same volumes of heptane. After flange and top extraction, the cartridge was filled with 900 µL heptane to extract the remaining silicone in the middle zone. Again, two rinsing steps were employed. Based on a previous study, the applied method led to a quantitative silicone extraction. Silicone extracts and FTIR analysis was further performed as previously described [40] (see chapter III).

According to considerations provided in ICH Q2 R1 Validation Analytical Procedure, the limit of detection of the developed FTIR method was below 1 µg/mL (number of calibration curves n = 22). The limit of quantification (LOQ) was 18 µg/mL (n = 22), equivalent to 4 µg per cartridge based on 250 µL dissolution volume.

2.7 3D-LASER SCANNING MICROSCOPY (3D-LSM)

The average silicone layer thickness (ALT) was determined using a VK-X210 microscope equipped with VK Viewer Software both from Keyence Deutschland GmbH (Neu-Isenburg, Germany) as previously reported [40] (see chapter III). The LOQ was 10 nm.

Cartridges were covered with adhesive tape, broken up and individual fragments were removed from the adhesive tape to enable direct measurements of the thin baked-on silicone layer. Cartridge fragments from the edge, flange, middle, and top of the cartridge were analyzed to determine the ALT distribution within the barrel.

To confirm the 3D-LSM measurements, a theoretical average layer thickness was calculated from the silicone level quantified via FTIR applying a silicone density of 0.972 g/cm^3 [41] and a cartridge interior surface of 2422 mm^2.

3D-LSM images were additionally employed to visualize the distribution of the silicone within an intact cartridge as previously described [40] (see chapter III).

2.8 EXTRUSION FORCE MEASUREMENTS

After bake-on siliconization, the piston and cartridges were manually assembled. The containers were filled with 5.16 mL highly purified water and sealed with stoppers and aluminum caps. Pistons in contact with lubricated container walls develop an initial resistance to movement. Therefore, movement is not initiated until a certain force is achieved, referred to as break-loose force. After a rapid relative movement, the movement sustains applying a gliding force. The break-loose, minimum and maximum gliding forces were evaluated by using a material testing

instrument TA.XT.plus from Winopal Forschungsbedarf GmbH (Elze, Germany) at a constant displacement speed of 5.6 mm/min over a distance of 17.5 mm, which was the maximum travel distance for the piston within the cartridge barrel. An approximate injection time of 3 min was mimicked for a high filling volume of 5.16 mL in a spring-controlled single injection patch device. For long-term extrusion forces, the filled cartridges were stored for 80 weeks at room temperature.

3 RESULTS AND DISCUSSION

3.1 IMPACT OF SPRAY PARAMETERS ON THE SPRAY PATTERN AND BAKED-ON SILICONE LAYER CHARACTERISTICS

3.1.1 IMPACT OF SPRAY QUANTITY

The effect of different spray quantities on the spray pattern and the baked-on silicone layer characteristics was investigated. Initially, the nozzle position was set to 10 mm below the flange, the spray pressure was 2 bar and the time for pump dosing was specified to be 150 ms. The initial concentration of the silicone emulsion was 1.75 % (w/w).

A nominal screw setting of 1 mm, 2 mm and 3 mm corresponded to an absolute spray amount of 4.0 ± 0.5 mg, 16.1 ± 0.7 mg and 29.0 ± 0.4 mg silicone emulsion, respectively. These tested spray quantities largely covered the range of applicable screw settings from 0 mm to 3 mm. A lower spray quantity was not further considered since the screw setting for this condition (e.g. 0.5 mm) was not sufficiently accurate.

A spray quantity of 4 mg emulsion could be instantaneously dispersed into a fine spray for approximately 255 ms (Fig. IV-1). The fine emulsion droplets were not visible after deposition within the cartridge barrel due to the fast evaporation of emulsion water. A quantity of 16 mg resulted in an emulsion jet for 135 ms initially before atomization was reached for 125 ms. A quantity of 29 mg emulsion led to a long-lasting solution jet for 150 ms followed by a poor atomization for 115 ms. The latter two spray quantities rendered larger emulsion droplets in the barrel forming runlets that deposited on the flared cartridge edge.

The quality of atomization highly depends on the air-to-liquid mass ratio, which decreases with higher liquid flow rates [42–45], i.e., with higher spray quantities. A complete theory to describe atomizing principles has not been fully developed yet. Basically, it involves the tearing of the liquid into filaments at the nozzle orifice, referred to as liquid sheets, and then large droplets. Subsequently, the high relative velocity and frictional forces between the air and the liquid result in a break-up into smaller droplets. High velocity air readily penetrates low velocity liquids, thus yielding the necessary turbulence and energy transfer to form a spray [46]. However, thick liquid jets as obtained at higher spray quantities of 16 mg and 29 mg could not be readily penetrated and therefore atomization was incomplete with an initial, compact jet in the center of the spray [47].

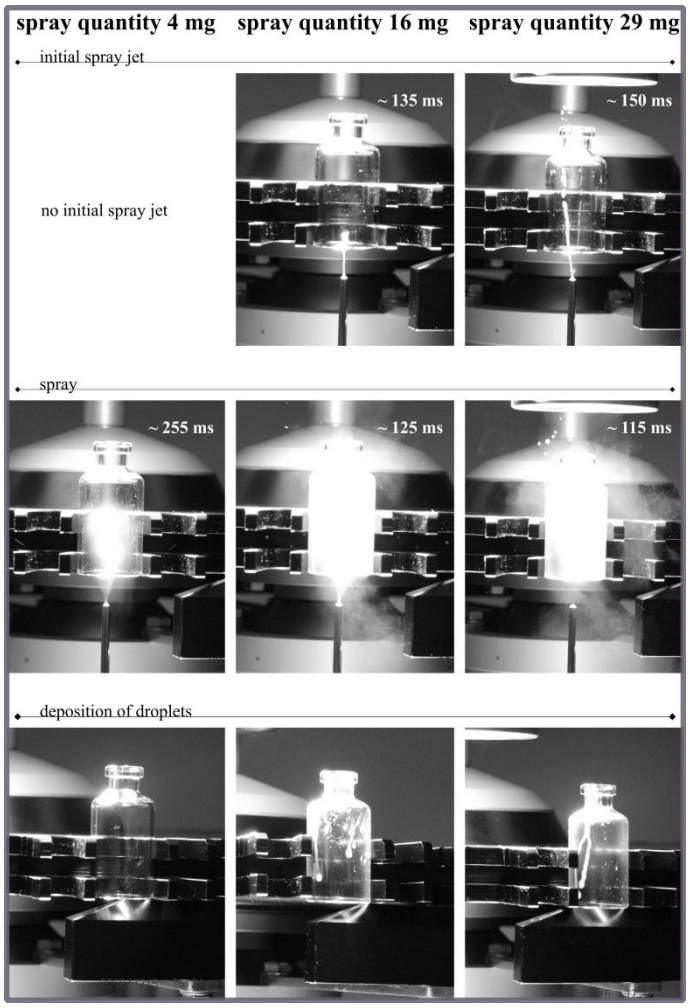

Fig. IV-1. High-speed images of a 4 mg, 16 mg, 29 mg spray quantity (10 mm nozzle position below the flange, spray pressure 2 bar, time for pump dosing 150 ms, 1.75 % (w/w) emulsion concentration).

The mean break-loose, minimum and maximum gliding forces were below 5 N regardless of the spray quantity (Fig. IV-2). The force profiles remained smooth and constant between 3 N to 5 N along the cartridge barrel (Fig. IV-2a). Interestingly, an increased spray quantity of 29 mg showed even slightly higher extrusion forces. A possible explanation for this observation could be that the long-lasting jet failed to sufficiently coat the inner glass barrel even though a high silicone quantity was deposited.

Overall, the theoretically sprayed silicone amount as derived from the absolute spray amount collected in tissue filled vials at an emulsion concentration of 1.75 % (w/w) increased from 70 ± 3 µg to 296 ± 1 µg to 504 ± 13 µg with the increase in spray quantity from 4 mg to 16 mg to 29 mg (Fig. IV-2b). This clear trend was not reflected in the baked-on silicone levels at the barrel inner surface (Fig. IV-2b). A spray quantity of 4 mg resulted in a baked-on silicone level of 33 ± 9 µg, a spray quantity of 16 mg in 171 ± 18 µg and a spray quantity of 29 mg in 164 ± 11 µg

as determined by FTIR. The difference between the sprayed silicone amount and the baked-on silicone level on the cartridge interior indicated a higher spray loss for larger spray quantities. This was reflected in the emulsion runlets depositing on the flared cartridge edge and the star wheel as well as spray blown out through the cartridge orifice as seen in the high-speed images. In particular for high spray quantities, also a rebound of the spray within the cartridge barrel and backward flow could be observed, which additionally increased the spray loss. It can be argued, that in addition to spray loss, silicone may be burned-off during heat-treatment at 316 °C for 12 min [31] (see chapter V). Overall, a good atomization process using low amounts of spray liquid appears to be important.

a. b.

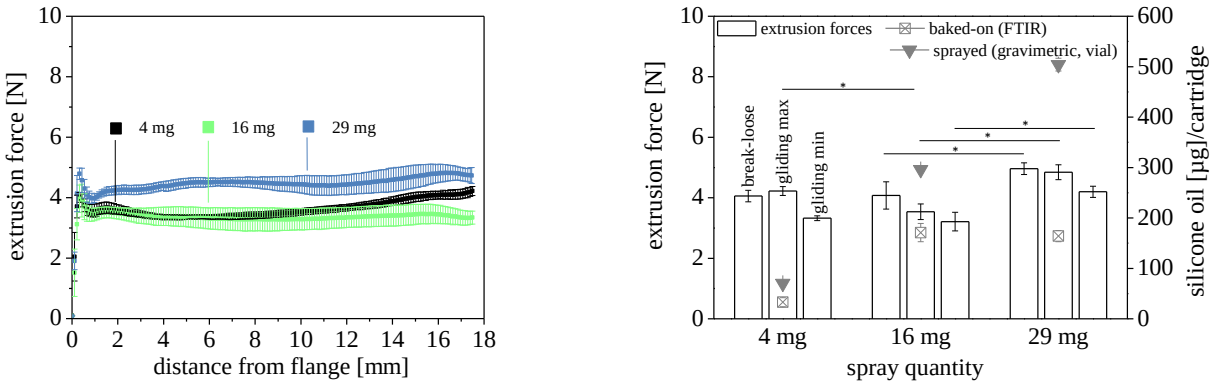

Fig. IV-2. Impact of a 4 mg, 16 mg, 29 mg spray quantity on (a) extrusion force profiles and (b) mean extrusion forces, baked-on silicone levels as determined by FTIR and theoretically sprayed silicone amounts derived from gravimetric vial analysis (* $p \leq 0.05$, ** $p \leq 0.01$, *** $p \leq 0.001$), (10 mm nozzle position below the flange, spray pressure 2 bar, time for pump dosing 150 ms, 1.75 % (w/w) emulsion concentration).

The baked-on silicone levels were below the range of 0.2-1 mg/barrel reported for sprayed-on 1 mL PFS [8,13,16–18,20–23]. Treatment at 16 mg and 29 mg spray quantities exceeded the silicone levels described for bake-on siliconization processes of < 0.1 mg/barrel [20,24,25] while at the same time leading to sub-optimal atomization and higher spray loss. Therefore, an approach to target sufficient and optimal baked-on silicone levels aimed to adapt the concentration of the silicone emulsion while maintaining a spray quantity of 4 mg, which has led to good atomization (see 3.2).

FTIR is a rapid method to quantify silicone with a reported LOQ down to 18 µg/mL [20,40] (see chapter III), but without the extraction of specific cartridge zones it fails to characterize the silicone distribution within the cartridge barrel. Therefore, additional 3D-LSM (LOQ ~ 10 nm,

see chapter III) was performed to analyze the thickness and distribution of the baked-on silicone layer (Fig. IV-3).

a.

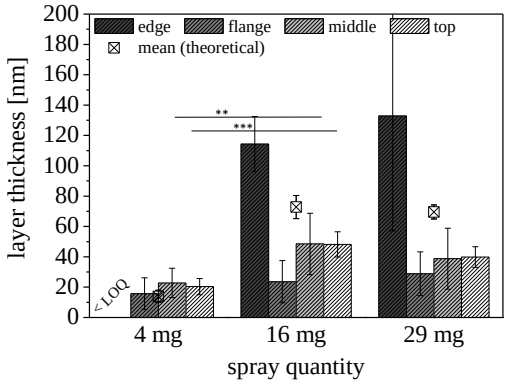

b.

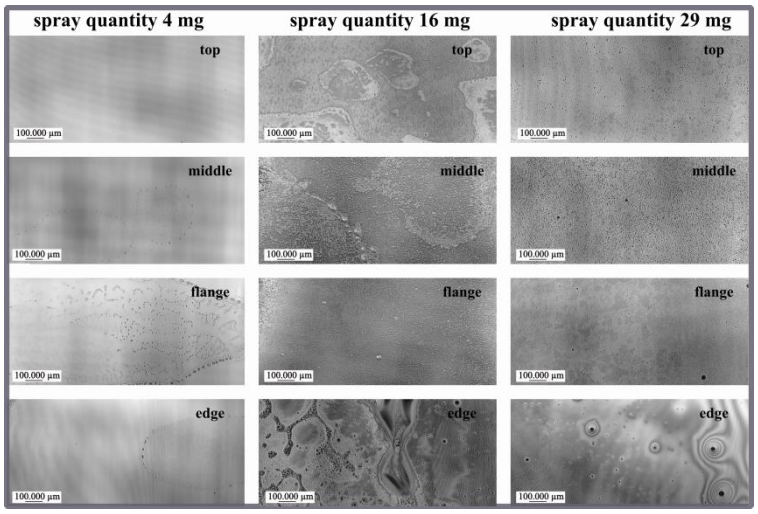

Fig. IV-3. 3D-LSM analysis after bake-on siliconization using a 4 mg, 16 mg, 29 mg spray quantity. (a) ALT in four different sections within the cartridge barrel (* $p \leq 0.05$, ** $p \leq 0.01$, *** $p \leq 0.001$) and (b) 3D-LSM images (10 mm nozzle position below the flange, spray pressure 2 bar, time for pump dosing 150 ms, 1.75 % (w/w) emulsion concentration).

A spray quantity of 4 mg led to a fine spray, which resulted in a thin, homogenous baked-on silicone layer of 16-23 nm from flange to top (Fig. IV-3a). 3D-LSM better imaged thin, baked-on silicone layers compared to optical microcopy [40] (see chapter III), but the baked-on silicone layer obtained by a spray quantity of 4 mg was even too thin to be clearly visualized by 3D-LSM (Fig. IV-3b). Spray quantities of 16 mg and 29 mg emulsion led to runlets forming 114-133 nm build-ups at the flared cartridge edge. These thicker, baked-on silicone layers showed plaque-like and micro-droplet structures comparable to sprayed-on silicone layers [9,17,18]. For both quantities, the ALT at the flange was 24-29 nm and increased at the middle and the top to 40-

48 nm. These thinner, baked-on layers exhibited a homogeneous micro-structure without any plaques or droplets. Furthermore, the 3D-LSM images showed more pronounced layer patterns at the middle and top, thereby reflecting the measured ALTs. This effective siliconization in the middle and top region could be attributed to the initial nozzle-to-flange distance of 10 mm, where the spray cone mainly reached the upper part of the cartridge (see 3.1.2). Thus, the different atomization qualities were reflected in the baked-on silicone layer distributions.

A theoretical layer thickness of 14 nm for 4 mg, 73 nm for 16 mg and 70 nm for 29 mg spray quantity calculated from FTIR analysis was in good agreement with the ALT obtained from 3D-LSM measurement (4 mg: 14 nm, 16 mg: 59 nm, 29 mg: 60 nm) (Fig. IV-3a). A spray quantity of 29 mg did not lead to thicker silicone layers compared to a spray quantity of 16 mg due to a markedly observed spray loss as discussed above.

Low and uniform extrusion forces are critical quality attributes. They did not benefit from high spray quantities and silicone accumulation at the flared cartridge edge. On the contrary, these higher silicone amounts may migrate to the cartridge lower edge and drip out onto the tub insert sheet when stored tip-up as observed in spray-on siliconized PFS [20]. During storage in horizontal position, silicone migration led to an increase of the silicone layer thickness from initially 350 nm to 1600 nm at the bottom-line already after three days [17].

Based on these result, a spray quantity of 4 mg was suggested as optimum within the tested range due to an improved atomization quality, adequate baked-on silicone levels in combination with low extrusion forces and most homogeneous, thin baked-on silicone layers. A lower range was not possible to be tested due to technical limitations.

3.1.2 IMPACT OF NOZZLE POSITION BELOW THE FLANGE

The nozzle position below the flange substantially affects the distribution of both the sprayed emulsion within the cartridge barrel and consequently the baked-on silicone layer later-on. Therefore, fixed nozzle positions of 0 mm, 10 mm, 20 mm, 30 mm and 40 mm below the cartridge flange were investigated while the initial spray quantity was 16 mg, the spray pressure was set to 2 bar and the spray time was specified to be 150 ms based on initial specifications of the manufacturer. The initial concentration of the silicone emulsion was 1.75 % (w/w).

At a fixed nozzle position of 0 mm close to the flange the spray mostly hit the middle and top of the cartridge while the flange was not reached (Fig. IV-4a). In addition, the spray was partially blown out through the cartridge orifice. Increasing the distance between nozzle and flange to

10 mm and 20 mm improved the spray distribution in the cartridge. At 20 mm the spray cone exactly reached the flange while the middle and top were still coated with emulsion. Longer nozzle-to-flange distances of 30 mm and 40 mm led to off-spray with emulsion passing outside the circumference of the cartridge barrel or being rebounded at the lower edge of the cartridge. Therefore, a nozzle position of 20 mm below the flange was suggested to yield an optimum distribution of the silicone emulsion over the entire barrel.

a.

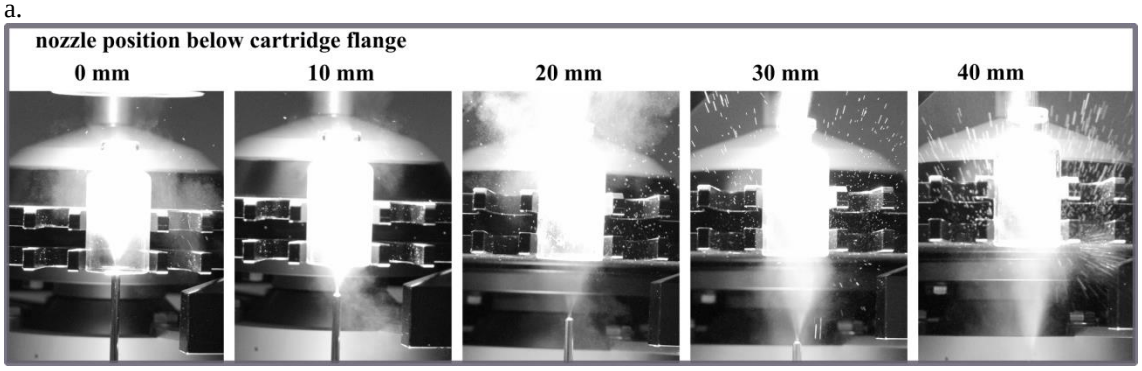

b.

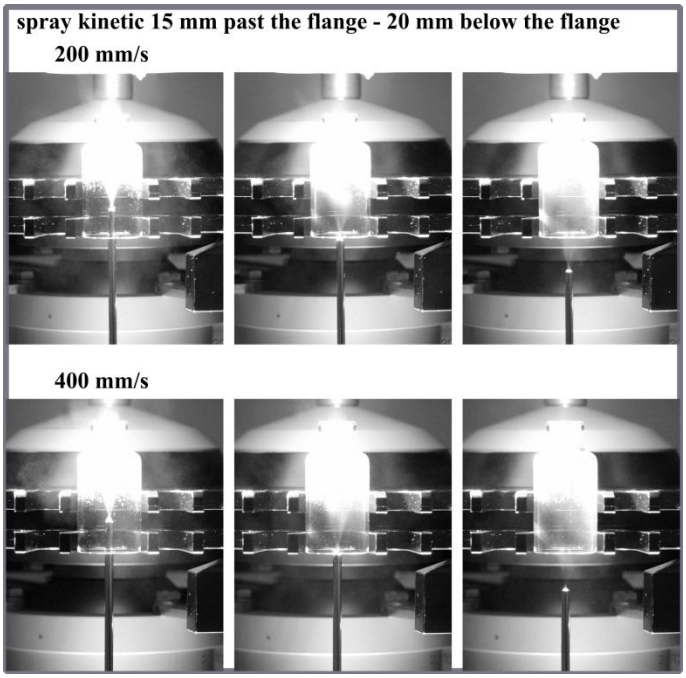

Fig. IV-4. High-speed images of (a) fixed nozzle positions 0-40 mm below the flange and (b) dynamic nozzle positions 15 mm past the flange to 20 mm below the flange at a retraction speed of 200 mm/s and 400 mm/s (16 mg spray quantity, spray pressure 2 bar, time for pump dosing 150 ms, 1.75 % (w/w) emulsion concentration).

Recently, diving and retracting nozzle positions were reported to be superior to the currently used static systems [12,13,16,20,25]. Therefore, retracting the nozzle position at 200 mm/s and 400 mm/s from 15 mm past the flange to 20 mm below the flange was investigated. In theory,

this should provide a sufficient siliconization at both the upper cartridge barrel and the flange. A slower retraction speed was shown to improve the silicone distribution in PFS as it offsets the upward velocity of the spray droplets less than higher retraction velocities. Thus, with faster downward retraction the spray fails to reach the needle-end of the barrel [13]. Conceptually, during the dosing step, the piston rotates at maximum speed for 180° to deliver a constant rate of spray medium. The initial and the subsequent 90° rotation are used to accelerate and brake the piston speed [7]. However, in this study, it was observed that initially a dense spray deposited at the top of the cartridge barrel, while with proceeding retraction the spray attenuated independent of the applied retraction speed (Fig. IV-4b.). These findings suggested that retracting the nozzle position yielded an inhomogeneous distribution. Therefore, fixed nozzle positions of 0-40 mm below the flange were further studied instead.

Independent of the nozzle position, the mean break-loose, minimum and maximum gliding forces remained below 6 N. A nozzle position of 0 mm below the flange revealed slightly higher mean extrusion forces (Fig. IV-5a and Fig. IV-5b) (will be discussed below).

a. b.

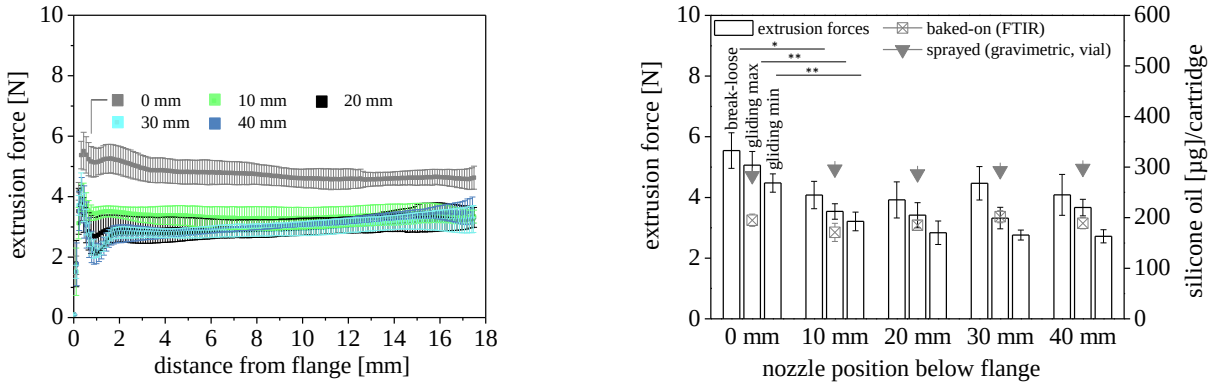

Fig. IV-5. Impact of fixed nozzle positions 0-40 mm below the flange on (a) extrusion force profiles and (b) mean extrusion forces, baked-on silicone levels as determined by FTIR and theoretically sprayed silicone amounts derived from gravimetric vial analysis (* $p \leq 0.05$, ** $p \leq 0.01$, *** $p \leq 0.001$), (16 mg spray quantity, spray pressure 2 bar, time for pump dosing 150 ms, 1.75 % (w/w) emulsion concentration).

The baked-on silicone levels were systematically lower (171 ± 18 µg to 202 ± 12 µg) than the absolute spray amount ranging between 287 ± 6 µg and 297 ± 6 µg independent of the nozzle position (Fig. IV-5b). Thus the total spray loss due to blowing out of emulsion through the cartridge orifice (particularly for higher nozzle positions), rebound of the spray within the cartridge barrel, backward flow out, and off-spray passing the circumference of the barrel (particularly for lower nozzle positions) was more or less independent of the nozzle position.

The impact of the nozzle position on the distribution of the baked-on silicone level was characterized by extracting specific cartridges zones. The total baked-on silicone level as the sum of the individual zone extractions ranged from 167 ± 16 µg to 197 ± 18 µg and was comparable to the respective baked-on silicone levels after extraction of the entire cartridge barrel (Tab. IV-1).

Tab. IV-1. Impact of fixed nozzle positions 0-40 mm below the flange on the baked-on silicone levels after extraction of the entire cartridge barrel and as the sum of individual zone extractions and subsequent FTIR analysis (16 mg spray quantity, spray pressure 2 bar, time for pump dosing 150 ms, 1.75 % (w/w) emulsion concentration).

Nozzle position below flange	Baked-on silicone level after extraction entire cartridge barrel [µg]	Baked-on silicone level as sum of individual zone extractions [µg]
0 mm	195 ± 12	197 ± 18
10 mm	171 ± 18	167 ± 16
20 mm	185 ± 10	187 ± 17
30 mm	202 ± 12	192 ± 18
40 mm	189 ± 11	178 ± 17

Consequently, the silicone distribution was further described as relative baked-on silicone contents within the specific cartridge areas (Fig. IV-6).

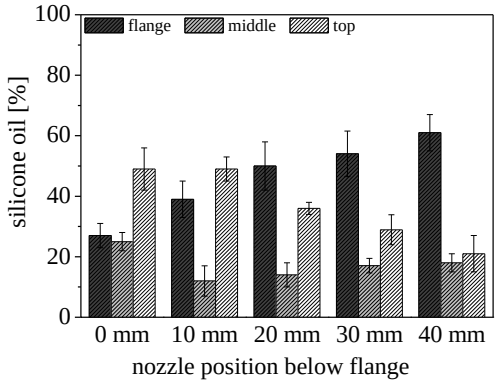

Fig. IV-6. Impact of fixed nozzle positions 0-40 mm below the flange on the relative baked-on silicone levels after individual zone extractions and subsequent FTIR analysis (16 mg spray quantity, spray pressure 2 bar, time for pump dosing 150 ms, 1.75 % (w/w) emulsion concentration). Note that during flange extraction, silicone was also extracted from the cartridge edge.

At a nozzle position of 0 mm and 10 mm below the flange, approximately 50 % baked-on silicone was recovered from the top region of the cartridge. The remaining 50 % silicone were distributed in the middle and flange region while at a nozzle position of 0 mm the amount in the middle region was slightly increased to 25 % compared to maximum 20 % at all other nozzle

positions. Longer nozzle-to flange distances of 20 mm, 30 mm and 40 mm led to a gradual increase of the baked-on silicone in the flange region up to 60 % at 40 mm at the expense of lower silicone ratios in the top region. The relative silicone content in the middle zone needs to be interpreted with caution since it was systematically reduced due to the spreading of the solvent during the extraction of the flange and top zones as observed in 3D-LSM (data not shown). Overall, the nozzle position substantially affected the silicone distribution along the cartridge barrel. Thus, the quantification of relative silicone contents within the different cartridge sections in addition to the total baked-on silicone level was crucial.

a.

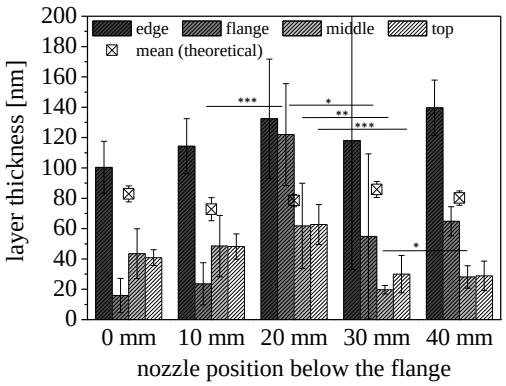

b.

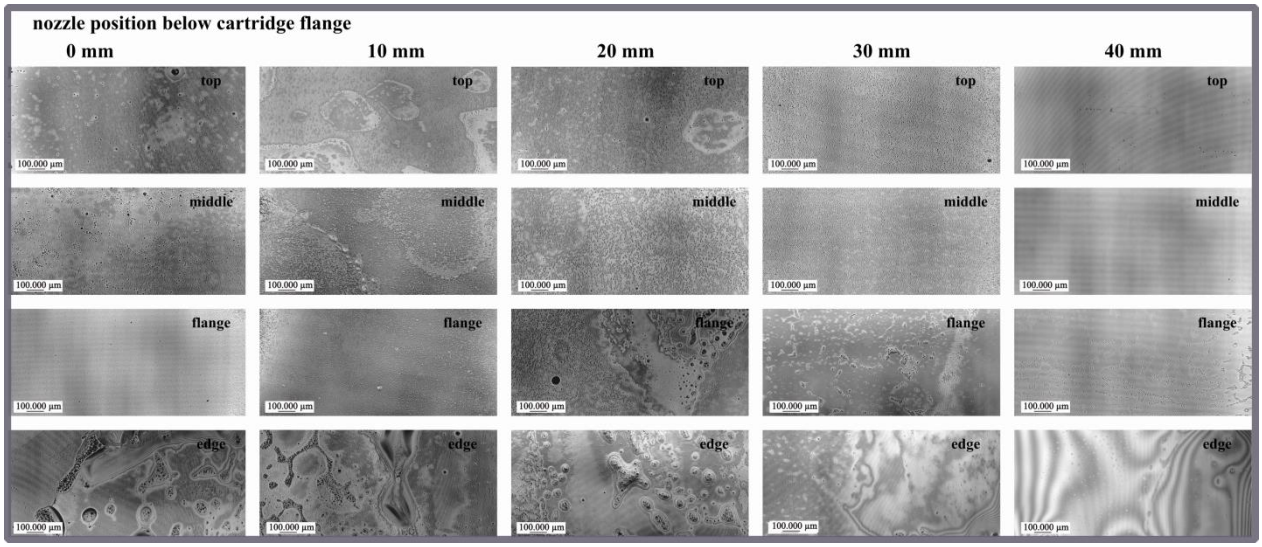

Fig. IV-7. 3D-LSM analysis after bake-on siliconization using nozzle positions from 0-40 mm below the flange. (a) ALT in four different sections within the cartridge barrel (* $p \leq 0.05$, ** $p \leq 0.01$, *** $p \leq 0.001$) and (b) 3D-LSM images (16 mg spray quantity, spray pressure 2 bar, time for pump dosing 150 ms, 1.75 % (w/w) emulsion concentration).

The thickness and distribution of the baked-on silicone layer was additionally characterized using 3D-LSM (Fig. IV-7). Independently of the nozzle position, the medium spray quantity of 16 mg partially drained off and induced thicker baked-on silicone layers of 100-140 nm at the flared cartridge edge (Fig. IV-7a). A thin silicone layer at the flange (16 nm and 24 nm, respectively) resulted at 0 mm to 10 mm nozzle-to-flange distances. At 20 mm the spray cone exactly reached the flange, which led to a thicker layer of 122 nm. At 30 mm to 40 mm nozzle positions, where the spray cone partially missed the cartridge, the thickness of the flange layer was decreased to 55-65 nm as compared to a nozzle-to-flange distance of 20 mm. The layer thickness at the middle and top was comparable for 0 mm to 20 mm nozzle-to-flange distances with 41 nm to 63 nm. At longer nozzle-to-flange distances of 30 mm to 40 mm the spray cone partially missed the circumference of the cartridge barrel, which led to decreased layer thicknesses of 20-30 nm at the middle and top. These quantitative data corresponded to the 3D-LSM images (Fig. IV-7b).

Overall, thin, baked-on silicone layers in the range of 15-65 nm showed a homogeneous micro-structure. As a result of emulsion runlets, thicker, baked-on silicone layers ranging from 100-140 nm were formed, which showed plaque-like and micro-droplet structures close to the flared cartridge edge. These structures are known from spray-on silicone layers [9,17,18].

Regardless of the nozzle position, the theoretical layer thicknesses calculated from FTIR analysis of approximately 73-86 nm were slightly higher compared to the ALT measured in 3D-LSM (0 mm: 51 nm, 10 mm: 59 nm, 20 mm: 95 nm, 30 mm: 56 nm, 40 mm: 66 nm) (Fig. IV-7a). Comparably, silicone levels quantified by AAS analysis following toluene extraction [17] or calculations using the silicone levels obtained from the PFS manufacturer and the inner barrel surface [9] were systematically higher than silicone contents obtained from vertical scanning interferometry (VSI) layer analysis. This can be either attributed to an inhomogeneous silicone distribution along the cartridge barrel depicting plaque-like structures [9,17] or limitations of VSI, which underestimates higher silicone levels due to multiple, interfering thickness values, when thick silicone droplets are formed [20]. However, for rather homogeneous silicone layers, the theoretical silicone levels derived from VSI are in good agreement with quantified silicone levels from FTIR [20].

Overall, the nozzle position below the flange was a key factor for the distribution of the baked-on silicone layer and its extrusion performance. A nozzle position of 20 mm below the flange was optimal as it led to a pronounced deposition of silicone emulsion at the flange. The thicker silicone layer and the increased relative baked-on silicone content at the flange particularly

facilitated smooth break-loose of the piston during injection. The homogeneous silicone layer at the middle and top of the cartridge enabled to sustain a smooth gliding of the piston along the cartridge barrel. On contrary, an insufficient siliconization at the flange as obtained from a nozzle position of 0 mm below the flange increased the extrusion forces. Thus, a certain amount of silicone was required at the flange for lubrication of the piston, in particular the flared ribs, which were in direct contact with the container wall. Additionally, it can be argued, that a sufficient siliconization at the flange substantially contributed to smooth piston gliding along the entire barrel as silicone is pushed forward by the piston movement [13] (see 3.3).

For longer cartridges or syringe barrels, this nozzle position of 20 mm below the flange may not be optimal. Wen *et al.* reported a significant increase of extrusion forces, or even worse stalling of the piston, at the end of injection for 1 mL syringes due to a silicone-rich flange and much less silicone at the needle-side [9]. Overall, fixed nozzle positions most commonly resulted in steadily decreasing silicone layers from flange to top ranging from 900 nm to 0 nm and 400 nm to 50 nm for “1 x” and “2 x” silicone levels, respectively [16], 600 nm to 100 nm [17] or even worse from 1-2 µm to approximately 250 nm [25]. Pronounced staining with talcum or glass powder of the flange and middle but not of the needle-side were observed [12,13,25]. Consequently, malfunctions during injection could be attributed to inhomogeneous silicone distributions along the cartridge barrel.

Recently, spray-on siliconization using diving nozzle positions were suggested to improve layer thickness homogeneity, thereby providing low extrusion forces and homogeneous coverage with talcum or glass powder [12,13,16,18,20,25]. Independent of the barrel position, sprayed-on silicone layers were initially 100-250 nm and after filling with protein formulation 50-150 nm thick, thereby yielding constant and smooth extrusion forces below 15 N along the 1 mL syringe barrel [18]. VSI layer profiles after diving nozzle siliconization demonstrated approximately 400 nm thick silicone layers at 0-35 mm barrel distance and the silicone layer thickness steadily decreased to 150 nm towards the needle-side at 50 mm [20]. Felsovalyi *et al.* reported homogeneous silicone layers ranging from 200 nm to 350 nm up to 40 mm barrel length followed by a drop in layer thickness to approximately 50 nm towards the needle-side at 50 mm [16]. In addition, diving nozzle position and a spray start close to the needle-side may yield the opposite extreme distribution compared to fixed nozzle positions, i.e., a pronounced siliconization at the needle-side with 300-600 nm thick layers and only 100 nm thick silicone layers at the flange [17]. Besides, the layer distribution after diving nozzle siliconization may be less reproducible [25].

There is no clear trend in literature, whether an insufficient siliconization at the flange or needle-side is more troublesome for functionality. In this study, the tailored bake-on siliconization process enabled defined, consistent silicone distributions, which correlated well with the applied spray positions and initial distribution of the sprayed emulsion. Thereby, the negative impact of an inadequate silicone distribution, e.g., an insufficient siliconization at the flange, was reflected in the extrusion profile.

3.1.3 IMPACT OF SPRAY PRESSURE AND TIME FOR PUMP DOSING

Parameters were selected to cover two extremes within the possible setting range (4-29 mg spray quantity, spray pressure 0.8-2.5 bar, time for pump dosing 60-175 ms) for either spraying small droplets (4 mg spray quantity, spray pressure 2.5 bar, time for pump dosing 175 ms) or large droplets (29 mg spray quantity, spray pressure 1 bar, time for pump dosing 60 ms) (Fig. IV-8). The nozzle position was set to 20 mm below the flange. The concentration of the silicone emulsion was 1.75 % (w/w).

At 2.5 bar a low spray quantity of 4 mg was atomized into a fine spray regardless of the pump dosing time. At pump dosing for 175 ms, a high spray pressure of 2.5 bar did not improve atomization, but led to uncontrolled splashing and an increased spray loss compared to a spray pressure of 1 bar (Fig. IV-8a). Regardless of the spray conditions, a high spray quantity of 29 mg resulted in a preliminary solution jet (Fig. IV-8b). A low spray pressure of 1 bar and a short time for pump dosing of 60 ms resulted in worst spray conditions: only a weak spray was achieved, shortly before the spray process ended. For a steady and fine atomized spray a prolonged time for pump dosing of 175 ms was crucial.

Atomization quality and droplet size are a direct function of the air-to-liquid mass ratio and are affected by the applied spray pressure, spray quantity and time for pump dosing. Droplet size decreases with higher air-to-liquid ratios and approaches an asymptote for a given nozzle design [13,42–44]. Therefore, a longer time for pump dosing of 175 ms compared to 60 ms resulted in a slower flow rate and increased the air-to-liquid ratio by a factor of three. Consequently, the atomization of a high spray quantity was improved. However, high spray pressure did not show the same beneficial effect although the air-to-liquid mass ratio was increased by a factor of 2.5. Juslin *et al.* reported that an insufficient spray pressure was not able to atomize fast flowing solutions, i.e., high spray amounts, which led to an increased volume of larger droplets [44]. It can be concluded, that a spray pressure of 2.5 bar was still too low to efficiently penetrate the

thick liquid jet of a high spray quantity and simply accelerated the jet to the air velocity, thereby minimizing the shear forces between air and liquid without inducing atomization [47]. Besides, the "true" pressure at the nozzle orifice could have been lower compared to the given gauge pressure [13]. In addition, high velocity air streams are suggested to initially form oscillating liquid surface and cavities of swirling air at the nozzle edge prior to disintegration [42,47]. Consequently, high spray pressure may result in initially turbulent, vibrating air cavities, which lead to a sudden, less controlled disintegration of the fed liquid and therefore increased spray loss (Fig. IV-8a). High spray pressure additionally disperses droplets farther [13], which contributes to the observed spray loss.

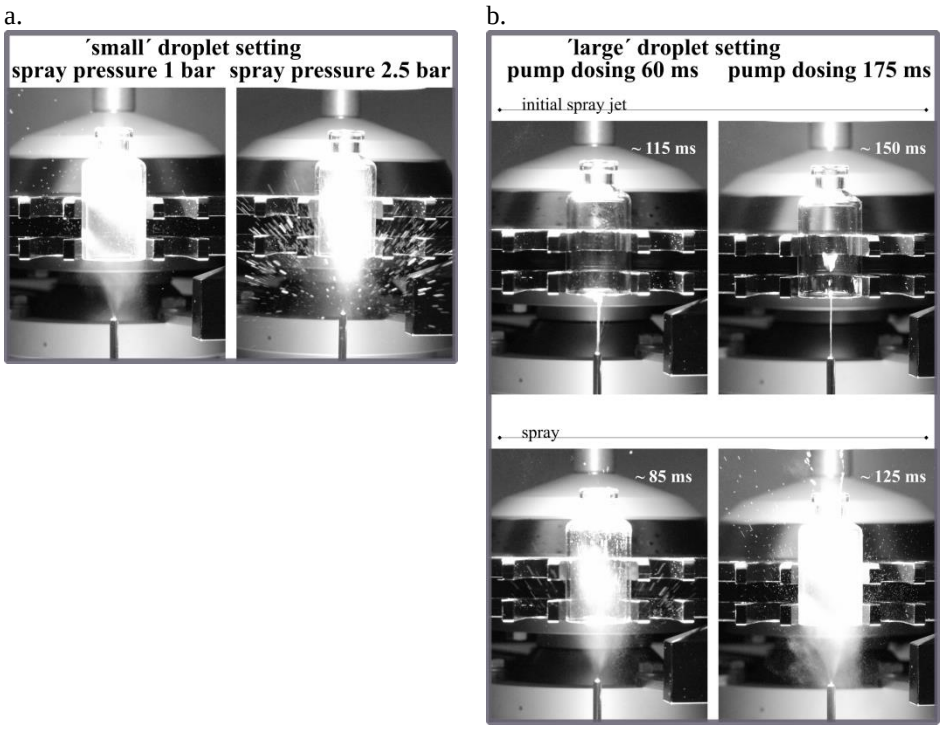

Fig. IV-8. High-speed images of (a) ´small´ droplet setting (4 mg spray quantity, time for pump dosing 175 ms, exemplary different spray pressures 1 bar vs. 2.5 bar) and (b) ´large´ droplet setting (29 mg spray quantity, spray pressure 1 bar, exemplary different times for pump dosing 60 ms vs. 175 ms). The nozzle position was set to 20 mm below the flange. The concentration of the silicone emulsion was 1.75 % (w/w).

Based on these findings, a prolonged time for pump dosing of 175 ms and a low spray pressure of 1 bar were most beneficial for atomization. High-speed imaging was presented as a valuable and fast approach to characterize the spray process. Further studies could aim to measure droplet size and distribution by more advanced techniques such as laser diffraction and phase-Doppler anemometry [46–48].

3.1.4 OPTIMIZED SPRAY PARAMETERS IN A BAKE-ON SILICONIZATION PROCESS – FINAL CONSIDERATIONS

Based on previous experiments, a low spray quantity of 4 mg resulted in a fine spray and was adequate to yield thin, but sufficient baked-on silicone layers. A nozzle position of 20 mm below the flange was chosen for optimal distribution of the silicone emulsion within the cartridge barrel. At 20 mm the spray cone exactly reached the cartridge flange and led to thicker, baked-on silicone layers of approximately 122 nm at the flange, thus ensuring functionality of the injection device in particular during break-loose of the piston. A prolonged time for pump dosing of 175 ms was crucial for a steady, fine spray, whereas a high spray pressure of 2.5 bar was not beneficial. On the contrary, a high spray pressure increased the spray loss near the flange compared to a lower spray pressure of 1 bar.

For further fine tuning, a spray quantity of 4 mg and alternatively 16 mg was dispersed using either an optimized nozzle position of 20 mm below the flange, a low spray pressure of 1 bar and a long time for pump dosing of 175 ms (Fig. IV-9a); or an initial nozzle position of 10 mm below the flange, a spray pressure of 2 bar and a time for pump dosing of 150 ms (see 3.1.1).

A spray quantity of 4 mg was immediately dispersed into a fine spray (Fig. IV-9a). An optimized pressure/time setting of 1 bar/175 ms did not further improve the atomization quality. On the contrary, for a spray quantity of 16 mg an improved pressure/time setting was beneficial. The previous solution jet was reduced to a marginal, conical tip initially followed by break-up into a strong spray.

Finally, experiments with nozzle positions of 15 mm, 20 mm and 25 mm below the flange were performed to further specify the optimal nozzle position (Fig. IV-9b). Overall, all three nozzle positions could be applied for a homogeneous coating of the cartridge barrel with silicone emulsion. However, at a nozzle position of 15 mm below the flange, the spray did not reach the flange well. A nozzle position of 20 mm below the flange was confirmed to be optimal as the spray cone exactly reached the cartridge flange. At 25 mm below the flange, the spray cone tended to pass the circumference of the cartridge barrel, thereby presumably increasing spray loss.

Fig. IV-9. High-speed images of an optimized spray process using (a) 4 mg and 16 mg spray quantity and (b) fixed nozzle positions of 15-25 mm below the flange (1.75 % (w/w) emulsion concentration; optimized spray parameters: spray pressure 1 bar, time for pump dosing 175 ms).

Based on these final experiments, a low spray quantity of 4 mg, and alternatively 16 mg silicone emulsion, a fixed nozzle position of 20 mm below the flange, a low spray pressure of 1 bar and a long time for pump dosing of 175 ms were identified as optimal spray parameters.

3.2 VARIATION OF THE SILICONE EMULSION CONCENTRATION

In addition to the spray parameters discussed in the previous chapters, the concentration of the silicone emulsion was further investigated to adjust the baked-on silicone level. An optimized spray quantity of 4 mg, a nozzle position of 20 mm below flange, a spray pressure of 1 bar and a time for pump dosing of 175 ms were adapted from previous experiments.

Siliconization with emulsions ranging from 0.175 % (w/w) to 3.5 % (w/w) silicone oil content resulted in steadily increasing baked-on silicone levels from 4 ± 1 µg to 94 ± 6 µg (Fig. IV-10). A 0.06 % (w/w) emulsion yielded levels below the LOQ of 18 µg/mL, i.e., below 4 µg/cartridge [40] (see chapter III). Correspondingly, the maximum gliding forces decreased from 34 ± 5 N to 4 ± 0 N with increasing concentrations from 0.06 % (w/w) to 1.2 % (w/w) and remained constant at approximately 4 N at higher concentrations of 1.75 % (w/w) and 3.5 % (w/w). The break-loose and minimum gliding forces showed the same trend, but less pronounced, with break-loose forces decreasing from 13 ± 1 N to 4 ± 1 N. The minimum gliding forces decreased from 11 ± 1 N to 3 ± 1 N.

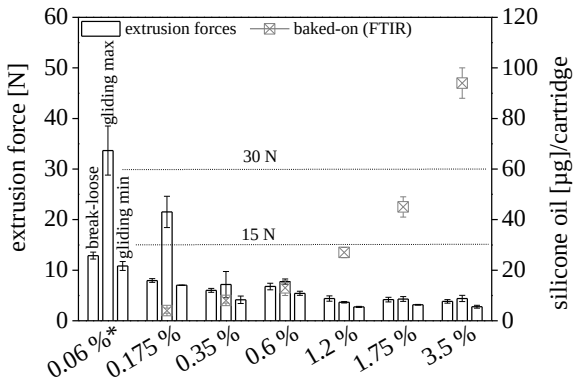

Fig. IV-10. Extrusion forces and baked-on silicone levels as determined by FTIR using silicone emulsion concentrations from 0.06 % (w/w) to 3.5 % (w/w) (optimized spray parameters: spray quantity 4 mg, fixed nozzle position of 20 mm below the flange, spray pressure 1 bar, time for pump dosing 175 ms). Asterisks indicate baked-on silicone levels below the LOQ of 18 µg/mL, i.e., < 4 µg/cartridge based on 250 µL dissolution volume [40] (see chapter III).

Reliable functionality over the product shelf life is a highly important parameter for a drug/device combination product. A baked-on silicone level of 8 ± 1 µg at an emulsion concentration of 0.35 % (w/w) was sufficient to achieve break-loose forces below 30 N and gliding forces below 15 N, which were considered as acceptable reference values in this study. A baked-on silicone level of 13 ± 3 µg, i.e., an emulsion concentration of 0.6 %, was used as assurance level for further experiments. Certainly, both break-loose and gliding forces have to be carefully assessed

for each combination product depending on the formulation, drug/device combination product technical features, intended user population and shelf life as well as technical requirements. In the literature, maximum forces for a manual injection were discussed being at 30 N [49] and rheumatoid arthritis patients could even exert maximum forces up to 45 N [50]. Patient-friendly injection was reported with gliding forces up to 15-20 N [51] while for empty cartridges a limit of 10 N is suggested in EN ISO 11608-3 [52]. Consequently, limited baked-on silicone levels as low as 10 µg were adequate to maintain functionality in this study.

The silicone layer may experience a phase transition upon contact with aqueous media as observed for other hydrophobic material layers [53]. The extrusion forces may thus be a function of different filling media due to a change in de-wetting behavior. In an exemplary experiment, different filling media did not affect the extrusion performance for cartridges siliconized with 4 mg of a 0.6 % (w/w) silicone emulsion and filled with either highly purified water or placebo (supporting Information Fig. S IV-2).

Talcum suspension was utilized for first visual assessment of the silicone level and its distribution over the cartridge barrel. Talcum did not adhere to cartridges siliconized with only 0.06 % (w/w) or 0.175 % (w/w) emulsions (Fig. IV-11). With increasing the concentrations from 0.35 % (w/w) to 3.5 % (w/w), talcum more adequately coated the container wall and the talcum distribution became improved, but still less coated areas remained at the top.

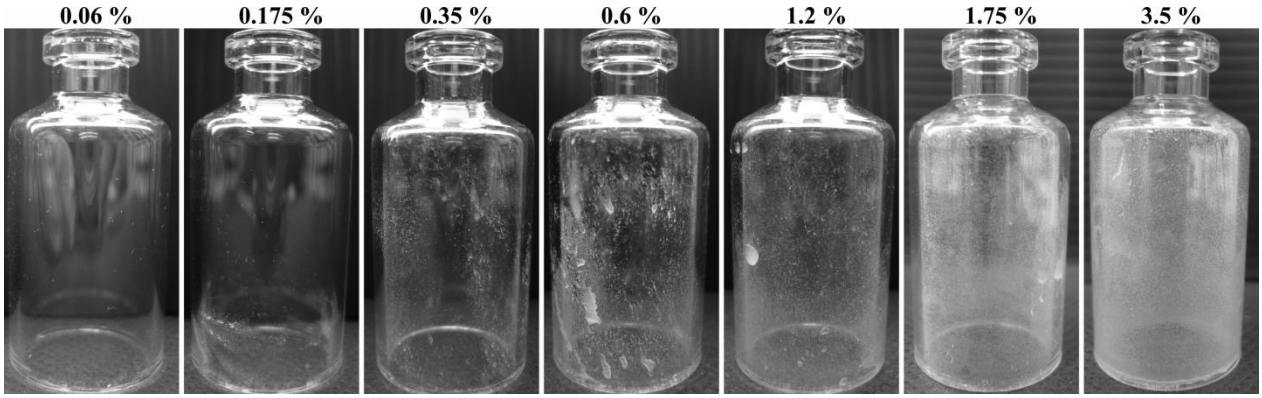

Fig. IV-11. Distribution of talcum suspension in cartridges coated with silicone emulsion concentrations from 0.06-3.5 % (w/w) (optimized spray parameters: spray quantity 4 mg, fixed nozzle position of 20 mm below the flange, spray pressure 1 bar, time for pump dosing 175 ms).

These observations were confirmed by 3D-LSM measurements (Fig. IV-12). Silicone layers obtained from 0.06-0.6 % (w/w) emulsions were thinner than the LOQ of 10 nm. 1.2 % (w/w) to 3.5 % (w/w) emulsions led to increasing baked-on silicone layers from 15 nm to 50 nm at the

flange (Fig. IV-12). The middle and top section revealed lower ALTs compared to the flange increasing from approximately 10 nm and below the LOQ to 20 nm and 40 nm, respectively. The pronounced siliconization of the flange was typical for the optimized nozzle position of 20 mm below the flange (see 3.1.2).

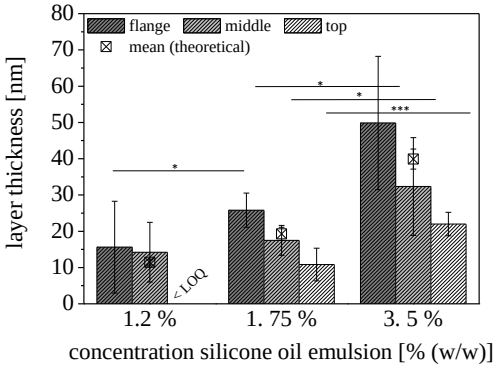

Fig. IV-12. 3D-LSM analysis after bake-on siliconization using silicone emulsion concentrations from 0.06-3.5 % (w/w) ALT in three different sections within the cartridge barrel (* $p \leq 0.05$, ** $p \leq 0.01$, *** $p \leq 0.001$) (optimized spray parameters: spray quantity 4 mg, fixed nozzle position of 20 mm below the flange, spray pressure 1 bar, time for pump dosing 175 ms).

The theoretical layer thicknesses calculated from FTIR quantification ranged from 11 nm to 40 nm and were in excellent agreement with the ALTs determined by 3D-LSM (1.2 % (w/w): 13 nm, 1.75 % (w/w): 18 nm, 3.5 % (w/w): 35 nm). It was demonstrated, that both FTIR and 3D-LSM were capable to describe the thickness of thin baked-on layers provided that an optimized siliconization process was established in advance.

Consequently, the study confirms that higher silicone emulsion concentrations (i.e., baked-on silicone levels and layer thicknesses) result in better functionality [13], but the extrusion forces reached a plateau value and were not further decreased, even when the emulsion concentration was further increased. Buch *et al*. observed a moderate reduction in break-loose and gliding forces from 4 N to 3 N with increasing the concentration of silicone oil in heptane solutions from 0.5 % to 1 % (dip siliconization was used) [15]. Spray-on silicone levels ranging from 0.2 mg-0.6 mg/barrel were reported to decrease gliding forces from 1.8 N to 0.5 N while the break-loose forces remained constant with approximately 2 N [25]. In both cases the actual silicone layer thickness is not known. But, high levels of silicone are prone to migration, thereby increasing silicone-related particulates and turbidity [23,28,54–57]. This could create artefacts during particulate measurements, that are, however, likely not relevant and of impact for product quality. Silicone has been discussed being a concern related to silicone-protein interactions, but adequate

formulation development, e.g., the addition of surfactant can hamper or even inhibit silicone-protein interactions with regard to adsorption and aggregation [58–62]. The reported protein instabilities are rather attributed to synergistic effects of silicone, elevated temperature [21,63], agitation [22,23,26,60,62,64], agitation at increased temperatures [60] or periodically rupture of the silicone oil-water interface [59]. Based on this study, a low, but sufficient baked-on silicone level of 13 ± 3 µg corresponding to a layer thickness of less than 10 nm was suggested as optimum.

3.3 EXTRUSION FORCES DURING STORAGE

The functional performance of the baked-on silicone layer obtained after siliconizing cartridges with 0.6 % (w/w) and 1.2 % (w/w) silicone emulsion was further assessed during storage for 80 weeks at room temperature. The baked-on silicone levels were 13 ± 3 µg and 27 ± 2 µg, respectively. Optimized spray parameters (spray quantity 4 mg, fixed nozzle position of 20 mm below flange, spray pressure 1 bar, time for pump dosing 175 ms) were adapted from previous experiments.

Initially, a baked-on silicone level of 13 ± 3 µg and 27 ± 2 µg resulted in mean extrusion forces of 5-8 N (Fig. IV-13a) and 3-6 N (Fig. IV-13b), respectively After storage, the low baked-on silicone level of 13 ± 3 µg showed a gradual increase in the mean break-loose and maximum gliding forces to 21-22 N (Fig. IV-13a). The increase for the higher silicone level was moderate to 10-12 N (Fig. IV-13b). The minimum gliding forces marginally increased for both silicone levels. The increase of both break-loose and gliding forces could be explained by the respective extrusion force profiles (Fig. IV-13c) along the cartridge barrel and 3D-LSM images (Fig. IV-14). The initial force profile of a 13 µg baked-on silicone cartridge was smooth with an increase in the gliding forces from 5 N to 8 N towards the barrel end (Fig. IV-13c). After fitting the piston into the container, the piston ribs were sufficiently lubricated. The baked-on silicone was visualized by 3D-LSM between the piston ribs and the container wall (Fig. IV-14a). During expelling, this contact area lost silicone. Thereby, the piston ribs became less lubricated (Fig. IV-14b), which resulted in an increase in gliding forces towards the top of the cartridge barrel. The baked-on silicone did not leach into the fill medium (see chapter VI), but rather accumulated between the upper piston plateau and the container wall (Fig. IV-14c). In addition, the baked-on silicone layer at the top was initially thinner (Fig. IV-12), which contributed to the lack of siliconization of the piston ribs towards the top of the cartridge.

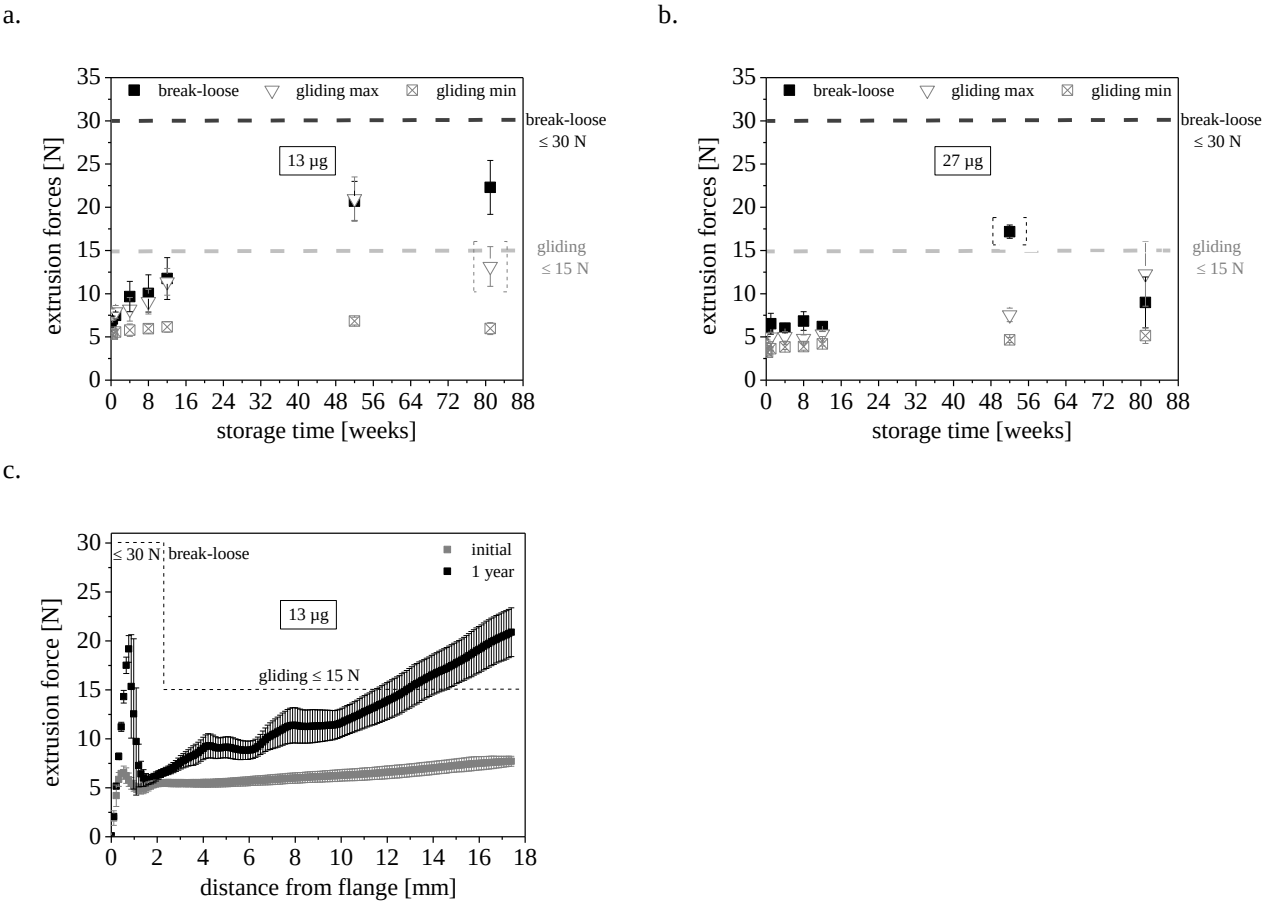

Fig. IV-13. Extrusion forces after bake-on siliconization with (a) 13 µg baked-on silicone, i.e. emulsion concentration of 0.6 % (w/w) and (b) 27 µg baked-on silicone, i.e., emulsion concentration of 1.2 % (w/w). (c) Exemplary extrusion force profiles for a 13 µg baked-on silicone level, initially and after 1 year of storage (optimized spray parameters (4 mg spray quantity, nozzle position below flange 20 mm, spray pressure 1 bar, time for pump dosing 175 ms). Values in brackets were not considered as they did not reflect the trend of the other extrusion force values.

After storage, the variability in the force profile increased and intermittently higher friction was built up (Fig. IV-13c), which may be an early warning sign for arising `slip-stick´ phenomena. In particular, for low volume dosages, ´slip-stick´ friction profiles are troublesome as they lead to irregular and imprecise dosages and are uncomfortable for both health care personnel and patients [7,8].

Conceptually, the diameter of the piston (19.55 ± 0.15 mm) was slightly greater than the inner diameter of the container wall (19.05 ± 0.15 mm) to obtain a sufficient liquid tight engagement between the piston and container to exclude leakage. Throughout storage, the adhesion between the piston and the container wall gradually increased as the initially compressed piston relaxed over time. Thereby the piston ribs partially displaced baked-on silicone from the contacting

surface and stuck to the container wall. This phenomenon has already been described for spray-on silicone layers [12,15,33]. The fingerprint of the piston ribs and upper piston plateau squeezing into the baked-on silicone layer at the flange was successfully visualized also after expelling stored cartridges (Fig. IV-14d). Potentially aging altered the viscoelastic properties of the silicone during storage. The silicone, accumulated close to the piston ribs, was not pushed forward during movement of the piston, but similarly remained as a fingerprint at the flange. Overall, the tighter contact between the piston and the container wall in combination with a less mobile silicone led to an additional increase in the gliding forces along the cartridge barrel after storage.

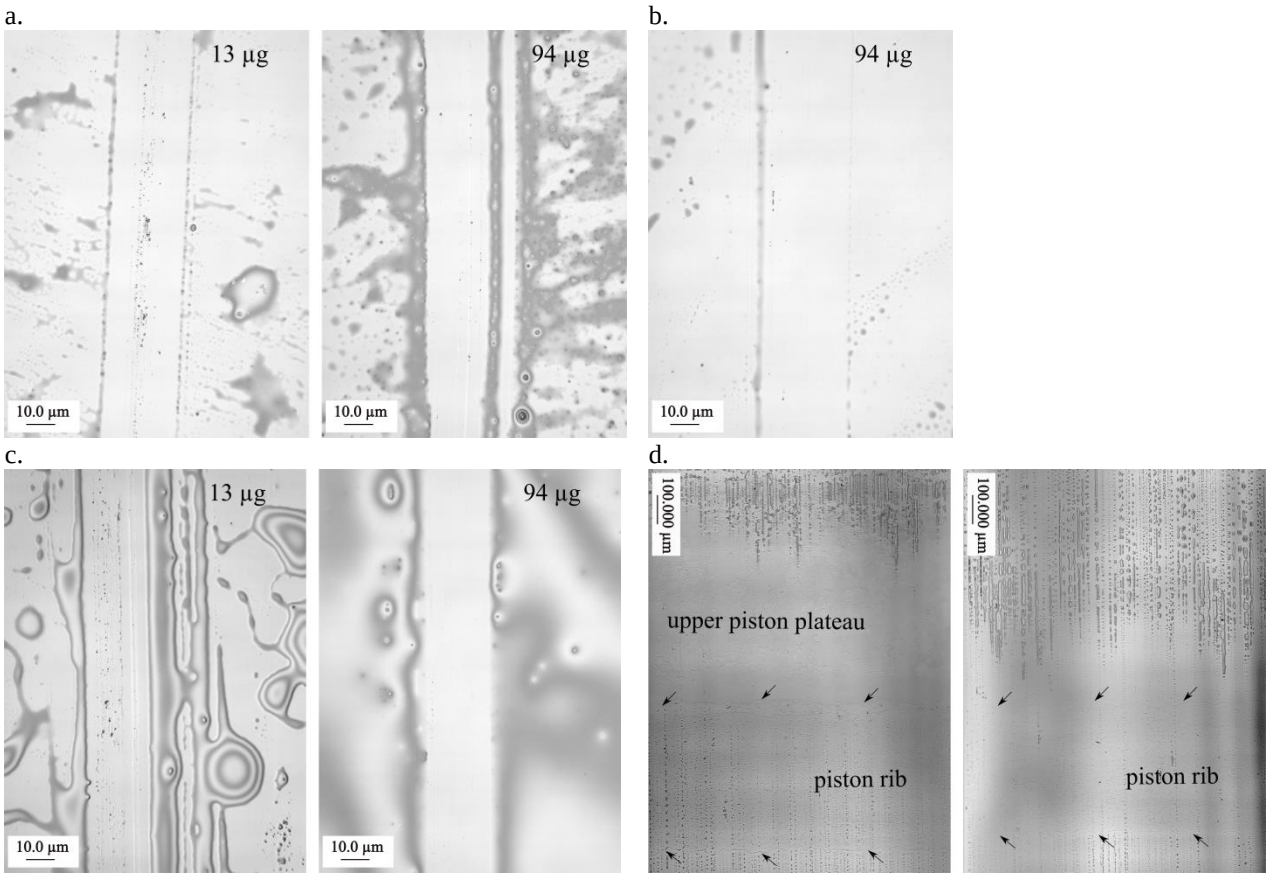

Fig. IV-14. 3D-LSM images of cartridges baked-on siliconized with 13 µg and 94 µg, respectively. Baked-on silicone in the contact surface between (a) piston rib and container wall initially after filling, (b) piston rib and container wall and (c) upper piston plateau and container wall both the latter initially after filling+expelling. (d) Fingerprint of pistons ribs (rib edges indicated by arrows) and upper piston plateau remaining at the flange after storage for 80 weeks and expelling (13 µg baked-on silicone). A high baked-on silicone level of 94 µg served to emphasize underlying mechanism during extrusion, but respective extrusion forces were not assessed during storage.

In addition to the silicone level, container and piston dimensions dictate the obtained extrusion forces. It is reported, that by increasing the inner diameter of the container from 9.23 mm to

9.44 mm compared to a piston of 9.6 mm in diameter, the pressure applied by the piston on the container surfaces and the friction forces are reduced [15].

Other studies showed that higher silicone levels up to 0.25 mg or 0.4 mg could enable constant extrusion forces of 2.5 N and 10 N for 24 month after filling with buffer and protein formulation, respectively [18]. But, spray-on siliconized syringes typically show a gradual increase in extrusion forces with storage time, even though higher silicone levels of 0.2-1 mg per 1 mL PFS are applied [8,13,16–18,20–23]. An increase in break-loose forces from 5 N to 12 N after 12 weeks of storage was found in combination with moderate gliding forces reaching 4 N compared to initially 2 N (silicone level was not disclosed) [33]. Comparably, in a dip siliconization process using 1 % silicone solution in heptane, break-loose forces increased from 3 N to 8 N after 91 days, whereas gliding forces increased much less from 3 N to 4 N [15]. Higher silicone levels can prevent or mitigate storage-related loss in performance, but excess spray-on silicone can migrate to the cartridge edge and drip out onto the tub insert sheet when stored tip-up [20], or accumulate at the bottom-line when stored horizontally [17].

Consequently, a reasonable silicone level balances reliable functionality throughout storage, but still limits excess silicone oil that may sloughs of into solution or redistributes. For functionality during storage, container and piston dimensions may play an important role to understand underlying mechanisms such as silicone displacement during expelling and squeezing of piston ribs into the silicone layer, which in turn impact extrusion forces during storage.

In this study, both baked-on silicone levels resulted in acceptable long-term break-loose forces below 30 N, which is considered as a reasonable reference value in this study. A baked-on silicone level of 13 µg was inadequate to maintain gliding forces below 15 N throughout storage. Therefore, a silicone level of 27 µg is recommended for longer storage times.

3.4 TRANSFER OF SPRAY PARAMETERS TO A DIFFERENT TWO-FLUID NOZZLE SYSTEM

Spray quantity and nozzle position below the flange were shown to be key parameters that determined the distribution of the baked-on silicone layer. A change in system design may also drastically affect the established optimized spray parameters. Therefore, the performance of a second two-fluid nozzle provided by Optima packaging group GmbH was investigated (Fig. IV-15 and Fig. IV-16).

a.

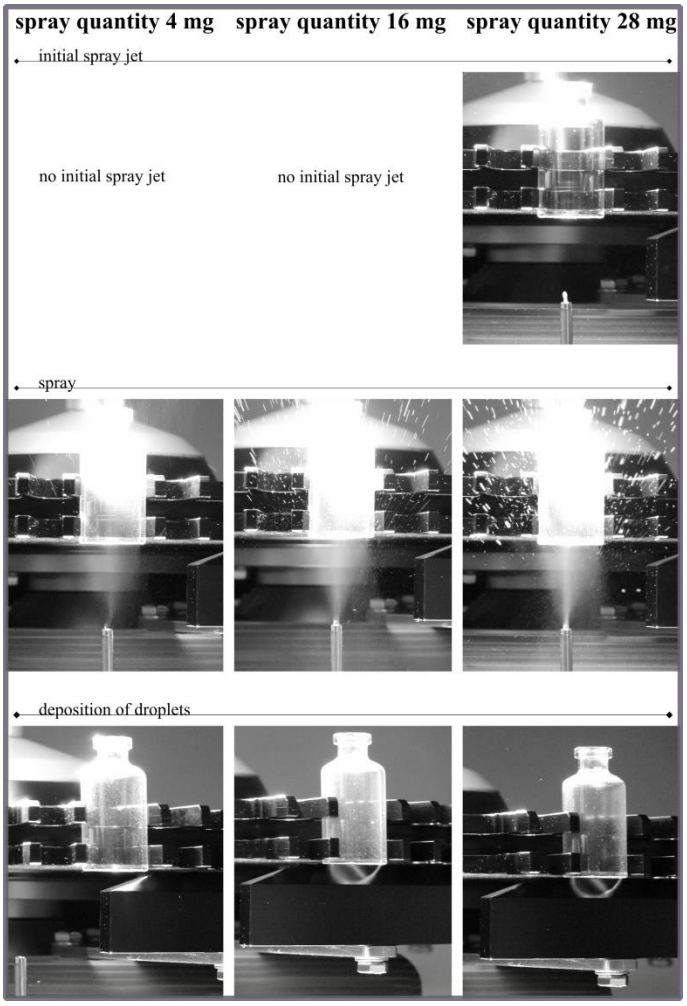

b.

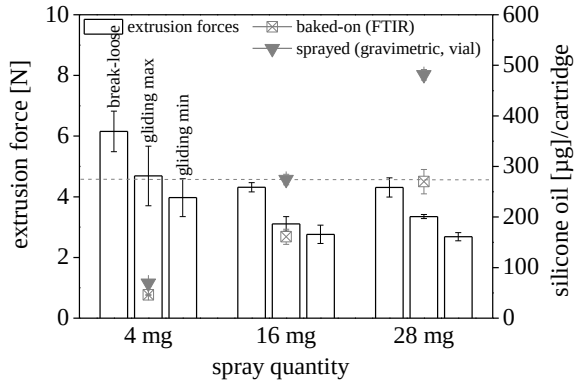

Fig. IV-15. Characterization of different spray quantities of an Optima spray nozzle using 4 mg, 16 mg, 28 mg in (a) high-speed images and (b) mean extrusion forces, baked-on silicone levels as determined by FTIR and theoretically sprayed silicone amounts derived from gravimetric vial analysis (30 mm nozzle position below the flange, spray pressure 1 bar, time for pump dosing 175 ms, 1.75 % (w/w) emulsion concentration).

The absolute spray amounts of the Optima and B+S spray nozzle were comparable with 3.7 ± 0.3 mg, 16.2 ± 0.7 mg, 27.5 ± 0.0 mg and 4.0 ± 0.5 mg, 16.1 ± 0.7 mg, 29.0 ± 0.4 mg silicone emulsion, respectively. The Optima nozzle was less capable to atomize low spray quantities of 4 mg, whereas it outperformed the B+S nozzle regarding higher spray quantities (Fig. IV-15a).

The poorer atomization of low spray quantities was reflected in higher extrusion forces (Fig. IV-15b). A spray quantity of 16 mg, i.e., a baked-on silicone level of 161 ± 15 µg, was required to achieve extrusion forces below 5 N. To the contrary, for the B+S nozzle a spray quantity of 4 mg, i.e., a baked-on silicone level of 45 ± 4 µg was sufficient for extrusion forces below 5 N. Consequently, spray quantity and atomization quality were confirmed as key parameters during development of an optimized bake-on siliconization process with low, but sufficient silicone levels.

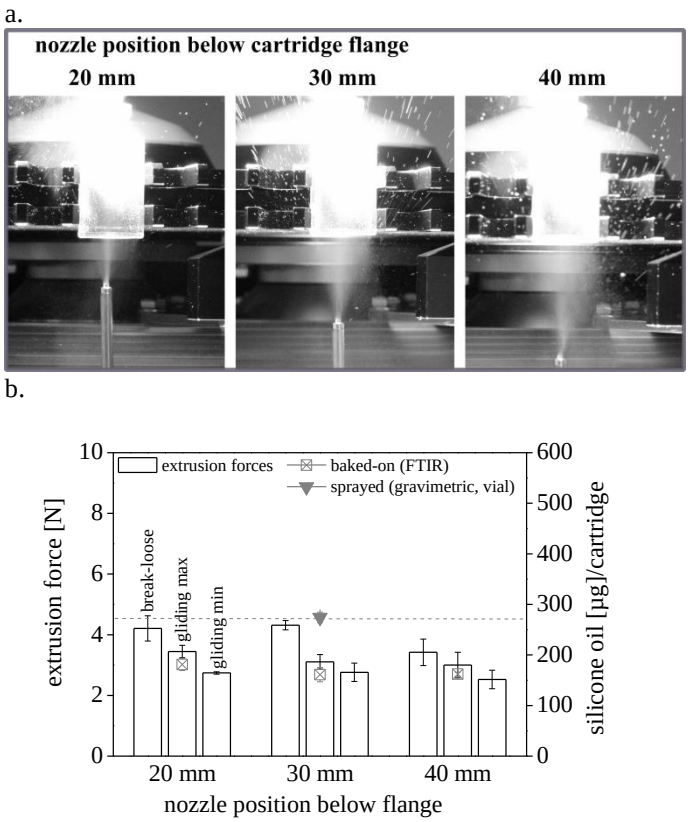

Fig. IV-16. Characterization of different nozzle positions of an Optima spray nozzle at 20 mm, 30 mm and 40 mm below the flange in (a) high-speed images and (b) extrusion forces, baked-on silicone levels as determined by FTIR and theoretically sprayed silicone amounts derived from gravimetric vial analysis (16 mg spray quantity, spray pressure 1 bar, time for pump dosing 175 ms, 1.75 % (w/w) emulsion concentration).

The swirl inset within the annular air channel of the more versatile B+S nozzle enabled a spray angle of approximately 45° compared to the simple external mixing Optima nozzle with its lower spray angle [47]. In particular, the more intense center of the spray cone with a low spray angle of approximately 15-20° led to a lower optimal nozzle position of 30 mm below the flange (Fig. IV-16a and Fig. IV-16b).

In theory, the Optima full cone nozzle design in combination with a steeper spray cone results in a poor atomization quality and increased droplet size compared to the wider, hollow, cone designed B+S nozzle [46,47]. Interestingly, the Optima spray nozzle showed a better atomization of higher spray quantities. It can be argued, that a longer wetted perimeter forms a thinner liquid film, which is disintegrated into smaller droplets [43,47].

Consequently, within siliconization processes based on similar equipment designs including pump and nozzle, optimized spray parameters may be easily transferable from bench-top to pilot-scale or even larger manufacturing-scale siliconization units [13]. However, a change of nozzle may be challenging and will most probably lead to a different set of optimal spray parameters.

4 CONCLUSION

An optimized bake-on siliconization process was designed to achieve defined baked-on silicone levels with lower limits of approximately 10 µg/cartridge barrel in combination with extrusion forces below 10 N. An improved atomization quality of a 4 mg spray quantity was most crucial to yield thin, homogeneous silicone layers. Spray quantities of 16 mg and 29 mg led to emulsion runlets forming thicker build-ups at the flared cartridge edge, which did not improve extrusion performance. A longer time for pump dosing was beneficial for the atomization of higher spray quantities, whereas higher spray pressures were not of advantage. To achieve adequate baked-on silicone levels ranging from 10-100 µg and thin homogeneous silicone layers below 50 nm, it can be recommended to maintain an optimized atomization quality, i.e., spray quantity, and adjust the emulsion concentration instead. The distribution of the baked-on silicone layer was substantially affected by the nozzle position. The silicone distribution was tailored and used in this particular case a nozzle position of 20 mm below the flange to yield thicker baked-on silicone layers at the flange, thereby facilitating smooth break-loose of the piston. Throughout long-term storage, a silicone level of approximately 30 µg resulted in adequate extrusion forces below 15 N.

The explored set of key process parameters affecting the spray pattern and characteristics of the baked-on silicone layer was successfully transferred to a second, differently designed nozzle using a fast optimization approach including high-speed images, FTIR quantification and extrusion force measurements. High-speed images were very effective in directly characterizing the atomization quality and the initial distribution of the silicone emulsion. From experiments performed with the B+S nozzle, this initial distribution of the silicone emulsion had a pivotal role for the uniformity of the baked-on silicone layer later-on. From an industry perspective, engineers and scientist can benefit from a fast optimization approach, but for advanced characterization of the baked-on silicone layer, additional 3D-LSM analysis is highly recommended.

The established bake-on siliconization process in this study balances both sufficient, but limited silicone levels in combination with specifically-tuned silicone distributions and adequate functionality, which presents a substantial challenge in current siliconization processes.

5 SUPPORTING INFORMATION

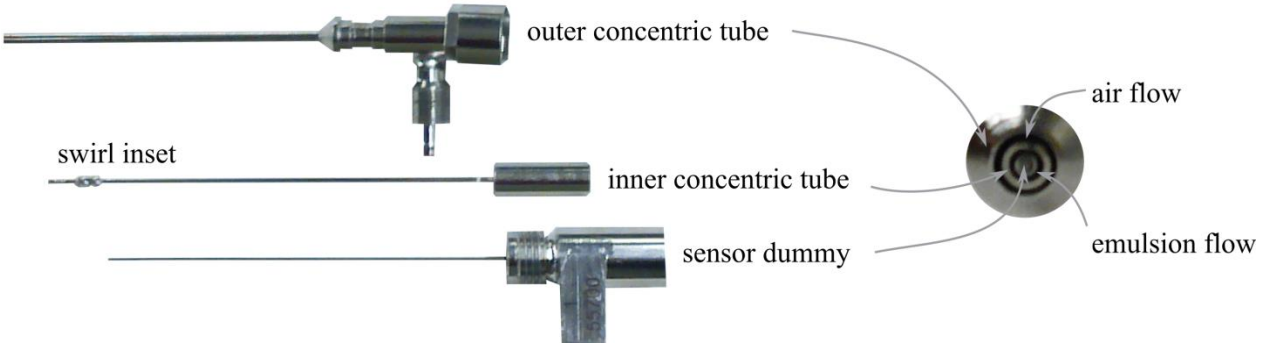

Fig. S IV-1. Design of the external mixing two-fluid nozzle from B+S with its individual components (left side) and nozzle orifice (right side). The nozzle consists of an inner concentric tube with a sensor dummy resulting in an annular slit for liquid supply. The air streams concentrically through the outer tube.

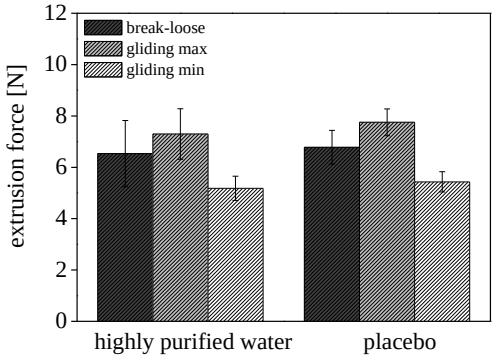

Fig. S IV-2. Mean extrusion forces after filling with highly purified water and placebo (20 mM histidine buffer, pH 6, 0.04 % (v/w) polysorbate 20 (optimized spray parameters: spray quantity 4 mg, fixed nozzle position of 20 mm below the flange, spray pressure 1 bar, time for pump dosing 175 ms).

6 ABBREVIATIONS

3D-LSM	3D-laser scanning microscopy
ALT	Average layer thickness
B+S	Bausch+Ströbel
FTIR	Fourier transform infrared (spectroscopy)
LOQ	Limit of quantification
PFS	Pre-filled syringes
VSI	Vertical scanning interferometry

7 REFERENCES

[1] B. Harrison, M. Rios, Big Shot: Developments in Prefilled Syringes, Pharm. Technol. 30 (2007) 42–48.

[2] D. Jenke, Suitability-for-use considerations for prefilled syringes, (2008). http://www.pharmtech.com/suitability-use-considerations-prefilled-syringes (accessed March 17, 2014).

[3] S. Makwana, B. Biswajit, Y. Makasana, A. Dharamasi, Prefilled syringes: An innovation in parenteral packaging, Int. J. Pharm. Inverstigations. 1 (2011) 200–206.

[4] B. Polin, The Ins and Outs of prefilles syringes, Pharmacutical Med. Packag. 11 (2003).

[5] J. Jezek, N.J. Darton, B.K. Derham, N. Royle, I. Simpson, Biopharmaceutical formulations for pre-filled delivery devices, Expert Opin. Drug Deliv. 10 (2013) 811–828.

[6] R.G. Ingle, A.S. Agarwal, Pre-filled syringe - a ready-to-use drug delivery system: a review, Expert Opin. Drug Deliv. 11 (2014) 1391–1399.

[7] G. Sacha, J.A. Rogers, R.L. Miller, Pre-filled syringes: a review of the history, manufacturing and challenges, Pharm. Dev. Technol. 20 (2015) 1–11.

[8] G.A. Sacha, W. Saffell-Clemmer, K. Abram, M.J. Akers, Practical fundamentals of glass, rubber, and plastic sterile packaging systems, Pharm. Dev. Technol. 15 (2010) 6–34.

[9] Z.-Q. Wen, A. Vance, F. Vega, X. Cao, B. Eu, R. Schulthesis, Distribution of Silicone Oil in Prefilled Glass Syringes Probed with Optical and Spectroscopic Methods, PDA J. Pharm. Sci. Technol. 63 (2009) 149–158.

[10] B. Eu, A. Cairns, G. Ding, X. Cao, Z.-Q. Wen, Direct visualization of protein adsorption to primary containers by gold nanoparticles., J. Pharm. Sci. 100 (2011) 1663–1670.

[11] A. Colas, Silicones in pharmaceutical applications. Part 5: Siliconization of parenteral packaging components, (2006). http://www.dowcorning.com/content/publishedlit/52-1094-01.pdf (accessed July 16, 2015).

[12] C. Petersen, Syringe Siliconisation. Trends, Methods, Analysis Procedures, Int. Pharm. Ind. 4 (2012) 92–99.

[13] E. Chan, A. Hubbard, S. Sane, Y.-F. Maa, Syringe siliconization process investigation and optimization, PDA J. Pharm. Sci. Technol. 66 (2012) 136–150.

[14] M. Bowen, N. Armstrong, Y.-F. Maa, Investigating high-concentration monoclonal antibody powder suspension in nonaqueous suspension vehicles for subcutaneous injection., J. Pharm. Sci. 101 (2012) 4434–4443.

[15] T. Buch-Rasmussen, P. Jannasch, E. Bonne Jorgsen, I. Johannesen, S. Ndoni, N. Berg Madsen, Coating systems providing low friction, U.S. Patent 6,482,509 B2, 1999.

[16] F. Felsovalyi, S. Janvier, S. Jouffray, H. Soukiassian, P. Mangiagalli, Silicone-oil-based subvisible particles: their detection, interactions, and regulation in prefilled container closure systems for biopharmaceuticals, J. Pharm. Sci. 101 (2012) 4569–4583.

[17] M. Lankers, Analyse von Silikonschichtdicken bei der Herstellung von Fertigspritzen mit Hilfe von Refektometriemessungen, Pharm. Ind. 72 (2010) 2148–2153.

[18] R.A. Depaz, T. Chevolleau, S. Jouffray, R. Narwal, M.N. Dimitrova, Cross-linked silicone coating: a novel prefilled syringe technology that reduces subvisible particles and maintains compatibility with biologics, J. Pharm. Sci. 103 (2014) 1384–1393.

[19] T. Klumpen, A. Janssen, High viscosity siliconization methods, International Publication Number WO 2009/124122 A2, 2009.

[20] J.S. Bee, V.V. Frey, U. Javed, J. Chung, M.L. Corcoran, P.S. Roussel, et al., Characterization of the Initial Level and Migration of Silicone Oil Lubricant in Empty Prefilled Syringes for Biologics Using Infrared Spectroscopy, PDA J. Pharm. Sci. Technol. 68 (2014) 494–503.

[21] A. Badkar, A. Wolf, L. Bohack, P. Kolhe, Development of Biotechnology Products in Pre-filled Syringes: Technical Considerations and Approaches, AAPS PharmSciTech. 12 (2011) 564–572.

[22] E. Krayukhina, K. Tsumoto, S. Uchiyama, K. Fukui, Effects of syringe material and silicone oil lubrication on the stability of pharmaceutical proteins, J. Pharm. Sci. 104 (2015) 527–535.

[23] S. Majumdar, B.M. Ford, K.D. Mar, V.J. Sullivan, R.G. Ulrich, A.J.M. D'Souza, Evaluation of the effect of syringe surfaces on protein formulations, J. Pharm. Sci. 100 (2011) 2563–2573.

[24] L. Khandke, R. Malone, X. Yang, H. Han, J.L. Look, Z. Jin, et al., Novel formulations which stabilize and inhibit precipitation of immunogenic compositions, U.S. Patent 2011/0172393 A1, 2011.

[25] B. Reuter, Silicone oil and its applications for parenteral products, PDA Europe Workshop, Cologne, (2010).

[26] A. Gerhardt, B.H. Nguyen, R. Lewus, J.F. Carpenter, T.W. Randolph, Effect of the siliconization method on particle generation in a monoclonal antibody formulation in pre-filled syringes, J. Pharm. Sci. 104 (2015) 1601–1609.

[27] A.J.M. D`Szouza, D.B. Montgomery, Medical components having coated surfaces exhibiting low frictiong and low reactivity, U.S. Patent US 2011/0313363 A1, 2011.

[28] K.B. Auge, A.W. Blake-Haskins, S. Devine, S. Rizvi, Y.-M. Li, M. Hesselberg, et al., Demonstrating the stability of albinterferon alfa-2b in the presence of silicone oil, J. Pharm. Sci. 100 (2011) 5100–5114.

[29] T. Mundry, T. Schurreit, P. Surmann, The Fate of Silicone Oil During Heat-curing Glass Siliconization - Changes in Molecular Parameters Analyzed by Size Exclusion and High Temperature Gas Chromatography, PDA J. Pharm. Sci. Technol. 54 (2000) 383–397.

[30] T. Mundry, P. Surmann, T. Schurreit, Surface characterization of polydimethylsiloxane treated pharmaceutical glass containers by X-ray-excited photo- and Auger electron spectroscopy, Fresenius. J. Anal. Chem. 368 (2000) 820–831.

[31] T. Mundry, Einbrennsilikonisierung bei pharmazeutischen Glaspackmitteln - Analytische Studien eines Produktionsprozesses, Dissertation, Humboldt-Universität Berlin, 1999.

[32] M. Adler, Challenges in the development of pre-filled syringes for biologics from a formulation scientist´s point od view, Am. Pharm. Rev. 15 (2012).

[33] J.D. Thornton, V.G. Sakhrani, A. Nagvekar, L. Jones Braun, Advanced lubrication systems for reducing subvisible particles based on downstream atmospheric gas plasma, Universe oft Prefilled Syringes and Injection Devices, Basel, (2013).

[34] K. Yoshino, K. Nakamura, A. Yamashita, Y. Abe, K. Iwasaki, Y. Kanazawa, et al., Functional evaluation and characterization of a newly developed silicone oil-free prefillable syringe system., J. Pharm. Sci. 103 (2014) 1520–1528.

[35] West Pharmaceutical Service Inc., CZ: The first silicone oil- and tungsten-free insert needle syringe, (2014).

http://www.westpharma.com/SiteCollectionDocuments/CZ Combined Brochure.pdf (accessed March 17, 2016).

[36] E.G.; Ashmead, E.C.. Gunzel, M.P.. Moritz, Syringe stopper, U.S. Patent US8722178 B2, 2014.

[37] A. Sardella, Fine tuning of process parameters for improving biocompatibility of prefilled syringes, Drug Deliv. (2010) 18–22.

[38] S.K. Singh, N. Afonina, M. Awwad, K. Bechtold-Peters, J.T. Blue, D. Chou, et al., An industry perspective on the monitoring of subvisible particles as a quality attribute for protein therapeutics, J. Pharm. Sci. 99 (2010) 3302–3321.

[39] Saphirwerk AG, mdp+ Pumpe. Product information, (n.d.). http://www.saphirwerk.com/downloads/Saphirwerk_mdp+_Pumpe_DE_EN.pdf (accessed June 22, 2015).

[40] S. Funke, J. Matilainen, H. Nalenz, K. Bechtold-Peters, H.-C. Mahler, W. Friess, Analysis of thin baked-on silicone layers by FTIR and 3D-Laser Scanning Microscopy, Eur. J. Pharm. Biopharm. 96 (2015) 304–313.

[41] Dow Corning Corporation, Product Information. Dow Corning 360 Medical Fluid. Ref. No. 51-0374N-01, (2009).

[42] K.Y. Kim, W.R. Marshall, Drop-size distributions from pneumatic atomizers, AIChE J. 17 (1971) 575–584.

[43] J. Gretzinger, W.R. Marshall, Characteristics of pneumatic atomization, AIChE J. 7 (1961) 312–318.

[44] L. Juslin, Droplet size measurement: I. Effect of three independent variables on droplet size distribution and spray angle from a pneumatic nozzle, Int. J. Pharm. 123 (1995) 247–256.

[45] L. Juslin, Droplet size measurement: II. Effect of three independent variables on parameters describing the droplet size distribution from a pneumatic nozzle studied by multilinear stepwise regression analysis, Int. J. Pharm. 123 (1995) 257–264.

[46] A.H. Lefebvre, Properties of Sprays, Part. Part. Syst. Charact. 6 (1989) 176–186.

[47] P.D. Hede, P. Bach, A.D. Jensen, Two-fluid spray atomisation and pneumatic nozzles for fluid bed coating/agglomeration purposes: A review, Chem. Eng. Sci. 63 (2008) 3821–3842.

[48] K. Bauckhage, Gleichzeitige Erfassung von Partikelmerkmalen und Eigenschaften mehrphasiger Strömungen mit Hilfe der Phasen-Doppler-Anemometrie, Chemie Ing. Tech. 68 (1996) 253–266.

[49] V. Burckbuchler, G. Mekhloufi, A.P. Giteau, J.L. Grossiord, S. Huille, F. Agnely, Rheological and syringeability properties of highly concentrated human polyclonal immunoglobulin solutions, Eur. J. Pharm. Biopharm. 76 (2010) 351–356.

[50] A. Sheikhzadeh, J. Yoon, D. Formosa, The effect of a new syringe design on the ability of rheumatoid arthritis patients to inject a biological medication, Appl. Ergon. 43 (2012) 368–375.

[51] L. Joseph, S. Martin, P. Kohle, K. Muthurania, Development of Syringeability Guide for Subcutaneous Protein Formulations, (2010). http://www.readbag.com/aapsj-abstracts-am-2010-w5265 (accessed August 14, 2015).

[52] European committee for standardization, EN ISO 11608-3. Needle-based injection systems for medical use - Requirements and test methods - Part 3: Finished containers, 2012.

[53] G. Reiter, Dewetting of thin polymer films, Phys. Rev. Lett. 68 (1992) 75–78.

[54] B. Demeule, S. Messick, S.J. Shire, J. Liu, Characterization of particles in protein solutions: reaching the

limits of current technologies., AAPS J. 12 (2010) 708–715.

[55] A. Lubiniecki, D.B. Volkin, M. Federici, M.D. Bond, M.L. Nedved, L. Hendricks, et al., Comparability assessments of process and product changes made during development of two different monoclonal antibodies., Biologicals. 39 (2011) 9–22.

[56] J.G. Barnard, K. Babcock, J.F. Carpenter, Characterization and quantitation of aggregates and particles in interferon-β products: potential links between product quality attributes and immunogenicity., J. Pharm. Sci. 102 (2013) 915–928.

[57] L. Liu, D.A. Ammar, L.A. Ross, N. Mandava, M.Y. Kahook, J.F. Carpenter, Silicone oil microdroplets and protein aggregates in repackaged bevacizumab and ranibizumab: effects of long-term storage and product mishandling, Invest. Ophthalmol. Vis. Sci. 52 (2011) 1023–1034.

[58] A. Gerhardt, K. Bonam, J.S. Bee, J.F. Carpenter, T.W. Randolph, Ionic strength affects tertiary structure and aggregation propensity of a monoclonal antibody adsorbed to silicone oil-water interfaces, J. Pharm. Sci. 102 (2013) 429–440.

[59] S.B. Mehta, R. Lewus, J.S. Bee, T.W. Randolph, J.F. Carpenter, Gelation of a monoclonal antibody at the silicone oil-water interface and subsequent rupture of the interfacial gel results in aggregation and particle formation., J. Pharm. Sci. 104 (2015) 1282–1290.

[60] R. Thirumangalathu, S. Krishnan, M.S. Ricci, D.N. Brems, T.W. Randolph, J.F. Carpenter, Silicone oil- and agitation-induced aggregation of a monoclonal antibody in aqueous solution, J. Pharm. Sci. 98 (2009) 3167–3181.

[61] K.A. Britt, D.K. Schwartz, C. Wurth, H.-C. Mahler, J.F. Carpenter, T.W. Randolph, Excipient effects on humanized monoclonal antibody interactions with silicone oil emulsions, J. Pharm. Sci. 101 (2012) 4419–4432.

[62] P. Basu, A.W. Blake-Haskins, K.B. O'Berry, T.W. Randolph, J.F. Carpenter, Albinterferon α2b adsorption to silicone oil-water interfaces: effects on protein conformation, aggregation, and subvisible particle formation, J. Pharm. Sci. 103 (2014) 427–436.

[63] L.S. Jones, A. Kaufmann, C.R. Middaugh, Silicone oil induced aggregation of proteins, J. Pharm. Sci. 94 (2005) 918–927.

[64] A. Gerhardt, N.R. Mcgraw, D.K. Schwartz, J.S. Bee, J.F. Carpenter, T.W. Randolph, Protein aggregation and particle formation in prefilled glass syringes, J. Pharm. Sci. 103 (2014) 1601–1612.

V Optimization of the Bake-On Siliconization of Cartridges. Part II: Investigations into Burn-In Time and Temperature

The following chapter is published as research article in the European Journal of Pharmaceutics and Biopharmaceutics:

S. Funke, J. Matilainen, H. Nalenz, K. Bechtold-Peters, H.-C. Mahler, F. Vetter, C. Müller, F. Bracher, W. Friess. Optimization of the Bake-On Siliconization Process of Cartridges. Part II: Investigations into Burn-In Time and Temperature. Accepted for publication.

Keywords

Bake-on siliconization, cartridge, heat-tunnel, heat-oven, siloxanes, FTIR, functionality, 3D-laser scanning microscopy, silicone layer thickness, silicone level

Graphical Abstract

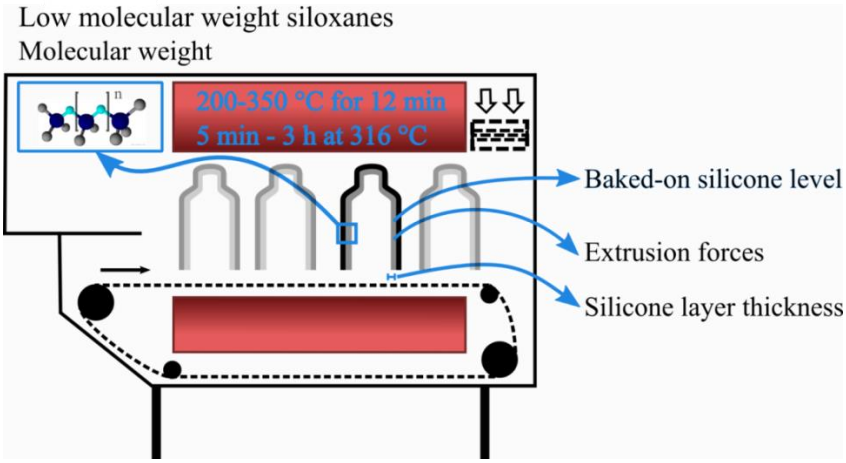

ABSTRACT

Combination products have become popular formats for the delivery of parenteral medications. Bake-on siliconization of glass syringes or cartridges allows good piston break-loose and gliding during injection at low silicone levels. Although widely implemented in industry, still little is known and published on the effect of the bake-on process on the silicone level, layer thickness and chemical composition. In this study, cartridges were bake-on siliconized in a heat-tunnel by varying both temperature from 200 to 350 °C for 12 min and time from 5 min to 3 h at 316 °C. Furthermore, a heat-oven with air-exchange was established as an experimental model. Heat treatment led to a time- and temperature-dependent decrease in the silicone level and layer thickness. After 1 h at 316 °C lubrication was insufficient. The silicone levels substantially decreased between 250 and 316 °C after 12 min. After bake-on, the peak molecular weight of the silicone remained unchanged while fractions below 5,000 g/mol were removed at 316 and 350 °C. Cyclic low molecular weight siloxanes below 500 g/mol were volatilized under all conditions. Despite most of the baked-on silicone was solvent-extractable, contact angle analysis indicated a strong binding of a remaining, thin silicone film to the glass surface.

1 INTRODUCTION

Pre-filled syringes and cartridge-based drug/device combination products have gained wide acceptance in the delivery of parenteral drug products due to several advantages including ease of self-administration, accurate dosing, decreased risk for contamination, and less overfill [1–5].

Silicone oil is used as lubricant allowing the piston to break-loose and glide smoothly within the glass barrel during injection [6–9]. Siliconization is performed by either spraying-on silicone oil, e.g., Dow Corning 360 Medical Fluid, referred to as spray-on siliconization, or by applying silicone emulsion such as diluted Dow Corning 365 35 % Dimethicone NF Emulsion, followed by bake-on at elevated temperature of approximately 300 °C for 10-30 min [10–16]. Bake-on siliconization results in relatively lower silicone levels < 0.1 mg/barrel [17–19] compared to spray-on siliconization with 0.2-1 mg/barrel [8,16,17,20–25]. Alternative siliconization methods include dip coating of Dow Corning 360 Medical Fluid dissolved in solvent [26,27] or applying cross-linkable silicone, such as VDT-731 by plasma-enhanced chemical vapor deposition [28] and Dow Corning MDX4-4159 with subsequent polymerization by ultraviolet irradiation or by curing at elevated temperature [27].

The main advantage of bake-on siliconization is to limit silicone migration into the drug product without compromising functionality [18,20,21,24,26,29,30]. However, based on thermal decomposition during bake-on, it has been argued that the processing window is narrow due to a change in the silicone bulk properties and the potential impact on extrusion forces [21]. Volatilization, depolymerization and thermo-oxidation have been identified as main mechanisms during thermal decomposition of silicone oil. The most commonly used lubricant trimethylsiloxy-endcapped polydimethylsiloxane (PDMS) [31] decomposes into volatile low molecular weight siloxanes (LMWS), SiO_2, H_2O and CO_2 [32–34]. In parallel, thermo-oxidation may initiate cross-linking via a complex radical mechanism [33]. As both processes overlap to some extent, the change in molecular weight of the polymer is hardly predictable. Thomas *et al.* found either a negligible change or decrease in molecular weight depending on both thermal depolymerization and rearrangement of siloxane bonds compensating each other in vacuum [34]. Mundry *et al.* suggested an increase in number and weight average molecular weight (M_n and M_w) attributed to the volatilization of a significant portion of LMWS while the peak average molecular weight (M_p) remained unchanged. Therefore, cross-linking was unlikely to be the main mechanism upon bake-on [10]. Suitable methods to analyze the molecular weight of PDMS are gel permeation chromatography (GPC) followed by matrix-assisted laser desorption/ionization time-of-flight

mass spectrometry [35,36], evaporative light scattering detection [37,38], inductively coupled plasma atomic emission spectrometry [39] or refractive index detection (RID) [10,40,41].

The application of silicone oil in health care includes usage as lubricant [31], for the treatment of retinal detachment and for soft tissue augmentation due to its biological inertness [42]. However, certain LMWS contained as residues from polymer synthesis [43,44] have been assessed for their toxic effect. Cyclic LMWS, i.e., cyclodimethylsiloxanes, are indicated as Dn where $D = [(CH_3)_2SiO]$. In particular, D4 has been associated with impaired fertility (D4 is labeled reproductive category II, globally harmonized system [45]). Both D4 and D5 were related to potential carcinogenic effects resulting in an increase in uterine tumors, as well as hepatomegaly in rats and mice [46,47]. LMWS are known to migrate into various, preferentially lipid-rich compartments [48], which increases the risk for a wide and persistent distribution throughout the body in mice [49] and human plasma of implant recipients [50]. Other studies suggested D4-induced denaturation and aggregation of fibronectin and fibrinogen [51,52]. Consequently, the thermal decomposition of PDMS into LMWS during bake-on may be of critical toxicological concern.

Most studies mainly investigated the decomposition of silicone bulk samples exposed to artificial heat-treatment rather than using baked-on silicone, solvent-extracted from syringes or cartridges. Therefore, though thermal “fixation” and “chemical binding” of silicone to the glass surface is often postulated [7,13], it is still rarely investigated. After solvent extraction, very thin baked-on silicone layers covalently bound to the glass surface have been found by Mundry *et al.*; however, most baked-on silicone was still solvent-soluble and therefore a general fixation of the baked-on silicone layer is postulated to be unlikely [12].

Thus, there is currently a substantial gap in understanding and analysis of the thermal decomposition of silicone emulsion upon bake-on. Although bake-on siliconization is an essential step during manufacturing of many parenteral drug products, minimal practical data is available. The purpose of this study was to investigate the impact of different burn-in times and temperatures on the characteristics of the baked-on silicone layer to identify an adequate processing range. Comparable to commercial bake-on siliconization processes, 0.6 % (w/w) silicone emulsion was sprayed-on using optimized spray parameters followed by bake-on in a heat-tunnel. We propose a toolbox of analytical methods towards full control of the baked-on silicone level, layer thickness distribution and coating functionality. The thermal decomposition of silicone and pharmaceutically relevant stabilizers of Dow Corning 365 35 % Dimethicone NF

Emulsion was characterized with respect to weight loss, cyclic LMWS content and molecular weight distribution of the silicone polymer. The formation of covalent bonds was functionally addressed by contact angle (CA) measurements after removal of the extractable silicone fraction. Finally, the silicone layer characteristics after bake-on in a heat-tunnel were compared with a heat-oven as an experimental model for lab-scale experiments.

2 MATERIALS AND METHODS

2.1 MATERIALS

Non-siliconized 5 mL cartridges, pistons, serum stoppers and aluminum seals were obtained from F. Hoffmann-La Roche Ltd (Basel, Switzerland). Elastomeric components were coated with fluoropolymer (FluroTec®). Microscope glass slides were obtained from VWR International GmbH (Darmstadt, Germany).

Chemicals were purchased as follows: 365 35 % Dimethicone NF Emulsion and 360 Medical Fluid, 350 cSt, from Dow Corning GmbH (Wiesbaden, Germany); heptane from Riedel-de Haën (Seelze, Germany); cyclic LMWS D3, D4, D5, methyl paraben, propyl paraben, *tert*-butylmethylether and toluene from VWR International GmbH (Darmstadt, Germany); Tween 20 from Croda GmbH (Nettetal-Kaldenkirchen, Germany); and cyclic LMWS D6, Triton X-100 from Sigma-Aldrich Chemie GmbH (Taufkirchen, Germany). ReadyCal-Kit polystyrene standards PSS-pskitr-04 were obtained from PSS Polymer Standards Service GmbH (Mainz, Germany).

2.2 BAKE-ON SILICONIZATION PROCESS

Bake-on siliconization was performed on a SVS9061 pilot-scale siliconization unit from Bausch + Ströbel Maschinenfabrik Ilshofen GmbH+Co. KG (Ilshofen, Germany) equipped with an external mixing, two-fluid nozzle. Optimized spray parameters were adapted from previous experiments: a spray quantity of 4 mg, or alternatively of 16 mg silicone emulsion, a fixed nozzle position of 20 mm below the flange, a spray pressure of 1 bar and time for pump dosing of 175 ms (see chapter IV).

For most experiments, Dow Corning 365 35 % Dimethicone NF Emulsion was diluted to 0.6 % (w/w) using highly purified water. A higher concentrated silicone emulsion of 3.5 % (w/w) was utilized for gas chromatography-mass spectrometry (GC-MS) analysis. For CA experiments, the emulsion was diluted to 1.75 % (w/w).

The cartridges were subsequently treated in a TSQ U03 heat-tunnel from Robert Bosch GmbH (Stuttgart, Germany). Burn-in temperatures were adjusted from 200 °C to 350 °C at a constant treatment time of 12 min. Varying burn-in times ranging from 5 min to 3 h were studied at a constant temperature of 316 °C.

The bake-on process was further investigated in a heat-oven Heraeus WU6100 from Thermo

Scientific Inc. (Waltham, MA, USA) without air-exchange and with air-exchange of 2.5 m^3/h. For temperature profile measurements, five cartridges in the center and at each side of a wire basket used as holder during bake-on were equipped with two T-type thermocouples (TC) from GE Sensing & Inspection Technologies GmbH (Hürth, Germany) at the top and bottom of the individual cartridge. TCs were affixed in the cartridge using Kapton 3M™ tape from Reinhard Krückemeyer GmbH & Co. KG (Wilnsdorf, Germany) to secure the TC firmly against the neck of the cartridge. An additional TC was directly placed into the oven. TCs were calibrated from 180 °C to 360 °C, and verified at 316 °C with a final accuracy of 315.5 °C ± 0.2 °C. At burn-in temperatures ≥ 200 °C a sensitivity of 1 °C is accepted to be sufficient [53].

2.3 EXTRACTION AND FOURIER TRANSFORM INFRARED (FTIR) QUANTIFICATION

The baked-on silicone level was determined by a combination of heptane extraction (900 µL heptane, two rinsing steps à 900 µL) and quantitative FTIR spectroscopy. According to considerations provided in ICH Q2 R1 Validation Analytical Procedure, the limit of detection of the developed FTIR method was found to be below 1 µg/mL (number of calibration curves n = 22). The limit of quantification was 18 µg/mL (n = 22), equivalent to 4 µg per cartridge based on 250 µL dissolution volume [54] (see chapter III).

2.4 GRAVIMETRIC ANALYSIS

After every adjustment of the spray parameters, the emulsion spray was initially collected in a 2R vial, which was previously loaded with a tissue to soak up the absolute spray amount without evaporation loss. The vial was weighted before and after the siliconization process using an AT261 DeltaRange System high precision balance from Mettler-Toledo GmbH (Gießen, Deutschland). The absolute spray amounts were converted into theoretically sprayed silicone amounts using the corresponding concentration of the silicone emulsion.

2.5 3D-LASER SCANNING MICROSCOPY (3D-LSM)

The average silicone layer thickness (ALT) was determined using a VK-X210 microscope equipped with VK Viewer Software both from Keyence Deutschland GmbH (Neu-Isenburg, Germany) as previously reported [54] (see chapter III). The lower limit of detection was 10 nm. Cartridges were covered with adhesive tape, broken up and individual fragments were removed from the adhesive tape to enable direct measurements of the thin baked-on silicone layer.

Cartridge fragments from the flange, middle and top of the cartridge were analyzed to determine the ALT distribution within the barrel.

2.6 EXTRUSION FORCE MEASUREMENTS

After bake-on siliconization, pistons and cartridges were manually assembled. The containers were filled with 5.16 mL highly purified water and sealed with serum stoppers and aluminum caps. Pistons in contact with lubricated container walls have shown to develop an initial resistance to movement. Therefore, movement is not initiated until a certain force is applied, referred to as break-loose force. After a sudden, rapid relative movement, the movement sustains applying a gliding force. The break-loose, minimum and maximum gliding forces were evaluated by using a material testing instrument TA.XT.plus from Winopal Forschungsbedarf GmbH (Elze, Germany) at a constant displacement speed of 5.6 mm/min over a distance of 17.5 mm (maximum travel distance for the piston within the cartridge barrel), thereby mimicking approximately 3 min injection time for a combination product with a high filling volume.

2.7 GAS CHROMATOGRAPHY-MASS SPECTROMETRY (GC-MS)

A higher concentrated silicone emulsion of 3.5 % (w/w) and a medium spray quantity of 16 mg baked-on at 316 °C for 12 min were utilized for GC-MS analysis. Cartridges were extracted as described above (900 µL heptane, two rinsing steps à 900 µL) (see 2.3). The extracts of four baked-on siliconized cartridges (baked-on silicone level 325 ± 68 µg) were pooled, evaporated to dryness using a flowtherm evaporator at 100 °C and constant nitrogen flow of 210 mL/min from Barkey GmbH & Co. KG (Leopoldshöhe, Germany). The dried sample was redissolved in 100 µL *tert*-butylmethylether. In addition, 108 ± 8 mg 35 % silicone emulsion (n = 8) were evaporated to dryness. 1 mg/mL solutions were prepared using *tert*-butylmethylether.

Cyclic LMWS and parabens were analyzed using a GC 3800 equipped with a Saturn 2000 MS detector using electron ionization at 70 eV both from Varian (Darmstadt, Germany). Separation was performed on a VF-5 MS column (30 m x 0.25 mm x 0.25 um) and a 10 m EZ-Guard column from Varian. Helium was used as carrier gas at a flow rate of 1.2 mL/min. The injector was settled to splitless for 1 min at an injection volume of 2 µL and an inlet temperature of 250 °C. The oven temperature was held at 50 °C for 5 min, ramped to 240 °C at 25 °C/min, followed by a second ramp to 310 °C at 50 °C/min, and then held for 6 min. The glass liner was exchanged on a regular basis to avoid artefacts due to high sample concentrations.

Peak identification was carried out by comparison with external standards with regard to retention times and mass spectra (full scan range *m/z* 40-500). For quantification, the area under the curve (AUC) for selected target ions was recorded following external standard calibration in the concentration range of 0.1-1.5 µg/mL (supporting information Fig. S V-1a and Fig. S V-1b). The following target ions were used: *m/z* 209+224 for D3, *m/z* 281 for D4, *m/z* 355 for D5, *m/z* 342+429 for D6, *m/z* 121+152 for methyl paraben and *m/z* 121+138 for propyl paraben. Correlation coefficients R^2 ranged between 0.976-1.000. Calibration was repeated in each sequence.

2.8 GEL PERMEATION CHROMATOGRAPHY-REFRACTIVE INDEX DETECTION (GPC-RID)

A high performance liquid chromatography system from the 1200 series from Agilent Technologies Deutschland GmbH (Waldbronn, Germany) equipped with RID was employed for GPC-RID on a SDV linear S, 300 x 8 mm, particle size 5 µm from PSS Polymer Standards Service GmbH (Mainz, Germany). The mobile phase was toluene with a flow rate of 0.5 mL/min. The temperature of the RID was set to 35 °C while the samples were cooled at 5 °C. Molecular weight averages were determined by ChemStation Software Rev. B 02.01 from Agilent, or alternatively WinGPC UniChrom Software from PSS Polymer Standards Service GmbH (Mainz, Germany).

The system was calibrated with 12 polystyrene standards with peak molecular weights (M_p) ranging from 266 g/mol to 66,000 g/mol (supporting information Tab. S V-1, supporting information Fig. S V-2a) and 3rd polynomial fitting with $R^2 = 0.999$ (supporting information Fig. S V-2b). Injections of a mixture of four polystyrenes at the beginning and the end of each sequence were reproducible (variation coefficient not more than 0.06 %).

The lowest injected silicone amount possible for sufficient baseline separation was 10 µg as determined from experiments using 0.5 mg/mL to 6 mg/mL silicone oil in toluene solutions and injection volumes of 10 µL, i.e., injected amounts of 5-60 µg (supporting information Fig. S V-3).

To meet these low detection limits for GPC-RID analysis, cartridges bake-on siliconized with a medium spray quantity of 16 mg and 0.6 % (w/w) silicone emulsion were used. Bake-on conditions in the heat-tunnel were performed as described above (see 2.2). The dried extract of

bake-on silicone (see 2.3) was redissolved in 100 µL toluene. As reference, 1 mL 35 % silicone emulsion was solvent-extracted with 1 mL toluene. The injection volume was 50 µL.

For describing the molecular weight distribution of silicone, the molecular weight of the peak maximum (M_p) in addition to the following parameters was used:

- the number average molecular weight (M_n), which is sensitive to changes in the low molecular weight fraction:

$$M_n = \frac{\sum N_i M_i}{\sum N_i}$$

Eq. V-1

with the number of particular molecules (N_i) having a particular molecular weight (M_i)

- the weight average molecular weight (M_w), which reflects changes in the high molecular weight fraction:

$$M_w = \frac{\sum N_i \, M_i{}^2}{\sum N_i \, M_i} = \frac{\sum W_i \, M_i}{\sum W_i}$$

Eq. V-2

given with the weight fraction (W_i) of each type of polymer molecule.

- the polydispersity index (PDI), which describes the width of the distribution [55]:

$$PDI = \frac{M_n}{M_w}$$

Eq. V-3

2.9 THERMOGRAVIMETRIC ANALYSIS (TGA)

A Hi-Res TGA 2950 from TA instruments (Eschborn, Germany) was used to follow the weight loss during heating at a constant rate of 2 °C/min in ramp mode. In isothermal mode, the temperature was increased to 55 °C at a rate of 28 °C/min, held for 12 min, followed by a second increase to 316 °C at 28 °C/min, held for 3 min, and finally decreased to 18.4 °C with a rate of 11 °C/min. Set target temperatures mimic the heat profile in the heat-tunnel, whereas the ramp increments in isothermal mode were derived from temperature mapping in the heat-oven. Approximately 20-30 mg sample was weighted into 40 µL aluminum pans from Mettler-Toledo GmbH (Gießen, Germany) and purged with air at a flow rate of approximately 60 mL/min during TGA analysis.

2.10 CONTACT ANGLE (CA) MEASUREMENTS

CAs of 2 µL purified water drops were determined using a Drop Shape Analyzer from Krüss GmbH (Hamburg, Germany) in sessile drop mode. CAs were calculated with Krüss Advance 1.1.02 software 20 s after drop deposition using ellipse (tanget-1) for siliconized samples and circle fitting for glass samples based on recommendations of the manufacturer. The baseline was set to manual or manual curved.

For CA analysis, samples were prepared as follows: 3 mL of diluted 1.75 % (w/w) silicone emulsion were transferred as a thin fluid layer in a borosilicate glass beaker of 9.5 cm diameter, heated at 295 °C for 12 min and extracted with 3 mL heptane. Aliquots of 200 µL were evaporated to dryness at room temperature and redissolved in 140 µL heptane to achieve final concentrations of 2.5 % (w/v). In addition, 2.5 % (w/v) silicone solutions in heptane were prepared. Glass slides were cut into 2.5 x 2.5 cm pieces and siliconized with 5 x 6 µL drops of silicone or heat-treated silicone in heptane on a SCI-20 spin-coater from Schaefer Technologies GmbH (Lange, Germany) at 100 rpm. Both coatings were established to model bake-on and spray-on siliconized glass surfaces, respectively.

The extraction of these siliconized glass slides was performed by rinsing with 884 µL heptane to maintain a similar volume-to-surface-ratio of 141 µL/cm^2 as valid for cartridge extraction using 3 x 900 µL heptane. Baked-on siliconized cartridges were initially extracted as described above (900 µL heptane, two rinsing steps à 900 µL) (see 2.3). Subsequently, cartridge fragments were prepared as described above (see 2.5). Additional extraction regimes included incubation of slide/cartridge pieces in 20 mL heptane and ultrasound bath treatment (VWR International GmbH, Darmstadt, Germany) for 10 min, as well as wiping with cotton swabs, soaked in heptane. After extraction, surfaces were rinsed 10 s with purified water to remove adhering heptane and subsequently dried at room temperature. Different harsh extraction regimes were employed to challenge the extractability of the different silicone coatings and to functionally assess the interactions between silicone and the glass surface.

3 RESULTS AND DISCUSSION

3.1 IMPACT OF BURN-IN TIME AND TEMPERATURE ON THE BAKED-ON SILICONE LEVEL, LAYER THICKNESS DISTRIBUTION AND COATING FUNCTIONALITY

Cartridges were bake-on siliconized in a heat-tunnel using both different burn-in temperatures from 200 °C to 350 °C for 12 min and burn-in times from 5 min to 3 h at 316 °C. The baked-on silicone level, layer thickness distribution and coating functionality were evaluated to identify an adequate processing range.

The baked-on silicone level markedly decreased from 26 ± 6 µg and 28 ± 4 µg at 200 °C and 250 °C, respectively, to 13 ± 3 µg and 11 ± 3 µg at temperatures of 316 °C and 350 °C (Fig. V-1a). The different burn-in temperatures did not affect the extrusion forces between 4-7 N.

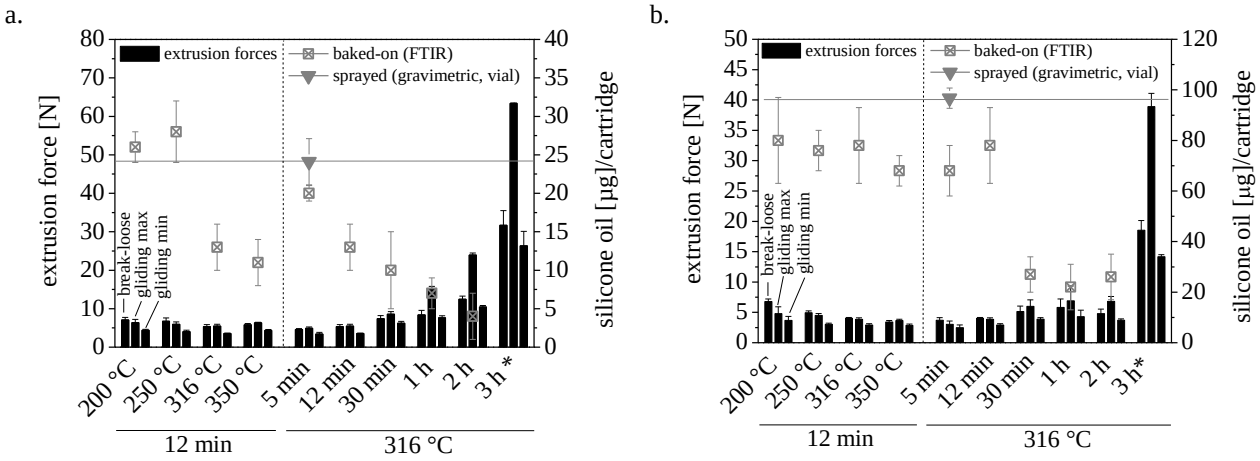

Fig. V-1. Extrusion forces, baked-on silicone levels as determined by FTIR and theoretically sprayed silicone amount derived from gravimetric vial analysis at burn-in temperatures between 200 °C and 350 °C (12 min) and burn-in times between 5 min and 3 h (316 °C) in a heat-tunnel using (a) 4 mg spray quantity and (b) 16 mg spray quantity. Asterisks indicate baked-on silicone levels below the limit of quantification of 18 µg/mL, i.e., < 4 µg/cartridge based on 250 µL dissolution volume [54] (see chapter III).

With increasing burn-in times from 5 min to 3 h, the baked-on silicone was steadily burned-off at 316 °C from 20 ± 1 µg to below 4 µg, which was the lower limit of detection [54] (see chapter III). After 1 h at 316 °C an insufficient lubrication was found as indicated by the increase in the maximum gliding force to 15 N, which was considered as reference value in this study. The break-loose forces exceeded 30 N after 3 h. Both break-loose and gliding forces have to be carefully evaluated depending on the injection device used. Overall, for patient-friendly injection, maximum gliding forces of 15-20 N were reported [56]. In addition, target values of 15 N were

suggested in studies comparing siliconized and BD-42 coated glass syringes [23] and assessing the gliding performance for high-concentration monoclonal antibody powder suspensions [57]. For empty cartridges a gliding force limit of 10 N is suggested in EN ISO 11608-3 [58]. In other studies, maximum forces were fixed at 30 N while rheumatoid arthritis patients were able to exert average forces of 28 N and up to a maximum of 45 N [59].

At moderate burn-in conditions, e.g., 200 °C, 250 °C for 12 min, the baked-on silicone levels were in good agreement with the theoretically sprayed silicone amount of 24 ± 3 µg. In a previous study, the difference between both values was established as an estimate for spray loss (see chapter IV). In this study, it additionally illustrates the reduction of silicone depending on the burn-in conditions. Consequently, at 200 °C and 250 °C for 12 min the optimized spray parameters led to a quantitative spray process without spray loss and minimal burn-off. Therefore, the decrease in the baked-on silicone level at 316 °C (△ 15 µg) could be exclusively attributed to burn-off rather than spray loss.

Higher baked-on silicone levels obtained with a medium spray quantity of 16 mg remained relatively constant at approximately 68 ± 6 µg to 80 ± 17 µg regardless of the burn-in temperature (Fig. V-1b). Extrusion forces remained between 3-7 N. After 30 min at 316 °C the baked-on silicone level dropped from 78 ± 15 µg to 27 ± 7 µg and further decreased below 4 µg after 3 h. Simultaneously, the gliding forces exceeded 15 N and the break-loose forces increased above 30 N.

At a medium spray quantity of 16 mg, the baked-on silicone level was systematically lower compared to the theoretically sprayed silicone amount, even at moderate burn-in conditions of 200 °C and 250 °C. Consequently, the spray loss was approximately 18-30 %. The rate of burn-off should be comparable to a low spray quantity of 4 mg, e.g., 15 µg between 250 °C and 316 °C, as elaborated above. However, a medium spray quantity resulted in a higher variability of baked-on silicone levels, which therefore did not directly reflect these slight reductions due to burn-off.

Silicone oil manufacturers suggest a burn-in temperature below 250 °C or even below 150 °C for less than two hours, or higher temperatures for substantially shorter time periods [11,60]. Also, temperatures above 250 °C [21], up to 320 °C for 15 min, 20 min, 28 min [10,12] or even 350 °C [61] are reported. Consequently, the investigated temperature range of 200°C to 350°C and burn-in time of 12 min, which was routinely used, were in agreement with literature. Nonetheless, bake-on conditions in siliconization processes are still not ´standardized´ and are in practice often

driven and limited by the temperature and passage time settings for the sterilization and depyrogenation of the containers. Adequate sterilization and depyrogenation were not within the scope of the study. Of course, this must be verified in a commercial bake-on siliconization process. Final temperature and time settings are mutually related: with increasing burn-in temperature, the burn-in time may be reduced. However, both settings eventually need to balance adequate evaporation of emulsion water, sterilization, depyrogenation and a decrease in silicone level, and ultimately extrusion performance [7,15,16,60]. Both applied spray quantities were low with 4 mg and 16 mg, thus emulsion water was completely evaporated after bake-on. Thermal decomposition started between 250 °C and 316 °C, which was well in line with TGA analysis (see 3.2.1). Consequently, only 5 min at 316 °C were sufficient to initiate thermal decomposition, but overall burn-in times up to 1 h were not critical with regard to extrusion performance. However, for bake-on siliconization processes with minimum silicone levels, interruptions longer than 1 h are suggested to be avoided.

The thin baked-on silicone layers ranged from 10 nm to 70 nm (10 nm was the lower limit of detection [54] (see chapter III)) (Fig. V-2).

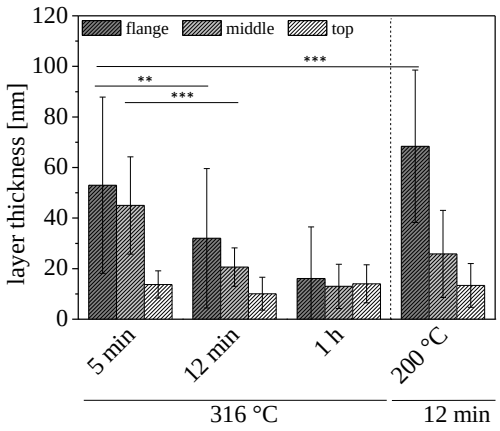

Fig. V-2. Baked-on silicone layer thickness after 5 min, 12 min and 1 h burn-in at 316 °C and after 12 min burn-in at 200 °C in a heat-tunnel using a spray quantity of 16 mg. ALT in three different sections within the cartridge barrel (* $p \leq 0.05$, ** $p \leq 0.01$, *** $p \leq 0.001$).

Overall, the achieved baked-on silicone layers were thin compared to spray-on silicone layers in the range of 50-400 nm with some areas up to 900 nm thickness [21,24,25,62]. Baked-on silicone layers of approximately 50 nm to 100 nm were only exemplarily determined using interferometry [25]. The effect of bake-on on the ALT was not as clearly reflected as compared to the decrease in the baked-on silicone levels. Still a short burn-in time of 5 min at 316 °C and a low burn-in temperature of 200 °C for 12 min resulted in a higher ALT. At less moderate burn-in conditions,

the thinner ALTs indicated thermal decomposition. However, the effect of the measuring position (flange, middle, top) was more pronounced. As described previously, the higher ALT in the flange and middle region was attributed to the fixed nozzle position of 20 mm below the flange, where the spray cone exactly reached the cartridge flange (see chapter IV).

To our knowledge, the processing window for bake-on siliconization processes is rarely investigated. A decrease in CA from 101° to 31° with increasing burn-in temperatures from 300-550° for 15 min [63] and from 97° to 26° at 320-600 °C for 15 min suggested silicone being burned-off with higher temperatures [14]. However, different CAs may also indicate a different orientation of PDMS on the glass surface [64,65], which aggravates interpretation. In this study, the effect of different burn-in times and temperatures on the baked-on silicone layer, layer thickness and extrusion performance was demonstrated.

3.2 THERMAL DECOMPOSITION BEHAVIOR OF SILICONE EMULSION

3.2.1 THERMAL DECOMPOSITION MECHANISMS AND THERMAL WEIGHT LOSS OF SILICONE EMULSION AND SELECTED STABILIZERS

Dow Corning 365 35 % Dimethicone NF Emulsion, which is most commonly used for bake-on siliconization processes, contains approximately 35 % Dow Corning 360 Medical Fluid, 350 cSt, in water and additional stabilizers such as preservatives (methyl paraben and propyl paraben), non-ionic surfactants (Tween 20 and Triton X-100) and co-solvents (propylene glycol) up to 5 % each [60,66]. Therefore, thermal decomposition and thermal weight loss of silicone emulsion and selected stabilizers in air were evaluated by TGA (Fig. V-3).

Silicone emulsion showed a weight loss of approximately 56 % upon a temperature increase from 50 °C to 100 °C, which can be attributed to the evaporation of emulsion water, followed by a second weight loss with three overlapping stages in the overall decomposition process (Fig. V-3a). TGA profiles for silicone oil and silicone emulsion in air were similarly reported in literature [14,33,34]. The small weight loss starting at 200 °C may be attributed to the volatilization of low molecular weight fractions remaining as precursors from polymer production, which has been described to occur between 150 °C and 250 °C [34,43,44]. The second stage with an onset of 313 ± 5 °C was assigned to thermo-oxidation, mainly resulting in SiO_2, H_2O and CO_2 [32,33], which was reported to take place around 290-350 °C [33,34,67]. In this study, 6 % remained as white silica powder. In literature, it was postulated that condensed phase oxidation via a radical mechanism crosslinks the polymer and slows down decomposition

of that stage [33]. Thermal depolymerization proceeds via cleavage and rearrangement of siloxane bonds to form cyclic LMWS that evaporate [34]. Depolymerization starts at about 350-410 °C [33,34,68] and is reflected in a third stage of decomposition around 400 °C in this study. Overall, both degradation steps finally result in a similar mixture of volatile LMWS with additional SiO_2, H_2O and CO_2 [32,33].

a. b.

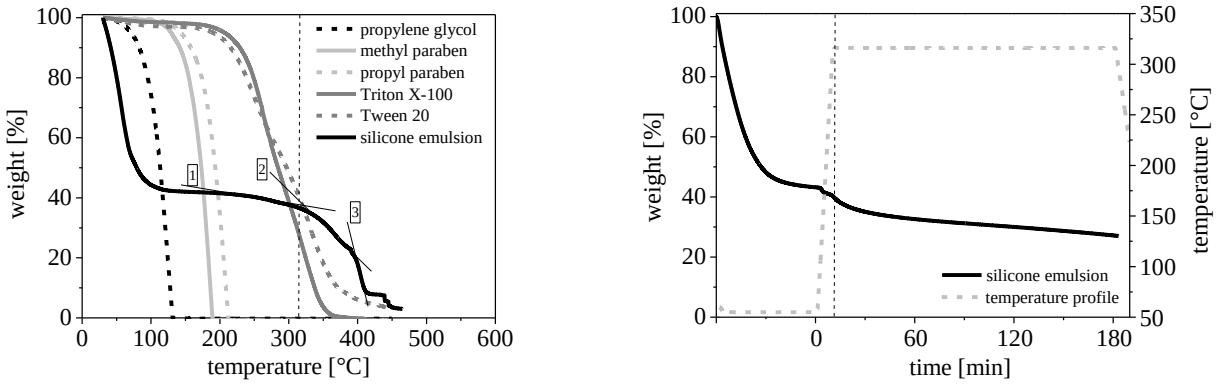

Fig. V-3. Exemplary TGA of Dow Corning 365 35 % Dimethicone NF Emulsion and its individual ingredients in (a) temperature ramp mode and (b) isothermal mode. Vertical, dashed lines indicate standard burn-in conditions of 316 °C for 12 min. Different stages of the thermal decomposition process were assigned to volatilization of low molecular weight fractions 1, thermo-oxidation 2 and depolymerization 3.

Interestingly, a substantial decrease in the baked-on silicone level was observed between 250 °C and 316 °C as described above, which correlates well with the onset of the second weight loss in TGA at 313 ± 5 °C. Although the different points of inflection and decomposition stages can be assigned to volatilization, thermo-oxidation and thermal depolymerization according to literature, all processes overlap to some extent [34] and therefore contribute to the decrease in the baked-on silicone level. In addition, oxygen further catalyzes thermal depolymerization, which results in lower onset temperatures [33].

In isothermal mode at 316 °C after the initial evaporation of water, the weight loss was less pronounced but steadily proceeded (Fig. V-3b). This was in agreement with the gradual decrease in baked-on silicone levels with increasing burn-in time.

Selected stabilizers of the silicone emulsion, including the preservatives methyl paraben and propyl paraben and the co-solvent propylene glycol, completely evaporated below the target burn-in temperature of 316 °C. Onset temperatures for the weight loss of propylene glycol, methyl and propyl paraben were 97 °C, 160 °C and 179 °C, respectively, in agreement with evaporation following zero-order kinetic [69–71]. Consequently, residues of parabens in the

baked-on silicone are unlikely. In addition, combinations of methyl paraben and propyl paraben in ratios of 7.5:1 or 9:1 are reported as preservative in parenteral formulation, but still the typical-in-use concentration for each paraben in parenteral biologics is limited to not more than 0.2 % [72–75]. Potential minute amounts of parabens remaining in the baked-on silicone were further investigated in GC-MS (see 3.2.3). Propylene glycol is not considered as a critical residue in the baked-on silicone due to complete evaporation below 316 °C. In addition, it is one of the most commonly used co-solvents in parenteral formulations and used up to 80 % in injectables [76,77]. For emulsion stability, it is beneficial as it prevents interactions between parabens and Tween 20 [78].

Surfactants such as Triton X-100 and Tween 20 were degraded up to 73 % and 60 % at 316 °C, respectively. The onsets for weight loss were at 211 °C for Tween 20 and 234 °C for Triton X-100. Tween 20 is widely found in parenteral products, e.g., as stabilizer inhibiting protein adsorption and aggregation [76,79,80]. Upon heating with and without the addition of water, autoxidation is the major degradation pathway, resulting in traces of acetaldehyde, hexane, pentane and heptanal, which immediately volatilize [81]. However, in therapeutic protein formulations during storage, degradation products such as peroxides, short chain acids (e.g., formic acid) and polyoxyethylene esters of fatty acids were found, which may eventually affect protein stability [81–85]. In a hypothetical situation with a maximum of 5 % Tween 20 in Dow Corning 365 35 % Dimethicone NF Emulsion [66], which was diluted to 0.6 % (w/w) in our study, a spray quantity of maximum 16 mg and a theoretical residue of 40 % Tween 20, approximately 6 µg Tween 20 would remain in the baked-on silicone layer. Based on a cartridge filling volume of 5.16 mL, a maximum of 0.0001 % Tween 20 may end up in the final drug product assuming complete migration from the baked-on silicone layer into the formulation. Compared to concentrations up to 0.4 % in antibody drugs [86], residues of Tween 20 remaining in the baked-on silicone layer can be considered not critical. A comparable low amount < 0.0001 % would be reached for Triton X-100. However, limited information are being published for the use of Triton X-100 as excipient [87,88] in parenteral formulations, but still, it is present in traces in marketed vaccine [89].

Overall, dilution of the emulsion prior to bake-on alone effectively dilutes all stabilizers to very low levels and reduces a potential interaction of emulsion stabilizers present in the silicone layer with the drug product formulation. This is further mitigated by fully or partially evaporation of these compounds during thermal bake-on.

3.2.2 MOLECULAR WEIGHT DISTRIBUTION OF BAKED-ON SILICONE

The molecular weight of untreated silicone emulsion and after bake-on was investigated using GPC-RID (Fig. V-4).

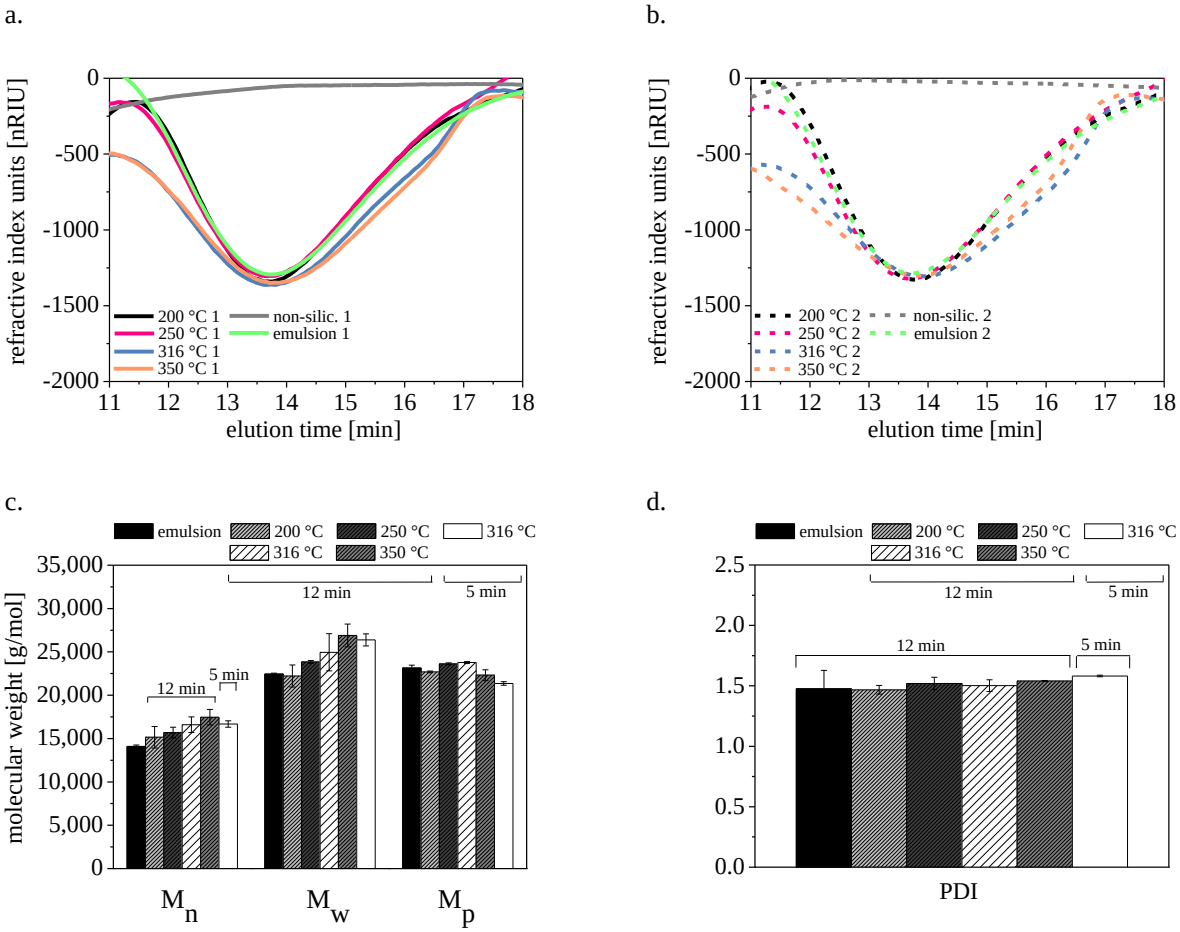

Fig. V-4. Molecular weight distribution of PDMS in untreated Dow Corning 365 35 % Dimethicone NF Emulsion and after bake-on at temperatures between 200 °C and 350 °C (12 min) in a heat-tunnel using a 16 mg spray quantity. (a) and (b) GPC-RID elution profiles of both duplicates, (c) average molecular weights and (d) PDI. Cartridge extracts were used for analysis (n = 2).

Molecular weight parameters for the silicone emulsion with M_n 14,373 ± 630 g/mol, M_w 22,700 ± 132 g/mol, M_p 22,914 ± 218 g/mol (Fig. V-4c), and PDI of 1.48 ± 0.15 (Fig. V-4d) were within the range reported for silicone oils of 350 cSt and 1,000 cSt [10,38,40,90]. After burn-in at 316 °C and 350 °C for 12 min the lower molecular weight fraction eluting later than 17 min, i.e., < 5,000 g/mol (Fig. V-4a and Fig. V-4b), was removed most likely due to volatilization [10]. Accordingly, with burn-in temperatures from 200 °C to 350 °C, the M_n steadily increased from 15,155 ± 1,236 g/mol to 17,463 ± 892 g/mol compared to a lower M_n of silicone emulsion of 14,373 ± 630 g/mol. Simultaneously, the relative proportion of higher molecular weight fractions

increased, which was reflected in the M_w increase from 22,217 ± 1,275 at 200 °C to 26,896 ± 1,304 g/mol at 350 °C. The M_w of the initial silicone emulsion (22,700 ± 132 g/mol) was comparable to the M_w at 200 °C.

Likewise, Mundry *et al.* found a reduction of volatile fractions between 0-7,400 g/mol after bake-on at 320 °C for 28 min, which led to a relative increase in higher molecular weight fractions. The M_n and M_w slightly increased from approximately 12,500 g/mol to 17,000 g/mol and 19,000 g/mol to 21,000 g/mol, respectively [10].

Furthermore, it can be argued that the M_w increase may be induced by thermo-oxidative cross-linking [33,34] rather than a change in the relative proportion of higher molecular weight fractions. In this study, insufficient baseline separation towards an artefact peak at 10.5 min, which was comparably found in non-siliconized and siliconized cartridges after extraction, rendered data interpretation difficult. But it has to be kept in mind that chain-lengthening has been only observed for hydroxyl-endblocked PDMS after intermolecular condensation rather than in trimethylsiloxy-endcapped PDMS [34].

In addition, at 316 °C and 350 °C tailing between 14.5-17 min was more pronounced, indicating a higher fraction of polymers between 5,000-15,000 g/mol as cleavage products after depolymerization. Depolymerization rapidly proceeds to completion until cleavage products below 5,000 g/mol finally evaporate [34].

The peak maxima at different temperatures from 200 °C to 350 °C were similar at 13.5-14 min. Consequently, the M_p remained unchanged between 22,685 ± 107 and 23,777 ± 114 g/mol and was comparable to the initial M_p of silicone emulsion with 22914 ± 218 g/mol. The PDI remained unchanged as well with 1.46 ± 0.04 to 1.58 ± 0.01. Likewise, Mundry *et al.* found a negligible change in M_p in the range of 18,000-19,000 g/mol after bake-on at 320 °C for 28 min [10]. Our findings were in good agreement with this study, although the GPC-RID system was calibrated with polystyrene instead of PDMS standards.

Overall, GPC-RID was successfully transferred to relevant baked-on silicone levels below 80 µg and a wider range of burn-in conditions. Interestingly, already burn-in temperatures of 200 °C and 250 °C slightly altered the average molecular weights. A more pronounced change in the molecular weight distribution was observed at 316 °C and 350 °C.

Burn-in times of 5 min and 12 min at 316 °C showed comparable average molecular weights. Analysis of longer burn-in times was not feasible due to poor baseline separation, indicating

depolymerization and evaporation of the decomposed silicone species under such conditions, even though two cartridge extracts were pooled.

3.2.3 ANALYSIS OF CYCLIC LOW MOLECULAR WEIGHT SILOXANES (LMWS) AND PARABENS IN BAKED-ON SILICONE

Similar, consecutive cyclic LMWS with repeating units of dimethylsiloxane are either formed together with the polymer in synthesis or produced in the thermal depolymerization process [34,44], independent of the applied pyrolysis temperature, initial silicone viscosity [91] or whether thermal decomposition is performed in air or inert atmosphere [32]. Dow Corning 365 35 % Dimethicone NF Emulsion and baked-on silicone (316 °C for 12 min) extracted from cartridges were analyzed for cyclic LMWS by GC-MS. In addition, GC-MS was utilized to track minute amounts of parabens. GC-MS has been reported as sensitive method to characterize LMWS [10,92,93] and parabens [94,95].

Referred to 100 µg silicone, the initial silicone emulsion contained 0.12 % (123 ± 50 ng) D3, 0.04 % (40 ± 22 ng) D5 and 0.03 % (30 ± 15 ng) D6 (Fig. V-5).

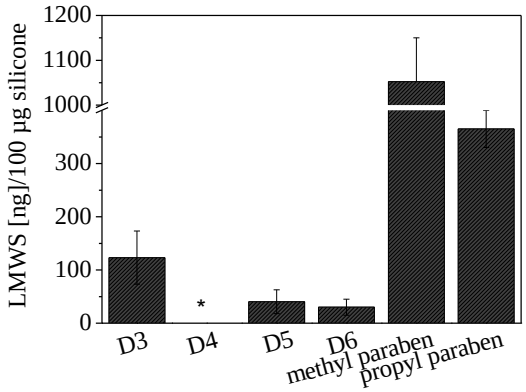

Fig. V-5. Cyclic LMWS in untreated Dow Corning 365 35 % Dimethicone NF Emulsion (n = 8, each performed as double injection). Asterisk indicates LMWS < calibration range 0.1 µg/mL, i.e. 10 ng LMWS/100 µg silicone.

D3 is used as precursor in polymer synthesis [43] and is consequently present at higher levels. The amounts of cyclic LMWS from D6 to D10 in Dow Corning Medical Fluids, 100-12500 cSt, have been reported to be below a detection limit of 1 µg/mL [96]. Species up to 3,700 g/mol, i.e., up to 50 siloxane units, are less than 1.65-2.35 % [10]. Overall, volatile species are limited to 2 % in the pertinent Ph. Eur. monograph [31]. Consequently, with approximately 0.2 % cyclic LMWS in untreated silicone in this study we were well within the limits given for LMWS.

GC-MS demonstrated that the amount of cyclic LMWS in the baked-on silicone after extraction was below 0.001 %, referred to the lowest calibration range for cyclic LMWS of 0.1 µg/mL and a high baked-on silicone concentration of 13 mg/mL used in this study (see 2.7). From TGA analysis it is known, that PDMS breaks down between 200-450 °C. Upon thermal decomposition in air, cyclic LMWS in the range of D3-D9 [44], D3-D14 [32], D3-D7 [91] are formed with D3 being the most prominent species [32,44,91]. However, these species are immediately removed during bake-on due to their volatile properties [10,96]. In addition, GPC showed a reduction in the lower molecular weight fraction < 5,000 g/mol (see 3.2.2) and volatilization in TGA started at 200 °C (see 3.2.1). Thus, after bake-on siliconization no toxicological concern exists regarding increased levels of cyclic LMWS potentially affecting protein stability in formulation [51,52] or distributing in human plasma after injection [50] as elaborated previously.

Additionally, GC-MS analysis demonstrated 1052 ± 98 µg methyl paraben and 365 ± 35 µg propyl paraben in the untreated silicone, which equals approximately 0.36 % methyl paraben and 0.1 % propyl paraben in 35 % silicone emulsion (definite paraben content not accessible for comparison due to proprietary reasons) (Fig. V-5). After bake-on, amounts of both parabens were below 0.001 % in baked-on silicone, which is in agreement with complete evaporation below 316 °C in TGA.

3.2.4 FORMATION OF COVALENT BONDS BETWEEN THE BAKED-ON SILICONE AND THE GLASS SURFACE

Baked-on silicone was extracted for analysis of the molecular weight distribution and to quantify cyclic LMWS. To directly characterize the silicone layer baked-on the glass surface and after extraction, the glass surface was analyzed by CA measurements.

A second solvent extraction of baked-on siliconized cartridges with a high silicone level of 202 µg ± 12 µg was performed as described previously (900 µL heptane, two rinsing steps à 900 µL heptane). Silicone concentrations in this second heptane extract were below the limit of quantification of 18 µg/mL (n = 22), equivalent to 4 µg per cartridge based on 250 µL dissolution volume. Consequently, one solvent extraction employing three solvent steps with heptane was sufficient for quantitative silicone recovery, even at high silicone levels [54] (see chapter III).

For CA analysis, cartridges with low baked-on silicone levels of 6 ± 2 µg were utilized, thereby enhancing quantitative extraction and enabling direct analysis of the non-extractable silicone fraction.

The CAs of non-siliconized glass slides were 8 ± 2° (Tab. V-1). Glass surfaces theoretically exhibit a CA of 0° [14,97], but due to the adsorption of hydrophobic, air-borne contaminants the CA may increase up to 31° [14] or 46.4° [97], which was reflected in the CA of 49 ± 5° for non-siliconized cartridges. Higher CAs of 47 ± 2° and 62 ± 2° were observed after heptane treatment for the glass slide and the cartridge, respectively. In theory, water on heptane results in a CA of 115°. On a microscopic scale, the water drop displaces a monolayer heptane film remaining on the glass surface, which yields the observed, merged CA between 8 ± 2° on glass and 115 ° on heptane [98].

Spin-coating with untreated silicone oil significantly increased the CA to 81 ± 1° (Tab. V-1 and Fig. V-6a). For vials siliconized with Dow Corning Medial Fluid 360 without additional heat treatment, Mathes found a comparable CA of 78° [97]. Silicone spread between glass slides or after dip coating in 1 % silicone solution in benzene exhibited lower CAs of 44° [14] and 31° [63], respectively, but this mode of preparation of experimental glass slides may have substantially affected the achieved CAs.

Tab. V-1. CA of purified water on glass slides; non-siliconized and after spin-coating with either silicone or heat-treated silicone and after multiple extraction sequences, in comparison to bake-on siliconized cartridges.

	Initial [°]	**After extraction [°]**		**After additional incubation with ultrasound [°]**	**After additional wiping [°]**		
Number of procedures	**-**	**#1**	**#2-3**	**#1**	**#1**	**#2**	**#3**
Slide							
Non-siliconized	8 ± 2	47 ± 2	-	-	-	-	-
Silicone	81 ± 1	68 ± 3	60 ± 1	65 ± 3	44 ± 3	-	-
Heat-treated silicone	101 ± 3	107 ± 8	107 ± 1	106 ± 0	58 ± 1	50 ± 2	53 ± 2
Cartridge							
Non-siliconized	49 ± 5	62 ± 2	-	-	-	-	-
Bake-on siliconized	103 ± 2	105 ± 3	101 ± 4	101 ± 1	98 ± 2	96 ± 3	97 ± 1

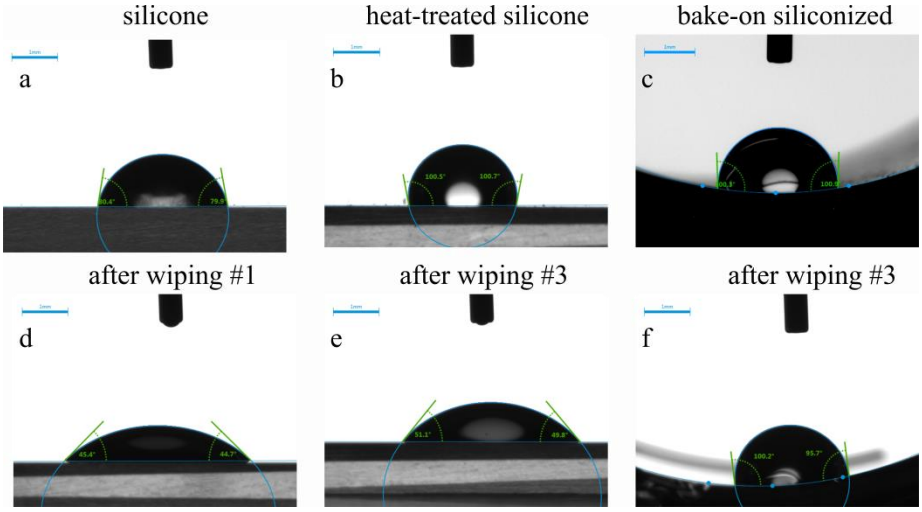

Fig. V-6. CA images of purified water on glass slides after spin-coating with either (a, d) silicone or (b, e) heat-treated silicone and after multiple extraction sequences in comparison to (c, f) bake-on siliconized cartridges.

Models describing defined states of orientation during compression of PDMS films on water can be transferred to solid surfaces, e.g., glass surfaces [65]. The polar glass surface induces a rearrangement of PDMS in a caterpillar-like, fully-stretched configuration with all silicon atoms in line and oxygen arranged towards the silanol groups of the glass surface by hydrogen bonds. The methyl groups closely assemble on the other side of the PDMS chain thereby yielding a hydrophobic surface [99–101]. In thin films, a gradual transformation to regular helices oriented parallel to the interface [102] or a horizontally folding multi-layer conformation of the caterpillar-like monolayer is described upon higher surface coverage [103]. In a three-dimensional, further compressed bulk state, the PDMS layer collapses resulting in irregular, standing coils [99,100,104] or circular, isolated domains of standing helices and multilayers that spread slowly [105–107]. Water may enter the wedges between the disordered methyl groups or sequences of water molecules access between neighboring PDMS chains as observed in hydrated states of PDMS [108]. Consequently, the CA for glass surfaces excessively coated with silicone in a bulk phase may exhibit a lower CA than thin spin-coated silicone surfaces.

Heat-treated silicone coated on glass slides and bake-on siliconized cartridges exhibited even higher CAs of 101 ± 3° and 103 ± 2°, respectively (Fig. V-6b and Fig. V-6c). Similarly, CAs after bake-on are reported with 97° (2.5 % emulsion, 330 °C for 20 min) [14], 100-104° (1 % silicone in benzene, 300 °C for 15-180 min) [63] and 95° (1.75 % emulsion, 300 °C for 20 min) [109]. The spin-coating method on glass slides was comparable for silicone and heat-treated silicone. Therefore, different orientation states of the silicone layer as previously discussed can be excluded. GPC indicated a decrease in the low molecular weight fraction < 5,000 g/mol, an

increase in the fraction between 500 g/mol and 15,000 g/mol and no substantial formation of molecules with more than 50,000 g/mol by cross-linking with increasing burn-in temperatures from 200 °C to 350 °C (see 3.2.2). Lower molecular weight fractions have shown to migrate into micro-inhomogeneities on the glass surface [110] or silicone rubber [111] due to great mobility and thereby lead to a disorientation of the applied layer [110]. This may results in a lower CA for untreated silicone oil.

Multiple extraction steps were required to decrease the CA of slides coated with untreated silicone from 81 ± 1° to 44 ± 3° (Fig. V-6a and Fig. V-6d) and heat-treated silicone from 101 ± 3° to 53 ± 2° (Fig. V-6b and Fig. V-6e). Those final values equal the CAs of glass slides treated with heptane as control. Silicone and heat-treated silicone were finally quantitatively extracted and the glass contact angle prevailed.

On contrary, after extraction of bake-on siliconized cartridges and all tested additional cleaning procedures, the CA remained high with 97 ± 1° (Fig. V-6f). The baked-on silicone becomes more intimately associated due to both stronger physical attraction after removal of hydration water from the glass surface and polymer matrix [11,64,112] and covalent siloxane bond formation with the glass surface [12]. Thus, CA analysis points to the formation of a thin covalently-bound silicone layer remaining after extraction of baked-on siliconized cartridges.

3.3 HEAT-OVEN TREATMENT AS AN EXPERIMENTAL MODEL FOR HEAT-TUNNEL BAKE-ON

Heat-tunnels are widely used for bake-on, continuous sterilization and concomitant depyrogenation in pharmaceutical manufacturing and pilot-scale set-ups, but for lab-scale experiments they are difficult to handle. Bake-on in a heat-tunnel showed a time- and temperature-dependent decrease in the silicone level and layer thickness. For functional performance the silicone level during bake-on is most critical. In addition, air velocity in the tunnel might be strongly equipment specific and also contributes to siliconization performance. The transferability of these parameters to a heat-oven as an experimental model is therefore of significant value and was investigated by controlling air-exchange and temperature.

Temperature profiles without and with air-exchange in the heat-oven were found to be comparable for all TCs positioned in the cartridge barrel with consistent maximum temperatures of 196 ± 0 °C and 196 ± 1 °C at an oven set temperature of 200 °C. Similarly, 312 ± 1 °C and 311 ± 1 °C were reached at a target temperature of 316 °C (Tab. V-2).

Tab. V-2. Average temperatures (T) for bake-on in a heat-oven at 316 °C and 200 °C for 12 min, either without or with air-exchange. Values given for cartridges average measured temperatures of five cartridges in the center and at each side of a wire basket. Each cartridge was equipped with two TCs at the cartridge top and the bottom. An additional TC was directly placed into the oven.

	Max. T oven	**Max. T cartridge**	**Max.T gradient TC_{top}-TC_{bottom} during heating**	**Max. T gradient TC_{top}-TC_{bottom} during cooling**
Without air-exchange at 200 °C	200 ± 1	196 ± 0	11 ± 7	-13 ± 5
With air exchange at 200 °C	198 ± 1	196 ± 1	8 ± 4	-15 ± 7
Without air-exchange at 316 °C	312 ± 4	312 ± 1	14 ± 8	-21 ± 7
With air exchange at 316 °C	312 ± 2	311 ± 1	11 ± 7	-19 ± 4

Besides facilitating bake-on siliconization, heat treatment is employed for sterilization and depyrogenation [7,15,16]. Therefore, temperature control without cold spots, i.e., areas with substantially lower temperatures, is crucial [113]. For temperature mapping in dry heat-tunnels and ovens at 250 °C and greater temperatures, an average of ± 15 °C of the setpoint is recommended [114]. In comparison, validation studies in a tunnel sterilizer showed maximum temperatures of 319 ± 13 °C for 10 mL containers at a set maximum temperature of 300 °C. Differences between the left and right side of the belt were between 3-4 °C [53]. In our study, maximum temperatures were within the range ± 15 °C of the setpoint and deviated less than 1 °C, thus temperature distribution was homogeneous and no cold spots were observed between cartridges in the center and at each side of a wire basket.

Interestingly, during heating and cooling, a temperature gradient built-up within the cartridge as the top of the cartridge heated and cooled faster (Supporting information Fig. S V-4). The effect that leads to this temperature gradient is not clear from this study. The thickness of the container wall apparently affects heat penetration [53], but in this study cartridges had a comparable wall thickness of 1.5 mm along the barrel.

Overall, the heat-oven allowed consistent, comparable temperature control regardless of the process conditions such as different target temperatures or airflow. On contrary, baked-on silicone levels were substantially affected by the investigated process conditions. Bake-on siliconization in the heat-oven without air-exchange led to higher silicone levels compared to the heat-tunnel (Fig. V-7a and Fig. V-7b). Consequently, an adequate experimental model mimicking heat-tunnel required air-exchange.

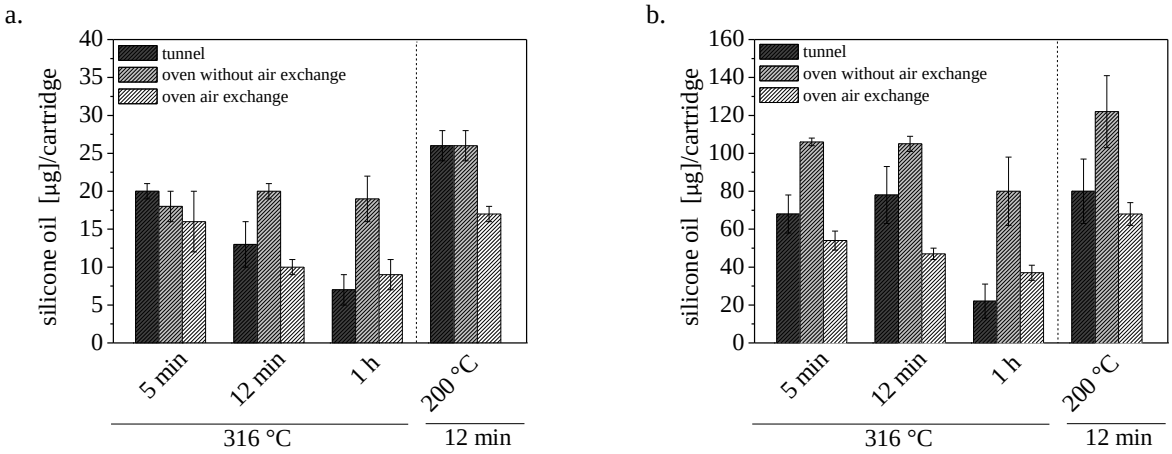

Fig. V-7. Baked-on silicone levels as determined by FTIR after 5 min, 12 min and 1 h burn-in at 316 °C and after 12 min burn-in at 200 °C in a heat-tunnel and heat-oven, either without or with air-exchange using (a) 4 mg spray quantity and (b) 16 mg spray quantity.

Both, heat-ovens and heat-tunnels, are used to sterilize and depyrogenate glass containers for parenteral drug products [115,116]. Overall, dry heat is transferred by convection, conduction or radiation [113]. In the heating zone of the tunnel, quartz tubes covered with polished reflector plates provide uniform heat distribution by radiation in addition to convective heat transfer due to laminar air circulation [117,118]. In case of parallel siliconization, silicone is burned-off and decomposition products are immediately blown out of the cartridge. In the oven, a fan at the back leads to a horizontal heat circulation by convection after jacket heating of fresh air [118,119]. At first, the cartridge glass wall heats up followed by heat conduction to the cartridge interior. In both processes heat may be partially conducted from the mesh conveyor belt in the heat-tunnel or wire basket and grid in the heat-oven. Without air-exchange in the heat-oven, burned-off silicone may accumulate within the cartridge interior or burn-off is slowed down due to saturation effects. In turn, air-exchange efficiently removes burned-off silicone from the cartridge and oven interior, thereby decreasing the final baked-on silicone level. As bake-on without and with air-exchange led to comparable temperature profiles, the different baked-on silicone levels in the heat-oven were exclusively attributed to differences in the air-exchange.

Air-exchange led to lower baked-on silicone levels, but the extrusion forces were comparable for bake-on processes without and with air-exchange. Regardless of the burn-in time, extrusion forces ranged between 4-7 N at a low spray quantity of 4 mg and 2-5 N at a medium spray quantity of 16 mg (Tab. V-3) (burn-in temperature of 200 °C discussed below).

Tab. V-3. Extrusion forces after 5 min, 12 min and 1 h burn-in at 316 °C and after 12 min burn-in at 200 °C in a heat-oven either without or with air-exchange using 4 mg spray quantity and 16 mg spray quantity.

Spray quantity 4 mg			
Without air-exchange	**Break-loose force [N]**	**Maximum gliding force [N]**	**Minimum gliding force [N]**
316 °C for 5 min	6 ± 1	6 ± 0	4 ± 0
316 °C for 12 min	6 ± 0	5 ± 0	4 ± 0
316 °C for 1 h	7 ± 1	6 ± 1	5 ± 0
200 °C for 12 min	7 ± 1	8 ± 1	5 ± 0
With air-exchange	**Break-loose force [N]**	**Maximum gliding force [N]**	**Minimum gliding force [N]**
316 °C for 5 min	6 ± 0	6 ± 1	4 ± 0
316 °C for 12 min	6 ± 0	7 ± 1	5 ± 0
316 °C for 1 h	6 ± 0	7 ± 1	5 ± 0
200 °C for 12 min	9 ± 1	8 ± 0	6 ± 0
Spray quantity 16 mg			
Without air-exchange	**Break-loose force [N]**	**Maximum gliding force [N]**	**Minimum gliding force [N]**
316 °C for 5 min	3 ± 1	4 ± 1	3 ± 0
316 °C for 12 min	4 ± 1	3 ± 0	2 ± 0
316 °C for 1 h	4 ± 1	4 ± 0	3 ± 0
200 °C for 12 min	7 ± 1	5 ± 1	4 ± 0
With air-exchange	**Break-loose force [N]**	**Maximum gliding force [N]**	**Minimum gliding force [N]**
316 °C for 5 min	3 ± 0	3 ± 0	3 ± 0
316 °C for 12 min	4 ± 0	3 ± 0	3 ± 0
316 °C for 1 h	5 ± 2	4 ± 1	4 ± 1
200 °C for 12 min	11 ± 1	8 ± 1	6 ± 1

Functionality does not ultimately benefit from higher silicone levels. Extrusion forces reach a minimum plateau value while the silicone levels still increase. In a previous study in the heat-tunnel, extrusion forces leveled at 4-8 N for baked-on silicone levels of approximately 10 µg/cartridge, and 3-4 N at higher baked-on silicone levels from 20-100 µg/cartridge (see chapter IV). This was well in line with extrusion forces obtained in this study

Only a substantial decrease in the baked-on silicone level to 4 µg was clearly reflected in high extrusion forces up to 22 N (see chapter IV). During bake-on in the heat-oven, silicone levels were 9 ± 2 µg or higher, thus moderate extrusion forces were maintained after 1 h at 316 °C. On contrary, during bake-on in the heat-tunnel extrusion forces increased to 15 N after 1 h at 316 °C

with final baked-on silicone levels of 7 ± 2 µg. Already these slight differences in the baked-on silicone level of 2 µg between the heat-oven with air-exchange and the heat-tunnel after 1 h may lead to different force profiles. However, for moderate burn-in times at 316 °C, the heat-oven represents an adequate experimental model to mimic silicone levels and extrusion forces obtained by bake-on in the heat-tunnel.

Interestingly, both bake-on at 200 °C for 12 min in the heat-tunnel and the heat-oven led to slightly higher extrusion forces compared to bake-on at 316 °C for 12 min although the baked-on silicone levels were higher. Wetting of polymers on solid surfaces can be described as spherical capped droplets with a set of horizontal layers in parallel to a precursor film in front of the drop [120,121]. Heat promotes spreading by lowering the liquid-surface tension and the liquid viscosity [122]. Thereby, a more uniform silicone layer is suggested [11]. The ALTs after bake-on at 200 °C and 316 °C for 12 min in a heat-oven without air-exchange were comparable, but the silicone layers after bake-on at 200 °C for 12 min exhibited an irregular texture with small, darker grey spots along the cartridge barrel (Fig. V-8).

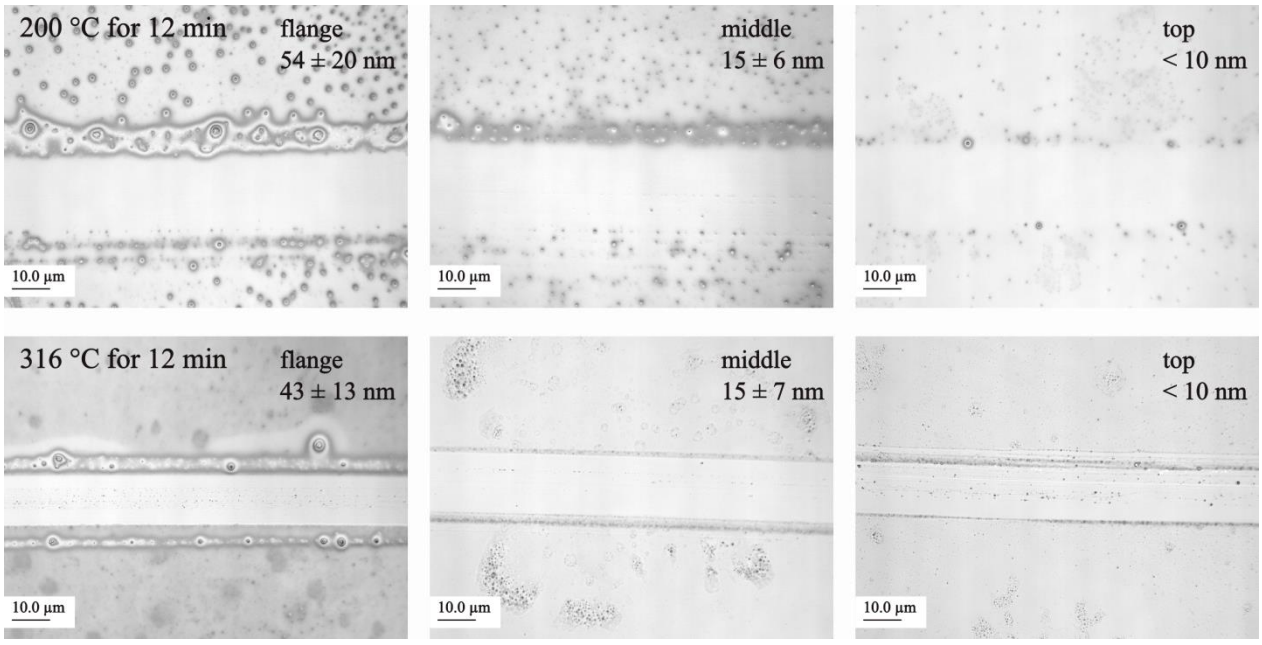

Fig. V-8. 3D-LSM analysis after bake-on siliconization in a heat-oven with air-exchange at 200 °C and 316 °C for 12 min using 16 mg spray quantity. Builds-ups next to the baseline derived from scratching with a 20 G cannula to create an artificial glass baseline and were not considered for ALT measurements. 3D-LSM images were similar for replicates.

At 316 °C the baked-on silicone layer was more homogeneous. In addition, larger, dark grey spots were observed indicating spreading and coalescence of the individual droplets.

Consequently, it can be argued that not only the baked-on silicone level, the measured ALTs and silicone distribution along the cartridge barrel substantially affect extrusion performance, but a certain temperature is essential to form a homogeneous baked-on silicone layer.

4 CONCLUSION

Bake-on siliconization for 12 min at 316 °C in a heat-tunnel provided functionality of cartridges with silicone levels as low as 13 ± 3 µg. A burn-in time of 1 h resulted in an insufficient lubrication as the maximum gliding forces increased due to decreased levels of silicone caused by burn-off. Thus, longer interruptions of the bake-on processes, i.e., longer exposure times at standard heat-tunnel conditions, should be avoided when using silicone levels below 30 µg/cartridge. However, at a baked-on silicone level of approximately 80 µg/cartridge longer burn-in times up to 2 h at 316 °C were well tolerated with regard to functionality.

A burn-in temperature around 300 °C correlated to the onset of the main weight loss in TGA at 313 ± 5 °C and at low baked-on silicone amounts, the layer thickness and the silicone level substantially decreased between 250 °C and 316 °C. Lower molecular weight fractions < 5,000 g/mol were removed at 316 °C and 350 °C and thus the relative proportion of higher molecular weight fractions increased. As a consequence, the average molecular weight of the bulk polymer remained rather constant at approximately 23,000 g/mol regardless of the burn-in temperature between 200 °C and 350 °C. In addition, peak tailing indicated an increased fraction between 5,000-15,000 g/mol as depolymerization products. Cyclic LMWS < 500 g/mol, which have been associated with toxicological concerns, did not remain in the baked-on silicone layer. Likewise, parabens and propylene glycol present as stabilizer in the silicone emulsion were quantitatively removed even below the standard burn-in temperature of 316 °C in this study, whereas thermal decomposition of non-ionic surfactants (Tween 20, Triton X-100) was incomplete.

Heat-oven treatment as an alternative to heat-tunnel bake-on led to comparable temperature profiles both without and with air-exchange. Air-exchange in the heat-oven was essential to model the baked-on silicone levels as achieved in the heat-tunnel at different burn-in times and temperatures since the airflow is necessary to remove silicone decomposition products. Bake-on studies at 200 °C and 316 °C for 12 min revealed, that a certain temperature above 200 °C was crucial to form a homogenous silicone layer.

Both untreated silicone oil and heat-treated silicone oil spin-coated on glass slides resulted in highly hydrophobic surfaces as indicated by CA measurements. These layers could apparently be removed from the glass surface. Although most of the silicone of directly baked-on siliconized cartridges was solvent-extractable, CA analysis suggested a thin silicone film remaining on the glass surface most likely due covalent siloxane bonds between silicone and the glass surface.

Bake-on siliconization processes are technically challenging as temperature and time settings are mutually related. Heat-treatment led to a time- and temperature-dependent decrease in the silicone level and layer thickness, but still for optimal spreading and uniform silicone layers temperatures as high as 300 °C may be essential. Overall, this study provides valuable insights into relevant parameters for bake-on siliconization processes. An extensive toolbox of methods was established to analyze associated heat-induced alterations of the baked-on silicone, which can be useful for the development of robust siliconization processes. For a short summary of all key results please refer to Tab. V-4.

Tab. V-4. Summary of key results.

Baked-on silicone layer characteristics	Impact of the bake-on process
Silicone level and coating functionality	• Silicone level decrease between 250 °C and 316 °C (12 min), no impact on functionality • Gradual silicone level decrease with longer burn-in times at 316 °C, insufficient functionality after 1 h • Higher silicone levels above 30 µg less dependent on burn-in conditions, bake-on induced changes covered by inherent variability in the initial silicone level
Silicone layer thickness distribution	• Thin silicone layers in the range of 10 nm to 70 nm (10 nm limit of detection [54], (see chapter III)) • Higher ALT at short burn-in time of 5 min at 316 °C • Higher ALT at low burn-in temperature of 200 °C for 12 min • Higher ALT at flange attributed to fixed nozzle position (20 mm below flange) (see chapter IV)
Thermal weight loss	• Onset main weight loss at 313 ± 5 °C correlated with silicone level decrease between 250 °C and 316 °C • Gradual weight loss in isothermal mode over time in agreement with gradual silicone level decrease with longer burn-in times • Residues of silicone emulsion stabilizers of no concern due to evaporation below 316 °C and effective dilution to low levels
Molecular weight distribution	• Decrease in molecular weight fraction < 5,000 g/mol at higher temperatures (316 °C, 350 °C) (M_n ↑) due to volatilization • Increase in relative proportion of higher molecular weight fractions (M_w↑) • Peak maxima unchanged (M_p) • Tailing at 316 °C and 350 °C indicating fraction of polymers between 5,000-15,000 g/mol as thermal cleavage products
Cyclic LMWS and parabens	• < calibration range, i.e., 0.001 % • No toxicological concern associated with LMWS
Covalent bonds	• Quantitative extraction of spin-coated silicone and heat-treated silicone, glass contact angle prevailed (glass slides) • Quantitative silicone recovery in FTIR from cartridges with high baked-on silicone levels • CA remained high on baked-on siliconized cartridges after harsh extraction indicating formation of thin covalently-bound silicone layer
Heat-oven as experimental model	• Consistent, comparable temperature profile at different target temperatures and airflow • Air-exchange to mimic silicone levels in heat-tunnel • Extrusion forces leveled at 4-7 N for silicone levels of approximately 10-20 µg/cartridge, 2-5 N for silicone levels of 20-100 µg/cartridge comparable to previous study in heat-tunnel (see chapter IV) • Coating functionality sensitive to silicone levels < 10 µg/cartridge • Certain temperature > 200 °C essential to form homogeneous silicone layer

5 SUPPORTING INFORMATION

Tab. S V-1. Peak molecular weights (M_p) and elution times of three different polystyrene standards in toluene (concentration 6 mg/mL, 5 µL injection volume).

Standard 1 (n = 5)		**Standard 2**		**Standard 3**	
Elution time [min]	**M_p [g/mol]**	**Elution time [min]**	**M_p [g/mol]**	**Elution time [min]**	**M_p [g/mol]**
11.591 ± 0.007	66000	13.296	28000	12.315	44200
13.956 ± 0.006	21500	15.580	9130	14.565	15700
17.136 ± 0.006	4920	20.787	682	17.827	3470
18.708 ± 0.006	2280	22.199	266	19.698	1250

a. b.

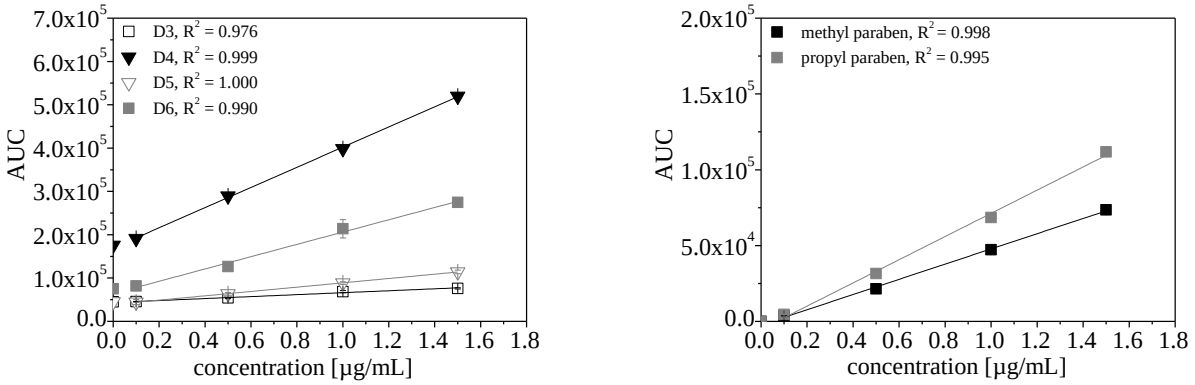

Fig. S V-1. Exemplary GC-MS calibration for (a) cyclic LMWS and (b) parabens ranging from 0.1-1.5 µg/mL.

a. b.

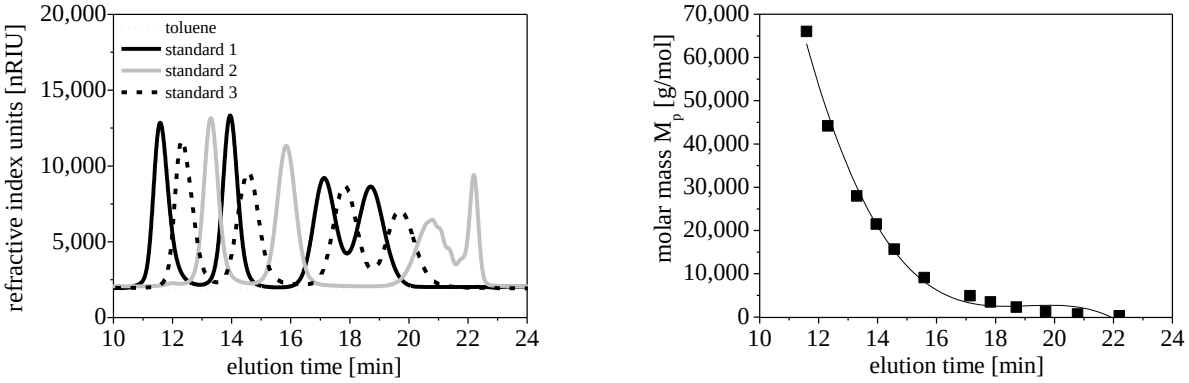

Fig. S V-2. GPC-RID calibration with three different polystyrene standards (concentration 6 mg/mL, 5 µL injection volume). (a) GPC-RID elution profiles and (b) 3rd polynomial fit calibration curve with $R^2 = 0.999$.

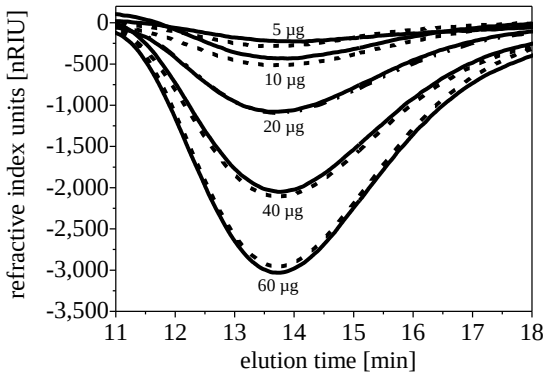

Fig. S V-3. GPC-RID elution profiles for double injections of 5-60 µg silicone oil in toluene (concentrations 0.5-6 mg/mL, 10 µL injection volume).

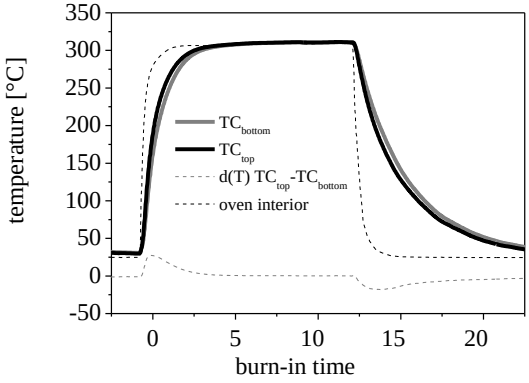

Fig. S V-4. Temperature profile within the oven interior and an exemplary cartridge, positioned at the left of the wire basket used during bake-on at 316 °C for 12 min, without air-exchange. TCs were positioned at the top and bottom of the cartridge.

6 ABBREVIATIONS

ALT	Average layer thickness
AUC	Area under the curve
CA	Contact angle
D3	Hexamethylcyclotrisiloxane
D4	Octamethylcyclotetrasiloxane
D5	Decamethylcyclopentasiloxane
D6	Dodecamethylcycloshexasiloxane
FTIR	Fourier transform infrared (spectroscopy)
GC-MS	Gas chromatography-mass spectrometry
GPC	Gel permeation chromatography
LMWS	Low molecular weight siloxanes
3D-LSM	3D-laser scanning microscopy
M_n	Number average molecular weight
M_w	Weight average molecular weight
M_p	Molecular weight of the peak maximum
PDI	Polydispersity index
PDMS	Polydimethylsiloxane
RID	Refractive index detection
TC	Thermocouple
TGA	Thermogravimetric analysis

7 REFERENCES

[1] B. Harrison, M. Rios, Big Shot: Developments in Prefilled Syringes, Pharm. Technol. 30 (2007) 42–48.

[2] D. Jenke, Suitability-for-use considerations for prefilled syringes, (2008). http://www.pharmtech.com/suitability-use-considerations-prefilled-syringes (accessed March 17, 2014).

[3] S. Makwana, B. Biswajit, Y. Makasana, A. Dharamasi, Prefilled syringes: An innovation in parenteral packaging, Int. J. Pharm. Inverstigations. 1 (2011) 200–206.

[4] B. Polin, The Ins and Outs of prefilles syringes, Pharmacutical Med. Packag. 11 (2003).

[5] J. Jezek, N.J. Darton, B.K. Derham, N. Royle, I. Simpson, Biopharmaceutical formulations for pre-filled delivery devices, Expert Opin. Drug Deliv. 10 (2013) 811–828.

[6] Y. Nashed-Samuel, D. Liu, K. Fujimori, L. Perez, H. Lee, Extractables and leachables implications on biological products in prefilled syringes, Am. Pharm. Rev. 14 (2011).

[7] G. Sacha, J.A. Rogers, R.L. Miller, Pre-filled syringes: a review of the history, manufacturing and challenges, Pharm. Dev. Technol. 20 (2015) 1–11.

[8] G.A. Sacha, W. Saffell-Clemmer, K. Abram, M.J. Akers, Practical fundamentals of glass, rubber, and plastic sterile packaging systems, Pharm. Dev. Technol. 15 (2010) 6–34.

[9] R.G. Ingle, A.S. Agarwal, Pre-filled syringe - a ready-to-use drug delivery system: a review, Expert Opin. Drug Deliv. 11 (2014) 1391–1399.

[10] T. Mundry, T. Schurreit, P. Surmann, The Fate of Silicone Oil During Heat-curing Glass Siliconization - Changes in Molecular Parameters Analyzed by Size Exclusion and High Temperature Gas Chromatography, PDA J. Pharm. Sci. Technol. 54 (2000) 383–397.

[11] A. Colas, Silicones in pharmaceutical applications. Part 5: Siliconization of parenteral packaging components, (2006). http://www.dowcorning.com/content/publishedlit/52-1094-01.pdf (accessed July 16, 2015).

[12] T. Mundry, P. Surmann, T. Schurreit, Surface characterization of polydimethylsiloxane treated pharmaceutical glass containers by X-ray-excited photo- and Auger electron spectroscopy, Fresenius. J. Anal. Chem. 368 (2000) 820–831.

[13] C. Petersen, Syringe Siliconisation. Trends, Methods, Analysis Procedures, Int. Pharm. Ind. 4 (2012) 92–99.

[14] T. Mundry, Einbrennsilikonisierung bei pharmazeutischen Glaspackmitteln - Analytische Studien eines Produktionsprozesses, Dissertation, Humboldt-Universität Berlin, 1999.

[15] K.B. Auge, A.W. Blake-Haskins, S. Devine, S. Rizvi, Y.-M. Li, M. Hesselberg, et al., Demonstrating the stability of albinterferon alfa-2b in the presence of silicone oil, J. Pharm. Sci. 100 (2011) 5100–5114.

[16] E. Chan, A. Hubbard, S. Sane, Y.-F. Maa, Syringe siliconization process investigation and optimization, PDA J. Pharm. Sci. Technol. 66 (2012) 136–150.

[17] J.S. Bee, V.V. Frey, U. Javed, J. Chung, M.L. Corcoran, P.S. Roussel, et al., Characterization of the Initial Level and Migration of Silicone Oil Lubricant in Empty Prefilled Syringes for Biologics Using Infrared Spectroscopy, PDA J. Pharm. Sci. Technol. 68 (2014) 494–503.

[18] L. Khandke, R. Malone, X. Yang, H. Han, J.L. Look, Z. Jin, et al., Novel formulations which stabilize and inhibit precipitation of immunogenic compositions, U.S. Patent 2011/0172393 A1, 2011.

[19] B. Reuter, Silicone oil and its applications for parenteral products, PDA Europe Workshop, Cologne, (2010).

[20] A. Badkar, A. Wolf, L. Bohack, P. Kolhe, Development of Biotechnology Products in Pre-filled Syringes: Technical Considerations and Approaches, AAPS PharmSciTech. 12 (2011) 564–572.

[21] F. Felsovalyi, S. Janvier, S. Jouffray, H. Soukiassian, P. Mangiagalli, Silicone-oil-based subvisible particles: their detection, interactions, and regulation in prefilled container closure systems for biopharmaceuticals, J. Pharm. Sci. 101 (2012) 4569–4583.

[22] E. Krayukhina, K. Tsumoto, S. Uchiyama, K. Fukui, Effects of syringe material and silicone oil lubrication on the stability of pharmaceutical proteins, J. Pharm. Sci. 104 (2015) 527–535.

[23] S. Majumdar, B.M. Ford, K.D. Mar, V.J. Sullivan, R.G. Ulrich, A.J.M. D'Souza, Evaluation of the effect of syringe surfaces on protein formulations, J. Pharm. Sci. 100 (2011) 2563–2573.

[24] R.A. Depaz, T. Chevolleau, S. Jouffray, R. Narwal, M.N. Dimitrova, Cross-linked silicone coating: a novel prefilled syringe technology that reduces subvisible particles and maintains compatibility with biologics, J. Pharm. Sci. 103 (2014) 1384–1393.

[25] M. Lankers, Analyse von Silikonschichtdicken bei der Herstellung von Fertigspritzen mit Hilfe von Refektometriemessungen, Pharm. Ind. 72 (2010) 2148–2153.

[26] A. Gerhardt, B.H. Nguyen, R. Lewus, J.F. Carpenter, T.W. Randolph, Effect of the siliconization method on particle generation in a monoclonal antibody formulation in pre-filled syringes, J. Pharm. Sci. 104 (2015) 1601–1609.

[27] T. Buch-Rasmussen, P. Jannasch, E. Bonne Jorgsen, I. Johannesen, S. Ndoni, N. Berg Madsen, Coating systems providing low friction, U.S. Patent 6,482,509 B2, 1999.

[28] A.J.M. D`Szouza, D.B. Montgomery, Medical components having coated surfaces exhibiting low frictiong and low reactivity, U.S. Patent US 2011/0313363 A1, 2011.

[29] J.D. Thornton, V.G. Sakhrani, A. Nagvekar, L. Jones Braun, Advanced lubrication systems for reducing subvisible particles based on downstream atmospheric gas plasma, Universe oft Prefilled Syringes and Injection Devices, Basel, (2013).

[30] M. Lankers, The relationship between silicone layer thickness, free silicone oil and protein aggregation on prefilled syringes, AAPS National Biotechnology Conference, San Francisco, (2010).

[31] European Directorate for the Quality of Medicines & HealthCare (EDQM), Ph. Eur. 3.1.8 Siliconöl zur Verwendung als Gleitmittel, (2014).

[32] G. Camino, S.. Lomakin, M. Lageard, Thermal polydimethylsiloxane degradation. Part 2. The degradation mechanisms, Polymer (Guildf). 43 (2002) 2011–2015.

[33] G. Camino, S.. Lomakin, M. Lazzari, Polydimethylsiloxane thermal degradation Part 1. Kinetic aspects, Polymer (Guildf). 42 (2001) 2395–2402.

[34] T.H. Thomas, T.C. Kendrick, Thermal analysis of polydimethylsiloxanes. I. Thermal degradation in controlled atmospheres, J. Polym. Sci. Part A-2 Polym. Phys. 7 (1969) 537–549.

[35] G. Montaudo, M.S. Montaudo, C. Puglisi, F. Samperi, Molecular weight distribution of poly(dimethylsiloxane) by combining matrix-assisted laser desorption/ionization time-of-flight mass spectrometry with gel-permeation chromatography fractionation, Rapid Commun. Mass Spectrom. 9 (1995)

1158–1163.

[36] M.S. Montaudo, C. Puglisi, F. Samperi, G. Montaudo, Application of size exclusion chromatography matrix-assisted laser desorption/ionization time-of-flight to the determination of molecular masses in polydisperse polymers, Rapid Commun. Mass Spectrom. 12 (1998) 519–528.

[37] K. Mojsiewicz-Pieńkowska, Size exclusion chromatography with evaporative light scattering detection as a method for speciation analysis of polydimethylsiloxanes. I: Influence of selected factors on the signal intensity of the detector., J. Pharm. Biomed. Anal. 53 (2010) 503–509.

[38] K. Mojsiewicz-Pieńkowska, Size exclusion chromatography with evaporative light scattering detection as a method for speciation analysis of polydimethylsiloxanes. II. Validation of the method for analysis of pharmaceutical formulations., J. Pharm. Biomed. Anal. 56 (2011) 851–858.

[39] S.B. Dorn, E.M.S. Frame, Development of a high-performance liquid chromatographic-inductively coupled plasma method for speciation and quantification of silicones: from silanols to polysiloxanes, Analyst. 119 (1994) 1687–1694.

[40] V.-P. Gabel, A. Kampik, J. Burkhardt, Analysis of intraocularly applied silicone oils of various origins, Graefe's Arch. Clin. Exp. Ophthalmol. 225 (1987) 160–162.

[41] T.C. Kendrick, Gel-permeation chromatography of polydimethylsiloxanes, J. Polym. Sci. Part A-2 Polym. Phys. 7 (1969) 297–307.

[42] R.S. Narins, K. Beer, Liquid injectable silicone: A Review of its history, immunology, technical considerations, complications, and potential, Plast Reconstr Surg. 118 (2006) 77S–84S.

[43] J. Ackermann, V. Damrath, Chemie und Technologie der Silicone II. Herstellung und Verwendung von Siliconpolymeren, Chemie Unserer ZEit. 3 (1989) 86–99.

[44] A. Ballistreri, D. Garozzo, G. Montaudo, Mass spectral characterization and thermal decomposition mechanism of poly(dimethylsiloxane), Macromolecules. 17 (1984) 1312–1315.

[45] Sigma-Aldrich Chemie GmbH, Material safety data sheet. Octamethylcyclotetrasiloxane, (2014) 8. http://www.sigmaaldrich.com/MSDS/MSDS/DisplayMSDSPage.do?country=DE&language=EN-generic&productNumber=235695&brand=ALDRICH&PageToGoToURL=http%3A%2F%2Fwww.sigmaaldrich.com%2Fcatalog%2Fproduct%2Faldrich%2F235695%3Flang%3Dde (accessed August 7, 2015).

[46] C. Rücker, K. Kümmerer, Environmental chemistry of organosiloxanes, Chem. Rev. 115 (2015) 466–524.

[47] C. Lassen, C.L. Hansen, S. Hagen Mikkelsen, J. Maag, Siloxanes - Consumption, Toxicity and Alternatives, Environmental project No. 1031 of the Danish Ministry of the Environment, (2005). http://www2.mst.dk/Udgiv/publications/2005/87-7614-756-8/pdf/87-7614-757-6.pdf (accessed July 13, 2015).

[48] E.D. Lykissa, S. V. Kala, J.B. Hurley, R.M. Lebovitz, Release of Low Molecular Weight Silicones and Platinum from Silicone Breast Implants, Anal. Chem. 69 (1997) 4912–4916.

[49] S. V Kala, E.D. Lykissa, M.W. Neely, M.W. Lieberman, Low molecular weight silicones are widely distributed after a single subcutaneous injection in mice., Am. J. Pathol. 152 (1998) 645–649.

[50] D. Flassbeck, B. Pfleiderer, R. Grümping, A. V. Hirner, Determination of Low Molecular Weight Silicones in Plasma and Blood of Women after Exposure to Silicone Breast Implants by GC/MS, Anal. Chem. 73

(2001) 606–611.

[51] L. Sun, H. Alexander, N. Lattarulo, N.C. Blumenthal, J.L. Ricci, G. Chen, Protein denaturation induced by cyclic silicone, Biomaterials. 18 (1997) 1593–1597.

[52] M. Prokopowicz, J. Łukasiak, B. Banecki, A. Przyjazny, In vitro measurement of conformational stability of fibrinogen adsorbed on siloxane., Biomacromolecules. 6 (2005) 39–45.

[53] M.J. Akers, K.E. Avis, B. Thompson, Validation Studies of the Fostoria Infrared Tunnel Sterilizer, PDA J. Pharm. Sci. Technol. 34 (1980) 330–347.

[54] S. Funke, J. Matilainen, H. Nalenz, K. Bechtold-Peters, H.-C. Mahler, W. Friess, Analysis of thin baked-on silicone layers by FTIR and 3D-Laser Scanning Microscopy, Eur. J. Pharm. Biopharm. 96 (2015) 304–313.

[55] J. Cazes, A Question of Molecular Weight, (1989). http://www.ampolymer.com/A Question of Molecular Weight.pdf (accessed July 22, 2015).

[56] L. Joseph, S. Martin, P. Kohle, K. Muthurania, Development of Syringeability Guide for Subcutaneous Protein Formulations, (2010). http://www.readbag.com/aapsj-abstracts-am-2010-w5265 (accessed August 14, 2015).

[57] M. Bowen, N. Armstrong, Y.-F. Maa, Investigating high-concentration monoclonal antibody powder suspension in nonaqueous suspension vehicles for subcutaneous injection., J. Pharm. Sci. 101 (2012) 4434–4443.

[58] European committee for standardization, EN ISO 11608-3. Needle-based injection systems for medical use - Requirements and test methods - Part 3: Finished containers, 2012.

[59] A. Sheikhzadeh, J. Yoon, D. Formosa, The effect of a new syringe design on the ability of rheumatoid arthritis patients to inject a biological medication, Appl. Ergon. 43 (2012) 368–375.

[60] Dow Corning Corporation, Frequently asked questions. Dow Corning 365, 35 % Dimethicone NF Emulsion, 2002.

[61] PDA, Technical report No. 12. Siliconization of parenteral drug packaging components, J. Parenter. Sci. Technol. 42 (1988) S2–S13.

[62] Z.-Q. Wen, A. Vance, F. Vega, X. Cao, B. Eu, R. Schulthesis, Distribution of Silicone Oil in Prefilled Glass Syringes Probed with Optical and Spectroscopic Methods, PDA J. Pharm. Sci. Technol. 63 (2009) 149–158.

[63] L.A. Spitze, D.O. Richards, Surface Studies of Glass. Part I. Contact Angles, J. Appl. Phys. 18 (1947) 904–911.

[64] H. Steinbach, C. Sucker, Über die Assoziation des Wassers an gespreiteten Filmen IV. Polyorganosiloxane, Colloid Polym. Sci. 252 (1974) 306–316.

[65] H. Steinbach, C. Sucker, Die Assoziation des Wassers an gespreiteten Filmen, Colloid Polym. Sci. 254 (1976) 656–669.

[66] Dow Corning Corporation, Material safety data sheet. Dow Corning 365, 35 % Dimethicone NF Emulsion, 2013.

[67] S.J. Clarson, J.A. Semlyen, Studies of cyclic and linear poly(dimethyl-siloxanes): 21. High temperature thermal behaviour, Polymer (Guildf). 27 (1986) 91–95.

[68] W. Patnode, D.F. Wilcock, Methylpolysiloxanes 1, J. Am. Chem. Soc. 68 (1946) 358–363.

[69] K. Chatterjee, D. Dollimore, K. Alexander, A new application for the Antoine equation in formulation development, Int. J. Pharm. 213 (2001) 31–44.

[70] K. Chatterjee, A. Hazra, D. Dollimore, K.S. Alexander, Estimating vapor pressure curves by thermogravimetry: a rapid and convenient method for characterization of pharmaceuticals, Eur. J. Pharm. Biopharm. 54 (2002) 171–180.

[71] A.S. Tatavarti, D. Dollimore, K.S. Alexander, A thermogravimetric analysis of non-polymeric pharmaceutical plasticizers: kinetic analysis, method validation, and thermal stability evaluation, AAPS PharmSci. 4 (2002) 1–12.

[72] Wissenschaftliche Verlagsgesellschaft Stuttgart, Commentary on Ph. Eur. 6.8/0409 Methyl-4-hydroxybenzoat., 2011.

[73] B.K. Meyer, A. Ni, B. Hu, L. Shi, Antimicrobial preservative use in parenteral products: past and present., J. Pharm. Sci. 96 (2007) 3155–3167.

[74] N. Vu, K. Nguyen, T.C. Kupiec, The essentials of United States Pharmacopeia Chapter <51> antimicrobial effectiveness testing and its application in pharmaceutical compounding., Int. J. Pharm. Compd. 18 (2014) 123–130.

[75] Wissenschaftliche Verlagsgesellschaft Stuttgart, Commentary on Ph. Eur. 6.8/0431 Propyl-4-hydroxybenzoat, (2011).

[76] M.J. Akers, Excipient-drug interactions in parenteral formulations., J. Pharm. Sci. 91 (2002) 2283–2300.

[77] S. Pramanick, D. Singodia, V. Chandel, Excipient selection in parenteral formulation development, Pharma Times. 45 (2013) 65–77.

[78] J. Poprzan, M.G. De Navarre, The interference of ninionic emulsifiers with preservatives VIII, J. Soc. Cosmet. Chem. 10 (1959) 81–87.

[79] H.J. Lee, A. McAuley, K.F. Schilke, J. McGuire, Molecular origins of surfactant-mediated stabilization of protein drugs, Adv. Drug Deliv. Rev. 63 (2011) 1160–1171.

[80] T.A. Khan, H.-C. Mahler, R.S.K. Kishore, Key interactions of surfactants intherapeutic proteinformulations: A review, Eur. J. Pharm. Biopharm. 97 (2015) 60–67.

[81] R.S.K. Kishore, A. Pappenberger, I.B. Dauphin, A. Ross, B. Buergi, A. Staempfli, et al., Degradation of polysorbates 20 and 80: studies on thermal autoxidation and hydrolysis., J. Pharm. Sci. 100 (2011) 721–731.

[82] B.A. Kerwin, Polysorbates 20 and 80 used in the formulation of protein biotherapeutics: structure and degradation pathways., J. Pharm. Sci. 97 (2008) 2924–2935.

[83] R.S.K. Kishore, S. Kiese, S. Fischer, A. Pappenberger, U. Grauschopf, H.-C. Mahler, The degradation of polysorbates 20 and 80 and its potential impact on the stability of biotherapeutics, Pharm. Res. 28 (2011) 1194–1210.

[84] X. Cao, R.M. Fesinmeyer, C.J. Pierini, C.C. Siska, J.R. Litowski, S. Brych, et al., Free fatty acid particles in protein formulations, part 1: microspectroscopic identification., J. Pharm. Sci. 104 (2015) 433–446.

[85] C.C. Siska, C.J. Pierini, H.R. Lau, R.F. Latypov, R.M. Fesinmeyer, J.R. Litowski, Free fatty acid particles in protein formulations, part 2: contribution of polysorbate raw material., J. Pharm. Sci. 104 (2015) 447–456.

[86] S. Uchiyama, Liquid formulation for antibody drugs., Biochim. Biophys. Acta. 1844 (2014) 2041–2052.

[87] United States Pharmacopeial Convention, United States Pharmacopeia. USP29-NF24 Octoxynol 9, (2007) 3381.

[88] G.E. Amidon, G.E. Peck, L.H. Block, R.C. Moreton, A. Katdare, R. Lafaver, et al., Proposed new USP general infomation chapter excipient performance <1059>, Pharmacopeial Forum. 33 (2007) 1311–1323.

[89] Sanofi Pasteur MSD GmbH, Fachinformation Vaxigrip 2015/2016, (2015) 1–4.

[90] K. Mojsiewicz-Pieńkowska, Size exclusion chromatography with evaporative light scattering detection: Method for the determination of polydimethylsiloxanes, J. Chromatogr. B. 865 (2008) 7–12.

[91] J. Kleinert, C. Weschler, Pyrolysis gas chromatographic-mass spectrometric identification of poly (dimethylsiloxanes), Anal. Chem. 52 (1980) 1245–1248.

[92] S. V Kala, E.D. Lykissa, R.M. Lebovitz, Detection and Characterization of Poly(dimethylsiloxane)s in Biological Tissues by GC/AED and GC/MS, Anal. Chem. 69 (1997) 1267–1272.

[93] S. Fujimoto, H. Ohtani, S. Tsuge, Characterization of polysiloxanes by high-resolution pyrolysis-gas chromatography-mass spectrometry, Fresenius' Zeitschrift Für Anal. Chemie. 331 (1988) 342–350.

[94] N. Ochiai, K. Sasamoto, M. Takino, S. Yamashita, S. Daishima, A.C. Heiden, et al., Simultaneous determination of preservatives in beverages, vinegar, aqueous sauces, and quasi-drug drinks by stir-bar sorptive extraction (SBSE) and thermal desorption GC-MS., Anal. Bioanal. Chem. 373 (2002) 56–63.

[95] H.-Y. Shen, H.-L. Jiang, H.-L. Mao, G. Pan, L. Zhou, Y.-F. Cao, Simultaneous determination of seven phthalates and four parabens in cosmetic products using HPLC-DAD and GC-MS methods, J. Sep. Sci. 31 (2008) 1864–1864.

[96] K. Nakamura, Factors contributing to the emulsification of intraocular silicone and fluorosilicone oils, Investig. Ophthalmol. Vis. Sci. 31 (1990) 2059–2069.

[97] J.M. Mathes, Protein Adsorption to Vial Surfaces – Quantification , Structural and Mechanistic Studies, Dissertation, Ludwig-Maximilians-Universität München, 2010.

[98] Krüss GmbH, Technical note TN306e. Models for sufaces free energy calculation, 1999.

[99] H. Fox, P. Taylor, W. Zisman, Polyorganosiloxanes...Surface Active Properties, Ind. Eng. Chem. 39 (1947) 1401–1409.

[100] W. Noll, H. Steinbach, C. Sucker, Das Spreitungsverhalten von Polyorganosiloxanen in Abhängigkeit von der Substitution, Fortschrittsberichte über Kolloide und Polym. 55 (1971) 131–142.

[101] S. Granick, S.. Clarson, T.. Formoy, J.. Semlyen, Studies of cyclic and linear poly(dimethylsiloxanes): 18. Surface pressures of the monolayers in the plateau region, Polymer (Guildf). 26 (1985) 925–929.

[102] T.D. Hahn, S.L. Hsu, H.D. Stidham, Reflectance Infrared Spectroscopic Analysis of Polymers at the Air−Water Interface. 4. Microstructure of Poly(dimethylsiloxane), Macromolecules. 30 (1997) 87–92.

[103] C. Kim, M.C. Gurau, P.S. Cremer, H. Yu, Chain conformation of poly(dimethyl siloxane) at the air/water interface by sum frequency generation., Langmuir. 24 (2008) 10155–10160.

[104] W. Noll, Zur Chemie und Technologie der Silicone, Angew. Chemie. 66 (1954) 41–55.

[105] L.T. Lee, E.K. Mann, D. Langevin, B. Farnoux, Neutron reflectivity and ellipsometry studies of a polymer molecular layer spread on the water surface, Langmuir. 7 (1991) 3076–3080.

[106] E.K. Mann, D. Langevin, Poly(dimethylsiloxane) molecular layers at the surface of water and of aqueous

surfactant solutions, Langmuir. 7 (1991) 1112–1117.

[107] Z. Liao, W.-T. Hsieh, T. Baumgart, I.J. Dmochowski, Measuring interactions between polydimethylsiloxane and serum proteins at the air-water interface., Langmuir. 29 (2013) 9420–9427.

[108] W. Noll, H. Steinbach, C. Sucker, Monolayers of polyorganosiloxanes on water, J. Polym. Sci. Part C Polym. Symp. 34 (1971) 123–139.

[109] E. Rödel, F. Blatter, J.-P. Büttiker, W. Weirich, H.-C. Mahler, Contact angle measurement on glass surfaces of injection solution containers, Pharm. Ind. 2 (2013) 328–332.

[110] V.A. Ogarev, V.M. Rudoi, A.A. Trapeznikov, Wettability of layers of polydimethylsiloxanes, transferred to glass by the langmuir method and produced by adsorption from solution, Bull. Acad. Sci. USSR Div. Chem. Sci. 21 (1972) 2421–2425.

[111] H. Hillborg, S. Karlsson, U.. Gedde, Characterisation of low molar mass siloxanes extracted from crosslinked polydimethylsiloxanes exposed to corona discharges, Polymer (Guildf). 42 (2001) 8883–8889.

[112] R.G. Horn, J.N. Israelachvili, Molecular organization and viscosity of a thin film of molten polymer between two surfaces as probed by force measurements, Macromolecules. 21 (1988) 2836–2841.

[113] T. Sandle, A practical approach to depyrogenation studies using bacterial endotoxin, J. GXP Compliance. 15 (2011) 90–96.

[114] U.S. Validation Services Inc., Validation knowledge base. Depyogenation, (2011). http://www.usvalidation.com/kb/eq_depyro_oven.aspx (accessed August 7, 2015).

[115] U.S. Food and Drug Administration (FDA), No. 40 Bacterial endotoxins/pyrogens, (1985). http://www.fda.gov/ICECI/Inspections/InspectionGuides/InspectionTechnicalGuides/ucm072918.htm (accessed August 10, 2015).

[116] U.S. Food and Drug Administration (FDA), Chapter 56 - Drug quality assurance. Subject: Sterile drug process inspections, (2012). http://www.fda.gov/downloads/ICECI/ComplianceManuals/CompliancePrograMManual/UCM125409.pdf (accessed August 10, 2015).

[117] H. Strunck GmbH + Co. Maschinenfabrik - Bosch Gruppe, Information brochure. Sterilisiertunnel der TSQ-Reihe. Die idealen Anlagen für Ampullen, Vials, Injektionsfläschen und Zylinderampulllen, n.d.

[118] L.B. Case, G.D. Heffernan, Dry heat sterilization and depyrogenation validation and monitoring, in: J.P. Agalloco, F.J. Carleton (Eds.), Valid. Pharm. Process., 3rd ed., CRC Press, 2007: pp. 223–240.

[119] Thermo Scientific Inc., Heraeus Wärme-Umluftschranke WU 6100, (n.d.). https://www.labmarket.com/pdf/Kendro/WU_6100_Waerme_Umluft_G_0599.pdf (accessed August 10, 2015).

[120] P. de Gennes, Wetting: statics and dynamics, Rev. Mod. Phys. 57 (1985) 827–863.

[121] J. De Coninck, M.J. de Ruijter, M. Voué, Dynamics of wetting, Curr. Opin. Colloid Interface Sci. 6 (2001) 49–53.

[122] R. Asthana, N. Sobczak, Wettability, spreading and interfacial phenomena in high-temperature coatings, JOM-E. 52 (2000).

VI SILICONE MIGRATION FROM BAKED-ON SILICONE LAYERS. PARTICLE CHARACTERIZATION IN PLACEBO AND PROTEIN SOLUTIONS

GRAPHICAL ABSTRACT

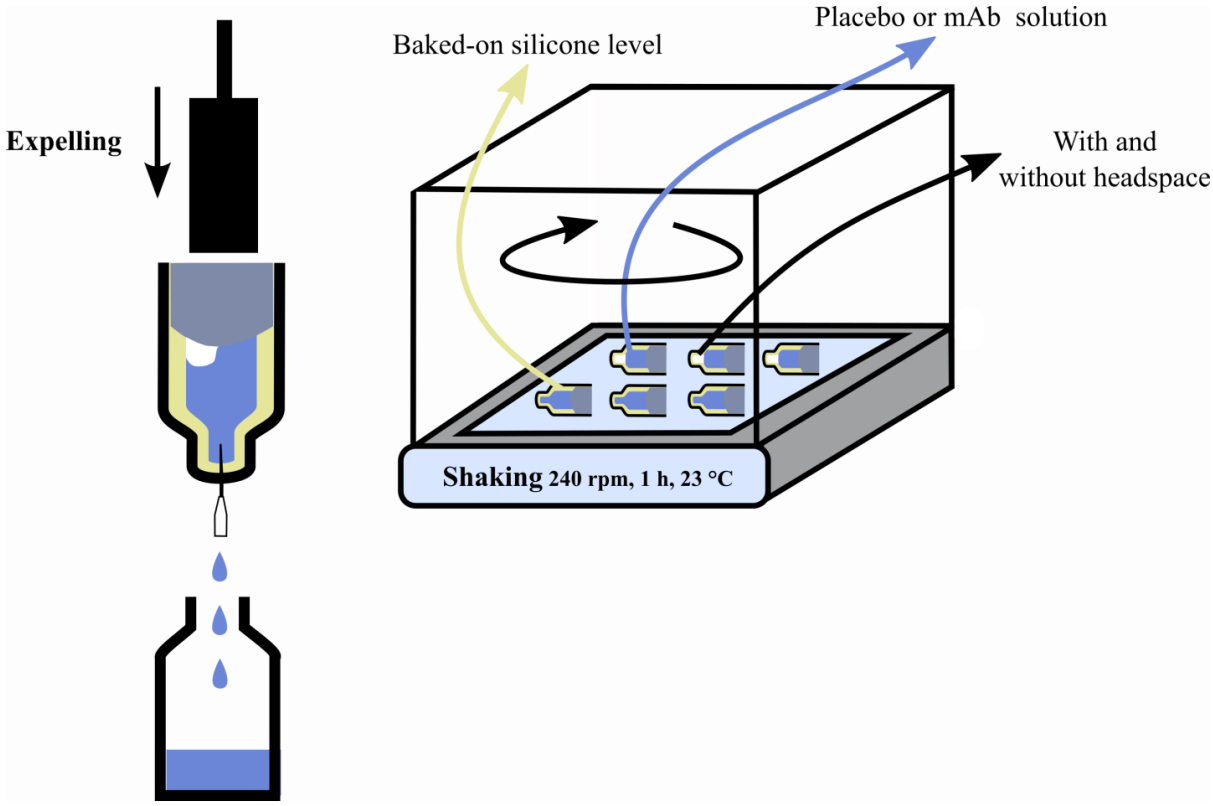

ABSTRACT

A significant amount of therapeutic proteins are marketed as pre-filled syringes or other drug/device combination products, and have been safely used in these formats for years. Silicone oil, which is used as lubricant, can migrate into the drug product and has been suggested to be potentially critical for protein stability. In this study, particles in the size range of 0.2-5 µm and ≥ 1 µm as determined by resonant mass measurement and micro-flow imaging/light obscuration, respectively, resulted from silicone sloughing off the container barrel after agitation. The degree of droplet formation correlated well with the applied baked-on silicone levels of 13 µg and 94 µg per cartridge. Silicone migration was comparable in placebo, 2 mg/mL and 33 mg/mL IgG1 formulations containing 0.04 % (w/v) polysorbate 20. Headspace substantially increased the formation of silicone droplets during agitation. The highest particle concentrations reached, however, were still very low compared to numbers described for spray-on siliconized containers. When applying adequate baked-on silicone levels below 100 µg, bake-on siliconization efficiently limits silicone migration into the drug product without compromising device functionality.

This chapter is intended for publication.

1 INTRODUCTION

Particle formation in biopharmaceutical drug products has become the subject of increasing scrutiny within the biopharmaceutical industry [1–3]. Aggregation and particle formation are important degradation pathway for proteins, possibly triggered by a wide range of stress conditions such as temperature, freeze/thaw and agitation [4–6]. Some levels of particles are ubiquitously found in marketed products, but without evidence of safety risks [3]. In addition to proteinaceous particles, the contact with various materials during manufacturing may result in heterogeneous or nonproteinaceous particles originating e.g., from stainless steel pumps, filters, tubing or glass containers [7–10].

In particular, the compatibility of proteins with siliconized drug product containers has been critically addressed in the literature as pre-filled syringes (PFS) and cartridges have become increasingly used primary containers in health care [11–14]. High levels of silicone have been reported to lead to protein aggregation in formulation when not appropriately formulated, in particular upon agitation [15–21], at increased temperatures [22,23] or upon periodically rupture of the silicone oil-water interface [24]. However, increased levels of spiked-in silicone did not result in aggregation or precipitation during quiescent storage at 4 °C and 37 °C [20] or room temperature [25,26]. Other studies also suggest that particle level and turbidity increase are most likely due to silicone migration rather than enhanced protein instability [18,27–31]. Nonetheless, proteins have a high propensity to interact with surfaces, making them susceptible to adsorption at the liquid-silicone oil interface, however, only in the absence of surfactants in the formulation [19,20,25,26,32].

Several approaches can be envisaged to mitigate protein-silicone oil interactions. First, state-of-the-art formulation development, e.g., the addition of surfactants, has been shown to prevent proteins from adsorption and degradation [19,20,24–26,32]. Second, optimized siliconization processes with sufficient, but limited silicone levels and well defined silicone distribution can be utilized (see chapter IV). Silicone oil is essential as lubricant for device functionality to ensure smooth and easy injection [12,13,33]. In traditional spray-on siliconization processes approximately 0.2 mg to 1 mg silicone oil per container is applied [17,18,23,33–39] compared to bake-on processes, which employ an aqueous silicone emulsion followed by bake-on at approximately 300 °C for 10-30 min [27,40–42]. Bake-on siliconization results in limited silicone levels below approximately 0.1 mg per container [34,43,44]. Thereby, bake-on siliconized primary containers present less likelihood to slough off silicone droplets into the formulation

compared to spray-on siliconized containers [15,23,35,37]. Recently, alternative siliconization methods using cross-linkable silicone have been reported to further prevent silicone transfer into the product [15,18,35,37].

In this work, we applied a bake-on siliconization process that has been developed and optimized previously (see chapter IV and V) to evaluate the effect of different baked-on silicone levels below 100 µg on the formation of particles in cartridges filled with placebo after expelling, shaking and a combination thereof. Different sampling via expelling and shaking stress as well as different silicone levels may result in entirely different particle concentrations [35]. In addition, the subvisible particle formation was assessed after filling with two different concentrations of monoclonal antibody solution (mAb) (2 mg/mL and 33 mg/mL) followed by shaking in the presence and absence of headspace. No single analytical technique is able to cover the entire range from soluble aggregates to visible particles. A number of reviews highlight the selection of appropriate orthogonal techniques including advantages and limitations to monitor aggregates and particulates [45–51]. Therefore, a set of different analytical techniques was applied also to benefit from advances that have been made to discriminate silicone oil droplets from proteinaceous particles using resonant mass measurements (RMM) and micro-flow imaging (MFI) [52–56]. As polysorbates are most frequently used as excipients [57–59], studies were performed in the presence of 0.04 % (w/v) polysorbate 20.

2 MATERIALS AND METHODS

2.1 MATERIALS

Non-siliconized 5 mL cartridges (barrel length 32 mm, inner diameter 19 mm, outer diameter 22 mm), pistons, serum stoppers and aluminum seals were provided by F. Hoffmann-La Roche Ltd (Basel, Switzerland). Elastomeric components were coated with fluoropolymer (FluroTec®). Polyethersulfone syringe filters (0.2 µm) were obtained from VWR International GmbH (Darmstadt, Germany). Whatman Anatop 10 (0.02 µm) filters were purchased from GE Healthcare Europe GmbH (Freiburg Germany). 4R vials and stoppers (both non-siliconized) were provided by Schott AG (Mainz, Germany) and West Pharmaceutical Services, Inc. (Exton, PA, USA), respectively. Disposable silicone oil-free1 mL plastic syringes and 22 G, 40 mm thin wall needles were obtained from Henke-Sass, Wolf GmbH (Tuttlingen, Germany) and Terumo Deutschland GmbH (Wettingen, Germany), respectively.

Chemicals were purchased as follows: 365 35 % Dimethicone NF Emulsion and 360 Medical Fluid, 350 cSt, from Dow Corning GmbH (Wiesbaden, Germany); heptane from Riedel-de Haën (Seelze, Germany); L-histidine monohydrochloride monohydrate and L-histidine both from Ajinomoto Europe S.A.S (Louvain-la-Neuve, Belgium); sodium hydroxide standard volumetric solution 1 M from AppliChem GmbH (Darmstadt, Germany); polysorbate 20 from Croda GmbH (Nettetal-Kaldenkirchen, Germany); polystyrene particle standards 0.994 µm from Thermo Scientific Inc. (Waltham, MA, USA) and tergazyme® enzyme detergent from Alconex Inc. (New York, NY, USA). A 33.4 mg/mL IgG1 mAb stock solution in 20 mM histidine buffer pH 5.4 was kindly provided by Roche Deutschland Holding GmbH (Penzberg, Germany).

2.2 BAKE-ON SILICONIZATION PROCESS

Bake-on siliconization was performed on a SVS9061 pilot-scale siliconization unit from Bausch + Ströbel Maschinenfabrik Ilshofen GmbH+Co. KG (Ilshofen, Germany) equipped with an external mixing, two-fluid nozzle. Optimized spray parameters were established in previous experiments: spray quantity of 4 mg silicone emulsion, fixed nozzle position of 20 mm below the flange, spray pressure of 1 bar and time for pump dosing of 175 ms (see chapter IV). The cartridges were subsequently treated at 316 °C for 12 min in a TSQ U03 heat-tunnel from Robert Bosch GmbH (Stuttgart, Germany).

Dow Corning 365 35 % Dimethicone NF Emulsion was diluted to 0.6 % (w/w) or 3.5 % (w/w)

with highly purified water to obtain a final baked-on silicone level of 13 ± 3 µg/cartridge and 94 ± 6 µg/cartridge, respectively (see chapter IV).

2.3 PREPARATION OF PROTEIN SAMPLES

20 mM histidine buffer, pH 6, containing 0.04 % (w/v) polysorbate 20 was used as placebo. Solutions of 2 mg/mL (mAb) and 33 mg/mL (mAb HC, higher concentration) in 20 mM histidine buffer, pH 6, and 0.04 % (w/v) polysorbate 20 were prepared from stock solutions. After filtration (0.2 µm), mAb concentrations were verified by UV at 280 nm using a NanoDrop 2000 spectrophotometer from Thermo Fisher Scientific Inc. (Waltham, MA, USA) and an extinction coefficient of 1.51 cm^2/mg.

2.4 SAMPLE PREPARATION/AGITATION STUDIES

After bake-on siliconization, the pistons and cartridges were manually assembled. The containers were filled with a target volume of 5.16 mL placebo, mAb or mAb HC solution and sealed with serum stoppers and aluminum caps. After stoppering, the headspace was calculated as 611 µL assuming a final fluid level of 9.6 ± 0.1 mm from the cartridge top. For experiments without headspace, cartridges were filled and carefully stoppered so that no visible air bubble remained.

Cartridges were expelled through the needle using a material testing instrument TA.XT.plus from Winopal Forschungsbedarf GmbH (Elze, Germany) at a constant displacement speed of 5.6 mm/min over a distance of 17.5 mm (maximum travel distance for the piston within the cartridge barrel), thereby mimicking approximately 3 min injection time.

Agitation was performed at 240 rpm on a 360° horizontal Certomat IS rotator from B. Braun Biotech International GmbH (Melsungen, Germany) for 1 h at 23 °C with cartridges positioned horizontally. The horizontal rotation frequency and test duration followed vehicle vibration tests from ISTA 2A and ASTM D 4169 – 08. Samples were collected by pipetting or decanting through the cartridge orifice after removing the serum stopper.

2.5 LIGHT OBSCURATION (LO)

LO analysis was performed using a PAMAS SVSS-C instrument equipped with a standard sensor HCB-LD-25/25 from Partikel- und Analysensysteme GmbH (Rutesheim, Germany). Prior to analysis, the system was flushed with highly purified water (at least 5 mL) until the cumulative particle concentration ≥ 1 µm was below 30 particles/mL. Samples were analyzed at least in triplicates. Each measurement consisted of a pre-run volume of 0.5 mL followed by three runs of

0.3 mL sample at an emptying and rinse rate of 5 mL/min. Particle concentrations were reported by PAMAS PMA V 2.1.2.0.

2.6 MICRO-FLOW IMAGING (MFI)

A MFI system DPA4100 from ProteinSimple (Santa Clara, CA, USA) equipped with a 470 nm LED light source and a high magnification (14 x) 100 µL flow cell was controlled by MFI View Software version 6.9. Placebo was used to "optimize illumination" prior or each measurement. The sample purge volume was 0.3 mL followed by 0.65 mL dispensed sample at a flow rate of 0.1 mL/min. "Edge particle rejection" and "fill particle" option were activated. Between each sample, the system was flushed with 5 mL highly purified water at maximum flow rate and visually checked for flow cell cleanliness. Samples were analyzed at least in duplicates. MVAS version 3.1 from ProteinSimple was used for data analysis. The "find similar" operation was employed to discriminate silicone-like from other particles based on the optical parameters of 30 particles ≥ 5 µm that were visually identified as silicone droplets. Optical filter parameters selected from MVAS for silicone-like particles were $514 \leq$ intensity mean ≤ 740, $0.8 \leq$ aspect ratio ≤ 1.1 and $0.4 \leq$ circularity ≤ 0.9.

2.7 TURBIDITY

A Nephla LPG239 turbidimeter from Hach Lange GmbH (Düsseldorf, Germany) was employed for turbidity measurements at $\lambda = 860$ nm in prerinsed 12 mm clear glass test tubes. Samples were analyzed at least in duplicates and results are given in formazin nephelometric units (FNU).

2.8 RESONANT MASS MEASUREMENTS (RMM)

RMM measurements were performed using an Archimedes system from Malvern Instruments Ltd. (Herrenberg, Germany) equipped with a Hi-Q micro sensor (size range 0.15-5 µm, channel dimension 8 µm x 8 µm). Initially, the sensor was calibrated with 0.994 ± 0.050 µm polystyrene size standards with an accuracy of ≥ 95 %. The lower limit of detection was determined in automatic mode for exemplary placebo and mAb HC samples. Subsequently, a mean value of 0.034 ± 0.013 Hz was manually selected as threshold limit for sample analysis. The density of positive buoyant particles was adjusted to 0.972 g/cm^3 [60] (referred to as "silicone-like"). Furthermore, the density of negative buoyant particles was set to 1.32 g/cm^3 ("other particles") as suggested by the RMM manufacturer and well within the density range reported for proteins in literature between 1.28 g/cm^3 to 1.43 g/cm^3 [61–63]. A fluid density of 1.000 g/cm was measured

for placebo and mAb samples, whereas for mAb HC samples the density was adjusted to 1.009 g/cm^3 (see 2.11). Before each measurement, the system was rinsed with highly purified water for 5 min, 1 % tergazyme® for 1 min and finally with highly purified water until a clean frequency trace was achieved. Between each rinsing step, additionally three "sneeze" operations were employed to remove possible impurities. Subsequently, the sample was loaded until a stable baseline was achieved (at least 45 s). The endpoint of measurement was 20 min with sample volumes ranging from 0.1-0.5 µL. The "autoreplenish" function was activated every 5 min for 5 s to periodically flush the fluidic tubing with fresh sample. Samples were analyzed at least in triplicates using ParticleLab software version 1.8.510 from Malvern Instruments Ltd. (Herrenberg, Germany).

2.9 DYNAMIC LIGHT SCATTERING (DLS)

DLS measurements were performed with a Zetasizer Nano-ZS ZEN3600 system from Malvern Instruments Ltd. (Herrenberg, Germany) equipped with a 633 nm He-Ne laser and non-invasive backscatter detection at an angle of 173°. Samples were analyzed at least in triplicates with three measurements each using automatic attenuation factor, measurement position and duration after 20 s equilibration time at 25 °C. A sample volume of 420 µL was measured in disposable semi-micro polymethyl methacrylate cuvettes from Brand GmbH + Co. KG (Wertheim, Germany). The Z-average diameter and polydispersity index (PDI) were calculated from the autocorrelation function obtained in "general purpose mode (normal resolution)" using Zetasizer software 7.03.

2.10 NANOPARTICLE TRACKING ANALYSIS (NTA)

NTA was performed using NS200, LM20 series from Nanosight Ltd (Amesbury, UK) equipped with a 405 nm laser. Prior to analysis, the sample chamber was flushed with 3 mL 0.02 µm filtered water. Samples were injected using a 1 mL syringe and a pre-run volume of 300 µL followed by 200 µL sample for first video analysis at stopped flow. For each triplicate sample, three video files were recorded with 200 µL sample flushed between each video. NTA 2.2 software was used for capturing and analyzing the data as well as automatic temperature acquisition. The focus was adjusted to obtain clear particle images without refractive rings. Initially, shutter and gain were optimized until no more new particles appeared on the screen and best contrast between background and particles was achieved. For placebo and mAb samples, the shutter was set to 597-603, the gain to 298-303 and the capture duration was 60 s for each video. In mAb HC samples, the gain was decreased to zero due to background light scattering of the

mAb solution matrix. For analysis the detection threshold was seven and the blur was set to 7 x 7. A minimum track length of ten and automatic minimum expected particle size were utilized. For placebo and low concentration mAb samples, the viscosity was 1.00 ± 0.01 mPa*s and 1.02 ± 0.01 mPa*s at 20 °C, respectively. Therefore, the viscosity was software-based adapted from water as dispersant (0.88 mPa*s at 25 °C) while for mAb HC the viscosity was adjusted to 1.42 ± 0.01 mPa*s at 20 °C (see 2.11).

2.11 PHYSICOCHEMICAL PROPERTIES OF THE SAMPLE SOLUTIONS

The refractive index (RI) was measured using an Abbé refractometer from Carl Zeiss (Jena, Germany) at a wavelength of 589 nm at room temperature.

Viscosity measurements were performed on a mVROC viscosimeter from Rheosense Inc. (San Ramon, CA, USA) equipped with an A-series chip with a flow channel depth of 50.8 µm at a constant shear rate of $1.90*10^{7}$ s^{-1} and 20 °C. Control software v2.6 was utilized for data analysis. The density was determined using DMA 38 density meter from Anton Paar GmbH (Graz, Austria) at 20 °C.

2.12 MIGRATED SILICONE AMOUNT IN PLACEBO BY FOURIER TRANSFORM INFRARED (FTIR) QUANTIFICATION

The migrated silicone amount in placebo was determined by FTIR spectroscopy after solvent extraction. Placebo samples after agitation were quantitatively decanted from the cartridges through the needle-side orifice into 4R vials and evaporated to dryness using a flowtherm evaporator at 100 °C and constant nitrogen flow of 210 mL/min from Barkey GmbH & Co. KG (Leopoldshöhe, Germany). Silicone in the dried extract was redissolved in 1 mL heptane. Two extracts were combined, followed by two rinsing steps à 1 mL heptane for each vial. The combined extracts were evaporated to dryness and finally redissolved in 250 µL heptane for FTIR analysis. According to considerations provided in ICH Q2 R1 Validation Analytical Procedure, the limit of detection of the developed FTIR method was found to be below 1 µg/mL (number of calibration curves n = 22). The limit of quantification was 18 µg/mL (n = 22). The analytical method was thus capable to quantify down to 4 µg per cartridge based on 250 µL dissolution volume [64] (see chapter III).

3 RESULTS

3.1 SILICONE MIGRATION IN PLACEBO

MFI and LO analysis were used to elucidate the effect of different baked-on silicone levels (13 µg and 94 µg per cartridge) on silicone migration into placebo. In addition, the effect of different sampling via expelling through the needle and shaking stress with and without headspace were evaluated as they may result in entirely different particle concentrations [35].

After expelling, low concentrations of particles ≥ 1 µm were detected in non-siliconized and different bake-on siliconized cartridges with headspace by MFI (3,200-4,100 particles/mL) and LO (2,000-2,400 particles/mL) (Fig. VI-1a). The concentration of particles generated through shaking with headspace increased to 3,500 particles/mL and 35,300 particles/mL in MFI, and to 1,300 particles/mL and 23,100 particles /mL in LO with higher silicone levels of 13 µg and 94 µg per cartridge, respectively. A combination of both shaking and expelling resulted in similar particle concentrations as compared to shaking alone.

a. b.

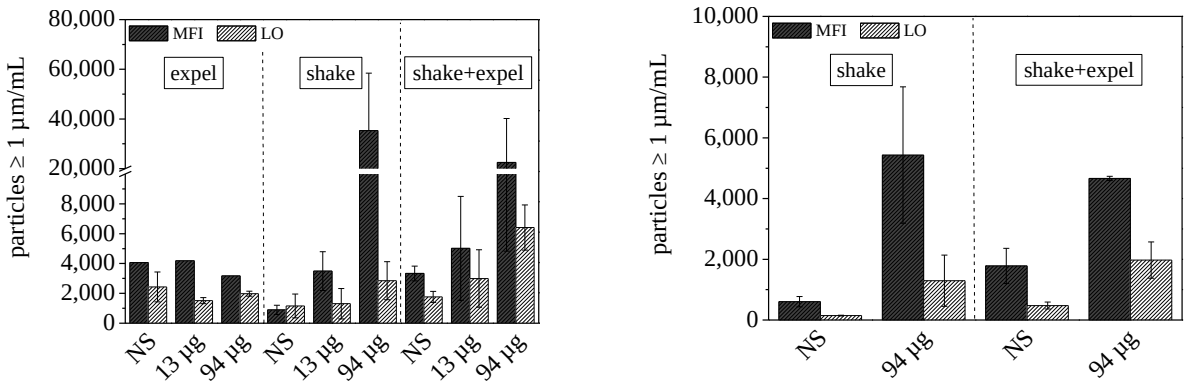

Fig. VI-1. Particle concentration ≥ 1 µm/mL (MFI and LO) in 20 mM histidine placebo, pH 6, as a function of baked-on silicone levels and different sampling/agitation stress (a) with headspace and (b) without headspace. Non-siliconized cartridges were abbreviated with NS.

Expelling had a less pronounced effect on particle formation and was therefore not further evaluated in cartridges without headspace (Fig. VI-1b). In the absence of headspace, fewer particles were formed. In non-siliconized cartridges, the particle concentration was below 1,800 particles/mL in MFI and below 500 particles/mL in LO after different sampling. Both shaking and shaking+expelling in combination with a higher silicone level of 94 µg per cartridge similarly increased the particle concentration to 4,700-5,400 particles/mL in MFI and to 1,300-2,000 particles/mL in LO.

MFI and LO reflected the same trends in particle concentrations, but MFI consistently detected higher particle concentrations, which can be attributed to an increased sensitivity for more transparent particles such as silicone droplets or protein particles [70,82–84].

None of these samples showed a change in turbidity (Tab. VI-1).

Tab. VI-1. Turbidity in 20 mM histidine placebo, pH 6, as a function of baked-on silicone levels and different sampling/agitation stress with and without headspace.

Sample description	**Turbidity [FNU]**	**Turbidity [FNU]**
Expel	**With headspace**	**Without headspace**
NS	< 1	-
13 µg	< 1	-
94 µg	< 1	-
Shake	**With headspace**	**Without headspace**
NS	< 1	< 1
13 µg	< 1	-
94 µg	< 1	< 1
Shake+expel	**With headspace**	**Without headspace**
NS	< 1	< 1
13 µg	< 1	-
94 µg	< 1	< 1

3.2 PARTICLE FORMATION AFTER AGITATION IN MAB SOLUTIONS

3.2.1 CONCENTRATION OF PARTICLES ≥ 1 µm/mL (MFI AND LO) AND TURBIDITY

Since shaking showed the most severe effect on particle formation in placebo, cartridges filled with 2 mg/mL mAb and 33 mg/mL mAb HC were also exposed to this stress. Non-siliconized cartridges with headspace contained 900-2,700 particles ≥ 1 µm per mL in MFI and 400-1,200 particles ≥ 1 µm per mL in LO for the different filling solutions (Fig. VI-2a). With higher silicone levels of 13 µg and 94 µg per cartridge, particle concentrations increased up to 6,300 particles/mL and 55,400 particles/mL in MFI, respectively, and to 1,400 particles/mL and 3,400 particles/mL in LO. The same trend but at lower particle concentrations was observed in cartridges without headspace (Fig. VI-2b). The mAb concentration did not affect the particle

counts ≥ 1 µm per mL in bake-on siliconized cartridges with and without headspace (Fig. VI-2a and Fig. VI-2b).

a.

b.

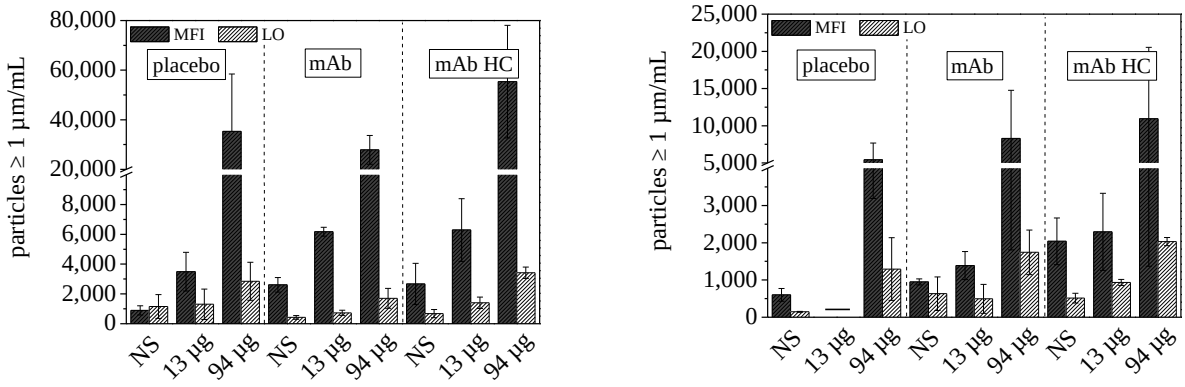

c.

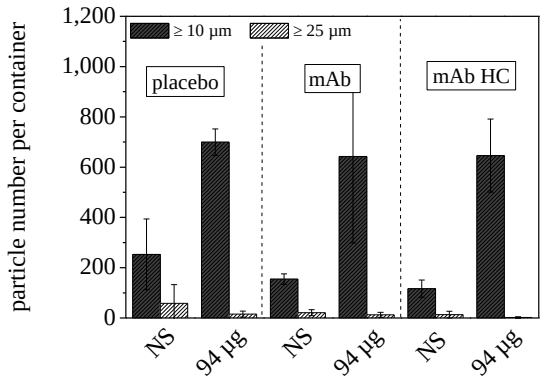

Fig. VI-2. Particle concentration ≥ 1 µm/mL (MFI and LO) after agitation as a function of baked-on silicone levels and mAb concentrations (a) with headspace and (b) without headspace. (c) Subvisible particles ≥ 10 µm and ≥ 25 µm per container (94 µg baked-on silicone, after agitation with headspace) by LO are additionally shown as outlined by pharmacopeia. Cartridges were filled with 20 mM histidine placebo, pH 6, 2 mg/mL mAb or 33 mg/mL mAb HC.

Also, the particle numbers in cartridges with a high silicone level of 94 µg per cartridge and agitated with headspace (650-700 particles/container ≥ 10 µm and 2-60 particles/container ≥ 25 µm (Fig. VI-2c) remained well below the limits of current pharmacopeia for parenteral products, in particular for protein injections (≤ 6,000 particles/container ≥ 10 µm and ≤ 600 particles/container ≥ 25 µm [68–70]).

Additionally, both mAb and mAb HC pre-filled in cartridges with a 13 µg silicone level met the requirements for ophthalmic solutions (≤ 50 particles/mL ≥ 10 µm and ≤ 5 particles/mL ≥ 25 µm [71]), whereas cartridges with a 94 µg baked-on silicone level failed these tight criteria (Tab. VI-2).

Tab. VI-2. Subvisible particle concentration ≥ 10 µm and ≥ 25 µm per mL by LO as outlined by pharmacopeia for ophthalmic solutions. Cartridges were filled with 20 mM histidine placebo, pH 6, 2 mg/mL mAb or 33 mg/mL mAb HC.

Sample description	LO ≥ 10 µm/mL	LO ≥ 25 µm/mL
Placebo		
NS	22 ± 14	4 ± 6
13 µg	25 ± 22	1 ± 2
94 µg	97 ± 21	2 ± 1
mAb		
NS	10 ± 5	2 ± < 1
13 µg	14 ± 6	1 ± 2
94 µg	64 ± 33	1 ± 1
mAb HC		
NS	7 ± 2	1 ± 1
13 µg	19 ± 3	1 ± 1
94 µg	90 ± 22	0 ± < 1

The turbidity was < 1 FNU for 2 mg/mL and 3-4 FNU for 33 mg/mL mAb formulations and did not change with higher silicone levels (Tab. VI-3).

Tab. VI-3. Turbidity after agitation as a function of baked-on silicone levels and mAb concentrations with and without headspace. Cartridges were filled with 20 mM histidine placebo, pH 6, 2 mg/mL mAb or 33 mg/mL mAb HC.

Sample description	Turbidity [FNU]	Turbidity [FNU]
Placebo	**With headspace**	**Without headspace**
NS	< 1	< 1
13 µg	< 1	-
94 µg	< 1	< 1
mAb	**With headspace**	**Without headspace**
NS	< 1	< 1
13 µg	< 1	< 1
94 µg	< 1	< 1
mAb HC	**With headspace**	**Without headspace**
NS	3 ± < 1	3 ± < 1
13 µg	4 ± < 1	4 ± < 1
94 µg	3 ± < 1	3 ± < 1

3.2.2 DISCRIMINATION BETWEEN SILICONE DROPLETS AND OTHER PARTICLES BY MFI AND RMM

In particular for biopharmaceutical drug products in PFS and other drug/device combination products lubricated with silicone oil, the discrimination between silicone droplets and other particles becomes increasingly important. The MFI built-in "find similar" filter (see 2.6) was initially based on visual analysis of particles and showed that discrimination between the two groups is reasonable for particles larger than 5 µm [54,56]. Therefore, a lower size limit of 5 µm was utilized in this study although "find similar" and customized filters were reported to resolve particle sizes down to 2 µm [53,55]. Cartridges filled with headspace showed highest particle numbers ≥ 1µm (see above) and were therefore further analyzed to evaluate the appearance of silicone droplets and other particles. The total concentration of particles ≥ 5 µm in non-siliconized and siliconized cartridges with 13 µg silicone was comparably low (50-300 particles/mL), which limits statistical representation of the sample population and discrimination (Fig. VI-3). Cartridges with a silicone level of 94 µg showed 2800 particles/mL to 4700 particles/mL ≥ 5 µm with 91 % to 97 % classified as silicone droplets independent of the contained formulation, i.e., placebo, 2 mg/mL mAb or 33 mg/mL mAb HC.

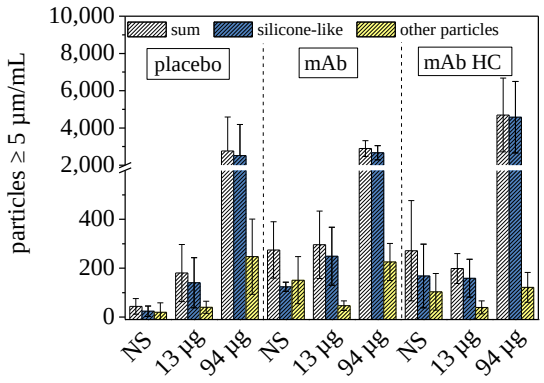

Fig. VI-3. Discrimination between silicone-like and other particles after agitation with headspace as a function of baked-on silicone levels and mAb concentrations as obtained by MFI for particles ≥ 5 µm. Cartridges were filled with 20 mM histidine placebo, pH 6, 2 mg/mL mAb or 33 mg/mL mAb HC.

Exemplary MFI particle images and scatter plots for placebo or mAb HC samples from cartridges with 94 µg silicone demonstrated the formation of well-defined spherical shapes (Fig. VI-4) as well as high values for aspect ratio (Fig. VI-5a) and circularity (Fig. VI-5b) as reported for silicone droplets [52–54,56]. Typically, silicone droplets ≥ 5 µm exhibit very dark edges and a bright center, which results in similar or lower mean object intensities compared to protein

aggregates (Fig. VI-5c) [27,55]. The remaining population exhibited a similar morphology and did not show irregular, dense clusters or fibrous like particles with noticeable different scatter values as described for protein [52–56]. These particles were therefore most likely falsely marked as other particles.

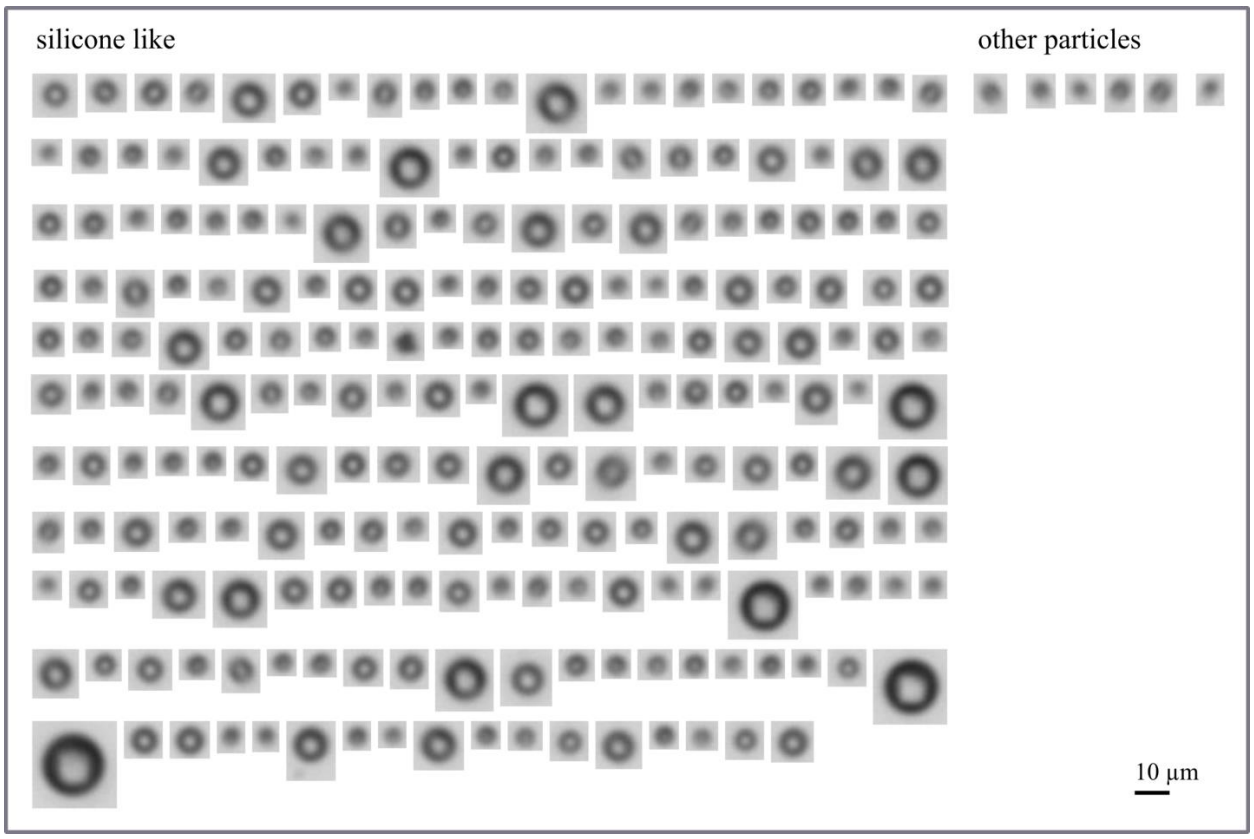

Fig. VI-4. Exemplary MFI images of silicone-like and other particles ≥ 5 µm detected in a sample of 33 mg/mL mAb HC after agitation with headspace in cartridges with 94 µg silicone.

a.

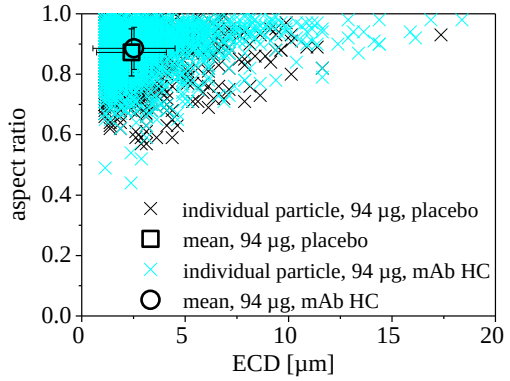

b.

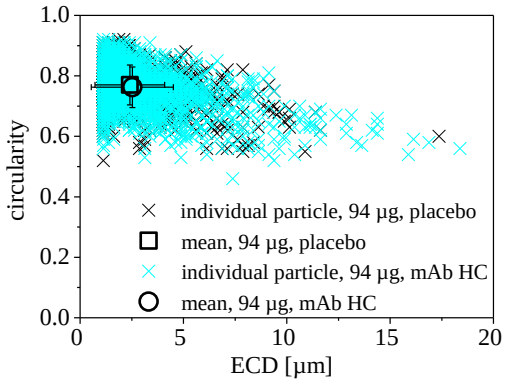

c.

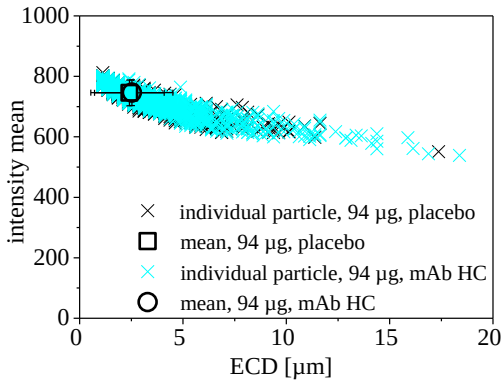

Fig. VI-5. Exemplary scatter plots of particle parameters in MFI: (a) aspect ratio, (b) circularity and (c) intensity mean for placebo and 33 mg/mL mAb HC after agitation with headspace. Cartridges were bake-on siliconized with 94 µg silicone.

In addition, selected agitated samples were analyzed by RMM. In the size range of 0.2-5 µm, all non-siliconized cartridges either filled with placebo, mAb or mAb HC showed similar particle concentrations below 8.8×10^4/mL (Fig. VI-6). In cartridges siliconized at a higher silicone level (94 µg per cartridge), RMM determined comparable particle concentrations up to 2.2×10^5/mL and 1.6×10^5/mL after filling with placebo and mAb, respectively. The highest particle concentration (4.9×10^5/mL) was observed in cartridges with 94 µg silicone filled with mAb HC. About 90-95 % of these particles could be attributed to silicone droplets regardless of the fill medium.

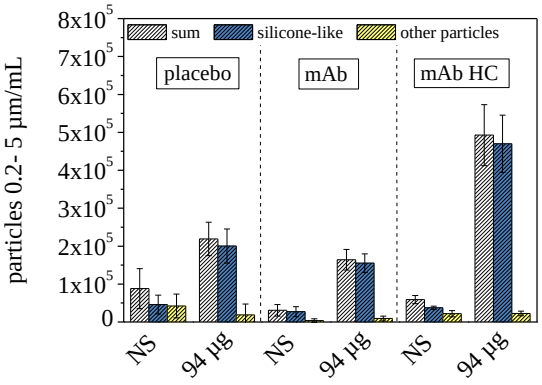

Fig. VI-6. Discrimination between silicone-like and other particles after agitation with headspace as a function of baked-on silicone levels and different mAb concentrations as obtained by RMM for particles in the range of 0.2 µm to 5 µm. Cartridges were filled with 20 mM histidine placebo, pH 6, 2 mg/mL mAb or 33 mg/mL mAb HC.

Samples revealed comparable particle size distributions in both MFI and RMM with the smaller particles being the largest fraction (Fig. VI-7). RMM detected more droplets of 1-3 µm, whereas

MFI determined the same number or more droplets in the size range from 3-5 µm. These results indicate that both methods do not yield comparable size information as described for MFI and RMM previously [55].

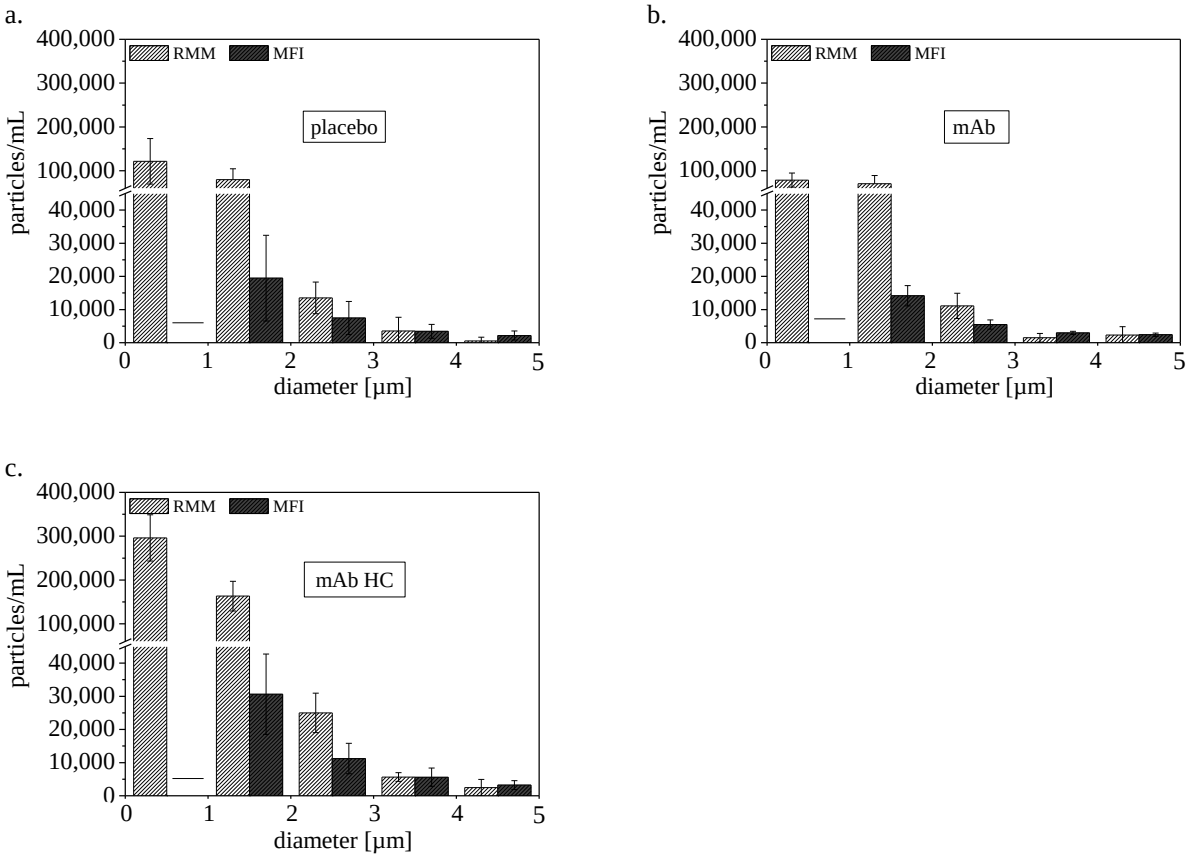

Fig. VI-7. Exemplary particle size distributions in the range of 0.2-5 µm/mL obtained from MFI and RMM after agitation with headspace in cartridges with 94 µg silicone. Cartridges were filled with (a) 20 mM histidine placebo, pH 6, (b) 2 mg/mL mAb and (c) 33 mg/mL mAb HC.

3.2.3 CHARACTERIZATION OF NANOSCALE PARTICLES USING NTA AND DLS

Additionally, NTA was applied to evaluate the different sample sets for particles in the submicron size range (Fig. VI-8).

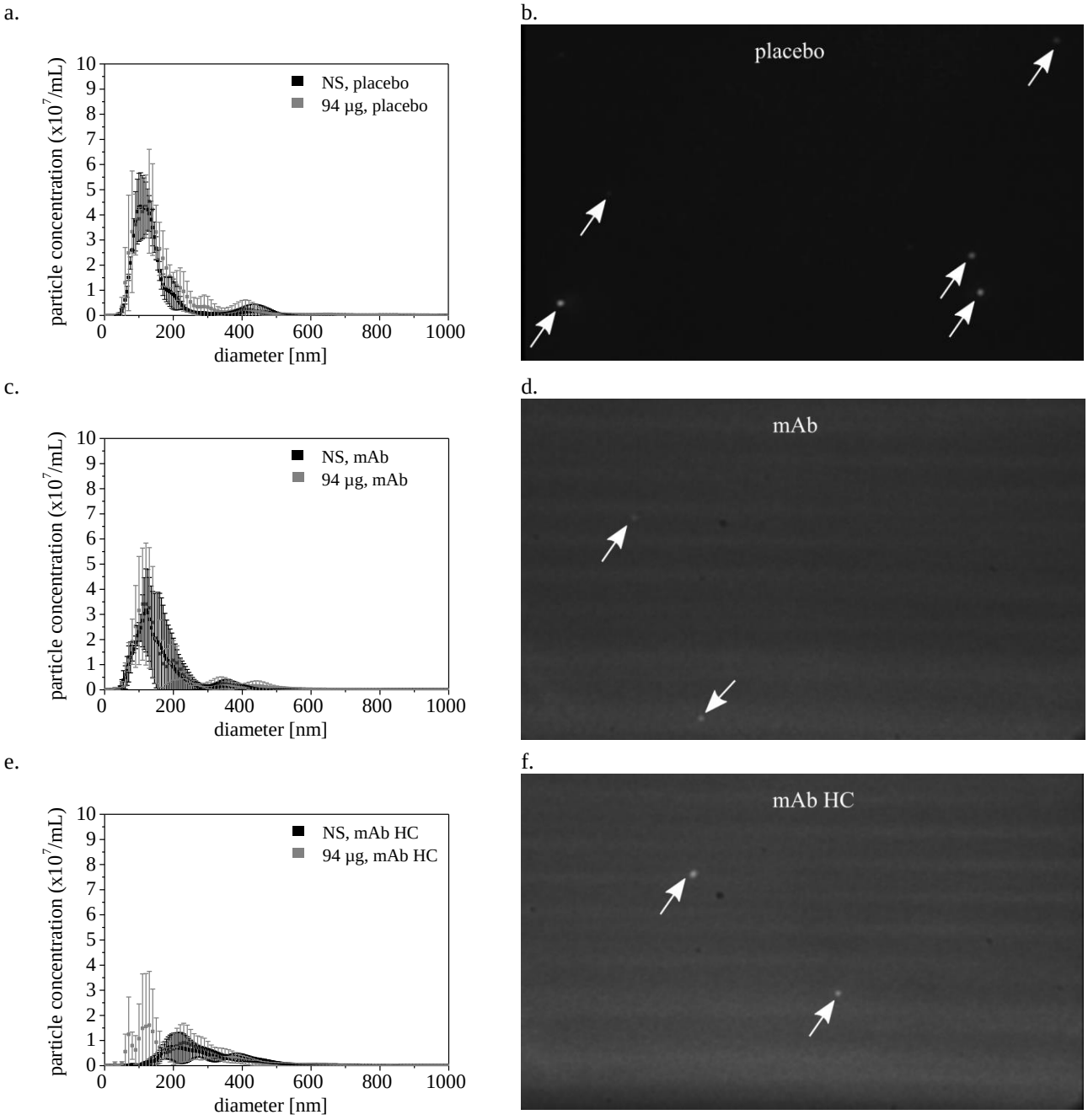

Fig. VI-8. (a, c, e) Particle size distributions by NTA after agitation with headspace in non-siliconized and siliconized cartridges (94 µg silicone) and (b, d, f) corresponding exemplary NTA frames. Cartridges were filled with (a, b) 20 mM histidine placebo, pH 6, (c, d) 2 mg/mL mAb and (e, f) 33 mg/mL mAb HC. For placebo and mAb samples, the shutter was set to 597-603 and the gain to 298-303. In mAb HC samples, the gain was decreased to zero due to high background scattering.

In NTA, sensitivity is inversely correlated with the mAb concentration, i.e., with higher protein concentration the background scattering from the solution matrix itself increased (Fig. VI-8b, Fig. VI-8d, Fig. VI-8f) as did turbidity (Tab. VI-3), which makes visualization of particles more

difficult [72,73]. Therefore NTA settings were adjusted for mAb HC (see 2.10). Comparison of particle concentrations between placebo and the different protein concentrations is thus not reasonable while particle sizing is less affected by protein concentration [73].

In placebo and mAb samples, the particle size distributions were fairly broad from 50 nm to 500 nm with a main peak at 110-130 nm (Fig. VI-8a, Fig. VI-8c). The concentrations for particles of the main peak were approximately 4×10^7/mL, which is at the lower end of the concentration range suggested as suitable for NTA (10^7-10^9 particles/mL [74]). As previously highlighted, particle detection was strongly impeded with higher protein concentration, hence the results do not allow a reliable determination of particle size for mAb HC (Fig. VI-8e). Overall, no change in the submicron particle distribution or increase in the particle level was observed between non-siliconized cartridges and the corresponding siliconized cartridges (94 µg).

DLS detected the monomeric mAb with a Z-average diameter between 8 nm to 11 nm fairly independent of silicone and mAb concentration (Tab. VI-4) [75,76]. A PDI ≤ 0.1 indicated monodisperse samples [76]. Minor differences in the Z-average as a function of concentration were within the variability of this method (± 2 nm) [75]. The particle fraction around 110-130 nm found by NTA was not detected by DLS due to the lower peak resolution and the low overall number of particles in that size range (peak intensity of the mAb monomer peak was 97-100 % in DLS) [74,77,78].

Tab. VI-4. PDI and Z-average diameter in DLS analysis after agitation with and without headspace as a function of baked-on silicone levels and mAb concentrations. Cartridges were filled with 20 mM histidine placebo, pH 6, 2 mg/mL mAb or 33 mg/mL mAb HC.

Sample description	**Z-average [d.nm]**	**PDI**	**Z-average [d.nm]**	**PDI**
mAb	**With headspace**		**Without headspace**	
NS	10.5 ± 0.1	0.04 ± 0.02	10.6 ± 0.2	0.06 ± 0.02
13 µg	11.2 ± 1.1	0.10 ± 0.07	10.7 ± 0.2	0.05 ± 0.03
94 µg	10.5 ± < 0.1	0.05 ± 0.01	11.3 ± 1.4	0.09 ± 0.08
mAb HC	**With headspace**		**Without headspace**	
NS	8.0 ± 0.1	0.03 ± 0.01	9.0 ± < 0.1	0.03 ± < 0.01
13 µg	8.8 ± < 0.1	0.02 ± < 0.01	8.9 ± < 0.1	0.03 ± 0.01
94 µg	8.9 ± < 0.1	0.03 ± < 0.01	8.9 ± < 0.1	0.03 ± 0.01

4 DISCUSSION

4.1 SILICONE MIGRATION IN PLACEBO

For each PFS and other drug/device combination product, a variety of factors such as the siliconization process, the formulation and the set-up for stress testing contributes to the number, size and morphology of particles present. In this paper, silicone migration from baked-on siliconized cartridges with two different silicone levels (13 ± 3 µg and 94 ± 6 µg per cartridge) was assessed in placebo after expelling, shaking and a combination thereof. Samples were filled with (Fig. VI-1a) and without headspace (Fig. VI-1b).

Previous work indicated that the method for sample collection substantially affects the amount of silicone droplets sloughing off from the container wall. Increased numbers of silicone droplets were observed in spray-on siliconized PFS with placebo after expelling compared to sample collection through the flange using a pipette after removal of the piston [35]. In this study, the particle levels ≥ 1 µm in placebo were comparably low in non-siliconized cartridges and at both silicone levels after expelling (Fig. VI-1). It has been previously observed that by expelling the thin baked-on silicone layer is pushed towards the needle-side of the cartridge and finally accumulates between the glass surface and the upper piston plateau (see chapter IV) rather than detaching into the fill medium. The expelling effect is likely highly relevant for sprayed-on silicone regarding silicone entry into solution, but of less relevance for thin baked-on silicone layers.

Mechanical stress methods such as agitation or stirring are commonly used during the development of therapeutic proteins to test robustness against different interfacial stresses, which they may encounter during manufacturing, transport and final administration [79]. The horizontal rotation frequency and test duration in this work followed vehicle vibration tests from ISTA 2A and ASTM D 4169 – 08 as guidelines for performance testing of shipping containers. With higher baked-on silicone levels, shaking substantially increased the particle counts ≥ 1 µm in placebo. Furthermore, a higher number of silicone droplets was displaced from the container wall of cartridges with headspace, likely induced by bulk fluid shear forces due to the movement of the air bubble [16]. Additional expelling after shaking had no effect on the particle counts, which is consistent with the negligible effect of expelling alone.

Consequently, for siliconization processes that have been previously optimized in terms of adequate silicone levels and reproducible silicone distributions, shaking studies with placebo can

be useful to understand if silicone is shed into product solution under worst-case conditions. They may serve to challenge the container performance and to guide the selection of siliconized product containers. However, this is not likely to reduce the number of testing (e.g., silicone in solution and functionality) for the particular container expected to be performed on stability.

4.2 PARTICLE FORMATION AFTER AGITATION IN MAB SOLUTIONS

As PFS and other drug/device combination products lubricated with silicone oil have become popular delivery formats for protein therapeutics [11–13], one of the aspects with potential quality impact proteins may encounter are silicone oil-water interfaces. The combination of different protein concentrations (2 mg/mL and 33 mg/mL), agitation and headspace on the particle formation in baked-on siliconized cartridges was investigated. Other authors have used silicone spiking studies to evaluate the impact on particle appearance [19,20,22,24–26,32]. These spiking studies miss relevant silicone levels as they utilize silicone concentrations far beyond the amount typically present in PFS and other drug/device combination products [79]. This is why we chose to evaluate two practically relevant baked-on silicone levels (13 ± 3 µg and 94 ± 6 µg per cartridge).

Overall, higher baked-on silicone levels led to higher particle concentrations ≥ 1 µm in LO and MFI (Fig. VI-2) and in the size range of 0.2-5 µm in RMM (Fig. VI-6). The particle concentrations were comparable in cartridges with placebo and at different mAb concentrations.

It may be argued that with an increased RI of the formulation, i.e., with a higher mAb concentration, the particle concentration is likely to be underestimated or in case of an RI match, particles disappear in MFI and LO [28,80–82]. In this study, the RI of 1.34 of the mAb formulation at higher protein concentration was very similar to the measured RI for mAb and placebo of 1.33. Thus, within this range, no substantial influence of formulation RI on both the number of silicone droplets (RI 1.40) and amorphous mAb particles (RI 1.41, [80]) was expected.

The majority of particles ≥ 5 µm in MFI (Fig. VI-3 - Fig. VI-5) and in the size range of 0.2-5 µm in RMM (Fig. VI-6) were silicone droplets without substantial protein-related matter independent of the formulation studied. RMM analysis was based on a small number of measured particles (< 300) due to the overall low particle concentration at the lower limit of the recommended range from 3×10^5 to 1×10^7/mL [55]. The sample volume (0.1-0.5 µL) was low, but within a range previously reported for RMM [55]. The statistical representation of the sample population in RMM was thus limited due to low sampling efficiency and the corresponding large extrapolations

factors [83], thereby questioning the noticeable difference in particle concentration between placebo, mAb and mAb HC. Nonetheless, solely silicone droplets contributed to the particle counts in RMM. In this study, applying both MFI and RMM brought noticeable benefit to cover a size range as broad as possible. As both methods are relatively new for the discrimination of silicone droplets and other particles and are not considered to be ready for quality control purposes, particle analysis with these methods is however challenging and results have to be interpreted with caution.

The submicron particle populations were comparable in non-siliconized and baked-on siliconized cartridges with an abundance of monomeric mAb in DLS (Tab. VI-4) and an additional particle subfraction around 110-130 nm as suggested by NTA data (Fig. VI-8). The increase in silicone droplets with higher baked-on silicone levels was moderate. Turbidity did not change compared to controls (Tab. VI-3), and was only reflecting turbidity as a function of protein concentration as described previously [72,75]. In cartridges siliconized with 94 µg silicone and filled with placebo, the migrated silicone amount after agitation was exemplarily determined to be 3 ± 1 µg by FTIR. This equals a weight fraction of 6×10^{-5} % (m/m) at a target filling volume of 5.16 mL placebo (see 2.4) with a density of 1.000 g/cm (see 2.8). A similar mass of approximately 2 µg and 5 µg was calculated from MFI and LO results, respectively, based on droplet counts and the density of silicone oil (0.972 g/cm^3 [60]). Similarly, Scherer observed a poor turbidity sensitivity at low weight fractions of 5×10^{-5} % (m/m) [78].

It has been previously indicated that the particles in PFS primarily consist of silicone droplets suggesting that silicone has a minimal impact on protein stability in the presence of surfactant [18,27–31]. On the contrary, in surfactant-free protein samples in PFS, increased particle concentrations were observed, and silicone droplets were suggested to be entangled in a fibrous protein aggregate structure due to silicone oil-water and air-water interfacial shear stress [15–18]. A disruption of the gelled protein layer at the silicone oil-water interface was considered followed by a release of gelled particles and agglomerates of silicone oil and protein aggregates [16]. In addition, agitation may provoke a collapse of the adsorbed protein layer at the air-water interface, gel buckling and subsequent detachment of protein particles into the bulk. [84]. In this work, the addition of polysorbate 20 0.04 % (w/v) protected mAb against aggregation and particle formation at both the silicone oil-water and air-water interface during agitation.

Overall, the baked-on silicone levels corresponded well with the number of silicone droplets. The highest numbers of silicone droplets were reached in cartridges with a silicone level of 94 µg

after agitation with headspace independent of the formulation. Still, particle counts ≥ 1 µm remained low with up to 3,400 particles/mL in LO and up to 55,500 particle/mL in MFI (Fig. VI-2a), and below 5,000 particles/mL above ≥ 5 µm in MFI (Fig. VI-3). In addition, particles ≥ 10 µm and ≥ 25 µm -650-700 particles/container and 2-60 particles/container (Fig. VI-2c), respectively- were well below the limits of current compendial monographs for parenteral products and protein injections [68–70]. The low silicone level of 13 µg was shown to be suitable as primary container for ophthalmic solutions with meeting the more stringent compendial limits for subvisible particle levels (Tab. VI-2) [71]. In the literature, both the siliconization method and the applied silicone level strongly affect the particle counts. High numbers of silicone droplets were reported for placebo samples in spray-on siliconized syringes with up to 10,000 particles/mL ≥ 2 µm in LO, 10^6 particles/mL ≥ 1 µm and 1.2×10^5 particles/mL ≥ 2 µm in MFI after agitation [35,37]. Similarly, baked-on siliconized vials with albinterferon alfa-2b fusion protein stabilized with 0.01 % polysorbate 80 contained 2.5×10^6 to 1.5×10^7 particles/mL from 1 µm to 10 µm in MFI with increasing baked-on silicone levels (specific silicone levels were not disclosed) [27]. In other studies using siliconized PFS and plastic syringes filled with IgG1, interferon beta-1a, bevacizumab and adalimumab, particle concentrations of 9,000 particles/mL ≥ 5 µm [28] and 3×10^5 to 6×10^5 particles/mL ≥ 1 µm were observed in MFI (surfactant was added for protein stability) [30,31,55]. Particles detected in these studies were primarily determined to be silicone droplets. Although the higher baked-on silicone level of 94 µg approached the upper limit of 0.1 mg/container reported for baked-on silicone levels [34,43,44], particle levels were clearly lower as compared to literature. Thus, adequate bake-on siliconization provides a viable alternative to limit subvisible particle formation compared to spray-on siliconization process [15,23,35,37].

Recently, cross-linked silicone layers were presented as an attractive method to achieve similar [15] or reduced subvisible particle levels compared to bake-on processes [35,37] and substantially less compared to spray-on layers [18]. Nevertheless, piston extrusion performance of these cross-linked layers needs to be further investigated as some studies have shown contradicting extrusion force profiles [15,18,35,37]. It was further suggested that in bake-on siliconization processes, high temperature exposure alters the bulk properties of silicone, thereby affecting gliding performance in addition to a narrow processing window [35]. From our experience, baked-on silicone levels below 100 µg were sufficient for adequate lubrication without a substantial change in the silicone bulk properties (see chapter V).

The biological relevance of visible and subvisible particles with respect to trigger an immunogenic response is still unclear and without consensus among academy, industry and regulatory authorities [85–90]. Considering subvisible particles consisting of silicone, safety is not seen to be a concern for parenteral and not even for intraocular administration [3,91]. However, it still remains important to consider the particle burden during formulation and process development as well as during in-use administration testing of parenteral drug products. Monitoring particles above 10 µm and 25 µm, which is required by current compendia using LO [68–70], remains the gold standard. Characterizing particles in the lower size range using more novel methods may provide further insight to differentiate the nature of particulates, e.g., by MFI and RMM [53–55], and enables relative ranking of samples. Yet, new methods such as NTA are not suggested for routine use and data evaluation needs to be done with care [73,77,83].

In summary, after shaking in the presence of headspace the number of particles for samples in siliconized cartridges increased as compared to expelling alone. Studies in absence of headspace provided further insight into the mechanism of silicone migration. Still, baked-on silicone levels below 100 µg resulted in low particle levels mainly comprising silicone droplets without compromising protein stability in formulations with 0.04 % (w/v) polysorbate 20. Lower baked-on silicone levels may even further limit silicone migration into the bulk solutions.

5 CONCLUSION

Particle formation is known to occur under a variety of different stress conditions. In this work, the particle appearance in mAb formulations in bake-on siliconized cartridges was investigated using two practically relevant baked-on silicone levels (13 µg and 94 µg per cartridge), different mAb concentrations (2 mg/mL and 33 mg/mL) as well as agitation with and without headspace. A toolbox of methods was utilized to cover a particle size range as broad as possible including DLS, NTA, RMM, turbidity, LO and MFI.

The robustness of mAb was demonstrated at both silicone levels independent of the protein concentration. The presence of 0.04 % (w/v) polysorbate 20 inhibited the formation of protein particles during agitation. Overall, the baked-on silicone levels corresponded well with the particle concentrations in the size range of 0.2-5 µm (RMM) and ≥ 1 µm (MFI, LO); and were comparable between placebo, 2 mg/mL mAb and 33 mg/mL mAb HC. The majority of particles was clearly identified as silicone droplets. Agitation with headspace caused an increase in particle concentration compared to samples without headspace, which was primarily attributed to silicone sloughing off from the container wall. Highest particle concentrations were observed in cartridges siliconized with 94 µg silicone after agitation with headspace independent of the filling medium (up to 55400 particles/mL ≥ 1 µm in MFI, 3400 particles/mL ≥ 1 µm in LO and 1.6-4.9×10^5/mL between 0.2-5 µm in RMM). Although the presence of baked-on silicone obviously increased the particle concentration, silicone migration was still efficiently minimized compared to spray-on siliconized primary containers as described in literature (see above). Based on silicone migration studies in placebo, highest silicone levels were observed after shaking, whereas expelling alone or after agitation did not enhance silicone migration.

Surely, silicone oil in sufficient concentration is essential as lubricant on the inner barrel of PFS and other drug/device combination products to maintain functionality over shelf life. An approach that could be taken to guide and limit the selection of siliconized primary containers may include i) optimized siliconization processes that balance adequate but limited silicone levels, reproducible silicone distributions and functionality; and ii) initial container performance testing with placebo, e.g., using shaking, which was most challenging for systems with low baked-on silicone levels; followed by iii) forced degradation and long-term protein stability studies including functionality testing (at intended and accelerated conditions) within the preselected containers under relevant formulation conditions such as the presence of surfactant.

6 ABBREVIATIONS

DLS	Dynamic light scattering
FNU	Formazine nephelometric units
FTIR	Fourier transform infrared (spectroscopy)
LO	Light obscuration
mAb	Monoclonal antibody
mAb HC	Monoclonal antibody at higher concentration (33 mg/mL)
MFI	Micro-flow imaging
NTA	Nanoparticle tracking analysis
NS	Non-siliconized
PDI	Polydispersity index
PFS	Pre-filled syringe
RMM	Resonant mass measurement
RI	Refractive index

7 REFERENCES

[1] S. Bukofzer, J. Ayres, A. Chavez, M. Devera, J. Miller, D. Ross, et al., Industry perspective on the medical risk of visible particles in injectable drug products., PDA J. Pharm. Sci. Technol. 69 (2015) 123–139.

[2] D. Ripple, M. Dimitrova, Protein particles: What we know and what we do not know, J. Pharm. Sci. 101 (2012) 3568–3579.

[3] S.K. Singh, N. Afonina, M. Awwad, K. Bechtold-Peters, J.T. Blue, D. Chou, et al., An industry perspective on the monitoring of subvisible particles as a quality attribute for protein therapeutics, J. Pharm. Sci. 99 (2010) 3302–3321.

[4] H.-C. Mahler, W. Friess, U. Grauschopf, S. Kiese, Protein aggregation: pathways, induction factors and analysis., J. Pharm. Sci. 98 (2009) 2909–2934.

[5] M.C. Manning, D.K. Chou, B.M. Murphy, R.W. Payne, D.S. Katayama, Stability of protein pharmaceuticals: an update., Pharm. Res. 27 (2010) 544–575.

[6] W. Wang, S. Nema, D. Teagarden, Protein aggregation--pathways and influencing factors., Int. J. Pharm. 390 (2010) 89–99.

[7] J.S. Bee, T.W. Randolph, J.F. Carpenter, S.M. Bishop, M.N. Dimitrova, Effects of surfaces and leachables on the stability of biopharmaceuticals, J. Pharm. Sci. 100 (2011) 4158–4170.

[8] B. Sharma, Immunogenicity of therapeutic proteins. Part 2: impact of container closures., Biotechnol. Adv. 25 (2007) 318–324.

[9] W. Wang, A.A. Ignatius, S. V Thakkar, Impact of residual impurities and contaminants on protein stability., J. Pharm. Sci. 103 (2014) 1315–1330.

[10] A.A. Wakankar, Y.J. Wang, E. Canova-Davis, S. Ma, D. Schmalzing, J. Grieco, et al., On developing a process for conducting extractable-leachable assessment of components used for storage of biopharmaceuticals, J. Pharm. Sci. 99 (2010) 2209–2218.

[11] J. Jezek, N.J. Darton, B.K. Derham, N. Royle, I. Simpson, Biopharmaceutical formulations for pre-filled delivery devices, Expert Opin. Drug Deliv. 10 (2013) 811–828.

[12] G. Sacha, J.A. Rogers, R.L. Miller, Pre-filled syringes: a review of the history, manufacturing and challenges, Pharm. Dev. Technol. 20 (2015) 1–11.

[13] R.G. Ingle, A.S. Agarwal, Pre-filled syringe - a ready-to-use drug delivery system: a review, Expert Opin. Drug Deliv. 11 (2014) 1391–1399.

[14] M. Adler, Challenges in the development of pre-filled syringes for biologics from a formulation scientist´s point od view, Am. Pharm. Rev. 15 (2012).

[15] A. Gerhardt, B.H. Nguyen, R. Lewus, J.F. Carpenter, T.W. Randolph, Effect of the siliconization method on particle generation in a monoclonal antibody formulation in pre-filled syringes, J. Pharm. Sci. 104 (2015) 1601–1609.

[16] A. Gerhardt, N.R. Mcgraw, D.K. Schwartz, J.S. Bee, J.F. Carpenter, T.W. Randolph, Protein aggregation and particle formation in prefilled glass syringes, J. Pharm. Sci. 103 (2014) 1601–1612.

[17] E. Krayukhina, K. Tsumoto, S. Uchiyama, K. Fukui, Effects of syringe material and silicone oil lubrication on the stability of pharmaceutical proteins, J. Pharm. Sci. 104 (2015) 527–535.

[18] S. Majumdar, B.M. Ford, K.D. Mar, V.J. Sullivan, R.G. Ulrich, A.J.M. D'Souza, Evaluation of the effect of syringe surfaces on protein formulations, J. Pharm. Sci. 100 (2011) 2563–2573.

[19] P. Basu, A.W. Blake-Haskins, K.B. O'Berry, T.W. Randolph, J.F. Carpenter, Albinterferon α2b adsorption to silicone oil-water interfaces: effects on protein conformation, aggregation, and subvisible particle formation, J. Pharm. Sci. 103 (2014) 427–436.

[20] R. Thirumangalathu, S. Krishnan, M.S. Ricci, D.N. Brems, T.W. Randolph, J.F. Carpenter, Silicone oil- and agitation-induced aggregation of a monoclonal antibody in aqueous solution, J. Pharm. Sci. 98 (2009) 3167–3181.

[21] M.K. Joubert, Q. Luo, Y. Nashed-Samuel, J. Wypych, L.O. Narhi, Classification and characterization of therapeutic antibody aggregates., J. Biol. Chem. 286 (2011) 25118–25133.

[22] L.S. Jones, A. Kaufmann, C.R. Middaugh, Silicone oil induced aggregation of proteins, J. Pharm. Sci. 94 (2005) 918–927.

[23] A. Badkar, A. Wolf, L. Bohack, P. Kolhe, Development of Biotechnology Products in Pre-filled Syringes: Technical Considerations and Approaches, AAPS PharmSciTech. 12 (2011) 564–572.

[24] S.B. Mehta, R. Lewus, J.S. Bee, T.W. Randolph, J.F. Carpenter, Gelation of a monoclonal antibody at the silicone oil-water interface and subsequent rupture of the interfacial gel results in aggregation and particle formation., J. Pharm. Sci. 104 (2015) 1282–1290.

[25] K.A. Britt, D.K. Schwartz, C. Wurth, H.-C. Mahler, J.F. Carpenter, T.W. Randolph, Excipient effects on humanized monoclonal antibody interactions with silicone oil emulsions, J. Pharm. Sci. 101 (2012) 4419–4432.

[26] D.B. Ludwig, J.F. Carpenter, J.-B. Hamel, T.W. Randolph, Protein adsorption and excipient effects on kinetic stability of silicone oil emulsions, J. Pharm. Sci. 99 (2010) 1721–1733.

[27] K.B. Auge, A.W. Blake-Haskins, S. Devine, S. Rizvi, Y.-M. Li, M. Hesselberg, et al., Demonstrating the stability of albinterferon alfa-2b in the presence of silicone oil, J. Pharm. Sci. 100 (2011) 5100–5114.

[28] B. Demeule, S. Messick, S.J. Shire, J. Liu, Characterization of particles in protein solutions: reaching the limits of current technologies., AAPS J. 12 (2010) 708–715.

[29] A. Lubiniecki, D.B. Volkin, M. Federici, M.D. Bond, M.L. Nedved, L. Hendricks, et al., Comparability assessments of process and product changes made during development of two different monoclonal antibodies., Biologicals. 39 (2011) 9–22.

[30] L. Liu, D.A. Ammar, L.A. Ross, N. Mandava, M.Y. Kahook, J.F. Carpenter, Silicone oil microdroplets and protein aggregates in repackaged bevacizumab and ranibizumab: effects of long-term storage and product mishandling, Invest. Ophthalmol. Vis. Sci. 52 (2011) 1023–1034.

[31] J.G. Barnard, K. Babcock, J.F. Carpenter, Characterization and quantitation of aggregates and particles in interferon-β products: potential links between product quality attributes and immunogenicity., J. Pharm. Sci. 102 (2013) 915–928.

[32] A. Gerhardt, K. Bonam, J.S. Bee, J.F. Carpenter, T.W. Randolph, Ionic strength affects tertiary structure and aggregation propensity of a monoclonal antibody adsorbed to silicone oil-water interfaces, J. Pharm. Sci. 102 (2013) 429–440.

[33] G.A. Sacha, W. Saffell-Clemmer, K. Abram, M.J. Akers, Practical fundamentals of glass, rubber, and plastic sterile packaging systems, Pharm. Dev. Technol. 15 (2010) 6–34.

[34] J.S. Bee, V.V. Frey, U. Javed, J. Chung, M.L. Corcoran, P.S. Roussel, et al., Characterization of the Initial Level and Migration of Silicone Oil Lubricant in Empty Prefilled Syringes for Biologics Using Infrared Spectroscopy, PDA J. Pharm. Sci. Technol. 68 (2014) 494–503.

[35] F. Felsovalyi, S. Janvier, S. Jouffray, H. Soukiassian, P. Mangiagalli, Silicone-oil-based subvisible particles: their detection, interactions, and regulation in prefilled container closure systems for biopharmaceuticals, J. Pharm. Sci. 101 (2012) 4569–4583.

[36] E. Chan, A. Hubbard, S. Sane, Y.-F. Maa, Syringe siliconization process investigation and optimization, PDA J. Pharm. Sci. Technol. 66 (2012) 136–150.

[37] R.A. Depaz, T. Chevolleau, S. Jouffray, R. Narwal, M.N. Dimitrova, Cross-linked silicone coating: a novel prefilled syringe technology that reduces subvisible particles and maintains compatibility with biologics, J. Pharm. Sci. 103 (2014) 1384–1393.

[38] M. Lankers, Analyse von Silikonschichtdicken bei der Herstellung von Fertigspritzen mit Hilfe von Refektometriemessungen, Pharm. Ind. 72 (2010) 2148–2153.

[39] M. Bowen, N. Armstrong, Y.-F. Maa, Investigating high-concentration monoclonal antibody powder suspension in nonaqueous suspension vehicles for subcutaneous injection., J. Pharm. Sci. 101 (2012) 4434–4443.

[40] T. Mundry, T. Schurreit, P. Surmann, The Fate of Silicone Oil During Heat-curing Glass Siliconization - Changes in Molecular Parameters Analyzed by Size Exclusion and High Temperature Gas Chromatography, PDA J. Pharm. Sci. Technol. 54 (2000) 383–397.

[41] A. Colas, Silicones in pharmaceutical applications. Part 5: Siliconization of parenteral packaging components, (2006). http://www.dowcorning.com/content/publishedlit/52-1094-01.pdf (accessed July 16, 2015).

[42] T. Mundry, P. Surmann, T. Schurreit, Surface characterization of polydimethylsiloxane treated pharmaceutical glass containers by X-ray-excited photo- and Auger electron spectroscopy, Fresenius. J. Anal. Chem. 368 (2000) 820–831.

[43] L. Khandke, R. Malone, X. Yang, H. Han, J.L. Look, Z. Jin, et al., Novel formulations which stabilize and inhibit precipitation of immunogenic compositions, U.S. Patent 2011/0172393 A1, 2011.

[44] B. Reuter, Silicone oil and its applications for parenteral products, PDA Europe Workshop, Cologne, (2010).

[45] J.F. Carpenter, T.W. Randolph, W. Jiskoot, D.J.A. Crommelin, C.R. Middaugh, G. Winter, et al., Overlooking subvisible particles in therapeutic protein products: gaps that may compromise product quality., J. Pharm. Sci. 98 (2009) 1201–1205.

[46] J. Carpenter, B. Cherney, A. Lubinecki, S. Ma, E. Marszal, A. Mire-Sluis, et al., Meeting report on protein particles and immunogenicity of therapeutic proteins: filling in the gaps in risk evaluation and mitigation., Biologicals. 38 (2010) 602–611.

[47] T.K. Das, Protein particulate detection issues in biotherapeutics development--current status., AAPS PharmSciTech. 13 (2012) 732–746.

[48] J. den Engelsman, P. Garidel, R. Smulders, H. Koll, B. Smith, S. Bassarab, et al., Strategies for the assessment of protein aggregates in pharmaceutical biotech product development, Pharm. Res. 28 (2011) 920–933.

[49] J.S. Philo, Is any measurement method optimal for all aggregate sizes and types?, AAPS J. 8 (2006) E564–E571.

[50] V.I. Razinkov, M.J. Treuheit, G.W. Becker, Accelerated formulation development of monoclonal antibodies (mAbs) and mAb-based modalities: review of methods and tools., J. Biomol. Screen. 20 (2015) 468–483.

[51] S. Zölls, R. Tantipolphan, M. Wiggenhorn, G. Winter, W. Jiskoot, W. Friess, et al., Particles in therapeutic protein formulations, Part 1: overview of analytical methods., J. Pharm. Sci. 101 (2012) 914–935.

[52] D.K. Sharma, D. King, P. Oma, C. Merchant, Micro-flow imaging: flow microscopy applied to sub-visible particulate analysis in protein formulations., AAPS J. 12 (2010) 455–464.

[53] R. Strehl, V. Rombach-Riegraf, M. Diez, K. Egodage, M. Bluemel, M. Jeschke, et al., Discrimination between silicone oil droplets and protein aggregates in biopharmaceuticals: a novel multiparametric image filter for sub-visible particles in microflow imaging analysis, Pharm. Res. 29 (2012) 594–602.

[54] S. Zölls, D. Weinbuch, M. Wiggenhorn, G. Winter, W. Friess, W. Jiskoot, et al., Flow imaging microscopy for protein particle analysis--a comparative evaluation of four different analytical instruments., AAPS J. 15 (2013) 1200–1211.

[55] D. Weinbuch, S. Zölls, M. Wiggenhorn, W. Friess, G. Winter, W. Jiskoot, et al., Micro-flow imaging and resonant mass measurement (Archimedes)--complementary methods to quantitatively differentiate protein particles and silicone oil droplets., J. Pharm. Sci. 102 (2013) 2152–2165.

[56] D.K. Sharma, P. Oma, S. Krishnan, Silicone microdroplets in protein formulations - detection and enumeration, Pharm. Technol. 33 (2009) 74–79.

[57] S. Uchiyama, Liquid formulation for antibody drugs., Biochim. Biophys. Acta. 1844 (2014) 2041–2052.

[58] M.J. Akers, Excipient-drug interactions in parenteral formulations., J. Pharm. Sci. 91 (2002) 2283–2300.

[59] A.L. Daugherty, R.J. Mrsny, Formulation and delivery issues for monoclonal antibody therapeutics., Adv. Drug Deliv. Rev. 58 (2006) 686–706.

[60] Dow Corning Corporation, Product Information. Dow Corning 360 Medical Fluid. Ref. No. 51-0374N-01, (2009).

[61] H. Fischer, I. Polikarpov, A.F. Craievich, Average protein density is a molecular-weight-dependent function, Protein Sci. 13 (2004) 2825–2828.

[62] M.L. Quillin, B.W. Matthews, Accurate calculation of the density of proteins, Acta Crystallogr. Sect. D Biol. Crystallogr. 56 (2000) 791–794.

[63] E. Folzer, T. Khan, R. Schmidt, C. Finkler, J. Huwyler, H.-C. Mahler, et al., Determination of the Density of Protein Particles Using a Suspended Microchannel Resonator, J. Pharm. Sci. (2015) 1–7.

[64] S. Funke, J. Matilainen, H. Nalenz, K. Bechtold-Peters, H.-C. Mahler, W. Friess, Analysis of thin baked-on silicone layers by FTIR and 3D-Laser Scanning Microscopy, Eur. J. Pharm. Biopharm. 96 (2015) 304–313.

[65] C.-T. Huang, D. Sharma, P. Oma, R. Krishnamurthy, Quantitation of protein particles in parenteral solutions using micro-flow imaging., J. Pharm. Sci. 98 (2009) 3058–3071.

[66] T. Werk, D.B. Volkin, H.-C. Mahler, Effect of solution properties on the counting and sizing of subvisible particle standards as measured by light obscuration and digital imaging methods, Eur. J. Pharm. Sci. 53 (2014) 95–108.

[67] K. Wuchner, J. Büchler, R. Spycher, P. Dalmonte, D.B. Volkin, Development of a microflow digital imaging assay to characterize protein particulates during storage of a high concentration IgG1 monoclonal antibody formulation., J. Pharm. Sci. 99 (2010) 3343–3361.

[68] European Directorate for the Quality of Medicines & HealthCare (EDQM), Ph. Eur. 2.9.19 Partikelkontamination - Nicht sichtbare -Partikeln, (2014).

[69] United States Pharmacopeial Convention, United States Pharmacopeia. General chapter -788-. Particulate matter in injections, (2012).

[70] United States Pharmacopeial Convention, United States Pharmacopeia. General chapter -787-.Subvisible particulate matter in therapeutic protein injections, (2014).

[71] United States Pharmacopeial Convention, United States Pharmacopeia. General chapter -789-. Particulate matter in opthalmic solutions, (2012).

[72] F. Gruia, A. Parupudi, A. Polozova, Practical Considerations for Detection and Characterization of Sub-Micron Particles in Protein Solutions by Nanoparticle Tracking Analysis, PDA J. Pharm. Sci. Technol. 69 (2015) 427–439.

[73] C. Zhou, A.B. Krueger, J.G. Barnard, W. Qi, J.F. Carpenter, Characterization of Nanoparticle Tracking Analysis for Quantification and Sizing of Submicron Particles of Therapeutic Proteins., J. Pharm. Sci. 104 (2015) 2441–2450.

[74] V. Filipe, A. Hawe, W. Jiskoot, Critical evaluation of Nanoparticle Tracking Analysis (NTA) by NanoSight for the measurement of nanoparticles and protein aggregates., Pharm. Res. 27 (2010) 796–810.

[75] M. Sukumar, B.L. Doyle, J.L. Combs, A.H. Pekar, Opalescent Appearance of an IgG1 Antibody at High Concentrations and Its Relationship to Noncovalent Association, Pharm. Res. 21 (2004) 1087–1093.

[76] H. Zhao, O. Graf, N. Milovic, X. Luan, M. Bluemel, M. Smolny, et al., Formulation development of antibodies using robotic system and high-throughput laboratory (HTL)., J. Pharm. Sci. 99 (2010) 2279–2294.

[77] W. Anderson, D. Kozak, V.A. Coleman, Å.K. Jämting, M. Trau, A comparative study of submicron particle sizing platforms: accuracy, precision and resolution analysis of polydisperse particle size distributions., J. Colloid Interface Sci. 405 (2013) 322–330.

[78] T.M. Scherer, S. Leung, L. Owyang, S.J. Shire, Issues and challenges of subvisible and submicron particulate analysis in protein solutions, AAPS J. 14 (2012) 236–243.

[79] A. Hawe, M. Wiggenhorn, M. van de Weert, J.H.O. Garbe, H.-C. Mahler, W. Jiskoot, Forced degradation of therapeutic proteins., J. Pharm. Sci. 101 (2012) 895–913.

[80] S. Zölls, M. Gregoritza, R. Tantipolphan, M. Wiggenhorn, G. Winter, W. Friess, et al., How subvisible particles become invisible-relevance of the refractive index for protein particle analysis., J. Pharm. Sci. 102 (2013) 1434–1446.

[81] Z. Hu, D.C. Ripple, The Use of Index-Matched Beads in Optical Particle Counters - jres.119.029.pdf, J. Res. Natl. Inst. Stand. Technol. 119 (2014) 674–682.

[82] R. Barer, S. Tkaczyk, Refractive Index of Concentrated Protein Solutions, Nature. 173 (1954) 821–822.

[83] A. Ríos Quiroz, J. Lamerz, T. Da Cunha, A. Boillon, M. Adler, C. Finkler, et al., Factors Governing the Precision of Subvisible Particle Measurement Methods - A Case Study with a Low-Concentration Therapeutic Protein Product in a Prefilled Syringe., Pharm. Res. (2015). doi:DOI 10.1007/s11095-015-1801-4.

[84] J.S. Bee, D.K. Schwartz, S. Trabelsi, E. Freund, J.L. Stevenson, J.F. Carpenter, et al., Production of particles of therapeutic proteins at the air–water interface during compression/dilation cycles, Soft Matter. 8 (2012) 10329–10335.

[85] L. Doessegger, H. Mahler, P. Szczesny, H. Rockstroh, G. Kallmeyer, A. Langenkamp, et al., The potential clinical relevance of visible particles in parenteral drugs, J. Pharm. Sci. 101 (2012) 2635–2644.

[86] A.S. Rosenberg, Effects of protein aggregates: an immunologic perspective, AAPS J. 8 (2006) E501–E507.

[87] H. Schellekens, Bioequivalence and the immunogenicity of biopharmaceuticals., Nat. Rev. Drug Discov. 1 (2002) 457–462.

[88] B. Sharma, Immunogenicity of therapeutic proteins. Part 3: impact of manufacturing changes., Biotechnol. Adv. 25 (2007) 325–331.

[89] B. Sharma, Immunogenicity of therapeutic proteins. Part 1: impact of product handling., Biotechnol. Adv. 25 (2007) 310–317.

[90] W. Jiskoot, G. Kijanka, T.W. Randolph, J.F. Carpenter, A. V Koulov, H.-C. Mahler, et al., Mouse Models for Assessing Protein Immunogenicity: Lessons and Challenges., J. Pharm. Sci. 105 (2016) 1567–1575.

[91] S. Bakri, N. Ekdawi, Intravitreal silicone oil droplets after intravitreal drug injections, Retina. 28 (2008) 996–1001.

VII QUARTZ CRYSTAL MICROBALANCE AND FLOW CYTOMETRY TO CHARACTERIZE PROTEIN ADSORPTION TO SILICONE SURFACES

GRAPHICAL ABSTRACT

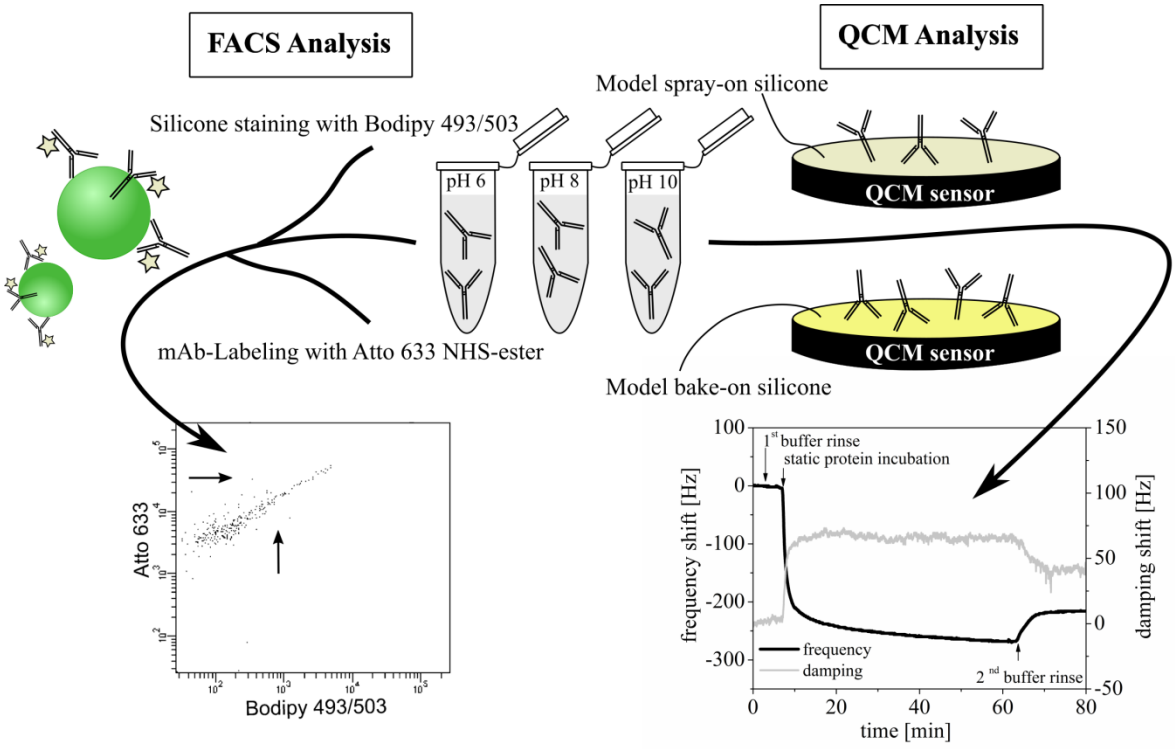

ABSTRACT

The adsorption of a monoclonal antibody (mAb) to model spray-on and bake-on silicone surfaces was investigated with a quartz crystal microbalance (QCM) and by fluorescence activated cell sorting (FACS). In QCM, maximum adsorption on spray-on silicone surfaces was found around the protein´s isoelectric point at pH 8 with 6.8 ± 0.2 mg/m^2. In comparison, adsorption to the slightly more hydrophobic bake-on silicone surface was increased at pH 8 (8.7 ± 1.6 mg/m^2) and pH 6 (7.0 ± 0.6 mg/m^2) and less reversible upon rinsing with buffer. In QCM, labeled mAb-Atto 633, which exhibited an increased hydrophobicity, adsorbed to a higher extent at pH 6 and pH 8 with 8.9-9.2 mg/m^2 and less reversible as compared to unlabeled mAb. The pH-dependent adsorption profile was similarly observed in FACS. In addition, mAb-Atto 633 was not exchanged with unlabeled species in FACS, which underscored the irreversible adsorption of mAb-Atto 633 in comparison to unlabeled mAb. Still, the addition of polysorbate 20 at a concentration of 0.005 % (m/v) markedly decreased the mAb-Atto 633 adsorption. Overall, both an increased hydrophobicity of the surface and of the adsorbed species strongly influenced the adsorption profile. Likewise, these results demonstrated that fluorescently labeled proteins have to be selected with care to clarify the label impact on the protein adsorption profile.

Parts of the following chapter are intended for publication.

Parts of the QCM protein adsorption and surface characterization experiments were performed by Samuel Scholl during his bachelor thesis ("The Effect of pH on the Adsorption of Monoclonal Antibody to Spray-On and Bake-On Silicone Oil Surfaces Studied by QCM", 2015).

1 INTRODUCTION

Protein adsorption at interfaces is a common phenomenon encountered in various areas of biotechnology including therapeutic proteins [1], biosensing [2], biomaterials [3], bioseparation in chromatography [4] and filtration [5]. Due to their complex molecular structure therapeutic proteins may interact with a number of surfaces during manufacturing (e.g., stainless steel tanks or pipes, filters, plastic tubing), storage (e.g., glass, rubber stoppers) and drug administration (e.g., plastic infusion bags, stainless steel needles) [1].

Silicone surfaces are particularly relevant since silicone oil is commonly used as lubricant to ease syringe piston movement during injection and enable good device performance, The silicone coating is applied by spraying either pure silicone oil without further treatment or silicone emulsion that is further baked-on the glass surface [6–8]. Bake-on siliconization typically results in silicone levels below 0.1 mg per container compared to 0.2 mg to 1 mg per container in spray-on siliconization processes [9–12].

One focus of research is to prevent or mitigate protein adsorption by the use of surfactants [13] or protein-resistant surface coatings (e.g., polyethylene glycol [14], polyglycerol [15]). Alternatively, studies seek to fundamentally understand the protein adsorption phenomenon [16,17]. Various models have been developed to describe the behavior of proteins in close proximity or adsorbed onto the surface, with the Langmuir isotherm being the most direct and simplest reference model [18,19]. Based on the assumption of a monomolecular layer of non-interacting substrates that reversibly occupy equivalent adsorption sites, the applicability of this model is limited [20]. Additional characteristics considered in certain models are heterogeneous adsorption sites [21] and discrete protein adsorption states arising from different orientations (e.g., for Y-shaped IgG end-on, side-on, flat-on) [22] or conformational changes that may allow further desorption [23,24] and/or self-exchange with other proteins [25]. Apart from the individual behavior of protein molecules at the interface, the structure of the adsorbed protein layer is described by random sequential adsorption (RSA). Accordingly, adsorbing proteins do not overlap with any other pre-adsorbed species, otherwise they are rejected back into the bulk [26]. Thus, the RSA model is equivalent to negative cooperative adsorption [16]. In this framework, positive cooperative adsorption implies that a protein molecule is more likely to adsorb if there are already pre-adsorbed protein molecules. Thereby, proteins may form two-dimensional clusters of protein monomers on the solid surface through direct attachment or surface diffusion of monomers to precursor clusters [27–29]. Alternatively, larger protein

assemblies formed in solution can deposit on the surface, subsequently spread, flatten and coalescence to surface clusters [30,31]. Furthermore, a combination of cooperative and non-cooperative adsorption is realized in a guiding mechanism. Accordingly, monomers are attracted by the surface in vertical direction and tracked laterally to the nearest available binding site by complex local electrostatic fields from pre-adsorbed proteins rather than being necessarily rejected from the surface. Thereby, proteins preferentially adsorb in the close vicinity of pre-adsorbed species but without direct contact [32,33]. Consequently, several adequate models are available to describe the formation of protein layers at solid interfaces, which should hold true for thin silicone layers in pre-filled syringes and other lubricated drug/device combination products.

Protein adsorption to silicone oil-water interfaces may be studied either by using emulsified silicone oil droplets or by the use of material surfaces coated with silicone oil. Interfacial adsorption at liquid-liquid interfaces is typically based on similar models with monomers forming homogeneous, closely packed, "soft glassy" layers or heterogeneous adsorption implying interfacial protein clustering [34,35].

The adsorption of proteins is affected by multiple factors such as the properties of the protein ("hard" or "soft" protein, isoelectric point (IEP), spatial charge distribution etc.) and the substrate surface (polarity, charge, morphology etc.) as well as environmental conditions (temperature, ionic strength, pH etc.). Depending on these factors protein adsorption can be governed by a combination of hydrogen bonding, electrostatic and hydrophobic forces [16,36,37]. In particular on hydrophobic surfaces, adsorption is substantially driven by a gain in entropy from dehydration of the sorbent surface, counter ion release and loss of ordered conformational structure within the protein molecule [38]. Overall, the total amount of adsorbed proteins is rather low and loss of protein may be only of concern for diluted protein therapeutics of low concentration [37,39]. Rather, a potential conformational change upon adsorption followed by exchange or desorption of these species back into solution receives attention since these altered structures are considered as precursor for protein aggregation and particle formation [40–42]. These subsequently induced protein particles may give rise to concerns about an increased risk of an immune response to the protein drug, which is controversially discussed in literature [43–48].

Among the many approaches used to investigate protein adsorption, quantifying the net protein accumulation over time, at different protein concentrations or in different formulations by bulk depletion technique [49,50] or after quantitative desorption from the surface [51,52] is rather popular. After fitting to an adequate model, the rate constant for adsorption and desorption, layer

thickness, average surface area per protein molecule and the irreversibly adsorbed fraction may be obtained. A direct measurement of the adsorbed amount and thus layer thickness, as well as *in situ* real-time adsorption/desorption kinetics can be conducted by surface plasmon resonance [53] and quartz crystal microbalance (QCM) with high sensitivity in the ng/cm^2 range [54,55]. Due to its ability to monitor the viscoelastic properties of the adsorbed layer and entrapped water in parallel to easy handling and flexibility in material surfaces, QCM has been increasingly used for protein adsorption studies [56,57]. Other applied techniques to assess the adsorbed layer thickness are ellipsometry [58], optical waveguide lightmode spectroscopy [58] and neutron reflection [59]. In addition, the average protein conformation can be determined using attenuated total internal reflectance-infrared spectroscopy [60], Raman spectroscopy [61] and circular dichroism [62]. Each of these techniques has its own advantages and constraints to investigate protein adsorption and its impact on protein conformation, which have been thoroughly reviewed [16,37,63].

In recent years, fluorescence based techniques such as total internal reflection fluorescence microscopy [17,34], Förster resonance energy transfer [30,64] and fluorescence correlation spectroscopy [65,66] have been increasingly applied to track individual protein species at interfaces with highest sensitivity. In addition, fluorescence activated cell sorting (FACS) has become a highly appreciated tool in protein analytics, e.g., for label-free counting [67] and preparative sorting of subvisible proteinaceous particles [68,69] as well as for the differentiation between silicone droplets, proteinaceous particles and protein-coated silicone droplets using combinations of different fluorescent dyes [70–72]. The utility of FACS to identify heterogeneous silicone droplets with adsorbed proteins particularly offers great potential for efficient monitoring of protein adsorption. Obviously, an inherent drawback of most fluorescence methods is the attachment of a fluorescent label, which may perturb the nature of the protein and thus change the adsorption behavior [73–76]. Therefore, the potential impact of these labels needs to be clarified.

In this study, we explored QCM and FACS to detect and characterize the adsorption of a monoclonal IgG1 antibody (mAb) on silicone oil surfaces. QCM was used as a highly sensitive method to determine the adsorbed mass, thickness and protein layer viscoelasticity on silicone oil and heat-treated silicone mimicking sprayed-on and baked-on siliconized surfaces. Furthermore, the adsorption of labeled mAb-Atto 633 to silicone droplets was studied in QCM and FACS for comparative evaluation of both novel techniques. The adsorption experiments were performed as

a function of protein concentration, time and at three different pH values, i.e., protein charge conditions, for a mechanistic understanding of the driving forces that trigger adsorption. In addition, a comprehensive set of experiments was performed in FACS to clarify the effect of Atto 633-labeling on the adsorption behavior of mAb.

2 MATERIALS AND METHODS

2.1 MATERIALS

Non-siliconized 2R vials from Schott AG (Mainz, Germany) and stoppers from West Pharmaceutical Services, Inc. (Exton, PA, USA) were used. Polyethersulfone (0.2 µm, Ø 27 mm), polytetrafluorethylene (0.2 µm, Ø 13 mm) and cellulose acetate (0.45 µm, Ø 27 mm) syringe filters were obtained from VWR International GmbH (Darmstadt, Germany). Cellulose acetate filters (0.2 µm, Ø 47 mm) were from Sartorius Stedim Biotech GmbH (Göttingen Deutschland). Slyde-A-Lyzer™ dialysis cassettes (molecular weight cut-off 10 kDa, volume 0.5-3 mL) were purchased from Thermo Scientific Inc. (Waltham, MA, USA).

Chemicals were obtained as follows: 365 35 % Dimethicone NF Emulsion and 360 Medical Fluid, 350 cSt, from Dow Corning GmbH (Wiesbaden, Germany); heptane from Riedel-de Haën (Seelze, Germany); diiodomethane, disodium hydrogen phosphate dihydrate, sodium chloride, diammonium sulfate and toluene from VWR International GmbH (Darmstadt, Germany); L-histidine monohydrochloride monohydrate and L-histidine both from Ajinomoto Europe S.A.S (Louvain-la-Neuve, Belgium); 1 M sodium hydroxide and 1 M hydrochloric acid standard volumetric solutions both from AppliChem GmbH (Darmstadt, Germany); sodium dodecyl sulfate (SDS) from Sigma-Aldrich Chemie GmbH (Taufkirchen, Germany); sodium dihydrogen phosphate dihydrate from Carl Roth GmbH + Co. KG (Karlsruhe, Germany); polysorbate 20 from Croda GmbH (Nettetal-Kaldenkirchen, Germany); potassium chloride from Caesar & Loretz GmbH (Hilden, Germany); dimethyl sulfoxid from Merck KGaA (Darmstadt, Germany); Atto 633 N-hydroxylsuccinimidyl (NHS)-ester from Atto-Tec GmbH (Siegen, Germany) and 4,4-difluoro-1,3,5,7,8-pentamethyl-4-bora-3a,4a-diaza-s-indacene (Bodipy 493/503) from Invitrogen/ Life Technologies GmbH (Darmstadt, Germany). A 33.4 mg/mL IgG1 mAb stock solution in 20 mM histidine buffer pH 5.4 was kindly donated by Roche Deutschland Holding GmbH (Penzberg, Germany). Silica microparticles with a diameter of 1.5 µm were purchased from Kisker Biotech GmbH & Company KG (Steinfurt, Germany).

2.2 QUARTZ CRYSTAL MICROBALANCE (QCM) EQUIPMENT AND MEASUREMENT PRINCIPLE

QCM experiments were performed on a qCell T from 3T GmbH & Co. KG (Tuttlingen, Germany) at 25 ± 0.1 °C equipped with an Ismatec peristaltic pump at a flow rate of 60 µL/min

from Cole-Parmer GmbH (Wertheim, Germany). Disc-shaped, AT-cut piezoelectric quartz crystals oscillating at a resonant frequency of 10 MHz with gold-plated electrodes and gold-coated active surfaces were obtained from 3T GmbH & Co. KG (Tuttlingen, Germany). 3T qGraph Software was utilized for instrument control and data analysis. Frequency and damping signals were monitored until stable values of ± 1 Hz and ± 10 Hz, respectively, were achieved for 10 min.

A homogeneous, thin, rigid mass deposition can be calculated from the frequency shift ($\Delta f_{Sauerbrey}$ in Hz) according to Sauerbrey:

$$\Delta m_{Sauerbrey} = \frac{C * \Delta f_{Sauerbrey}}{A}$$

Eq. VII-1

with $\Delta m_{Sauerbrey}$ as the mass change per area (in mg/m^2), C as the instrument specific crystal sensitivity constant (0.86×10^{-6} mg/Hz) and A as electrode active area (1.96×10^{-5} m^2) [77,78]. The above equation only holds for vacuum and gaseous phase. Kanazawa and Gordon expanded this model to sensors immersed in Newtonian liquid with a frequency shift ($\Delta f_{Kanazawa}$ in Hz) due to the viscosity (η) and density (ρ) of the surrounding medium defined by:

$$\Delta f_{Kanazawa} = -\sqrt{f_0^3 \frac{\eta\rho}{\Pi\mu_q\rho_q}}$$

Eq. VII-2

where f_0 is the fundamental resonant frequency (10×10^6 Hz) [77], μ_q is the shear module of the quartz (2.947×10^{16} mg/m·s^2) and ρ_q is the density of the quartz (2.648×10^9 mg/m^3) [79]. In a model system composed of a rigidly adsorbed layer immersed in liquid, the Sauerbrey and Kanazawa frequency shift both add up to an overall final shift [55]. This model for rigid and liquid-loaded sensors was further developed by various contributors, remarkably Rodahl *et al.* [80,81] and Voinova *et al.* [82]. Viscoelastic layers induce an exponentially-damped sinusoidal frequency decay of a freely oscillating crystal. Here, damping (ΔD) for liquid-loaded sensors can be derived from:

$$\Delta D = 2\sqrt{\frac{f_0}{\eta\Pi}}\frac{1}{\upsilon_q\rho_q}\sqrt{\rho\eta}$$

Eq. VII-3

with υ_q as the speed of sound in quartz (3340 m/s) [83].

The dissipation factor (D) (e.g., in QCM-D instruments from Q-Sense), half the bandwidth at half maximum of the resonance frequency (Γ) (e.g., in qCell T from 3T GmbH & Co. KG) and the motional resistance (R) are interchangeable terms and are commonly used to describe dissipation:

$$D = \frac{2\Gamma}{f_0} = \frac{R * f_0}{2\,\Pi * L_q}$$

Eq. VII-4

with L_q as the equivalent (motional) inductance of the bare quartz crystal (8.2×10^{-3} Ω/Hz) [80,84,85]. The dissipation thus gives valuable information on the film´s complex viscoelasticity since energy is dissipated due to oscillatory motion within the soft film, trapped liquid that moves within the film after deformation and load from bulk liquid [56].

2.3 SILICONE MODEL SURFACES FOR QCM

2.3.1 SPIN-COATING PROCESS FOR MODEL SPRAY-ON AND BAKE-ON SILICONE COATINGS

Silicone oil was dissolved in heptane at a final concentration of 1.75 % (w/v) and 3.5 % (w/v). Silicone emulsion was diluted to 1.75 % (w/w) using highly purified water. 3 mL of the diluted silicone emulsion were transferred as a thin fluid layer in a borosilicate glass beaker of 9.5 cm diameter, heated at 295 °C for 12 min and extracted with 3 mL heptane. Aliquots of 200 µL were evaporated to dryness at room temperature and redissolved in 140 µL or 200 µL heptane to achieve final concentrations of 1.75 % (w/v) and 2.5 % (w/v), respectively.

Initially, the resonant frequency of the blank quartz chip was recorded. Quartz chips were then siliconized with 5 x 6 µL drops of silicone (i.e., model spray-on coating) or heat-treated silicone (i.e., model bake-on coating) in heptane on a SCI-20 spin-coater from Schaefer Technologies GmbH (Lange, Germany) at 100 rpm. After drying, the coated mass was derived from the frequency shift between the uncoated and the siliconized quartz chip according to Sauerbrey (Eq. V-1). For reuse, the quartz chips were cleaned with 6 x 6 µL drops of toluene during spinning at 100 rpm and additional wiping with cotton swab, soaked in solvent.

A silicone layer density of 0.97 g/cm^3 [86] was utilized to calculate the coated layer thickness. In addition, ΔΓ/Δf was introduced as a measure for layer rigidity. Comparable to ΔD/Δf quotients, more rigid layer yield small ΔΓ/Δf and vice versa [87] (see 2.4.3).

2.3.2 CONTACT ANGLE AND SURFACE FREE ENERGY

Contact angles of 1 µL purified water drops were determined at four different positions of the siliconized quartz chip using a Drop Shape Analyzer from Krüss GmbH (Hamburg, Germany) in sessile drop mode. Contact angles were calculated with Krüss Advance 1.1.02 software 20 s after drop deposition by ellipse (tangent-1) fitting and automatic baseline adjustment. For the calculation of the surface free energy including disperse and polar fractions, the Owens, Wendt, Rabel and Kaeble method was applied using the contact angles of 0.9 µL diiodomethane droplets as second liquid with known polar and disperse fractions [88].

2.3.3 ZETA POTENTIAL AND ISOELECTRIC POINT (IEP)

The zeta potential (ζ-potential) was determined using a Zetasizer Nano-ZS ZEN3600 from Malvern Instruments Ltd (Herrenberg, Germany) in monomodal mode (50 V const.) with three measurements per sample with 10-40 subruns each at 25 °C. For the determination of IEP, the disposable zeta cell was connected to a Malvern MPT-2 Autotitrator. The pH of 12 mL sample in a polypropylene tube was automatically adjusted from pH 12.5 to pH 1.5 in increments of 0.5 pH using 1 M NaOH and 1 M HCl under constant stirring. The ζ-potential and IEP were calculated by Zetasizer Software v6.32.

Pure silicone oil was dispersed in highly purified water to a final concentration of 10 % (w/v). After vortexing briefly with Vortex Genie 2 from VWR International GmbH (Darmstadt, Germany) and ultrasound treatment (VWR International GmbH, Darmstadt, Germany) both for 10 min, the emulsion was diluted to 5 % (w/v). Heat-treated silicone was dispersed in highly purified water to a final concentration of 1.5 % (w/v) using ultrasound treatment for 30 min. The emulsion was further diluted to 0.5 % (w/v). Both emulsions were exposed to a second ultrasound treatment for 10 min followed by 0.45 µm filtration prior to analysis. The emulsion preparation was adjusted to obtain adequate mean count rates. Fresh silicone emulsions were prepared on the day of the measurement.

2.3.4 3D-LASER SCANNING MICROSCOPY (3D-LSM)

The average silicone layer thickness was determined using a VK-X210 microscope from Keyence Deutschland GmbH (Neu-Isenburg, Germany) as previously reported [89] (see chapter III). The limit of quantification was 10 nm. The silicone coating was artificially removed from the quartz chip surface by smoothly scratching an Eppendorf pipette tip (0.1-10 µL) over the surface. Height profile measurements of 1.5 x 1.1 mm surface areas (10 x magnification) were

performed using Keyence VK Viewer Software in EasyMode. The average layer thickness at the center, right and left side of the chip was determined as the difference in the average height between the gold surface and the silicone coating in multi-line average profile (400 lines) after area and line plane tilt correction. The integrated optical microscope (10 x magnification) was additionally employed to visualize the intact silicone coating at the center and each side of the chip.

2.4 ANALYSIS OF MAB AND MAB-ATTO 633 ADSORPTION IN QCM

2.4.1 PREPARATION OF BUFFERS AND PROTEIN SAMPLES FOR QCM MEASUREMENTS

The standard buffer was 20 mM histidine, pH 6. For additional mAb adsorption experiments, the pH was adjusted to pH 8 and pH 10 using 1 M NaOH. A consistent ionic strength of 50 mM for all histidine buffers was obtained by adding adequate amounts of sodium chloride based on iterative calculations previously described by Mathes [90]. Buffers were 0.2 µm filtered using pressurized nitrogen.

A concentrated solution (33.4 mg/mL) of mAb was diluted into the corresponding buffers to final concentrations from 0.1 mg/mL to 4 mg/mL. The equilibrium concentration in QCM was reached at 2 mg/ml (supporting information Fig. S VII-1). Thus, for further adsorption experiments, a 2 mg/mL mAb concentration was used. Similarly, mAb-Atto 633 (see 2.5.1) was diluted to 2 mg/mL using histidine buffers of defined pH and consistent ionic strength of 50 mM.

Prior to analysis, all solutions were 0.2 µm filtered and mAb concentrations were verified by UV absorption at 280 nm using a NanoDrop 2000 spectrophotometer from Thermo Fisher Scientific Inc. (Waltham, MA, USA) and an extinction coefficient of 1.51 cm^2/mg. The mAb-Atto 633 concentration was determined as recommended in the procedure for labeling [91]. All buffers and samples were carefully degassed in a desiccator equipped with a Laboport vacuum pump from KNF Neuberger GmbH (Freiburg, Germany) before analysis.

2.4.2 SUMMARY OF THE EXPERIMENTAL SEQUENCE FOR PROTEIN SAMPLES IN QCM

For protein adsorption studies, measurements started with buffer at a flow rate of 60 µL/min until a stable baseline in frequency (± 1 Hz for 10 min) and damping (± 10 Hz for 10 min) was achieved. Equilibration of the silicone coating in buffer prior to each measurement was crucial

since up to 0.5-1.9 mg/m^2 silicone leached upon rinsing with buffer (supporting information Fig. S VII-2). An aliquot of 244 µL protein solution in the respective buffer was then injected at 60 µL/min corresponding to a surface-to-volume ratio of 0.447 µL/cm^2 as exemplarily valid for 5 mL cartridges (tubing dead volume of 74 µL and 0.38 cm^2 chip area exposed to liquid were considered). Protein samples were further statically incubated until frequency and damping signals were stabilized. Subsequently, the corresponding buffer was introduced at 60 µL/min until damping and frequency became stable. The sequential steps involved in the experiments are exemplarily illustrated in Fig. VII-1.

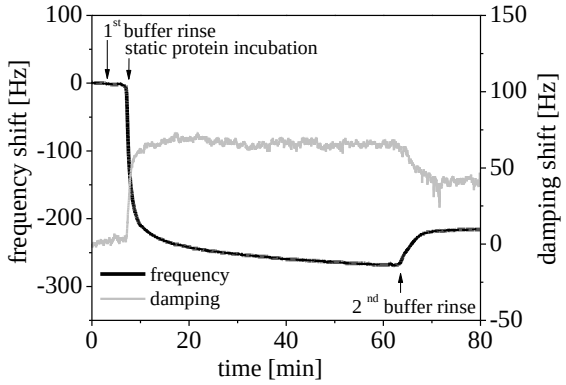

Fig. VII-1. Typical time course of frequency and damping changes in QCM upon adsorption of mAb at the silicone oil-buffer interface as a function of time.

After each measurement the QCM system was rinsed with 10 mM phosphate buffer containing 145 mM sodium chloride and 0.05 % (w/v) SDS (pH 7.2) to desorb bound protein followed by highly purified water. SDS increased silicone leaching up to 3.7-8.4 mg/m^2 (supporting information Fig. S VII-2). Therefore, frequency shifts during/after SDS exposure were not considered for further analysis. The silicone coating was subsequently removed as described above.

2.4.3 DATA ANALYSIS OF PROTEIN SAMPLES IN QCM

The frequency shift between the first buffer rinse and the equilibrium during static protein incubation was utilized to determine total adsorption (irreversible plus reversible). The liquid-induced frequency and damping shifts (Kanazawa contributions) due to the different media were calculated according to Eq. VII-2 and Eq. VII-3, respectively, based on the densities and viscosities of both buffer and protein solutions, and finally subtracted from the corresponding

initial frequency and damping shifts. This final corrected frequency shift was transferred into total adsorbed mass according to Sauerbrey (Eq. VII-1).

The frequency shift between the first buffer rinse and the end of the second buffer rinse directly corresponded to the irreversibly adsorbed mass based on Sauerbrey (Eq. VII-1) without Kanazawa contributions due to the same bulk media.

The density of the adsorbed protein layer was assumed to be 1.35 g/cm^3 to calculate the adsorbed layer thickness [92]. In addition, $\Delta\Gamma/\Delta f$ was introduced as a measure for layer rigidity. Comparable to $\Delta D/\Delta f$ quotients, more rigid layers result in small $\Delta\Gamma/\Delta f$ and vice versa [87]. Rigid layers are described by $\Delta\Gamma/\Delta f < 0.25$ as suggested by *Paul et al.* [93] while Muramatsu *et al.* found $\Delta\Gamma/\Delta f < 0.1$ (given $\Delta R/\Delta f$ and $\Delta D/\Delta f$ terms were transferred according to Eq. VII-4. Thus, for rigid layers, a rigidity quotient $\Delta\Gamma/\Delta f \sim 0\text{-}0.25$ was considered reasonable.

In this study, we present QCM adsorption data based on the Sauerbrey model, well aware that for highly viscoelastic films in liquid media the adsorbed mass becomes underestimated compared to Voigt-based data modeling [94]. However, it was reported that for frequency shifts up to 2 % of the unloaded frequency [95] and for layer thicknesses below 100 nm [96] or less than 10 nm [97] the Sauerbrey model is adequate.

2.5 ANALYSIS OF MAB-ATTO 633 ADSORPTION IN FLUORESCENCE ACTIVATED CELL SORTING (FACS)

2.5.1 MAB FLUORESCENT LABELING WITH ATTO 633 NHS-ESTER

mAb was fluorescently labeled with amine-reactive Atto 633 NHS-ester according to the manufacturer´s recommended procedure for labeling [91]. Atto 633 shows best excitation at $\lambda_{ex} = 629$ nm and emission at $\lambda_{em} = 657$ nm [98]. Before labeling, a 33.4 mg/mL concentrated mAb solution was dialyzed (ratio 1:600) into 10 mM phosphate-buffered saline (pH 7.4, 135 mM NaCl, 3 mM KCl) to mitigate dye reactions with histidine in the initial buffer bulk. The dialyzed mAb solution was diluted to 5 mg/mL and pH adjusted with 0.2 M sodium bicarbonate solution (pH 9) to pH 8.3. The mAb concentration was verified by UV absorption at 280 nm as described above followed by labeling an aliquot of 3.5 mL protein solution with 16 µL of Atto 633 NHS-ester at 10 mg/mL in dimethyl sulfoxide for 1 h at room temperature protected from light. After labeling, the mAb-Atto 633 conjugate was immediately dialyzed (ratio 1:600) in the corresponding histidine buffers of defined pH and consistent ionic strength of 50 mM to remove excess unassociated dye.

The mAb-Atto 633 concentration and the degree of labeling (DOL), i.e., average number of molecules coupled to a protein, were determined as recommended in the procedure for labeling [91]. The DOL was 1.3 ± 0.1. The concentration of mAb-Atto 633 after dialysis and 0.2 µm filtration ranged between 3.5 mg/mL to 4.7 mg/mL (further referred to as mAb-Atto 633 stock solution).

2.5.2 SILICONE STAINING WITH BODIPY 493/503

A 100 mg aliquot of silicone oil (0.2 µm filtered) was dissolved in 300 µL toluene and mixed with 16 µL Bodipy 493/503 at a concentration of 2.5 mg/mL in dimethyl sulfoxide. Both solvents were removed under constant nitrogen flow of 210 mL/min at 30 °C for 3 h protected from light using a thermal evaporator from Barkey GmbH & Co. KG (Leopoldshöhe, Germany). Bodipy 493/503 shows best excitation at λ_{ex} = 493 ± 3 nm and emission at λ_{em} = 504 ± 4 nm [99].

2.5.3 PREPARATION OF SILICONE OIL EMULSION

An aliquot of 40 mg silicone (0.2 µm filtered) or Bodipy 493/503-stained silicone was dispersed in 200 µL highly purified water to generate an emulsion without additives, which may affect the emulsification process. After vortexing for 30 s with Vortex Genie 2 form VWR International GmbH (Darmstadt, Germany), the emulsion was homogenized using an ultraturrax T 10 basic from IKA Laboratories (Staufen, Germany) for 1 min and diluted to 8 mg/mL in highly purified water. Fresh 8 mg/mL silicone stock emulsion was prepared on the day of the measurement.

2.5.4 PREPARATION OF MIXED SAMPLES OF SILICONE OIL AND PROTEIN FOR FACS MEASUREMENTS

2.5.4.1 FLUORESCENCE CONTRIBUTIONS FROM UNSPECIFIC SILICONE INTERACTIONS

A set of mixtures with final protein concentrations of 0.05 mg/mL mAb-Atto 633, equimolar concentrations of free Atto 633 and 0.2 mg/mL Bodipy 493/503-stained or non-stained silicone oil in 20 mM histidine buffer, pH 6, was prepared from the stock solutions described above. At least 2 h prior to sample preparation, the 10 mg/mL Atto 633 NHS-ester stock solution in dimethyl sulfoxide was diluted 1:100 in 20 mM histidine buffer, pH 6, such that the functional groups were hydrolyzed followed by 0.2 µm filtration.

2.5.4.2 CONCENTRATION DEPENDENT ADSORPTION OF MAB-ATTO 633 AND FREE ATTO 633

mAb-Atto 633 stock solution (dialyzed in 20 mM histidine buffer, pH 6, 0.2 µm filtrated) was mixed at concentrations from 0.01 mg/mL to 1 mg/mL with 0.2 mg/mL Bodipy 493/503-stained silicone emulsion in the corresponding histidine buffer. Similarly, mixtures of free Atto 633 dye and silicone emulsion were prepared (Atto 633 concentration was equimolar to the corresponding mAb concentration).

2.5.4.3 DISPLACEMENT STUDIES

A mixture of 0.01 mg/mL mAb-Atto 633 and 0.2 mg/mL Bodipy 493/503-stained silicone emulsion in 20 mM histidine buffer, pH 6, was allowed to incubate for 2 h (time based on previous experiments where the equilibrium was reached after approximately 2 h, supporting information Fig. S VII-3). Subsequently, an excess of unlabeled mAb was added to obtain a final ratio of 1:10 mAb-Atto 633 to mAb. Experiments were performed incubating mAb first followed by addition of an excess of mAb-Atto 633. Bodipy 483/503 and Atto 633 fluorescence signals were recorded up to 6 h after the second incubation step.

2.5.4.4 MAB-ATTO 633 ADSORPTION AS A FUNCTION OF PH AND ADDITION OF POLYSORBATE 20

Experiments were performed with mixtures of 0.05 mg/mL mAb-Atto 633 and 0.2 mg/mL Bodipy 493/503-stained silicone emulsion in histidine buffer of defined pH at constant ionic strength of 50 mM. Samples with surfactant additionally contained 0.005 % (m/v) to 0.04 % (m/v) polysorbate 20. The mixtures were allowed to adsorb for 2 h before analysis.

2.5.5 DETECTION OF PROTEIN ADSORPTION IN FACS

A 200 µL sample aliquot was analyzed for 1 min using a FACSCanto II flow cytometer from Becton, Dickinson and Company (Heidelberg, Germany) at a low sample flow (approximately 10 µL/min). Fluorescence signals of both Bodipy 493/503 and Atto 633 were simultaneously analyzed after excitation using a 488 nm blue laser (air-cooled, solid state, 20 mV laser output) and a 633 nm red laser (HeNe, 17 mW laser output); and fluorescence detector bands of 530/30 nm and 660/20 nm at 509 V and 400 V, respectively. A multicolor approach facilitated minimum overlap of the fluorescence response of both dyes and thus less spill-over in the emission filters (max. 1.4 %) [100]. Low angle forward light scatter (FSC) and 90° side scatter (SSC) detector voltages were set to 85 V and 300 V, respectively. Mean Bodipy 483/503 and

Atto 633 fluorescence intensities, FSC and SSC were recorded immediately after sample preparation unless otherwise stated. The approximate size range detected in FSC was studied with silica microparticle suspensions with a diameter of 1.5 µm after dilution in 20 mM histidine buffer, pH 6.

2.6 PHYSICOCHEMICAL PROPERTIES OF THE SAMPLE SOLUTIONS

Viscosity measurements were performed with a mVROC viscosimeter from Rheosense Inc. (San Ramon, CA, USA) equipped with an A-series chip with a flow channel depth of 50.8 µm at a constant shear rate of $1.90*10^{7}$ s^{-1}. Control software v2.6 was utilized for data analysis. Densities were determined using DMA 38 density meter from Anton Paar GmbH (Graz, Austria) at 20 °C.

2.7 HYDROPHOBIC INTERACTION CHROMATOGRAPHY (HIC)

HIC analysis was performed on a 35 x 4.6 mm TSKgel Butyl-NR column from Tosoh Bioscience GmbH (Darmstadt, Germany) and an Alliance 2695 high performance liquid chromatography system from Waters GmbH (Eschborn, Germany) with gradient elution (buffer A: 1.5 M $(NH_4)_2SO_4$, 20 mM histidine, pH 6; buffer B: 20 mM histidine, pH 6; linear gradient 0-100 % buffer B until 17 min, 100 % buffer B until 21.5 min, linear gradient buffer A 0-100 % until 26 min, 100 % buffer A until 34.5 min) at a flow rate of 0.8 mL/min and 25 °C column temperature. mAb and mAb-Atto 633 samples were diluted to 1 mg/mL in 20 mM histidine buffer, pH 6, and cooled at 4 °C before injecting 20 µg. The elution was monitored with UV detection at λ = 280 nm (mAb absorption) and λ = 629 nm (Atto 633 absorption).

3 RESULTS AND DISCUSSION

3.1 DEVELOPMENT OF MODEL SPRAY-ON AND BAKE-ON SILICONE COATINGS IN QCM

Different silicone coatings were established as model surfaces for therapeutic drug product containers, which are lubricated by either spraying-on silicone oil or silicone emulsion that is further baked-on the glass surface [6–8]. The coatings were optimized in terms of coated mass, thickness and rigidity to exclude an effect of these parameters on protein adsorption (Tab. VII-1). Comparable amounts of approximately 60-65 mg/m^2 silicone or heat-treated silicone were finally deposited yielding a layer thickness of 60-70 nm. The bound layer was rigid in nature as indicated by rigidity quotients of $\Delta\Gamma/\Delta f$ = 0.04-0.05. A thicker silicone layer of 170 nm resulting from a higher coated amount of approximately 160 mg/m^2 silicone was slightly less rigid ($\Delta\Gamma/\Delta f$ = 0.07) and was therefore not considered in further studies. The coated layer thickness was exemplarily confirmed in 3D-LSM (Tab. VII-1, Fig. VII-2c, Fig. VII-2d), which revealed thinner layers of 40-50 nm. For 3D-LSM analysis, a low 10 x magnification was employed, which has been previously shown to underestimate the layer thickness by 5-20 % [89] (see chapter III). Overall, both coatings were found to be comparable in terms of coated mass, layer thickness and rigidity.

Tab. VII-1. Optimization of frequency shift (Δf), coated mass (Δm), rigidity quotient ($\Delta\Gamma/\Delta f$), and layer thickness based on calculations according to Sauerbrey (Eq. VII-1) after spin-coating QCM chips with model spray-on and model bake-on silicone. Grey panels indicate coating solutions and characteristics used for further experiments.

Sample description	**Concentration silicone solution**	**Δf [Hz]**	**Δm [mg/m^2]**	**$\Delta\Gamma/\Delta f$**	**Layer thickness [nm]**	
					QCM	**3D-LSM**
Spray-on coating	3.5 %	-3695.7 ± 95.6	162.2 ± 4.2	0.07 ± 0.01	167.2 ± 4.3	-
	1.75 %	-1478.7 ± 131.8	64.9 ± 5.8	0.05 ± 0.02	66.9 ± 6.0	50 ± 9
Bake-on coating	1.75 %	-889.7 ± 20.1	39.0 ± 0.9	0.04 ± 0.02	40.2 ± 0.9	-
	2.5 %	-1313.7 ± 81.1	57.6 ± 3.6	0.04 ± 0.03	59.4 ± 3.7	42 ± 11

The morphology of both silicone surfaces was similar exhibiting a relatively smooth structure with circular, brighter yellowish marks in particular on the model spray-on silicone surface. The surface coverage at the center and each side of the quartz chip was homogeneous (Fig. VII-2a, Fig. VII-2b). Note that the yellow color is due to the gold surface on the quartz chip. The surface

additionally revealed micro-scratches, which are also present on untreated chip surfaces [101,102] or may be partially introduced during chip cleaning with cotton swabs. Atomic force and scanning electron micrographs of the untreated gold surface showed pyramid-like gold structures and nm-scale airborne-contaminants [101,102] that may preferentially adhere silicone during spin-coating and thus give rise to the circular structures observed in 3D-LSM.

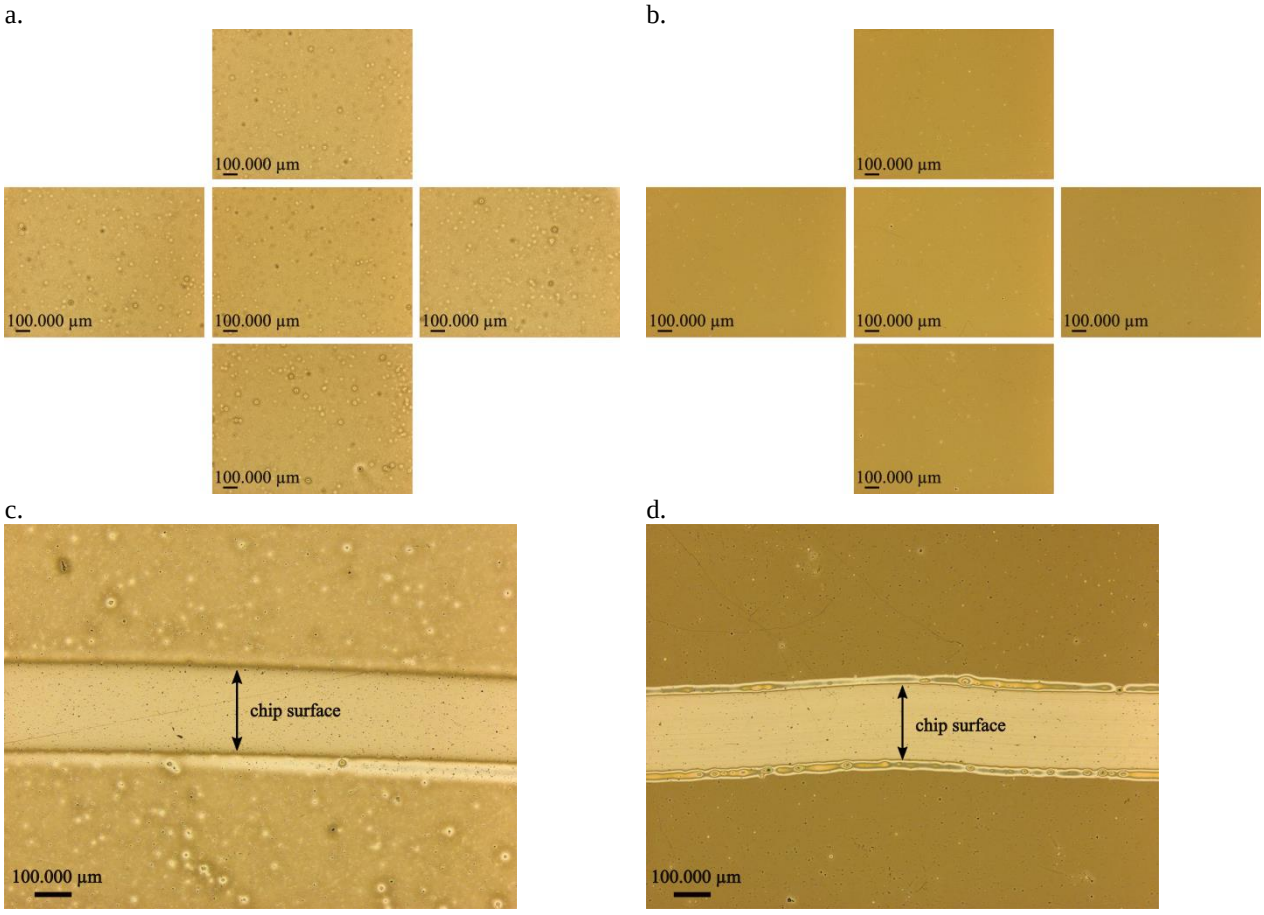

Fig. VII-2. Visual appearance of model (a) spray-on and (b) bake-on silicone surfaces in optical microscopy at the center and each side of the coated QCM chip. Exemplary micrographs of the (c) spray-on and (d) bake-on coating used for the determination of the coated layer thickness by 3D-LSM analysis as the difference in the average height between the chip surface and the silicone layer.

Studies indicate that proteins readily adsorb to hydrophobic surfaces governed by hydrophobic interactions and the entropy gain upon dehydration of the hydrophobic surface, counter ion release and loss of ordered conformational structure within the protein molecule [38,103]. To understand the influence of surface hydrophobicity on protein adsorption, water contact angles on both silicone coatings were determined. The model spray-on and bake-on silicone coatings were highly hydrophobic with contact angles of 78.1 ± 1.3° and 91.9 ± 1.2°, respectively (Fig. VII-3, Tab. VII-2).

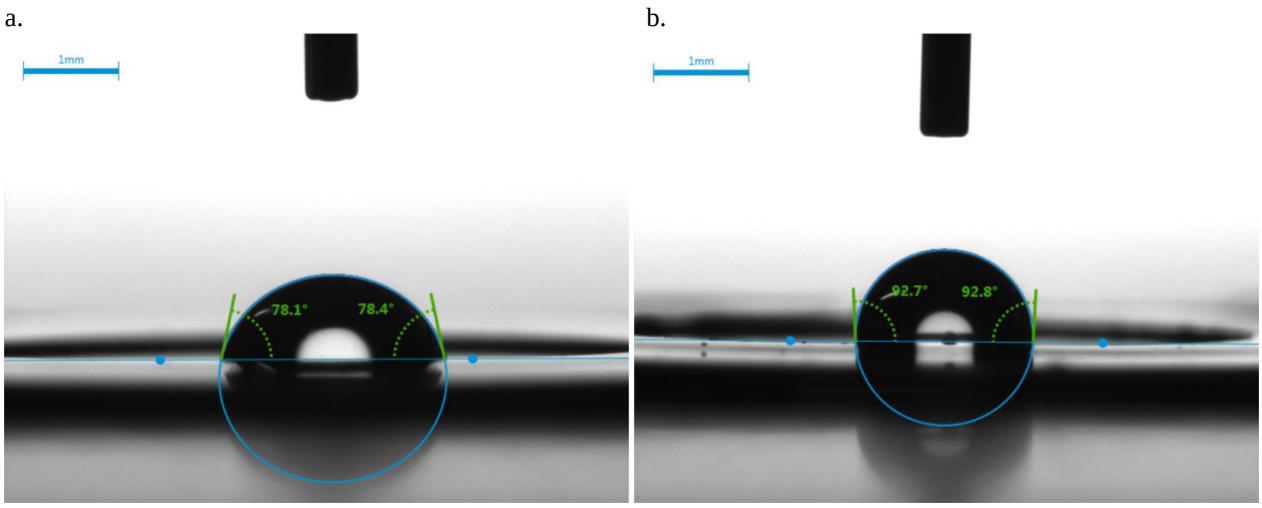

Fig. VII-3. Contact angle images of water on QCM chips after spin-coating with (a) model spray-on and (b) model bake-on silicone.

Tab. VII-2. Measured contact angles of water and values for the dispersive and polar components of the surface free energy after spin-coating QCM chips with model spray-on and bake-on silicone.

Measurement parameter	**Spray-on coating**	**Bake-on coating**
Contact angle water (four different chip positions)	78.1 ± 1.3°	91.9 ± 1.2°
Surface free energy γ [mN/m]	39.9 ± 0.6	29.4 ± 0.3
Dispersive component γ_d [mN/m]	34.9 ± 0.2 (87 %)	27.4 ± 0.1 (93 %)
Polar component γ_p [mN/m]	5.0 ± 0.3 (13 %)	2.0 ± 0.3 (7 %)

For vials siliconized with Dow Corning Medical Fluid 360 without additional heat treatment, Mathes found a comparable contact angle of 78° [90] while bake-on siliconized cartridges exhibited a higher contact angle of 103 ± 2° (see chapter V). Previous studies suggested a decrease in the low molecular weight fraction of silicone below 5,000 g/mol, an increase in the fraction between 500 g/mol and 15,000 g/mol and no substantial formation of molecules with more than 50,000 g/mol upon bake-on. It can be argued, that lower molecular weight fractions migrate into micro-inhomogeneities on the sorbent surface due to a greater mobility and thereby lead to a disorientation of the applied, hydrophobic layer [104,105]. This may result in a slightly lower contact angle for untreated silicone oil (i.e., model spray-on) (for more comprehensive discussion please refer to chapter V).

Contact angle measurements with different test liquids of known polar and disperse fractions (in this study water and diiodomethane) are widely used to calculate surface energetic properties

based on the Owens, Wendt, Rabel and Kaeble method. London dispersion forces arising from instantaneous dipoles due to a permanent electron density fluctuation within an atom and polar forces due to permanent dipole-dipole, dipole-induced and ion-dipole polarization as well as hydrogen bonding both sum up to the total surface free energy [106,107]. The surface free energy of the bake-on coating was determined to be less with 29.4 ± 0.3 mN/m compared to 39.9 ± 0.6 mN/m found for the spray-on coating (Tab. VII-2). The bake-on coating showed a dispersive interaction energy of 93 % compared to 87 % for the spray-on coating in excess of the polar fraction and indicating a slightly stronger hydrophobicity and weaker polar contributions (e.g., due to dipole-dipole interaction with water [107]). In literature, comparable surface free energies for silicone oil, siliconized vials and silicone rubber were reported with 20-22 mN/m up to 45 mN/m and 91-97 % dispersive contributions [90,108–110]. In consequence, the model spray-on and bake-on silicone coatings were considered as suitable surrogates for spray-on and bake-on siliconized glass surfaces in therapeutic drug product containers. Interestingly, the bake-on silicone coating was slightly more hydrophobic with higher dispersive force contributions.

Furthermore, the surface IEP and surface charge at defined pH dictate the electrostatic interactions proteins may encounter upon adsorption. Starting at approximately 8 mV at pH 1.5, the ζ-potential of silicone droplets in highly purified water (model spray-on) decreased to zero ζ-potential at the IEP of 3.9 ± 0.0 and reached -38 mV at pH 12.5 (Fig. VII-4). The ζ-potential determined for silicone emulsions containing heat-treated silicone droplets (model bake-on) with a slightly lower IEP of 2.9 ± 0.5 was in good agreement with the data obtained for pure silicone droplets.

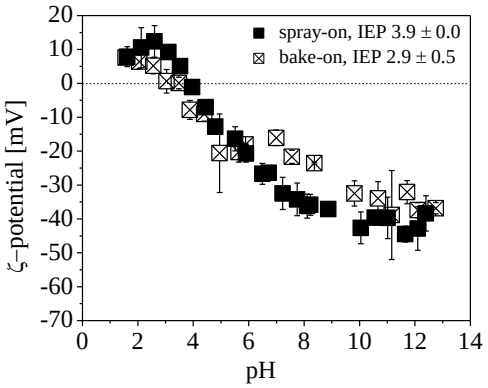

Fig. VII-4. The ζ-potential of droplets of pure silicone (model spray-on) and heat-treated silicone oil (model bake-on) in highly purified water versus pH.

Electric charge in aqueous solution results from selective adsorption of hydrogen and hydroxide ions at the shear plane between the surrounding solution and a layer of surface bound ions at the neural silicone surface [111]. In the case of strongly acidic or alkaline solution, charge may also be introduced by partial hydrolysis of the siloxane backbone and dissociation of the resulting silanol groups [112]. The IEPs were well in line with reported values for siliconized glass powder and slides of 3.4-3.6 [51]. Other studies suggest a higher IEP for silicone droplets in aqueous media and silicone rubber ranging from 4.5-5.5 [113–115], which may be due to different sample materials and measurements techniques. Overall, ζ-potential measurements indicated similar surface charges in the pH range of 1.5-12.5 for both coatings investigated in QCM. Consequently, the model spray-on and bake-on coating are expected to exhibit negative ζ-potentials of approximately -20 mV to -40 mV at the tested pH values of pH 6, pH 8 and pH 10.

3.2 THE ADSORPTION OF MAB TO MODEL SPRAY-ON AND BAKE-ON SILICONE SURFACES AS A FUNCTION OF PH STUDIED BY QCM

3.2.1 ADSORBED AMOUNT AS A FUNTION OF PH

The influence of pH on the adsorption of mAb to model spray-on and bake-on silicone surfaces was investigated in QCM.

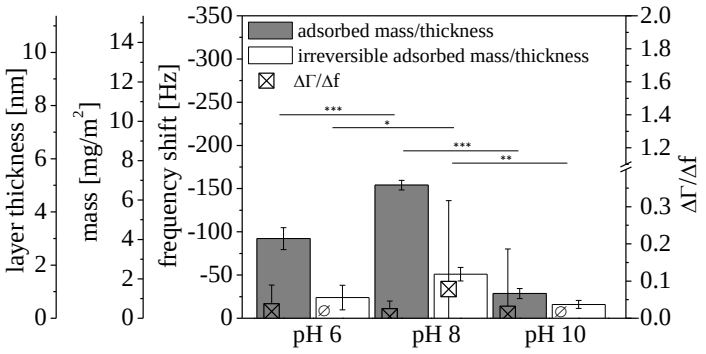

Fig. VII-5. Effect of pH on mAb adsorption (2 mg/mL) to model spray-on silicone surfaces in histidine buffer at consistent ionic strength of 50 mM as determined by QCM. Adsorbed mass was corrected for liquid-induced frequency and damping contributions according to Kanazawa (Ø - ΔΓ/Δf could not be quantified (≤ 0)). Statistical significance for bars is shown with * $p \leq 0.05$, ** $p \leq 0.01$, *** $p \leq 0.001$.

For spray-on silicone surfaces, the highest surface concentration with 6.8 ± 0.2 mg/m^2 was found at pH 8 close to the mAb´s IEP at pH 8.0-8.5 [116] (Fig. VII-5). At pH 6, mAb still markedly adsorbed with 4.0 ± 0.6 mg/m^2. The most pronounced drop in adsorption to 1.3 ± 0.3 mg/m^2 was observed at pH 10.

As described above the spray-on silicone surface was rather hydrophobic with contact angles of 78.1 ± 1.3°, but also exhibited a substantial negative charge of about -20 mV to -40 mV at the tested pH values. Consequently, adsorption resulted from interplay of hydrophobic and electrostatic forces.

At pH 8 close to the IEP, the mAb molecules carried least net charge, thus adsorption to the negatively charged silicone surface was suggested to be mainly driven by hydrophobic interactions. Furthermore, least inter-protein repulsion was expected close to the IEP, which enables closer packaging of the mAb molecules [117].

At pH 6 the silicone surface and mAb were oppositely charged with strong electrostatic attractive forces triggering adsorption while electrostatic repulsion amongst the mAb molecules themselves makes close packaging unfavorable. Thus, a decreased adsorption at pH 6 compared to pH 8 was anticipated.

At pH 10, where both the silicone surface and the mAb molecules were negatively charged, surface repulsion of the protein as well as amongst the mAb molecules themselves impeded adsorption. Nonetheless, adsorption to silicone surfaces was described even under electrostatically unfavorable conditions due to strong hydrophobic interactions as main driving force [118,119]. Even though the mAb carried net negative charge, charges are spatially distributed on the protein surface. Thus, local positively charged patches may exist, that still drive adsorption to the negatively charged silicone surface [120]. Additionally, incorporation of ions in the inner region of the adsorbed layer was described to mitigate high charge densities in the contact region [38]. This might further enable adsorption even under electrostatically unfavorable conditions.

The adsorption of mAb to baked-on silicone surfaces also revealed a similar pH-dependent profile with higher maxima of 8.7 ± 1.6 mg/m^2 at pH 8 and 7.0 ± 0.6 mg/m^2 at pH 6. The adsorbed mass at pH 10 remained low with 1.2 ± 0.7 mg/m^2 (Fig. VII-6).

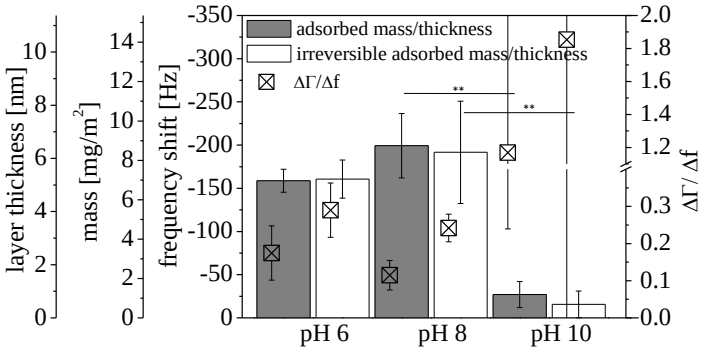

Fig. VII-6. Effect of pH on mAb adsorption (2 mg/mL) to model bake-on silicone surfaces in histidine buffer at consistent ionic strength of 50 mM as determined by QCM. Adsorbed mass was corrected for liquid-induced frequency and damping contributions according to Kanazawa. Statistical significance for bars is shown with ** $p \leq 0.01$.

A wide range of adsorbed amounts from approximately 1 mg/m^2 to 10 mg/m^2 has been described in literature obviously depending on buffer composition, measurement technique, surface characteristics as well as the protein under investigation [37,52]. In QCM, a pronounced adsorption maximum of approximately 7 mg/m^2 close to the IEP was described for a Fc-fusion protein on untreated silicone surfaces compared to approximately 3 mg/m^2 at pH values away from the IEP [119]. This is in agreement with what is generally observed for protein adsorption on hydrophobic surfaces with highest adsorbed amounts around the IEP [103,117]. On baked-on siliconized vials, two adsorption maxima with 5-7 mg/m^2 (depending on ionic strength) were suggested for IgG at pH 5-6 and close to the IEP of 7.8 [51], which was similarly observed in this study. However, the adsorption of albumin on baked-on silicone surfaces was found to be rather pH-independent [121].

The present study was performed on electrostatically comparable surfaces. Thus, different electrostatic attractive forces were less likely responsible for the higher adsorption at pH 6 on baked-on silicone surfaces compared to spray-on silicone surfaces. Rather, a change in hydrophobicity may be considered since slightly higher contact angles with stronger dispersive components were observed (Tab. VII-2, Fig. VII-3). Mathes found a linear dependence of IgG1 adsorption on the surface polarity (expressed as γ_p/γ) with higher adsorbed amounts on hydrophobic surfaces [90]. Similar results were described by Warkentin *et al.* and Elwing *et al.* for mAb and γ-globulin adsorption to methylated silicon surfaces with increasing contact angles [122,123]. Ortega reported a 20 % higher IgG adsorption with an increase in contact angle from

78° to 94° [124]. Stronger hydrophobic interactions may thus have led to the increase in adsorption on baked-on silicone surfaces at pH 6 and pH 8 and additionally may have compensated electrostatic repulsive forces between the oppositely charged mAb molecules occupying the sorbent surface at pH 6 [117].

3.2.2 MAB ORIENTATION AND PROTEIN LAYER THICKNESS

A straightforward approach to determine the approximate orientation of mAb on the silicone surface is to compare the adsorbed mass in QCM with the theoretical monolayer coverage based on generally accepted models in literature assuming close packaging and RSA (Tab. VII-3).

Tab. VII-3. Comparison between the theoretical protein monolayer coverage for end-on, side-on and flat-on adsorption assuming close packaging and RSA models.

Orientation	**Adsorbed dimensions [nm]**	**Surface contact area [nm^2]** [a]	**Monolayer coverage [mg/m^2]** [b]	
			Close packaging	**RSA**
End-on [c]	14×4.5	63	4.0	2.2
Side-on	10×4.5	45	5.6	3.1
Flat-on	14×10	140	1.8	1.0

[a] *Surface contact area was based on adsorption of aligned squares comparable to [58,125].*
[b] *Theoretical monolayer coverage was calculated using the Avogadro`s number with 6×10^{23}/mol, the molecular weight of approximately 150 kDa [126] and for RSA a jamming limit of 0.562 for aligned squares [26].*
[c] *End-on orientation holds for both F_{ab}-up and F_{ab}-down adsorption.*

As expected, the RSA surface exclusion model led to surface densities well below close-packaging. Assuming no or only minor structural rearrangements, the experimental results in this work of 1.2 mg/m^2 to 8.7 mg/m^2 (Fig. VII-5, Fig. VII-6) do not allow an assignment of one particular protein orientation at the interface.

A surface coverage higher than expected for a closely packed layer may likely be attributed to the co-existence of a second or more adlayers as previously suggested [87,97,127–129]. A second layer may also refer to systems with spread molecules interspersed with some intact molecules, which have insufficient free surface left for structural arrangement [130]. It is also possible that some clustering of the mAb occurs on the sorbent surface [129,131]. In QCM, it is additionally important to consider that the measured adsorbed mass corresponds to the protein layer and associated water, e.g., in the protein hydration shell or capillary-like water between the adsorbed molecules. Generally 1.7-2.7× higher adsorbed amounts were reported for QCM compared to other techniques (e.g., in situ ellipsometry, optical waveguide lightmode spectroscopy) [53,58]. The adsorbed amounts may thus still correspond to monolayer coverage.

To obtain additional information about structural and orientational arrangements on the surface, the adsorbed protein layer thickness was calculated based on an average protein density of 1.35 g/cm^3 [92] and compared to the approximate dimensions of IgG with 10×14×4.5 nm^3 [132]. Assuming monolayer coverage, the relatively high adsorbed amounts suggest a closely packed layer of either end-on or side-on adsorbed species extending approximately 10 nm and 14 nm in solution, respectively (Fig. VII-7). Close to the IEP, a more contracted, end-on conformation is likely with F_{ab}-fragments that lie close together with adsorbed amounts up to 5.5 mg/m^2 as reported by Buijs *et al.* [131]. It has been previously found that on hydrophobic surfaces, the mAb molecule is preferentially adsorbed in an end-on orientation [131,133].

However, the determined layer thickness between 0.9 nm and 6.5 nm in this study (Fig. VII-5, Fig. VII-6) was systematically lower than 10 nm and 14 nm as anticipated for end-on and side-on adsorption, respectively. This may be attributed to surface induced spreading [58,134], which particularly explains the rather questionable adsorbed layers thinner than the shortest axis of the molecule.

Alternatively, flat-on adsorption has been reported for CH_3-terminated surfaces and surfaces where electrostatic interactions are weak [135,136]. Flat-on adsorbed mAb extending approximately 5 nm in solution would roughly correspond to the calculated layer thickness, but it is rather unlikely due to the relatively high adsorbed amounts.

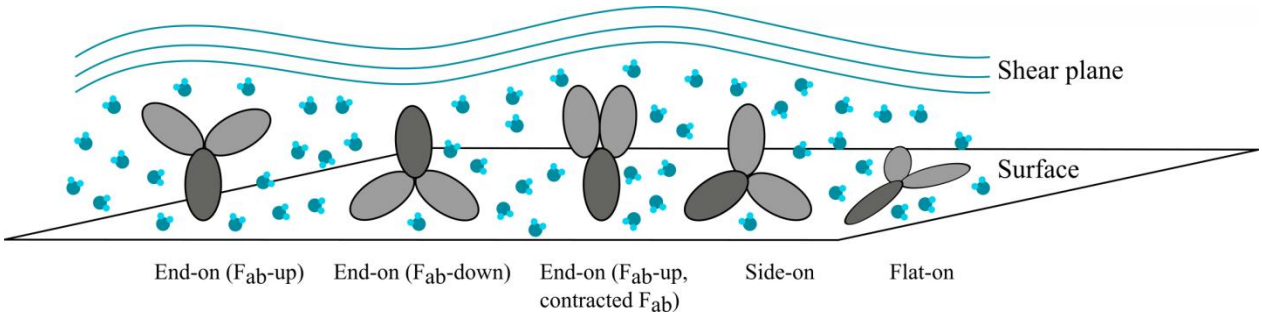

Fig. VII-7. Schematic drawing of some orientations of adsorbed mAb in aqueous media modified from [130,131,137].

In addition, it has to be taken into account that the density of the adsorbed layer depends on protein size, experimental conditions (e.g., layer water content) and surface characteristics [130]. Malmsten *et al.* found a comparable layer thickness for IgG of approximately 17-18 nm on both silica and methylated silica corresponding with different low adsorbed amounts of 1.2 ± 0.1 mg and 3.0 ± 0.2 mg, respectively [133]. Therefore, calculation of the layer thickness may be inherently misleading while in turn, predicted orientations associated with the surface coverage

results do not account for surface induced structural changes. It was not within the scope of the current experiments to probe the loss of the structural component, thus it could not be unambiguously clarified whether alterations of the protein´s structure contributed to the surface coverage at the different pH values.

3.2.3 ADSORPTION REVERSIBILITY UPON DILUTION

The fraction of mAb reversibly associated was between 44 % and 74 % for spray-on silicone layers upon rinsing with buffer, while for baked-on silicone layers the adsorption was apparently irreversible (Fig. VII-5, Fig. VII-6).

In protein adsorption studies, the concepts of reversibility and reconformation are often closely connected, but still not fully understood [16,36,37]. A simple explanation involves that “soft” proteins adapt its shape and assemble hydrophobic peptide moieties to interact with hydrophobic surface patches resulting in a loss of ordered structure and concomitant conformation entropy gain [38,103]. A perturbed protein structure was shown for IgG adsorption on hydrophobic polytetrafluoroethylene surfaces with a decrease in β-sheet and β-turn content, whereas α-helices and random coils were increased [62]. Upon adsorption the F_c-fragment remained unperturbed whereas the F_{ab}-fragment denatured due to a higher hydrophobicity [138]. Disruption of the native structure was also reported for several other proteins upon adsorption on hydrophobic surfaces [103,139–141].

Thereby, in particular on hydrophobic surfaces, protein adsorption was often found to be irreversible [119] or partially reversible by dilution [22,73,127]. This may indicate that two conformational populations are adsorbed to the surface with one being more loosely attached, which can be removed by rinsing [142]. The desorbed fraction may also be linked to molecules adsorbed above monolayer coverage that are not directly associated to the surfaces [127,143].

In the literature, the fraction of protein irreversibly adsorbed to hydrophobic surfaces was generally higher than to hydrophilic surfaces [117,144,145], which may explain the observed discrepancies in adsorption reversibility for spray-on and bake-on silicone surfaces in this study.

Although desorption experiments with buffer revealed a (partially) irreversible adsorption, a dynamic equilibrium with molecules arriving and displacing adsorbed species at the interface has been suggested by Lundström *et al.* [25]. and Norde *et al.* [103] (see 3.4.2).

3.2.4 VISCOELASTIC PROPERTIES OF THE ADSORBED PROTEIN LAYER

QCM with dissipation monitoring can be employed to investigate the viscoelastic properties of the adsorbed protein layer. The highest rigidity quotient for mAb adsorption on spray-on silicone layers was $\Delta\Gamma/\Delta f = 0.08$ (Fig. VII-5) indicating a rather rigid layer. On baked-on silicone layers higher $\Delta\Gamma/\Delta f$ up to 0.29 were observed (Fig. VII-6) (exceptional high value at pH 10, see below). The less rigid layer on baked-on silicone layers may be explained by both the higher surface load and/or a larger amount of coupled water. A linear correlation was found in literature between the measured dissipation and the total water content of the layer [130]. Considering the irregular Y-shape of mAb, this was well expected since such a film is relatively porous and hence associates more water [58].

There was no clear trend whether the rigidity increased or decreased upon buffer rinse, i.e., desorption. A higher rigidity and a concomitant lower surface coverage after rinsing as observed for spray-on silicone surfaces may be consistent with a more rigidly attached, dense layer after surface-induced spreading since the spread molecules closely fill up the free surface [97]. It can be further argued, that with lower surface coverage interfacial relaxation from an end-on to a flat-on orientation by rollover increased rigidity [22]. These effects are most likely cooperative while their relative contributions cannot be precisely quantified. The quantitatively different rigidity behavior on bake-on silicone surfaces where the surface coverage remained high after desorption pointed towards a different mechanism. At present, we do not have a clear explanation for this behavior.

The exceptionally large rigidity quotients > 1 at low surface coverage at pH 10 indicated a highly fluidic layer (Fig. VII-6). Dixit *et al.* reported a $\Delta R/\Delta f = 0.68\ \Omega/Hz$ for a purely viscous coupling of sucrose solutions [119], which equals $\Delta\Gamma/\Delta f = 6.6$ (calculation based on Eq. VII-4). Thus, the rigidity values observed at pH 10 could be indicative for loosely attached mAb molecules due to electrostatic repulsion from the negatively charged surface.

The reported negative $\Delta\Gamma/\Delta f$ values as a consequence of negative damping drifts were more difficult to interpret. They may derive from interfacial slip between the silicone layer and the adsorbed protein molecules or the quartz surface, respectively, which reduces the coupling of the layer and/or liquid to the crystal [87,146].

3.3 THE ADSORPTION OF MAB-ATTO 633 TO MODEL SPRAY-ON SILICONE SURFACES AS A FUNCTION OF PH STUDIED BY QCM

In this study, Atto 633 was covalently labeled to mAb to enable analysis in FACS (see 3.4). The main obstacle to be clarified was how the fluorescent label affected the adsorption behavior of the protein. In particular, the effect on the adsorption of mAb-Atto 633 to spray-on silicone surfaces was investigated in QCM at different pH values and consistent ionic strength of 50 mM.

Compared to unlabeled mAb (Fig. VII-5), higher amounts of approximately 9 mg/m^2 labeled mAb-Atto 633 adsorbed at both pH 6 and pH 8 (Fig. VII-8). At pH 10 the adsorption level dropped sharply to 0.8 ± 0.7 mg/m^2 similar to the adsorption of unlabeled mAb. In contrast to the adsorption of mAb to model spray-on silicone surfaces with a reversibly adsorbed fraction of 44-74 %, mAb-Atto 633 did not desorb upon rinsing with buffer.

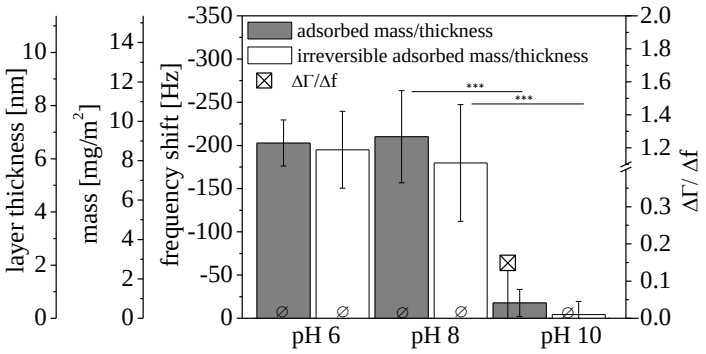

Fig. VII-8. Effect of pH on mAb-Atto 633 adsorption (2 mg/mL) to model spray-on silicone surfaces in histidine buffer at consistent ionic strength of 50 mM as determined by QCM. Adsorbed mass was corrected for liquid-induced frequency and damping contributions according to Kanazawa (Ø - ΔΓ/Δf could not be quantified (≤ 0)). Statistical significance for bars is shown with *** $p \leq 0.001$.

Changed charge properties of the labeled proteins [147] as compared to the unlabeled species as well as the hydrophobicity of the fluorescent label itself [148,149] are properties, which could impact the adsorption behavior of the dye-mAb conjugate.

For adsorption experiments on hydrophobic silicone surfaces, the hydrophobicity of the labeled species is probably the most important factor. HIC analysis revealed a heterogeneously labeled population with unlabeled mAb being present up to approximately 61-63 % (Fig. VII-9). The labeled species were not clearly separated due to their high degree of heterogeneity. Two prominent peaks could be exemplarily assigned to species with approximately one and two attached Atto-633 molecules based on the UV signal intensity in HIC at 280 nm and 633 nm (see

2.5.1). The DOL of 1.3 ± 0.1 as determined spectroscopically thus averaged the unlabeled main peak and the different labeled fractions.

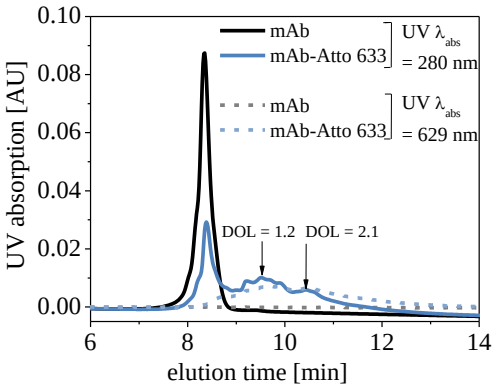

Fig. VII-9. Effect of Atto 633-labeling on the elution profile of mAb in HIC. Elution was monitored with UV detection at λ = 280 nm (protein absorption) and λ = 629 nm (Atto 633 absorption). Exemplary DOLs are given at specific time points calculated according to the recommended procedure for labeling [104].

The ε-amino groups of lysine residues and the N-terminal α-amino group are the primary sites used for amine-directed labeling and drug conjugation. Thus, the high degree of heterogeneity suggests species labeled at different lysine residues in addition to different labeling degrees [150,151]. Studies investigating the amine-directed conjugation for antibody-drug conjugates described that both the light and heavy chain have been modified [151]. For modified trastuzumab, an actual substitution ranging from 1 to 7 payloads was found at an average drug antibody ratio (DAR) of 3.5 [152]. Furthermore 50 % unconjugated mAb and a DAR of 4-6 were reported for modified gemtuzumab resulting in an average DAR of 2-3 [153].

Thus, Atto 633 labeling yielded a rather typical heterogeneous distribution of amine-labeled species. More importantly, these results clearly showed, that Atto 633-labeled mAb exhibited a substantially higher hydrophobicity compared to unlabeled mAb. As a consequence, mAb-Atto 633 adsorbed to a higher extent and less reversible to hydrophobic silicone surfaces. Similarly, on hydrophobic surfaces, a higher protein hydrophobicity corresponded with a higher surface coverage when two different mAbs were investigated [127].

3.4 THE ADSORPTION OF MAB-ATTO-633 TO MODEL SPRAY-ON SILICONE SURFACES STUDIED BY FACS

3.4.1 IMPACT OF UNSPECIFIC SILICONE INTERACTIONS

FACS has emerged as a powerful technique to differentiate silicone droplets, proteinaceous particles and protein-coated silicone droplets using combinations of fluorescently-labeled proteins (e.g., Alexa Fluor 647), or non-covalently binding dyes such as SYPRO Orange [71], Bis-ANS and DCVJ [72] and stained silicone oil (e.g., Bodipy 493/503) [70]. The utility of FACS to identify heterogeneous silicone droplets with adsorbed proteins particularly offers an interesting approach to monitor protein adsorption. In most cases, experiments with fluorescently labeled proteins are based on two crucial assumptions: i) that the fluorescent dye does not alter the physicochemical properties and adsorption behavior of the protein and ii) that the dye itself does not interact with the sorbent surface. Clearly, these generalized assumptions require further assessment since recent studies indicated that fluorescently-labeled mAbs exhibit different aggregation [154] and adsorption behaviors [155].

Selecting an appropriate fluorescent dye in terms of a minimum change in relative protein charge, IEP and size [147], protein aggregation behavior [156] or hydrophobicity of the fluorescent probe itself [148,149] surely mitigates concerns arising from the presence of a fluorescent label. However, in this study the choice of the fluorescent label was limited. Bodipy 493/503 is a lipophilic, non-charged fluorophore well-known to track lipid trafficking, as membrane probe and as specific tracer for cellular lipid droplets in FACS [99,157]. In addition, it was successfully used to stain silicone droplets in earlier studies [158,159]. mAb was labeled with Atto 633, which is described as pH-independent, cationic, moderately hydrophilic dye [98]. A combination of both dyes was thus considered reasonable and allowed a multicolor approach in FACS with minimum spectral spill-over in the emission filters (< 1.4 %) [100]. To mitigate label-induced alterations in the mAb properties, we used a relatively low DOL of 1.3 ± 0.1 compared to a DOL of 7-8 applied for IgG in former FACS studies [158,159].

Contributions to the fluorescence detected in FACS could be divided into four categories arising from i) the adsorbed mAb, ii) unspecific Atto 633-to-silicone, iii) dye-to-dye and iv) mAb-to-Bodipy 493/503 interactions. A mixture of Bodipy 493/503-stained or non-stained silicone emulsion, Atto-633-labeled mAb and free Atto 633 dye was consequently examined in order to investigate these different fluorescence contributions (Fig. VII-11, Fig. VII-10).

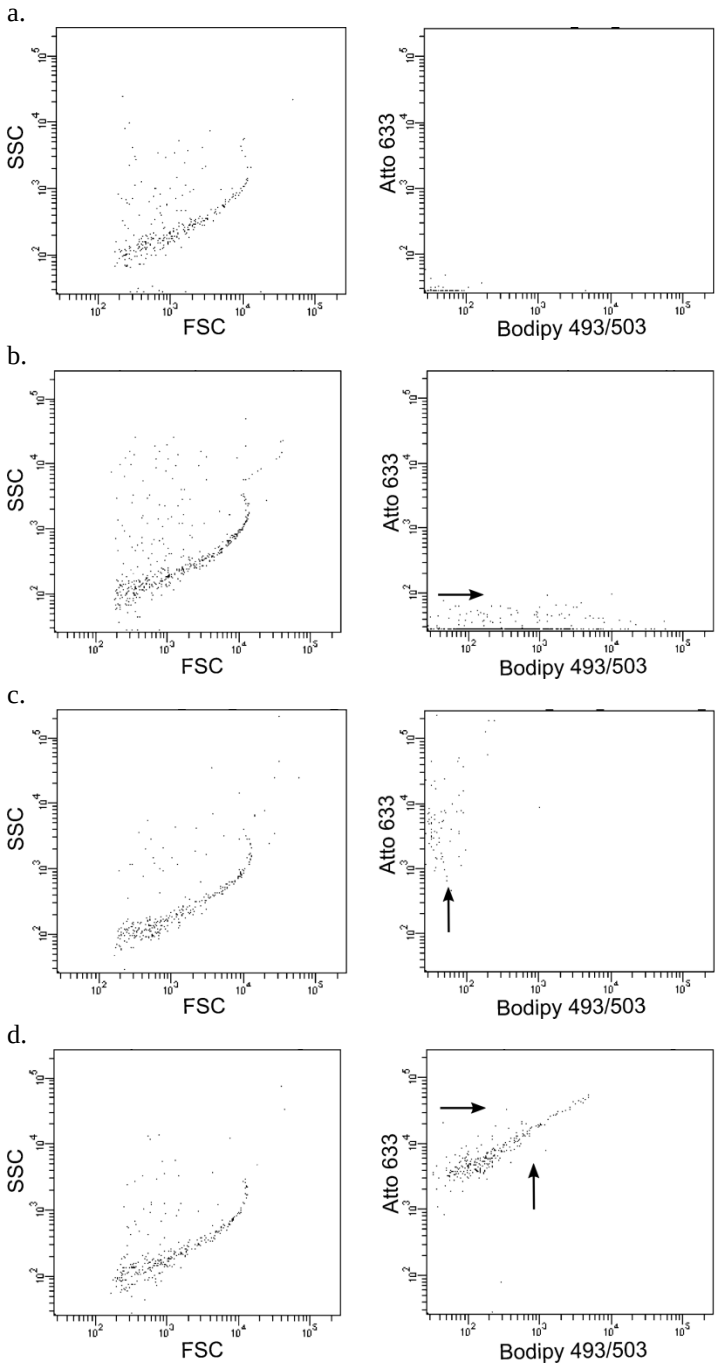

Fig. VII-10. Representative FACS dot plots of SSC versus FSC; and the fluorescence detected at 660/20 nm (i.e., Atto 633 fluorescence) versus 530/30 nm (i.e., Bodipy 493/503 fluorescence) for samples containing (a) 0.2 mg/mL non-stained silicone emulsion, (b) 0.2 mg/mL Bodipy 493/503-stained silicone emulsion, (c) a mixture of 0.2 mg/mL non-stained silicone emulsion and 0.05 mg/mL mAb-Atto 633 and (d) a mixture of 0.2 mg/mL Bodipy 493/503-stained silicone oil and 0.05 mg/mL mAb-Atto 633 in 20 mM histidine buffer, pH 6. Arrows indicate an increase in the corresponding fluorescence due to labeling mAb with Atto 633 and silicone staining with Bodipy 493/503, respectively.

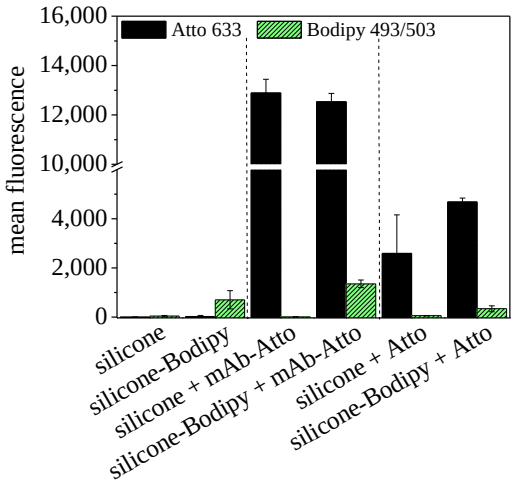

Fig. VII-11. Fluorescence contributions from mAb adsorption to silicone as well as unspecific Atto 633-to-silicone, dye-to-dye and mAb-to-Bodipy 493/503 interactions. Samples contained 0.2 mg/mL Bodipy 493/503-stained or non-stained silicone emulsion in 20 mM histidine buffer, pH 6, a final protein concentration of 0.05 mg/mL mAb-Atto 633 or equimolar concentrations of free Atto 633. In FACS, Atto 633 was excited with a 633 nm red laser and the mean fluorescence was detected with a detector band of 660/20 nm. For the excitation of Bodipy 493/503, a 488 nm blue laser was used followed by detection with a 530/30 nm detector band.

While non-stained silicone oil emulsion showed a minimum fluorescence < 40 for both fluorescence filters, staining silicone oil with Bodipy 493/503 caused an increase in the corresponding Bodipy 493/503 fluorescence to 700 (Fig. VII-10a and Fig. VII-10b, Fig. VII-11 left panel). The addition of Atto 633-labeled mAb increased the corresponding Atto 633 fluorescence at a similar ratio to 12,500 and 12,900, respectively, in samples containing non-stained or stained silicone emulsion (Fig. VII-10c and Fig. VII-10d, Fig. VII-11 middle panel). This indicated an adsorption of mAb primarily attributed to mAb-to-silicone interactions rather than a substantial binding affinity of mAb-to-Bodipy 493/503 or dye-to-dye interactions. Interestingly, experiments with free Atto 633 dye suggested a binding to silicone oil but to a markedly lesser extent, associated with an increase in the corresponding Atto 633 fluorescence to 2600 (Fig. VII-11 right panel). The Atto 633 fluorescence signal after addition of free dye was rather comparable in non-stained and Bodipy 493/503-stained silicone emulsion thus excluding additional dye-to-dye interactions.

Hydrophobic dyes such as Bodipy 630/650 were found to non-specifically bind to the protein interior through hydrophobic interactions [149]. The influence of this should, however, be negligible within the scope of this study. Nonetheless, the first obstacles using fluorescently-labeled protein for adsorption experiments were clear from these results since Atto 633 dye itself

partially associated with silicone oil. Similarly, free Cy5 dye was found to substantially interact with sorbent surfaces such as CH_3-silane, polystyrene and polydimethylsiloxane [76].

We further tested, if choosing a suitable concentration range may mitigate fluorescence contributions from the Atto 633 dye alone. The influence of different mAb-Atto 633 concentrations ranging from 0.01 mg/mL to 1 mg/mL and equivalent concentrations of free Atto 633 based on a DOL of 1.3 ± 0.1 is depicted in Fig. VII-12.

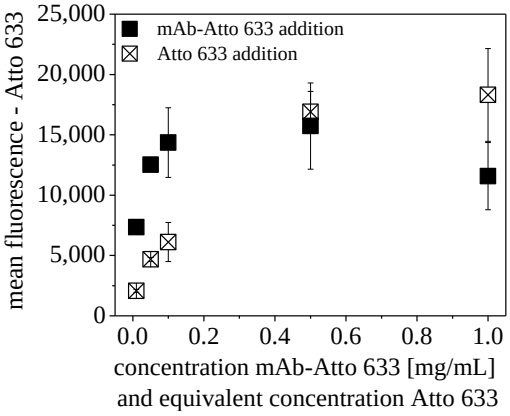

Fig. VII-12. Concentration dependent mean fluorescence of mAb-Atto 633 at 0.01-1 mg/mL or equimolar concentrations of free Atto 633. Samples contained 0.2 mg/mL Bodipy 495/503-stained silicone emulsion in 20 mM histidine buffer, pH 6.

For Atto 633-labeled mAb, surface saturation was reached at around 0.5 mg/mL. The curve characteristics coincided with a Langmuir adsorption isotherm [18,19]. However, the application of the Langmuir model with its implication of dynamic equilibrium and adsorption reversibility, is not necessarily justified by the agreement of the data [20]. Surface saturation may also be understood using the more relevant RSA model in which proteins readily adsorb to form an inefficiently packed layer with undefined gaps. The probability to find an available adsorption site decreases faster with increasing surface coverage [26]. However, the free Atto 633 dye exhibited a similar saturation plateau, but with an initially less steep slope. Due to the small size of the Atto 633 dye (535 Da [91]) relative to the overall size of the protein (~ 150 kDa [126]) and the corresponding much smaller footprint occupied upon adsorption, it is unlikely that both species achieved saturation coverage at equivalent concentrations. Instead, the stagnating fluorescence in addition to the indicated overshoot of fluorescence at 0.5 mg/mL mab-Atto 633 compared to 1 mg/mL may be attributed to intermolecular concentration quenching as with higher concentration the fluorophores come in close proximity [160,161]. The plateau may thus

derive from competition between an increase in the number of fluorophores at the interface and the concomitant decrease in fluorescence quantum yield.

The steeper slope for mAb-Atto 633 adsorption pointed to a greater surface affinity compared to the free Atto 633 dye, most probably due to long-range electrostatic attractive forces at pH 6, which trigger the transport of the positively charged mAb-Atto (IEP = 8-8.5 [116]) to the negatively charged silicone surface (IEP = 3.9).

Overall, an easy set-up was established to assess the fluorescence contributions from unspecific Atto 633-to-silicone interactions. On the basis of these results, adsorption studies in FACS are recommended to be performed in a concentration range of 0.01-0.1 mg/mL mAb-Atto 633.

3.4.2 REVERSIBILITY OF MAB-ATTO 633 ADSORPTION UPON DILUTION, EXCHANGE WITH UNLABELED MAB AND ADDITION OF POLYSORBATE 20

Conceptually, reversibility testing of mAb adsorption to silicone oil in this work can be divided into three categories. i) reversibility upon buffer rinse, ii) exchange against dissolved proteins and iii) replacement of protein by surfactant.

As depicted above for QCM experiments, mAb-Atto-633 adsorbed irreversible to model spray-on silicone surfaces upon dilution (Fig. VII-8) compared to unlabeled mAb (Fig. VII-5) most likely attributed to an increased hydrophobicity of the labeled species (Fig. VII-9).

The first experiment in FACS involved an exchange study between unlabeled mAb and Atto 633-labeled mAb to further probe discrepancies in the adsorption reversibility of both species. After a defined adsorption period of 2 h, which is sufficient for surface saturation of mAb-Atto 633 (supporting information Fig. S VII-3), a ten-fold excess of unlabeled mAb was added and the mean Atto 633 fluorescence was monitored over a 6 h time period (Fig. VII-13a). The Atto 633 fluorescence remained rather constant indicating that mAb-Atto 633 was not displaced by unlabeled mAb. In contrast, in experiments that were performed in reverse order, mAb-Atto 633 steadily displaced the unlabeled mAb from the silicone surface since the Atto 633 fluorescence increased over time (Fig. VII-13b). Thus, a stronger surface binding of Atto 633-labeled mAb as compared to unlabeled mAb was indicated in FACS.

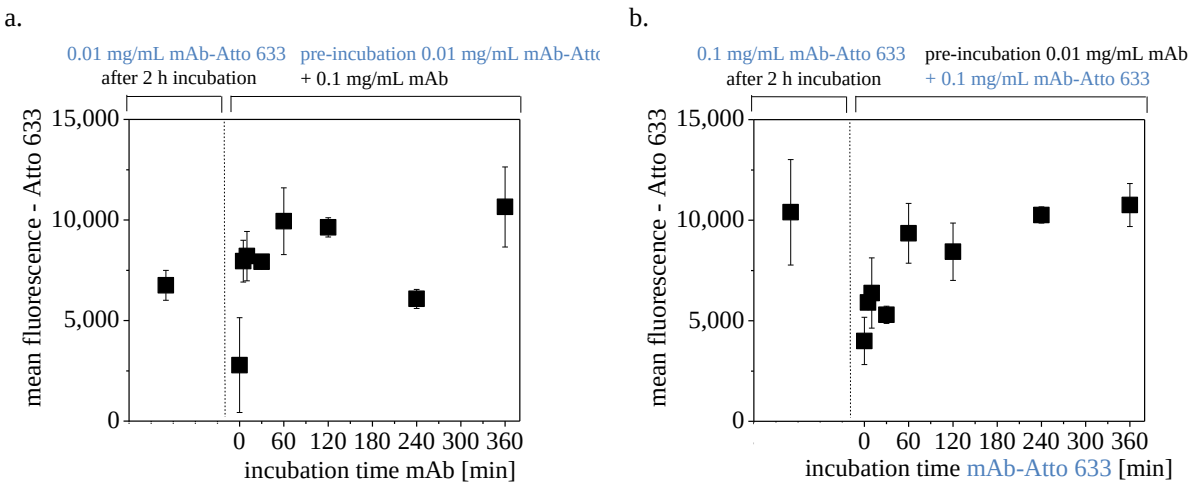

Fig. VII-13. Sequential adsorption assay for mAb and mAb-Atto 633 onto 0.2 mg/mL Bodipy 493/503 stained silicone emulsion in 20 mM histidine buffer, pH 6. (a) mAb-Atto 633 was incubated for 2 h followed by adding an excess of mAb in a ratio of 1:10. (b) Experiments were performed in reverse order, incubating mAb first followed by an excess addition of mAb-Atto 633.

For adsorption experiments on hydrophobic silicone surfaces, the hydrophobicity of the labeled species is a highly important factor (see 3.3), but also a difference in protein charge may play a role. At the tested pH 6, the silicone surface and protein carried opposite electrostatic charge. Note that, Atto NHS-ester primarily attack the highly polar primary amino groups of lysine, which are usually positively charged at pH 6 ($pK_a = 10.4$ for lysine [162]). The conjugation reaction thus leads to the loss of a positive charge while, simultaneously, a positive charge is introduced due to the cationic Atto-label [98]. Thus, the influence of charge should be nullified and less strong than a change in hydrophobicity [74,148].

Upon addition of a surfactant, the adsorption of mAb-Atto 633 was clearly reduced in mixed samples containing polysorbate 20 in concentrations as low as 0.005 % (m/v) (Fig. VII-14).

In therapeutic protein formulations, the addition of nonionic surfactants has shown to prevent adsorption induced protein monomer loss [13,49,158,159] and different mechanism have been proposed [163,164]. Sequential and competitive protein adsorption experiments on hydrophobic surfaces primarily pointed at an interfacial competition mechanism with the low molecular surfactant arriving faster at the interface [165,166]. A protein repellent detergent layer is formed, which sterically prevents proteins from adsorption similar to polyethylene glycol-modified surfaces [167]. Initially adsorbed proteins may be also displaced by surfactant molecules in a later stage [168,169]. A direct association of nonionic surfactants to hydrophobic protein sites was described in some cases, thereby shielding these hydrophobic protein sites and mitigating

interfacial protein adsorption or protein aggregation [170,171]. However, a few studies on IgG suggest a negligibly weak protein-surfactant binding [172].

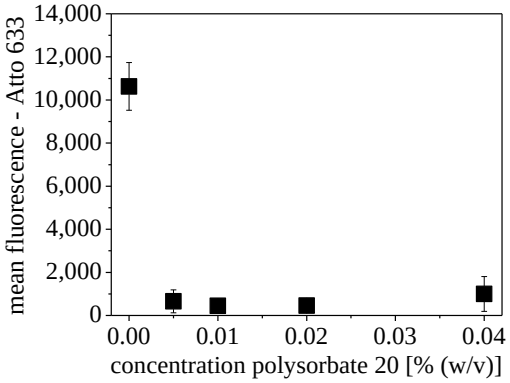

Fig. VII-14. mAb-Atto 633 (0.05 mg/mL) adsorption to 0.2 mg/mL Bodipy 493/503 stained silicone emulsion in histidine buffer, pH 6, 50 mM, as a function of polysorbate 20 concentration ranging from 0.005 % (w/v) to 0.04 % (w/v). The mixtures were allowed to adsorb for 2 h before FACS analysis.

For Atto 633-labeled mAb, maximum adsorption suppression was achieved close to the critical micelle concentration (CMC) of polysorbate 20 at around 0.005-0.006 % [173–175]. In the literature, comparable results were observed for polysorbate 20, polysorbate 80 and poloxamer 188 with adsorption minima for albumin and mAb onto hydrophobic surfaces close to the CMC [118,176]. It was suggested that surfactant monomers are the competing species. This makes a most effective surfactant concentration close to the CMC, where the concentration of monomer in the bulk is high, conceivable. The extent of adsorption depression depends on the protein, surfactant and surface properties among others factors, thus no general trend could be observed.

Overall, labeling induced a substantially altered reversibility profile for both dilution with buffer in QCM (see 3.3) and exchange against unlabeled species in FACS. The adsorption of Atto 633-labeled mAb was still inhibited by polysorbate 20. Both QCM and FACS thus demonstrated a high potential to study adsorption reversibility, but the complex nature of fluorescence-based adsorption studies was clearly highlighted. It is thus noteworthy that results derived from mechanistic adsorption studies based on single molecule tracking, but also FACS, may be essentially perturbed by the altered adsorption behavior of labeled protein species.

3.4.3 THE ADSORPTION OF MAB-ATTO 633 TO MODEL SPRAY-ON SILICONE SURFACES AS A FUNCTION OF PH STUDIED BY FACS

As described above (see 3.3), the adsorption of mAb-Atto 633 was investigated in QCM as a function of pH and at consistent ionic strength of 50 mM. mAb-Atto 633 markedly adsorbed at

pH 6 and pH 8 to a comparable extent, while at pH 10 the adsorption level dropped sharply. FACS was capable to qualitatively reflect this pH-dependent adsorption, but the pH effect was less pronounced (Fig. VII-15). In addition, FACS adsorption results may be affected by the composition of the sheath fluid that was not matched in these experiments.

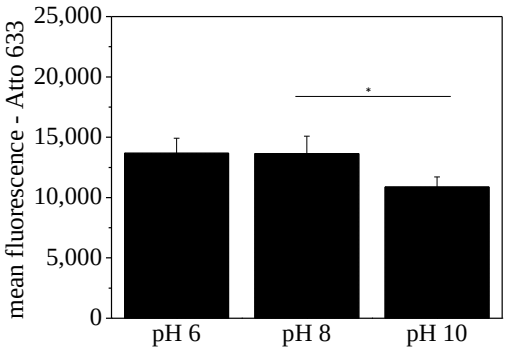

Fig. VII-15. Effect of pH on mAb-Atto 633 (0.05 mg/mL) adsorption to 0.2 mg/mL Bodipy 493/503-stained silicone emulsion in histidine buffer at consistent ionic strength of 50 mM (* $p \leq 0.05$). The samples were allowed to adsorb for 2 h before FACS analysis.

For comparison, a protein sample without silicone emulsion was particle-free in the detected size range as no signals in the scatter plots were observed (lower size range covered in FSC was approximately 1.5 µm, supporting information Fig. S VII-4). Consequently, the particles detected were attributed to silicone droplets with adsorbed mAb. Additional sample information can be derived from the number of detected events, i.e., particles, and from FSC as a measure for particle size. No additional particles (e.g., protein aggregates) were introduced compared to the initial silicone emulsion since the mean number of detected events ranged between 260 and 350 (supporting information Fig. VII-5a). Also, the mean FSC was consistent with 3100-3600 for all samples (supporting information Fig. VII-5b), thereby indicating no substantial change in the size of droplet species, e.g., due to coalescence of silicone droplets, which has been previously reported for relatively highly concentrated silicone emulsions (0.5-1 %) [70]. In contrast, low silicone levels of 0.2 mg/mL (0.02 %) were employed in this study. In preliminary experiments, this concentration was identified to yield lowest reasonable particle counts in FACS.

4 CONCLUSION

The choice of methods to study protein adsorption at the solid-liquid or liquid-liquid interface is large and ever-increasing. In this study, QCM and FACS were utilized to detect and characterize the adsorption of a model mAb to silicone surfaces.

For QCM experiments, quartz chips were coated with silicone oil and heat-treated silicone to mimic the different silicone surfaces in drug product containers that are present after spray-on and bake-on siliconization, respectively. A spin-coating method was established to yield comparable rigid, homogeneous coatings with approximately 60-70 mg/m^2 and a layer thickness of 40-50 nm in QCM. The model bake-on silicone coating was slightly more hydrophobic with contact angles of 91.9 ± 1.2° and 91 % dispersive components compared to the spray-on coating with a contact angle of 78.1 ± 1.3° and 87 % dispersive components. ζ-potential measurements of silicone droplets indicated similar negative surface charges of approximately -20 mV to -40 mV for both coatings at the tested pH 6, pH 8 and pH 10.

Adsorption experiments were performed with mAb in histidine buffer at three different pH values (i.e., charge of the protein) and consistent ionic strength of 50 mM to investigate driving forces that trigger adsorption to hydrophobic silicone surfaces. On spray-on siliconized surfaces, the highest surface concentration for mAb with 6.8 ± 0.2 mg/m^2 was found at pH 8 close to the mAb´s IEP at pH 8.0-8.5 [116] and lower adsorbed amounts if shifting away from the IEP. The adsorption of mAb to baked-on silicone surfaces exhibited a higher maximum of 8.7 ± 1.6 mg/m^2 at pH 8, but also a second adsorption maximum with 7.0 ± 0.6 mg/m^2 was observed at pH 6. Overall, the adsorbed masses ranging between 1.2 mg/m^2 and 8.7 mg/m^2 entirely covered the predicted range for closely-packed and RSA adsorption models implying a diversity of molecular orientation on the surface when assuming no or only minor structural changes. However, the calculated layer thickness did not necessarily corroborate the surface coverage results, which may be attributed to surface-induced spreading. More than monolayer coverage could be assigned to additional adlayers or surface clustering, but might also be an inherent artefact of the QCM technique. QCM was reported to yield generally higher adsorbed amounts than other techniques due to layer entrapped water. On baked-on silicone surfaces, the adsorption of mAb was apparently irreversible upon rinsing with buffer while on spray-on silicone surfaces between 44-74 % were reversibly associated. Overall, our results showed that the adsorption of mAb was noticeably influenced by surface hydrophobicity.

Atto 633-labeled mAb exhibited a higher hydrophobicity as compared to unlabeled mAb and as a consequence a different adsorption profile in QCM. The adsorption to model spray-on silicone surfaces was increased up to approximately 9 mg/m^2 and irreversible compared to unlabeled mAb. In FACS, we have additionally demonstrated that mAb-Atto 633 was not exchanged against unlabeled mAb, but adsorption of mAb-Atto 633 was clearly reduced by the addition of polysorbate 20 in concentrations as low as 0.005 % (m/v). Adsorption was also partially driven by unspecific Atto 633-to-silicone interactions as confirmed in a set of control experiments in FACS. Both QCM and FACS revealed a similar pH dependent effect on the mAb-Atto 633 adsorption, but the pH effect was less pronounced in FACS.

Thus, based on our results the hydrophobicity of both the surface and adsorbed species markedly affected the adsorption properties. The use of fluorescently labeled proteins for adsorption studies has to be selected with care and the effect of the label needs to be clarified. We therefore suggest that the unlabeled and labeled species are comparatively evaluated, e.g., in terms of i) adsorbed mass, ii) adsorption reversibility towards rinsing with buffer, exchange against unlabeled species and surfactants, iii) non-specific binding of the dye to the investigated surface within the investigated concentration range, and iv) physicochemical properties such as hydrophobicity, charge, size and IEP. The experimental set-up in this study largely covered these suggestions, but only with high experimental effort. Thus, for further adsorption experiments particularly on hydrophobic surfaces, the hydrophobicity of the labeled species appeared to be a valuable indicator for a changed adsorption behavior. Another approach could thus aim to specifically tune fluorescence labeling with regard to a low DOL, and more importantly, fluorescence labels that induce no or minor alterations in the protein´s hydrophobicity.

5 SUPPORTING INFORMATION

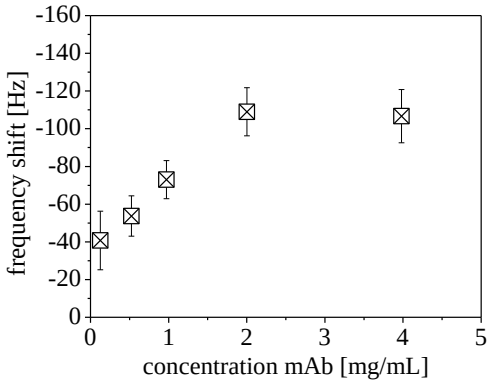

Fig. S VII-1. Effect of mAb concentration ranging from 0.1 mg/mL to 4 mg/mL on frequency shifts in QCM upon adsorption to spray-on silicone surfaces in 20 mM histidine buffer, pH 6.

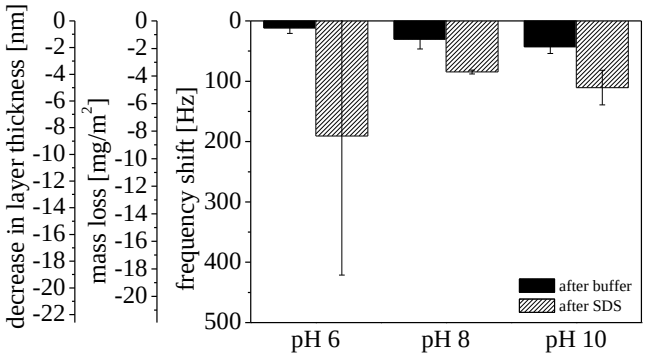

Fig. S VII-2. Exemplary physical stability of the spray-on silicone coating. The coating was exposed to highly purified water followed by histidine buffer of different pH and consistent ionic strength of 50 mM and then water, all at flow rate of 60 µL/min until frequency and damping signals were stable for 10 min with ± 1 Hz and ± 10 Hz, respectively. Similarly, the silicone coating was exposed to 10 mM phosphate buffer containing 145 mM NaCl and 0.05 % (w/v) SDS (pH 7.2) between two runs of highly purified water. Frequency shifts between both water runs were used for modeling the mass of detached silicone coating according to Sauerbrey (Eq. VII-1).

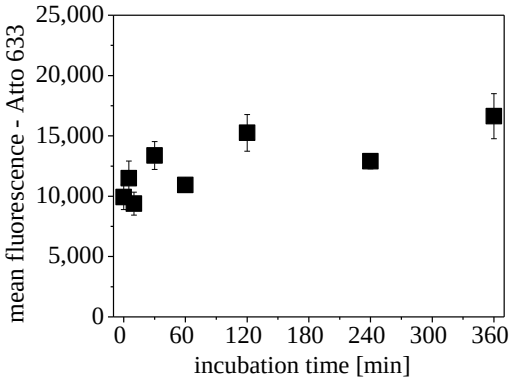

Fig. S VII-3. Mean fluorescence of mAb-Atto 633 (0.05 mg/mL) as a function of incubation time in samples containing 0.2 mg/mL Bodipy 495/503-stained silicone emulsion in 20 mM histidine buffer, pH 6.

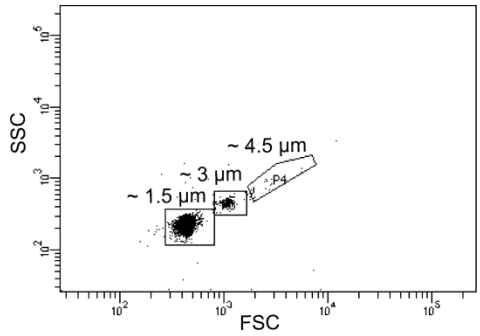

Fig. S VII-4. Representative FACS dot plot of SSC versus FSC for silica standards in 20 mM histidine, pH 6.

a.

b.

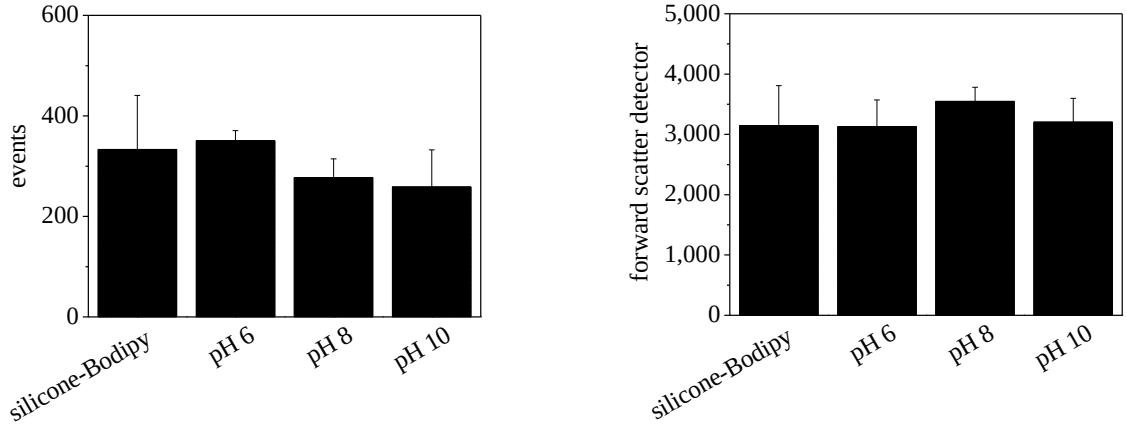

Fig. S VII-5. Effect of pH on the detected events and FSC in FACS for samples containing mAb-Atto 633 (0.05 mg/mL) and 0.2 mg/mL Bodipy 493/503-stained silicone emulsion in histidine buffer of different pH and consistent ionic strength of 50 mM (n = 3). Average for Bodipy 493/503-stained silicone emulsion (n = 14) was derived as average from all experiments during the course of the FACS study.

6 ABBREVIATIONS

Atto 633 NHS-ester	Atto 633 N-hydroxylsuccinimidyl-ester
Bodipy 493/503	4,4-difluoro-1,3,5,7,8-pentamethyl-4-bora-3a,4a-diaza-s-indacene
CMC	Critical micelle concentration
3D-LSM	3D-laser scanning microscopy
DOL	Degree of labeling
DAR	Drug antibody ratio
FACS	Fluorescence activated cell sorting
FSC	Forward scatter
HIC	Hydrophobic interaction chromatography
IEP	Isoelectric point
mAb	Monoclonal antibody
QCM	Quartz crystal microbalance
RSA	Random sequential adsorption
SDS	Sodium dodecyl sulfate
SSC	Side scatter

7 REFERENCES

[1] J.S. Bee, T.W. Randolph, J.F. Carpenter, S.M. Bishop, M.N. Dimitrova, Effects of surfaces and leachables on the stability of biopharmaceuticals, J. Pharm. Sci. 100 (2011) 4158–4170.

[2] S. Choi, J. Chae, Methods of reducing non-specific adsorption in microfluidic biosensors, J. Micromechanics Microengineering. 20 (2010) 1–9.

[3] Q. Wei, T. Becherer, S. Angioletti-Uberti, J. Dzubiella, C. Wischke, A.T. Neffe, et al., Protein interactions with polymer coatings and biomaterials, Angew. Chem. Int. Ed. Engl. 53 (2014) 8004–8031.

[4] L. Yu, L. Zhang, Y. Sun, Protein behavior at surfaces: orientation, conformational transitions and transport, J. Chromatogr. A. 1382 (2015) 118–134.

[5] H.-C. Mahler, F. Huber, R.S.K. Kishore, J. Reindl, P. Rückert, R. Müller, Adsorption behavior of a surfactant and a monoclonal antibody to sterilizing-grade filters, J. Pharm. Sci. 99 (2010) 2620–2627.

[6] R.G. Ingle, A.S. Agarwal, Pre-filled syringe - a ready-to-use drug delivery system: a review, Expert Opin. Drug Deliv. 11 (2014) 1391–1399.

[7] G. Sacha, J.A. Rogers, R.L. Miller, Pre-filled syringes: a review of the history, manufacturing and challenges, Pharm. Dev. Technol. 20 (2015) 1–11.

[8] G.A. Sacha, W. Saffell-Clemmer, K. Abram, M.J. Akers, Practical fundamentals of glass, rubber, and plastic sterile packaging systems, Pharm. Dev. Technol. 15 (2010) 6–34.

[9] E. Chan, A. Hubbard, S. Sane, Y.-F. Maa, Syringe siliconization process investigation and optimization, PDA J. Pharm. Sci. Technol. 66 (2012) 136–150.

[10] J.S. Bee, V.V. Frey, U. Javed, J. Chung, M.L. Corcoran, P.S. Roussel, et al., Characterization of the Initial Level and Migration of Silicone Oil Lubricant in Empty Prefilled Syringes for Biologics Using Infrared Spectroscopy, PDA J. Pharm. Sci. Technol. 68 (2014) 494–503.

[11] B. Reuter, Silicone oil and its applications for parenteral products, PDA Europe Workshop, Cologne, (2010).

[12] L. Khandke, R. Malone, X. Yang, H. Han, J.L. Look, Z. Jin, et al., Novel formulations which stabilize and inhibit precipitation of immunogenic compositions, U.S. Patent 2011/0172393 A1, 2011.

[13] P. Basu, A.W. Blake-Haskins, K.B. O'Berry, T.W. Randolph, J.F. Carpenter, Albinterferon α2b adsorption to silicone oil-water interfaces: effects on protein conformation, aggregation, and subvisible particle formation, J. Pharm. Sci. 103 (2014) 427–436.

[14] S. Pasche, J. Vörös, H.J. Griesser, N.D. Spencer, M. Textor, Effects of Ionic Strength and Surface Charge on Protein Adsorption at PEGylated Surfaces, J. Phys. Chem. B. 109 (2005) 17545–17552.

[15] K. Höger, T. Becherer, W. Qiang, R. Haag, W. Frieß, S. Küchler, Polyglycerol coatings of glass vials for protein resistance, Eur. J. Pharm. Biopharm. 85 (2013) 756–764.

[16] M. Rabe, D. Verdes, S. Seeger, Understanding protein adsorption phenomena at solid surfaces, Adv. Colloid Interface Sci. 162 (2011) 87–106.

[17] M. Kastantin, B.B. Langdon, D.K. Schwartz, A bottom-up approach to understanding protein layer formation at solid-liquid interfaces, Adv. Colloid Interface Sci. 207 (2014) 240–252.

[18] I. Langmuir, Vapor pressured, evaporation, condensation and adsorption, J. Am. Chem. Soc. 54 (1932) 2798–2832.

[19] I. Langmuir, The adsorption of gases on plane surfaces of glass, mica and platinum, J. Am. Chem. Soc. 40 (1918) 1361–1403.

[20] R. Latour, The langmuir isotherm: A commonly applied but misleading approach for the analysis of protein adsorption behavior, J. Biomed. Mater. Res. Part A. 103 (2015) 949–958.

[21] R. Sips, On the Structure of a Catalyst Surface, J. Chem. Phys. 16 (1948) 490–495.

[22] M.E. Wiseman, C.W. Frank, Antibody adsorption and orientation on hydrophobic surfaces, Langmuir. 28 (2012) 1765–1774.

[23] R. Beissinger, E. Leonard, Plasma protein adsorption and desorption rates on quartz: approach to multi-component systems, ASAIO J. XXVII (1981) 225–230.

[24] M.. Soderquist, A.. Walton, Structural changes in proteins adsorbed on polymer surfaces, J. Colloid Interface Sci. 75 (1980) 386–397.

[25] I. Lundström, H. Elwing, Simple kinetic models for protein exchange reactions on solid surfaces, J. Colloid Interface Sci. 136 (1990) 68–84.

[26] J. Feder, Random sequential adsorption, J. Theor. Biol. 87 (1980) 237–254.

[27] A.P. Minton, Adsorption of globular proteins on locally planar surfaces. II. Models for the effect of multiple adsorbate conformations on adsorption equilibria and kinetics, Biophys. J. 76 (1999) 176–187.

[28] R.C. Chatelier, A.P. Minton, Adsorption of globular proteins on locally planar surfaces: models for the effect of excluded surface area and aggregation of adsorbed protein on adsorption equilibria, Biophys. J. 71 (1996) 2367–2374.

[29] A.P. Minton, Effects of excluded surface area and adsorbate clustering on surface adsorption of proteins, Biophys. Chem. 86 (2000) 239–247.

[30] M. Rabe, D. Verdes, S. Seeger, Surface-induced spreading phenomenon of protein clusters, Soft Matter. 5 (2009) 1039–1047.

[31] P.A. Mulheran, D. Pellenc, R.A. Bennett, R.J. Green, M. Sperrin, Mechanisms and dynamics of protein clustering on a solid surface., Phys. Rev. Lett. 100 (2008) 068102(1)–068102(4).

[32] M. Rabe, D. Verdes, J. Zimmermann, S. Seeger, Surface Organization and Cooperativity during Nonspecific Protein Adsorption Events, J. Phys. Chem. B. 112 (2008) 13971–13980.

[33] M. Rabe, D. Verdes, S. Seeger, Understanding cooperative protein adsorption events at the microscopic scale: a comparison between experimental data and Monte Carlo simulations, J. Phys. Chem. B. 114 (2010) 5862–5869.

[34] M. Kastantin, R. Walder, D.K. Schwartz, Identifying mechanisms of interfacial dynamics using single-molecule tracking, Langmuir. 28 (2012) 12443–12456.

[35] A.C. McUmber, N.R. Larson, T.W. Randolph, D.K. Schwartz, Molecular Trajectories Provide Signatures of Protein Clustering and Crowding at the Oil/Water Interface, Langmuir. 31 (2015) 5882–5890.

[36] W. Norde, My voyage of discovery to proteins in flatland ...and beyond, Colloids Surf. B. Biointerfaces. 61 (2008) 1–9.

[37] K. Nakanishi, T. Sakiyama, K. Imamura, On the adsorption of proteins on solid surfaces, a common but very complicated phenomenon, J. Biosci. Bioeng. 91 (2001) 233–244.

[38] W. Norde, J. Lyklema, Thermodynamics of protein adsorption. Theory with special reference to the adsorption of human plasma albumin and bovine pancreas ribonuclease at polystyrene surfaces, J. Colloid Interface Sci. 71 (1979) 350–366.

[39] C.J. Burke, B.L. Steadman, D.B. Volkin, P.-K. Tsai, M.W. Bruner, C.R. Middaugh, The adsorption of proteins to pharmaceutical container surfaces, Int. J. Pharm. 86 (1992) 89–93.

[40] V. Sluzky, J.A. Tamada, A.M. Klibanov, R. Langer, Kinetics of insulin aggregation in aqueous solutions upon agitation in the presence of hydrophobic surfaces, Proc. Natl. Acad. Sci. 88 (1991) 9377–9381.

[41] W. Norde, C.E. Giacomelli, BSA structural changes during homomolecular exchange between the adsorbed and the dissolved states, J. Biotechnol. 79 (2000) 259–268.

[42] T. Vermonden, C.E. Giacomelli, W. Norde, Reversibility of Structural Rearrangements in Bovine Serum Albumin during Homomolecular Exchange from AgI Particles, Langmuir. 17 (2001) 3734–3740.

[43] L. Doessegger, H. Mahler, P. Szczesny, H. Rockstroh, G. Kallmeyer, A. Langenkamp, et al., The potential clinical relevance of visible particles in parenteral drugs, J. Pharm. Sci. 101 (2012) 2635–2644.

[44] L. Emmi, F. Chiarini, The role of intravenous immunoglobulin therapy in autoimmune and inflammatory disorders., Neurol. Sci. 23 Suppl 1 (2002) S1–8.

[45] A.S. Rosenberg, Effects of protein aggregates: an immunologic perspective, AAPS J. 8 (2006) E501–E507.

[46] H. Schellekens, Bioequivalence and the immunogenicity of biopharmaceuticals., Nat. Rev. Drug Discov. 1 (2002) 457–462.

[47] R. Purcell, R. Lockey, Immunologic response to therapeutic biologic agents, J Investig Allergol Clin Immunol. 18 (2008) 335–342.

[48] B. Sharma, Immunogenicity of therapeutic proteins. Part 3: impact of manufacturing changes., Biotechnol. Adv. 25 (2007) 325–331.

[49] A. Gerhardt, K. Bonam, J.S. Bee, J.F. Carpenter, T.W. Randolph, Ionic strength affects tertiary structure and aggregation propensity of a monoclonal antibody adsorbed to silicone oil-water interfaces, J. Pharm. Sci. 102 (2013) 429–440.

[50] R. Thirumangalathu, S. Krishnan, M.S. Ricci, D.N. Brems, T.W. Randolph, J.F. Carpenter, Silicone oil- and agitation-induced aggregation of a monoclonal antibody in aqueous solution, J. Pharm. Sci. 98 (2009) 3167–3181.

[51] K. Höger, J. Mathes, W. Frieß, IgG1 adsorption to siliconized glass vials-influence of pH, ionic strength, and nonionic surfactants, J. Pharm. Sci. 104 (2015) 34–43.

[52] J. Mathes, W. Friess, Influence of pH and ionic strength on IgG adsorption to vials, Eur. J. Pharm. Biopharm. 78 (2011) 239–247.

[53] G. Diaconu, T. Schäfer, Study of the interactions of proteins with a solid surface using complementary acoustic and optical techniques, Biointerphases. 9 (2014) 029015(1)–029015(6).

[54] R.E. Speight, M.A. Cooper, A survey of the 2010 quartz crystal microbalance literature, J. Mol. Recognit. 25 (2012) 451–473.

[55] M.A. Cooper, V.T. Singleton, A survey of the 2001 to 2005 quartz crystal microbalance biosensor literature: applications of acoustic physics to the analysis of biomolecular interactions, J. Mol. Recognit. 20 (2007)

154–184.

[56] F. Höök, B. Kasemo, T. Nylander, C. Fant, K. Sott, H. Elwing, Variations in Coupled Water, Viscoelastic Properties, and Film Thickness of a Mefp-1 Protein Film during Adsorption and Cross-Linking: A Quartz Crystal Microbalance with Dissipation Monitoring, Ellipsometry, and Surface Plasmon Resonance Study, Anal. Chem. 73 (2001) 5796–5804.

[57] C. Galli Marxer, M. Collaud Coen, L. Schlapbach, Study of adsorption and viscoelastic properties of proteins with a quartz crystal microbalance by measuring the oscillation amplitude, J. Colloid Interface Sci. 261 (2003) 291–298.

[58] F. Höök, J. Vörös, M. Rodahl, R. Kurrat, P. Böni, J.. Ramsden, et al., A comparative study of protein adsorption on titanium oxide surfaces using in situ ellipsometry, optical waveguide lightmode spectroscopy, and quartz crystal microbalance/dissipation, Colloids Surfaces B Biointerfaces. 24 (2002) 155–170.

[59] T. Werk, D.B. Volkin, H.-C. Mahler, Effect of solution properties on the counting and sizing of subvisible particle standards as measured by light obscuration and digital imaging methods, Eur. J. Pharm. Sci. 53 (2014) 95–108.

[60] C. Giacomelli, M. Bremer, W. Norde, ATR-FTIR Study of IgG Adsorbed on Different Silica Surfaces, J. Colloid Interface Sci. 220 (1999) 13–23.

[61] M. Jang, I. Cho, P. Callahan, Raman detection of protein interfacial conformation, J Biochem Mol Biol. 30 (1997) 352–355.

[62] A.W.P. Vermeer, M.G.E.G. Bremer, W. Norde, Structural changes of IgG induced by heat treatment and by adsorption onto a hydrophobic Teflon surface studied by circular dichroism spectroscopy, Biochim. Biophys. Acta - Gen. Subj. 1425 (1998) 1–12.

[63] M. Wahlgren, Protein adsorption to solid surfaces, Trends Biotechnol. 9 (1991) 201–208.

[64] D.M. Togashi, A.G. Ryder, Assessing protein-surface interactions with a series of multi-labeled BSA using fluorescence lifetime microscopy and Förster Energy Resonance Transfer, Biophys. Chem. 152 (2010) 55–64.

[65] J. Donsmark, C. Rischel, Fluorescence correlation spectroscopy at the oil-water interface: hard disk diffusion behavior in dilute beta-lactoglobulin layers precedes monolayer formation, Langmuir. 23 (2007) 6614–6623.

[66] J. Donsmark, L. Jorgensen, S. Mollmann, S. Frokjaer, C. Rischel, Kinetics of insulin adsorption at the oil-water interface and diffusion properties of adsorbed layers monitored using fluorescence correlation spectroscopy, Pharm. Res. 23 (2006) 148–155.

[67] H. Nishi, R. Mathäs, R. Fürst, G. Winter, Label-Free Flow Cytometry Analysis of Subvisible Aggregates in Liquid IgG1 Antibody Formulations, J. Pharm. Sci. 103 (2014) 90–99.

[68] V. Rombach-Riegraf, C. Allard, E. Angevaare, A. Matter, B. Ossuli, R. Strehl, et al., Size fractionation of microscopic protein aggregates using a preparative fluorescence-activated cell sorter, J. Pharm. Sci. 102 (2013) 2128–2135.

[69] B. Boll, E. Folzer, C. Finkler, J. Huwyler, H.-C. Mahler, R. Schmidt, et al., Comparative Evaluation of Two Methods for Preparative Fractionation of Proteinaceous Subvisible Particles-Differential Centrifugation and FACS, Pharm. Res. 32 (2015) 3952–3964.

[70] D.B. Ludwig, J.T. Trotter, J.P. Gabrielson, J.F. Carpenter, T.W. Randolph, Flow cytometry: a promising technique for the study of silicone oil-induced particulate formation in protein formulations, Anal. Biochem. 410 (2011) 191–199.

[71] H. Mach, A. Bhambhani, B.K. Meyer, S. Burek, H. Davis, J.T. Blue, et al., The use of flow cytometry for the detection of subvisible particles in therapeutic protein formulations, J. Pharm. Sci. 100 (2011) 1671–1678.

[72] C. Lubich, M. Malisauskas, T. Prenninger, T. Wurz, P. Matthiessen, P.L. Turecek, et al., A Flow-Cytometry-Based Approach to Facilitate Quantification, Size Estimation and Characterization of Sub-visible Particles in Protein Solutions, Pharm. Res. 32 (2015) 2863–2876.

[73] S.H. Mollmann, L. Jorgensen, J.T. Bukrinsky, U. Elofsson, W. Norde, S. Frokjaer, Interfacial adsorption of insulin conformational changes and reversibility of adsorption, Eur. J. Pharm. Sci. 27 (2006) 194–204.

[74] A. Gajraj, R.Y. Ofoli, Effect of Extrinsic Fluorescent Labels on Diffusion and Adsorption Kinetics of Proteins at the Liquid−Liquid Interface, Langmuir. 16 (2000) 8085–8094.

[75] T.M. Scherer, S. Leung, L. Owyang, S.J. Shire, Issues and challenges of subvisible and submicron particulate analysis in protein solutions, AAPS J. 14 (2012) 236–243.

[76] K.E. Sapsford, F.S. Ligler, Real-time analysis of protein adsorption to a variety of thin films, Biosens. Bioelectron. 19 (2004) 1045–1055.

[77] 3T GmbH & Co.KG, Sensor Instrument for Surface Interaction Analysis in Real Time. qCell / qCell T. Information brochure, (n.d.). http://www.3t-analytik.de/sites/default/files/Prospekt_qCell_T_120913_web.pdf (accessed November 24, 2015).

[78] G. Sauerbrey, Verwendung von Schwingquarzen zur Wägung dünner Schichten und zur Mikrowägung, Zeitschrift Für Phys. 155 (1959) 206–222.

[79] K.K. Kanazawa, J.G. Gordon, Frequency of a quartz microbalance in contact with liquid, Anal. Chem. 57 (1985) 1770–1771.

[80] M. Rodahl, F. Höök, A. Krozer, P. Brzezinski, B. Kasemo, Quartz crystal microbalance setup for frequency and Q-factor measurements in gaseous and liquid environments, Rev. Sci. Instrum. 66 (1995) 3924–3930.

[81] M. Rodahl, B. Kasemo, A simple setup to simultaneously measure the resonant frequency and the absolute dissipation factor of a quartz crystal microbalance, Rev. Sci. Instrum. 67 (1996) 3238–3241.

[82] M. V Voinova, M. Rodahl, M. Jonson, B. Kasemo, Viscoelastic Acoustic Response of Layered Polymer Films at Fluid-Solid Interfaces: Continuum Mechanics Approach, Phys. Scr. 59 (1999) 391–396.

[83] M.F. Cuddy, A.R. Poda, L.N. Brantley, Determination of isoelectric points and the role of pH for common quartz crystal microbalance sensors, ACS Appl. Mater. Interfaces. 5 (2013) 3514–3518.

[84] D. Johannsmann, Piezoelectric sensors, Springer-Verlag Berlin Heidelberg, 2007.

[85] 3T GmbH & Co. KG, The relation between, dissipation, damping and resistance. Personal communication with Dr. F. K. Gehring, (n.d.).

[86] Dow Corning Corporation, Product Information. Dow Corning 360 Medical Fluid. Ref. No. 51-0374N-01, (2009).

[87] M. Rodahl, F. Höök, C. Fredriksson, C.A. Keller, A. Krozer, P. Brzezinski, et al., Simultaneous frequency

and dissipation factor QCM measurements of biomolecular adsorption and cell adhesion, Faraday Discuss. 107 (1997) 229–246.

[88] G. Ström, M. Fredriksson, P. Stenius, Contact angles, work of adhesion, and interfacial tensions at a dissolving Hydrocarbon surface, J. Colloid Interface Sci. 119 (1987) 352–361.

[89] S. Funke, J. Matilainen, H. Nalenz, K. Bechtold-Peters, H.-C. Mahler, W. Friess, Analysis of thin baked-on silicone layers by FTIR and 3D-Laser Scanning Microscopy, Eur. J. Pharm. Biopharm. 96 (2015) 304–313.

[90] J.M. Mathes, Protein Adsorption to Vial Surfaces – Quantification , Structural and Mechanistic Studies, Dissertation, Ludwig-Maximilians-Universität München, 2010.

[91] ATTO-TEC GmbH, Recommended Procedure for Labeling, (2014). https://www.atto-tec.com/fileadmin/user_upload/Katalog_Flyer_Support/Procedures.pdf (accessed November 26, 2015).

[92] H. Fischer, I. Polikarpov, A.F. Craievich, Average protein density is a molecular-weight-dependent function, Protein Sci. 13 (2004) 2825–2828.

[93] S. Paul, D. Paul, T. Basova, A.K. Ray, Studies of Adsorption and Viscoelastic Properties of Proteins onto Liquid Crystal Phthalocyanine Surface Using Quartz Crystal Microbalance with Dissipation Technique, J. Phys. Chem. C. 112 (2008) 11822–11830.

[94] M.V. Voinova, M. Jonson, B. Kasemo, "Missing mass" effect in biosensor's QCM applications, Biosens. Bioelectron. 17 (2002) 835–841.

[95] C.E. Reed, K.K. Kanazawa, J.H. Kaufman, Physical description of a viscoelastically loaded AT-cut quartz resonator, J. Appl. Phys. 68 (1990) 1993–2001.

[96] M. Rodahl, B. Kasemo, On the measurement of thin liquid overlayers with the quartz-crystal microbalance, Sensors Actuators A Phys. 54 (1996) 448–456.

[97] F. Hook, M. Rodahl, B. Kasemo, P. Brzezinski, Structural changes in hemoglobin during adsorption to solid surfaces: Effects of pH, ionic strength, and ligand binding, Proc. Natl. Acad. Sci. 95 (1998) 12271–12276.

[98] ATTO-TEC GmbH, Atto 633, (2001). https://www.atto-tec.com/attotecshop/product_info.php?info=p110_atto-633.html (accessed November 25, 2015).

[99] Molecular Probes Inc., Molecular probes. Certificate of analysis, (2015). https://tools.thermofisher.com/content/sfs/COAPDFs/2015/1715409_D3922.pdf (accessed November 25, 2015).

[100] Becton Dickinson and Company, BD fluorescence spectrum viewer, (2015). http://www.bdbiosciences.com/sg/research/multicolor/spectrum_viewer/index.jsp (accessed April 7, 2014).

[101] J. Claußen, Eintwicklung biologischer Schichten für die Blutanalytik mit Schwingquarzsensoren, Dissertation, Technische Universität Kaiserslautern, 2006.

[102] F.K. Gehring, Schwingquarzsensorik in Flüssigkeiten. Entwicklung einer Blutanalysegerätes, 1st ed., Cuvillier, E, 2005.

[103] W. Norde, F. MacRitchie, G. Nowicka, J. Lyklema, Protein adsorption at solid-liquid interfaces: Reversibility and conformation aspects, J. Colloid Interface Sci. 112 (1986) 447–456.

[104] V.A. Ogarev, V.M. Rudoi, A.A. Trapeznikov, Wettability of layers of polydimethylsiloxanes, transferred to glass by the langmuir method and produced by adsorption from solution, Bull. Acad. Sci. USSR Div. Chem. Sci. 21 (1972) 2421–2425.

[105] H. Hillborg, S. Karlsson, U.. Gedde, Characterisation of low molar mass siloxanes extracted from crosslinked polydimethylsiloxanes exposed to corona discharges, Polymer (Guildf). 42 (2001) 8883–8889.

[106] D.K. Owens, R.C. Wendt, Estimation of the surface free energy of polymers, J. Appl. Polym. Sci. 13 (1969) 1741–1747.

[107] F.M. Fowkes, Attractive forces at interfaces, Ind. Eng. Chem. 56 (1964) 40–52.

[108] K. Nakamura, Factors contributing to the emulsification of intraocular silicone and fluorosilicone oils, Investig. Ophthalmol. Vis. Sci. 31 (1990) 2059–2069.

[109] H.-H. Moretto, M. Schulze, G. Wagner, Silicone. Ullmann´s encyclopedia of industrial chemistry, Vol. 32, Wiley-VCH Verlag GmbH & Co. KGaK, Weinheim, 2012.

[110] J.M. Schakenraad, H.J. Busscher, C.R. Wildevuur, J. Arends, The influence of substratum surface free energy on growth and spreading of human fibroblasts in the presence and absence of serum proteins, J. Biomed. Mater. Res. 20 (1986) 773–784.

[111] Y. Gu, D. Li, An Electrical Suspension Method for Measuring the Electric Charge on Small Silicone Oil Droplets Dispersed in Aqueous Solutions, J. Colloid Interface Sci. 195 (1997) 343–352.

[112] C. Rücker, K. Kümmerer, Environmental chemistry of organosiloxanes, Chem. Rev. 115 (2015) 466–524.

[113] J. Song, J.F.L. Duval, M.A.C. Stuart, H. Hillborg, U. Gunst, H.F. Arlinghaus, et al., Surface ionization state and nanoscale chemical composition of UV-irradiated poly(dimethylsiloxane) probed by chemical force microscopy, force titration, and electrokinetic measurements, Langmuir. 23 (2007) 5430–5438.

[114] J. Roth, V. Albrecht, M. Nitschke, C. Bellmann, F. Simon, S. Zschoche, et al., Surface functionalization of silicone rubber for permanent adhesion improvement, Langmuir. 24 (2008) 12603–12611.

[115] Y. Gu, D. Li, The zeta-Potential of Silicone Oil Droplets Dispersed in Aqueous Solutions, J. Colloid Interface Sci. 206 (1998) 346–349.

[116] V. Saller, Interactions of formulation and disposables in biopharmaceutical drug product manufacturing, Dissertation, Ludwig-Maximilians-Universität München, 2015.

[117] J. Buijs, P.A.W. van den Berg, J.W.T. Lichtenbelt, W. Norde, J. Lyklema, Adsorption Dynamics of IgG and Its F(ab′)2and Fc Fragments Studied by Reflectometry, J. Colloid Interface Sci. 178 (1996) 594–605.

[118] K. Höger, J. Mathes, W. Frieß, IgG1 adsorption to siliconized glass vials-influence of pH, ionic strength, and nonionic surfactants, J. Pharm. Sci. 104 (2015) 34–43.

[119] N. Dixit, K.M. Maloney, D.S. Kalonia, Application of quartz crystal microbalance to study the impact of pH and ionic strength on protein-silicone oil interactions, Int. J. Pharm. 412 (2011) 20–27.

[120] D. Asthagiri, A.M. Lenhoff, Influence of Structural Details in Modeling Electrostatically Driven Protein Adsorption, Langmuir. 13 (1997) 6761–6768.

[121] T. Mizutani, Estimation of protein and drug adsorption onto silicone-coated glass surfaces, J. Pharm. Sci. 70 (1981) 493–496.

[122] P. Warkentin, B. Wälivaara, I. Lundström, P. Tengvall, Differential surface binding of albumin,

immunoglobulin G and fibrinogen, Biomaterials. 15 (1994) 786–795.

[123] H. Elwing, S. Welin, A. Askendal, U. Nilsson, I. LundstrÖm, A wettability gradient method for studies of macromolecular interactions at the liquid/solid interface, J. Colloid Interface Sci. 119 (1987) 203–210.

[124] J. Ortega-Vinuesa, P. Tengvall, I. Lundström, Aggregation of HSA, IgG, and Fibrinogen on Methylated Silicon Surfaces, J. Colloid Interface Sci. 207 (1998) 228–239.

[125] J.S. Bee, D. Chiu, S. Sawicki, J.L. Stevenson, K. Chatterjee, E. Freund, et al., Monoclonal antibody interactions with micro- and nanoparticles: adsorption, aggregation, and accelerated stress studies, J. Pharm. Sci. 98 (2009) 3218–3238.

[126] L. Fornelli, E. Damoc, P.M. Thomas, N.L. Kelleher, K. Aizikov, E. Denisov, et al., Analysis of intact monoclonal antibody IgG1 by electron transfer dissociation Orbitrap FTMS, Mol. Cell. Proteomics. 11 (2012) 1758–1767.

[127] A. Oom, M. Poggi, J. Wikström, M. Sukumar, Surface interactions of monoclonal antibodies characterized by quartz crystal microbalance with dissipation: impact of hydrophobicity and protein self-interactions, J. Pharm. Sci. 101 (2012) 519–29.

[128] M. Wahlgren, T. Arnebrant, I. Lundström, The Adsorption of Lysozyme to Hydrophilic Silicon Oxide Surfaces: Comparison between Experimental Data and Models for Adsorption Kinetics, J. Colloid Interface Sci. 175 (1995) 506–514.

[129] H. Xu, X. Zhao, C. Grant, J.R. Lu, D.E. Williams, J. Penfold, Orientation of a monoclonal antibody adsorbed at the solid/solution interface: a combined study using atomic force microscopy and neutron reflectivity, Langmuir. 22 (2006) 6313–6320.

[130] J. Vörös, The density and refractive index of adsorbing protein layers, Biophys. J. 87 (2004) 553–561.

[131] J. Buijs, J.W.T. Lichtenbelt, W. Norde, J. Lyklema, Adsorption of monoclonal IgGs and their F(ab′)2 fragments onto polymeric surfaces, Colloids Surfaces B Biointerfaces. 5 (1995) 11–23.

[132] L.J. Harris, E. Skaletsky, A. McPherson, Crystallographic structure of an intact IgG1 monoclonal antibody, J. Mol. Biol. 275 (1998) 861–872.

[133] M. Malmsten, Ellipsometry studies of the effects of surface hydrophobicity on protein adsorption, Colloids Surfaces B Biointerfaces. 3 (1995) 297–308.

[134] C. Zhou, J.-M. Friedt, A. Angelova, K.-H. Choi, W. Laureyn, F. Frederix, et al., Human Immunoglobulin Adsorption Investigated by Means of Quartz Crystal Microbalance Dissipation, Atomic Force Microscopy, Surface Acoustic Wave, and Surface Plasmon Resonance Techniques, Langmuir. 20 (2004) 5870–5878.

[135] Y.-J. Sheng, H.-K. Tsao, J. Zhou, S. Jiang, Orientation of a Y-shaped biomolecule adsorbed on a charged surface, Phys. Rev. E. Stat. Nonlin. Soft Matter Phys. 66 (2002) 011911(1)–011911(5).

[136] S. Chen, L. Liu, J. Zhou, S. Jiang, Controlling Antibody Orientation on Charged Self-Assembled Monolayers, Langmuir. 19 (2003) 2859–2864.

[137] J. Zhou, S. Chen, S. Jiang, Orientation of Adsorbed Antibodies on Charged Surfaces by Computer Simulation Based on a United-Residue Model, Langmuir. 19 (2003) 3472–3478.

[138] A. Vermeer, Adsorption of IgG onto hydrophobic teflon. Differences between the Fab and Fc domains, Biochim. Biophys. Acta - Gen. Subj. 1526 (2001) 61–69.

[139] A.B. Anderson, C.R. Robertson, Absorption spectra indicate conformational alteration of myoglobin adsorbed on polydimethylsiloxane, Biophys. J. 68 (1995) 2091–2097.

[140] M.C.L. Maste, W. Norde, A.J.W.G. Visser, Adsorption-Induced Conformational Changes in the Serine Proteinase Savinase: A Tryptophan Fluorescence and Circular Dichroism Study, J. Colloid Interface Sci. 196 (1997) 224–230.

[141] M.C.L. Maste, E.H.W. Pap, A. van Hoek, W. Norde, A.J.W.G. Visser, Spectroscopic Investigation of the Structure of a Protein Adsorbed on a Hydrophobic Latex, J. Colloid Interface Sci. 180 (1996) 632–633.

[142] M. Rankl, T. Ruckstuhl, M. Rabe, G.R.J. Artus, A. Walser, S. Seeger, Conformational reorientation of immunoglobulin G during nonspecific interaction with surfaces, Chemphyschem. 7 (2006) 837–846.

[143] S.H. Mollmann, J.T. Bukrinsky, S. Frokjaer, U. Elofsson, Adsorption of human insulin and AspB28 insulin on a PTFE-like surface, J. Colloid Interface Sci. 286 (2005) 28–35.

[144] R.J. Marsh, R.A.. Jones, M. Sferrazza, Adsorption and displacement of a globular protein on hydrophilic and hydrophobic surfaces, Colloids Surfaces B Biointerfaces. 23 (2002) 31–42.

[145] V. Krisdhasima, J. McGuire, R. Sproull, Surface hydrophobic influences on β-lactoglobulin adsorption kinetics, J. Colloid Interface Sci. 154 (1992) 337–350.

[146] F. Höök, M. Rodahl, P. Brzezinski, B. Kasemo, Measurements Using the Quartz Crystal Microbalance Technique of Ferritin Monolayers on Methyl-Thiolated Gold: Dependence of Energy Dissipation and Saturation Coverage on Salt Concentration., J. Colloid Interface Sci. 208 (1998) 63–67.

[147] S. Bingaman, V.H. Huxley, R.E. Rumbaut, Fluorescent Dyes Modify Properties of Proteins Used in Microvascular Research, Microcirculation. 10 (2003) 221–231.

[148] L.C. Zanetti-Domingues, C.J. Tynan, D.J. Rolfe, D.T. Clarke, M. Martin-Fernandez, Hydrophobic fluorescent probes introduce artifacts into single molecule tracking experiments due to non-specific binding, PLoS One. 8 (2013) e74200(1)–e74200(11).

[149] V. Buschmann, K.D. Weston, M. Sauer, Spectroscopic study and evaluation of red-absorbing fluorescent dyes, Bioconjug. Chem. 14 (2002) 195–204.

[150] G. Grunwaldt, S. Haebel, C. Spitz, M. Steup, R. Menzel, Multiple binding sites of fluorescein isothiocyanate moieties on myoglobin: photophysical heterogeneity as revealed by ground- and excited-state spectroscopy, J. Photochem. Photobiol. B Biol. 67 (2002) 177–186.

[151] L. Wang, G. Amphlett, W.A. Blättler, J.M. Lambert, W. Zhang, Structural characterization of the maytansinoid-monoclonal antibody immunoconjugate, huN901-DM1, by mass spectrometry, Protein Sci. 14 (2005) 2436–2446.

[152] A.A. Wakankar, M.B. Feeney, J. Rivera, Y. Chen, M. Kim, V.K. Sharma, et al., Physicochemical stability of the antibody-drug conjugate Trastuzumab-DM1: changes due to modification and conjugation processes, Bioconjug. Chem. 21 (2010) 1588–1595.

[153] FDA professional durg information, Mylotarg (gemtuzumab ozagamicin for injection) fir intravenous use only., (2010). http://www.drugs.com/pro/mylotarg.html (accessed December 14, 2015).

[154] G.M. Cockrell, M.S. Wolfe, J.L. Wolfe, C. Schöneich, Photoinduced aggregation of a model antibody-drug conjugate, Mol. Pharm. 12 (2015) 1784–1797.

[155] C.A. Teske, E. von Lieres, M. Schröder, A. Ladiwala, S.M. Cramer, J.J. Hubbuch, Competitive adsorption of labeled and native protein in confocal laser scanning microscopy, Biotechnol. Bioeng. 95 (2006) 58–66.

[156] V. Filipe, R. Poole, O. Oladunjoye, K. Braeckmans, W. Jiskoot, Detection and characterization of subvisible aggregates of monoclonal IgG in serum, Pharm. Res. 29 (2012) 2202–2212.

[157] Molecular Probes Inc., Bodipy Lipid Probes. Product information, (2003). https://tools.thermofisher.com/content/sfs/manuals/mp03792.pdf (accessed November 25, 2015).

[158] K.A. Britt, D.K. Schwartz, C. Wurth, H.-C. Mahler, J.F. Carpenter, T.W. Randolph, Excipient effects on humanized monoclonal antibody interactions with silicone oil emulsions, J. Pharm. Sci. 101 (2012) 4419–4432.

[159] D.B. Ludwig, J.F. Carpenter, J.-B. Hamel, T.W. Randolph, Protein adsorption and excipient effects on kinetic stability of silicone oil emulsions, J. Pharm. Sci. 99 (2010) 1721–1733.

[160] F. Gruia, A. Parupudi, A. Polozova, Practical Considerations for Detection and Characterization of Sub-Micron Particles in Protein Solutions by Nanoparticle Tracking Analysis, PDA J. Pharm. Sci. Technol. 69 (2015) 427–439.

[161] B.K. Lok, Y.-L. Cheng, C.R. Robertson, Total internal reflection fluorescence: a technique for examining interactions of macromolecules with solid surfaces, J. Colloid Interface Sci. 91 (1983) 87–103.

[162] D.G. Isom, C.A. Castañeda, B.R. Cannon, B. García-Moreno, Large shifts in pKa values of lysine residues buried inside a protein, Proc. Natl. Acad. Sci. U. S. A. 108 (2011) 5260–5265.

[163] T.A. Khan, H.-C. Mahler, R.S.K. Kishore, Key interactions of surfactants intherapeutic proteinformulations: A review, Eur. J. Pharm. Biopharm. 97 (2015) 60–67.

[164] H.J. Lee, A. McAuley, K.F. Schilke, J. McGuire, Molecular origins of surfactant-mediated stabilization of protein drugs, Adv. Drug Deliv. Rev. 63 (2011) 1160–1171.

[165] N. Dixit, K.M. Maloney, D.S. Kalonia, Protein-silicone oil interactions: comparative effect of nonionic surfactants on the interfacial behavior of a fusion protein, Pharm. Res. 30 (2013) 1848–1859.

[166] O. Joshi, J. McGuire, Adsorption behavior of lysozyme and Tween 80 at hydrophilic and hydrophobic silica-water interfaces, Appl. Biochem. Biotechnol. 152 (2009) 235–248.

[167] S.I. Jeon, J.H. Lee, J.D. Andrade, P.G. De Gennes, Protein—surface interactions in the presence of polyethylene oxide, J. Colloid Interface Sci. 142 (1991) 149–158.

[168] S.H. Mollmann, U. Elofsson, J.T. Bukrinsky, S. Frokjaer, Displacement of adsorbed insulin by Tween 80 monitored using total internal reflection fluorescence and ellipsometry, Pharm. Res. 22 (2005) 1931–1941.

[169] A.R. Mackie, A.P. Gunning, P.J. Wilde, V.J. Morris, Orogenic Displacement of Protein from the Oil/Water Interface, Langmuir. 16 (2000) 2242–2247.

[170] H.L. Kim, A. McAuley, B. Livesay, W.D. Gray, J. McGuire, Modulation of protein adsorption by poloxamer 188 in relation to polysorbates 80 and 20 at solid surfaces, J. Pharm. Sci. 103 (2014) 1043–1049.

[171] N.B. Bam, J.L. Cleland, J. Yang, M.C. Manning, J.F. Carpenter, R.F. Kelley, et al., Tween protects recombinant human growth hormone against agitation-induced damage via hydrophobic interactions, J. Pharm. Sci. 87 (1998) 1554–1559.

[172] P. Garidel, C. Hoffmann, A. Blume, A thermodynamic analysis of the binding interaction between

polysorbate 20 and 80 with human serum albumins and immunoglobulins: a contribution to understand colloidal protein stabilisation, Biophys. Chem. 143 (2009) 70–8.

[173] K.L. Mittal, Determination of CMC of polysorbate 20 in aqueous solution by surface tension method, J. Pharm. Sci. 61 (1972) 1334–1335.

[174] S.K. Hait, S.P. Moulik, Determination of critical micelle concentration (CMC) of nonionic surfactants by donor-acceptor interaction with lodine and correlation of CMC with hydrophile-lipophile balance and other parameters of the surfactants, J. Surfactants Deterg. 4 (2001) 303–309.

[175] L.S.C. Wan, P.F.S. Lee, CMC of polysorbates, J. Pharm. Sci. 63 (1974) 136–137.

[176] M. Zhang, M. Ferrari, Reduction of albumin adsorption onto silicon surfaces by Tween 20, Biotechnol. Bioeng. 56 (1997) 618–625.

VIII SUMMARY OF THE THESIS

During the development of drug/device combination products comprising syringes or cartridges as primary packaging components, siliconization of the interior glass barrel is an essential step to enable device functionality with adequate piston extrusion performance. Bake-on siliconization is a complex, multi-step process with a set of parameters to be precisely regulated. In addition to functionality, compatibility of the formulation with the siliconized container surface is equally important and needs to be assessed, in particular for sensitive protein therapeutics. Both aspects were presented in the general introduction **(chapter I)**.

Adequate siliconization balances both sufficient silicone for lubricity and limited silicone levels to mitigate an impact on drug product, e.g., due to migrating silicone droplets. This challenge is met by bake-on siliconization processes applying low silicone levels and resulting in thin silicone layers, which, however, cannot be easily characterized by standard methods. Therefore, in **chapter III**, Fourier transform infrared spectroscopy (FTIR) after a multi-step solvent extraction was established to quantify baked-on silicone levels as low as 4 µg/cartridge barrel (limit of quantification = 18 µg/mL). FTIR showed a good linear response (R^2 = 0.994-0.999) and an excellent sensitivity (limit of detection < 1 µg/mL). Additionally, 3D-laser scanning microscopy (3D-LSM) was introduced as a novel technique to visualize the baked-on silicone at such low levels and to determine the layer thickness down to 10 nm. 3D-LSM was further developed to characterize the silicone distribution along the cartridge barrel. Both methods were able to overcome the current limitations of other standard techniques to characterize such thin baked-on silicone layers and thus enabled further optimization of the bake-on siliconization process.

The bake-on siliconization process comprises two steps, namely spraying diluted silicone emulsion into the interior cartridge barrel followed by baking at elevated temperature. An optimized spray process using a pilot scale siliconization unit was designed in **chapter IV** supported by the methods developed in chapter III. A spray quantity of 4 mg showed best atomization behavior and led to relatively thin, homogeneous silicone layers compared to a spray quantity of 16 mg and 29 mg. These higher spray quantities led to runlets and thus inhomogeneous silicone build-ups at the flared cartridge edge. A long time for pump dosing was beneficial for the atomization of higher spray quantities, whereas a high spray pressure did not result in an improvement. Adequate baked-on silicone levels ranging from 10 µg to

100 µg/cartridge barrel and layer thicknesses from 10 nm to 50 nm were targeted by adjusting the emulsion concentration while an optimized spray quantity of 4 mg was maintained. Initially, a low baked-on silicone level of approximately 10 µg/cartridge barrel was sufficient for adequate extrusion forces below 10 N. However, for optimal extrusion performance throughout long-term storage, a baked-on silicone level of 30 µg/cartridge barrel is advisable for extrusion forces below 15 N. The spray nozzle position had a fundamental impact on the silicone distribution since it determined the matching area of the spray cone and the cartridge barrel. A spray nozzle position of 20 mm below the cartridge flange resulted in thicker silicone layers at the cartridge flange, which may be beneficial for break-loose of the piston during injection. A reduced set of methods and the identification of key spray parameters further allowed a fast optimization approach for a second, different nozzle design. The fundamental process understanding was a prerequisite to enable a fully controlled spray-on process. Overall, the optimized process yielded sufficient, but limited baked-on silicone levels, a specifically tuned silicone distribution and adequate functionality.

Chapter V aimed to clarify the impact of the bake-on process in the heat-tunnel on the silicone layer characteristics. A baked-on silicone level of 13 ± 3 µg/cartridge barrel provided adequate functionality at considered standard burn-in conditions of 316 °C for 12 min. Burn-in times equal to or longer than 1 h cannot be recommended due to an increase in gliding forces above 15 N. Thus, long interruptions of the bake-on process need to be avoided at such low baked-on silicone levels. Alternatively, a baked-on silicone level of approximately 80 µg/cartridge barrel should be preferred to enable burn-in times up to 2 h. In thermogravimetric analysis, silicone showed an onset of the main weight loss at 313 ± 5 °C, which correlated well with the decrease in the baked-on silicone level between 250 °C and 316 °C and a decrease in the layer thickness at 316 °C compared to 200 °C. The average molecular weight of the silicone polymer remained unchanged at approximately 23,000 g/mol independent of the burn-in temperatures between 200 °C and 350 °C. However, at higher temperatures of 316 °C and 350 °C, the molecular weight distribution showed an increased fraction between 5,000-15,000 g/mol as depolymerization products and fractions below 5,000 g/mol were removed. Cyclic low molecular weight species of less than 500 g/mol were not found in the baked-on silicone layer. In addition, emulsion stabilizers were either quantitatively removed upon bake-on (parabens, propylene glycol) or remained in the baked-on silicone layer only in small traces (polysorbate 20, Triton X-100). A toxicological effect or an adverse impact on the drug product associated with low molecular weight species or

stabilizer residues were thus not considered to be of concern. During bake-on in a heat-oven as an experimental model, sufficient air exchange was required to mimic the time and temperature-dependent siliconization process in the heat-tunnel. Air-exchange likely prevented saturation effects within the heat-oven and contributed to the removal of silicone decomposition products. Interestingly, for optimal spreading and uniform silicone layers, temperatures as high as 300 °C may be essential despite the concomitant decrease in the baked-on silicone level. Contact angle analysis suggested a thin silicone film remaining on the glass surface most likely due to covalent siloxane bonds between silicone and the glass surface although extraction was performed under harsh conditions. Overall, the performed experiments provided valuable insight into the thermal decomposition of silicone. The silicone layer characteristics were comprehensively studied to identify an adequate processing window for robust bake-on siliconization processes.

Adequate piston extrusion performance governs the lower silicone level while higher silicone levels might compromise drug product quality, e.g., due to a higher number of silicone droplets in solution. Therefore, the impact of two practically relevant baked-on silicone levels (13 ± 3 µg and 94 ± 6 µg/cartridge barrel, i.e., 4 mg of a 0.6 % (w/w) and 3.5 % (w/w) silicone emulsion), on the formation of silicone droplets and protein particles in formulation containing surfactant was assessed in **chapter VI**. Agitation resulted in silicone migration whereas expelling alone or in addition to agitation did not enhance silicone migration in placebo. A therapeutic protein formulation containing a model monoclonal antibody (mAb) at a concentration of 2 mg/mL and 33 mg/mL and additionally 0.04 % (m/v) polysorbate 20 was therefore assessed after agitation with and without headspace. The different baked-on silicone levels had no impact on the submicron particle size range in nanoparticle tracking analysis and the monomeric mAb in dynamic light scattering. The number of particles in the size range of 0.2-5 µm in resonant mass measurement and ≥ 1 µm in micro-flow imaging and light obscuration increased with higher baked-on silicone levels. Particles were identified as silicone droplets and the particle numbers were comparable in placebo and solutions containing mAb at 2 mg/mL or 33 mg/mL. Cartridges that were filled with headspace showed higher numbers of silicone droplets mobilized by bulk fluid shear forces due to the movement of the air bubble as compared to cartridges filled without headspace. Still, the optimized bake-on siliconization process in combination with adequate silicone levels resulted in considerably lower particles as compared to literature. Overall, the particle numbers were well below the limits of current pharmacopeias and were thus of no

concern for product quality. It was further demonstrated that the different baked-on silicone levels and migrated silicone droplets did not induce protein particle formation.

In this study, the number of silicone droplets was reasonable low due to an optimized bake-on siliconization process. However, since proteins may interact with surfaces, adsorption to the silicone oil-water interface is also thought to occur and could be critical for the specified drug product concentration. In any case, adsorption studies are recommended to ensure drug product quality and provide adsorption mechanisms. **Chapter VII** thus aimed to evaluate quartz crystal microbalance (QCM) and fluorescence activated cell sorting (FACS) as novel methods to characterize protein adsorption to silicone surfaces. In QCM, sprayed-on and baked-on silicone layers were successfully modeled by spin-coating quartz chips with silicone oil and heat-treated silicone oil, respectively. Maximum adsorption on sprayed-on silicone surfaces was found around the protein´s isoelectric point at pH 8 with 6.8 ± 0.2 mg/m^2. At the isoelectric point, protein molecules carry least net charge, which results in minimized inter-protein repulsion and thus enables close packaging. In comparison, adsorption to the slightly more hydrophobic baked-on silicone surface was increased with a broader maximum between pH 6 (7.0 ± 0.6 mg/m^2) and pH 8 (8.7 ± 1.6 mg/m^2) and less reversible upon rinsing with buffer. The literature suggests greater adsorption to hydrophobic surfaces and by more hydrophobic proteins. The latter was confirmed by adsorption studies using Atto 633-labeled mAb, which exhibited a significantly higher hydrophobicity and higher adsorbed amounts with 8.9-9.2 mg/m^2 at pH 6 and pH 8. In contrary to the unlabeled mAb, the adsorption of mAb-Atto 633 was irreversible upon rinsing with buffer in QCM and exchange with unlabeled mAb in FACS. The pH effect on the adsorption of mAb-Atto 633 was similarly observed in QCM and FACS, but it was less clear presented in FACS. Polysorbate 20 at a concentration as low as 0.005 % (w/v) efficiently prevented mAb-Atto 633 from adsorption. Overall, the hydrophobicity of both the sorbent surface and adsorbed species thus dominated the adsorption behavior. Labeling provided an interesting approach to artificially modulate the protein´s hydrophobicity and investigate the associated impact on adsorption. However, these results also clearly demonstrated that the effect of the label needs to be clarified before undertaking experiments where labeled proteins are applied as surrogates for the unlabeled species.

In summary, this work highlighted challenges, which are encountered during the development of protein therapeutics in siliconized drug/device combination products. An exemplary bake-on siliconization process was systematically optimized by applying novel analytical tools. The

described experiments shall encourage further investigation and development of robust and fully controlled siliconization processes. They further underscored the complexity of developing a suitable bake-on siliconization process. Currently, there has been a considerable interest into the assessment of particles from many academic and industrial researchers, particularly for those particles smaller than 10 µm. For bake-on siliconized cartridges filled with therapeutic protein formulations containing surfactant, silicone droplet and protein particle formation was of no concern for drug product quality. Protein adsorption was efficiently mitigated by the addition of surfactant. Overall, this work provided a substantial contribution to rational formulation and packaging development for protein therapeutics.

ABBREVIATIONS

FACS	Fluorescence activated cell sorting
FTIR	Fourier transform infrared (spectroscopy)
3D-LSM	3D-laser scanning microscopy
mAb	Monoclonal antibody
PFS	Pre-filled syringe
QCM	Quartz crystal microbalance